UNIVERSITY OF NOTTINGHAM

DEPARTMENT OF CIVIL ENGINEERING

APPLICATION OF THE DISSIPATED ENERGY CONCEPT TO

FATIGUE CRACKING IN ASPHALT PAVEMENTS

by

Geoffrey M. Rowe, BSc(Hons)

Thesis submitted to the University of Nottingham

for the degree of Doctor of Philosophy

January 1996

TO RACHEL

ABSTRACT

Following a description of the general properties of asphaltic materials, a review is presented on fatigue damage.

Fatigue element tests have been carried out using two types of procedures; uniaxial tension-compression and a trapezoidal cantilever beam. The data from the Trapezoidal test has been used to develop relationships between dissipated energy and the number of load cycles to crack initiation. A method has been developed which enables the stiffness loss during a fatigue test to be quantified in terms of the initial mixture rheology. In addition, an improved method for defining the crack initiation point, *N1*, has been developed along with the definition of an energy ratio to enable determination of fatigue life for intermediate modes of loading. An assessment of two tests involving indirect tension has been made.

A series of tests were conducted in the Slab Test Facility to determine the performance of various asphaltic mixtures with respect to fatigue. These have been used to validate the results from the element tests and assess the suitability of different shift factors.

A 2 dimensional Finite Element visco-elastic analysis method has been used to calculate dissipated energy in pavement structures. This method has been compared to an elastic analysis method. It was observed that the F.E. method is less sensitive to pavement thickness. The F.E. method has some potential

for prediction of surface cracking and fatigue life but further work is needed to implement a 3 dimensional model.

Finally, based upon an assessment of the results obtained, recommendations have been made for additional work involving materials testing, model development and pavement design.

the numerical procedures used in the analysis of data and the Finite Element procedures; Mr. Keith Cooper who instructed me on computer programming methods for running the various fatigue tests and Mr. Barry Brodrick for his help with the Slab Test Facility experiments.

I thank Mrs. Bettina Bouldin and Mr. John Buxbaum for their help with scanning many of the figures in this thesis.

Finally, I wish to thank my wife, Rachel, for enduring many lonely evenings as I worked on this document and for proof reading the text with great accuracy.

APPLICATION OF THE DISSIPATED ENERGY CONCEPT TO FATIGUE CRACKING IN ASPHALT PAVEMENTS

- CONTENTS -

Page Number

i

CHAPTER 3. LITERATURE REVIEW

CHAPTER 4. EXPERIMENTAL

CHAPTER 5. TEST PROCEDURES

CHAPTER 9. FATIGUE ANALYSIS OF PAVEMENTS

CHAPTER 10. PREDICTION OF FATIGUE LIFE

CHAPTER 11. CONCLUSIONS AND RECOMMENDATIONS

REFERENCES

APPENDICES

Appendix A - Strain Gauge Results from fatigue Wheel Tracking

LIST OF TABLES

LIST OF FIGURES

xiii

xv

CHAPTER 1

Introduction

1.0   THE PROBLEM OF FATIGUE CRACKING

Fatigue cracking occurs when materials are subjected to repeated application of loads at a level which induces stresses generally below the tensile strength. In road pavements, traffic induced stresses/strains at the underside of the bound asphaltic layer have been linked to this form of cracking. The cracking can result in moisture penetration and this in turn can cause weakening of the soil foundation, accelerating the failure of pavement structures. The need to protect the considerable value invested in road pavements prompts the need to understand the fatigue mechanism in relation to road pavement performance.

1.1   EARLY PAVEMENT DESIGN

The engineering properties of asphaltic paving materials and analysis of the pavement structure are both so complex that, for many years, detailed structural analysis was not attempted. When pavements for road vehicles consisted essentially of unbound materials such as, gravels, crushed stone etc, covered with thin asphaltic treatments, such as a surface dressing or a thin asphaltic mixture, the choice of materials, and the thickness required to carry traffic, were based on experience. This experience was originally that of

individual pavement engineers but gradually it was rationalized and presented in the form of tables or charts, so that the data could be used by less experienced engineers. Many such systems were developed for particular locations by making appropriate allowances for factors such as climate, soil type, drainage and effects of frost.

These purely empirical systems were fairly reliable but, since they were based on experience, their use was restricted to the same circumstances as the original experience. The limitations of these systems have became apparent as traffic volumes have increased and the trend in pavement design has been towards the gradual adoption of a more mechanistic approach. This approach requires a knowledge of the engineering properties of the materials and an ability to model the pavement structure theoretically.

1.2   DEVELOPMENT OF MECHANISTIC PAVEMENT DESIGN

The possibility of using conventional structural design methods, which require a mathematical model of the structure, was first considered in the 1940's. Equations were developed by Burmister (1943) for the calculation of stresses and deflections in a two-layer system. These equations assumed that the layers were homogeneous, isotropic and elastic and indicated the potential benefit of using higher quality materials in the upper layers. The solutions for stress were, however, not widely used because of the mathematical complexity of the equations. Recently, with the development of increased computing facilities, these use of these complex mathematical procedures have become relatively

routine.

Considerable progress has been made in understanding structural behaviour, including the interaction between layers and the concept of pavement deterioration. Pavements do not normally fail catastrophically but by gradual accumulation of permanent deformation or cracking, caused by repeated applications of load, eventually leading to unacceptable pavement quality. The use of structural analysis techniques led to the realization that layers of high stiffness would develop high tensile stresses. The inspection of test pavements confirmed that cracking is generally initiated at the bottom of the asphalt layer and propagates upward through the bound pavement layers (van Dijk, 1975). Thus, the adoption of stiff bound layers to protect the soil foundation, can result in fatigue failure due to the traffic loading with cracks initiating at the bottom of the layer. However, other researchers (Matsuno et al., 1992) have reported the incidence of surface cracks initiating first, particularly in hot arid climates where UV light can cause brittleness of the surface through high levels of oxidation. Considerable progress has been made in understanding the mechanisms of fatigue cracking and these developments have been used in various design methods for flexible pavements (Shell International Petroleum Company, 1978; Brown et al., 1985; and The Asphalt Institute, 1984). These have been generally been based on, or incorporated, a theoretical analysis carried out by computers.

1.3   BACKGROUND TO THE RESEARCH PROJECT

The research work undertaken and presented in this thesis evolved from a series of research contracts awarded to SWK Pavement Engineering Ltd. and the University of Nottingham by contractors working on the U.S. Strategic Highway Research Program, SHRP, (Strategic Highway Research Program, 1986). This program was funded by the government of the USA and concentrated on four specific areas of research related to highways; asphalt, concrete and structures, highway operations and long term pavement performance. The largest amount of work in this thesis formed part of the asphalt research which was conducted via a series of main research contracts as given in Table 1.1. Two other contracts (A-002B, "Novel Approaches for Investigating Asphalt Binders" and A-002C, Nuclear Magnetic Resonance Investigation of Asphalt) supported the work of contractor A-002A. In addition, a series (fifteen total) of small innovative research contracts were awarded. The work on fatigue cracking was carried out for contracts A-003A and A-004. In addition, a small amount of work was done directly with the management contractor (SHRP contract A-001).

During the course of the SHRP research, additional research contracts were awarded to SWK(PE) following discussions between the author and Shell Development Company in Houston. The combination of the SHRP and SHELL contracts provided a basis for an extensive investigation of the fatigue cracking phenomenon. Due to the larger scale of these projects some of the technical work carried out by the author involved developments by co-workers who are referred to from time to time in the text. The transatlantic nature of the research provided for an excellent opportunity for interactions with

American universities and at some stage in the research program all the places listed in Table 1.1 were visited.

The specific work conducted on each of the projects outlined above was as follows:-

SHRP-A-003A: Refinement of the procedures and equipment at Nottingham for two types of fatigue test followed by the subsequent testing of 64 specimens in each apparatus as part of a test development plan.

Testing of 6 slabs with an apparatus, in which the load was applied with a rolling wheel, to assist with the validation of the selected test method for fatigue.

Testing of 40 specimens removed from a circular test track in France[1] as part of an inter-laboratory study on repeatability/reproducibility of the preferred test methods.

SHRP-A-004: Testing of 12 slabs with an apparatus, in which the load was applied with a rolling wheel, to assist with validation of the selected fatigue test for mixtures with modified binders.

SHELL-02: Fatigue testing of 45 specimens using a standard mixture

---

[1]Laboratoire Central des Ponts et Chaussées, Nantes

Contract No.	Description	Organization/Principle Investigator
A-001	Improved Asphaltic Materials, Experiment Design, Coordination and Control of Experimental Materials.	University of Texas, Austin, Texas. Professor T. Kennedy
A-002A	Binder Characterization and Evaluation.	Pennsylvania State University, State College, Pennsylvania. Professor D. Anderson
A-003A	Performance Related Testing and Measuring of Asphalt-Aggregate Interactions and Mixtures.	University of California at Berkeley, California. Professor C.L. Monismith
A-003B	Fundamental Properties of Asphalt-Aggregate Interactions and Mixtures.	University of Auburn, Auburn, Alabama Professor C. Curtis
A-004	Asphalt Modification.	South Western Laboratories, Houston, Texas. Mr D. F. Martinez and Dr D. Rowlett
A-005	Performance Models and Validation of Test Results.	Texas A&M University, College Station, Texas. Professor R.L. Lytton

Table 1.1: SHRP Asphalt Projects

with 11 different types of binder, 9 of which were modified.

SHELL-03: Development of a visco-elastic pavement model for the prediction of fatigue life (and permanent deformation) of asphalt pavements.

SHELL-D: Testing of 60 specimens of asphalt aggregate mixtures to obtain visco-elastic properties.

While the results of the individual contracts have been separately reported, the combination of the all the work allowed the author to further develop existing methods and improve understanding of the fatigue cracking problem.

1.4   OBJECTIVES OF THE RESEARCH

The objectives of the research work presented in this thesis were to evaluate and develop the concept of dissipated energy to explain the fatigue process in asphaltic materials. The work involved the development of new, improved fatigue test procedures making full use of data acquisition with modern PC's which has only recently become possible. Consequently, the work on this project had the advantage of a significantly greater level of data acquired for analysis than on previous research conducted at Nottingham on the fatigue performance of asphaltic mixtures (for example Cooper, 1976).

In addition, methods were investigated which made use of visco-elastic

analysis to calculate pavement damage using dissipated energy. This work involved model development for asphaltic materials and the use of transfer functions to estimate the damage associated with dissipated energy.

In addition to the theoretical model and transfer function development, the series of tests in the Slab Test Facility provide a first stage validation of the methods developed above. An effort was also made to develop simplified test procedures.

1.5   CONTENTS OF THESIS

This thesis is divided into eleven chapters. Chapters 2 and 3 provide a literature review on the properties of asphaltic materials and their fatigue characteristics including background information on visco-elastic behaviour.

The details of the experimental work are given in Chapter 4 which also provides information on material properties and other basic reference data. The laboratory test procedures are described in detail in Chapter 5.

Chapter 6 contains a detailed analysis of the fatigue test results and a method for defining crack initiation is presented. A mode of loading factor is developed and statistical analysis of the data result in predictive equations for estimating fatigue cracking of laboratory specimens using the concepts of dissipated energy.

The results of the wheel tracking experiments conducted in the Slab Test Facility are presented in Chapter 7. This includes comparisons with bending beam fatigue test results and performance rankings.

Chapter 8 contains analysis of data collected in the Indirect Tensile Test which was used as a "simplified" test procedure.

The fatigue analysis method using visco-elastic modelling is presented in Chapter 9. This contains a discussion on the "case for" visco-elastic analysis and discusses material models which can be used. Comparisons are made with conventional elastic analysis.

The prediction of fatigue life for real pavements includes the effects of temperature variations, traffic, rest periods and other considerations. These aspects are discussed in Chapter 10 which makes recommendations and suggestions for fatigue prediction.

Conclusions and recommendations are presented in Chapter 11.

Physical Properties of Asphaltic

Mixtures

2.0 COMPONENTS OF ASPHALTIC MATERIALS

Asphaltic materials are made from the combination of mineral aggregates with an asphaltic binder. The aggregates are described as belonging to one of three categories depending upon the size fraction. The fraction retained on 2.36 mm (or 3.35 mm), passing 2.36 mm (or 3.35 mm) retained 75 μm and passing 75 μm sieves are generally referred to as coarse aggregate, fine aggregate and filler respectively. The filler, although present in many aggregates, is normally obtained from limestone due to both improved physical and chemical effects that this alkaline aggregate imparts to the mixture.

2.1 BINDERS

2.1.1 Asphaltic Binders

The most common asphaltic binder is *bitumen*[1] which is obtained from crude

---

[1] In the United States of America "Bitumen" is referred to as "Asphalt Cement" or simply "Asphalt".
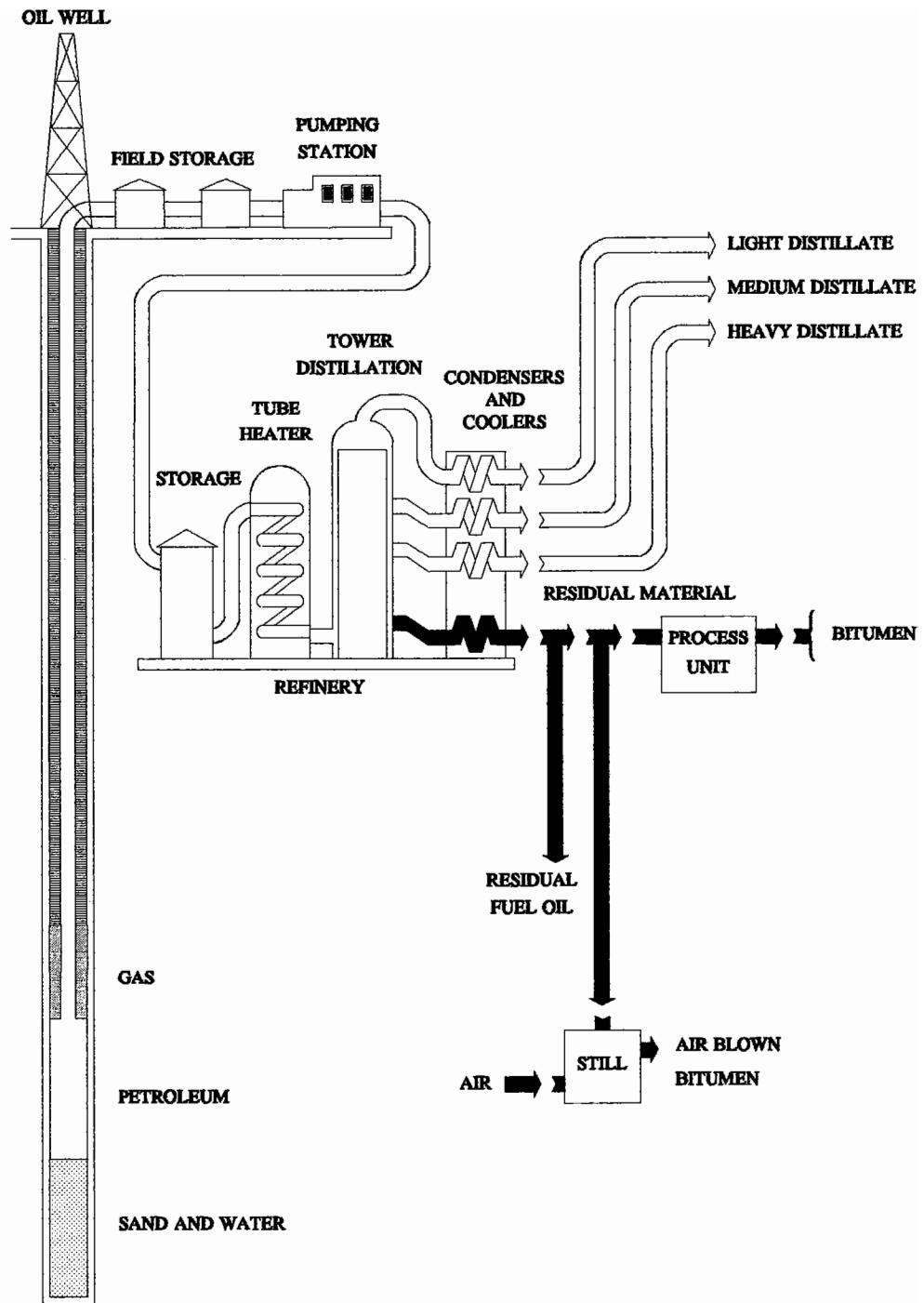
Figure 2.1 : Production of Bitumen

oil. Figure 2.1 shows the flow of oil and the fractionalizing into principal components of which it should be noted bitumen is last to be obtained. It is often referred to as being obtained from the "bottom of the barrel" and is a dark (black) thick viscous liquid. Bitumen consists of a highly complex arrangement of mainly hydro-carbon molecular matter.

Several other types of "natural" hydrocarbons are used in limited quantities for asphaltic mixtures, such as Trinidad Lake Asphalt (Attwooll et al., 1962) and Gilsonite (American Gilsonite Company). Tar, a byproduct of the manufacture of coke from coal has been extensively used in the past but is rarely used today.

In addition, the use of chemically modified binders (such as Styrene-Butadiene-Styrene (SBS), Ethylene Vinyl Acetate (EVA) and many others) have been gaining popularity due to their improved performance (Brown et al., 1990). These binders have enhanced physical behaviour and better performance in road pavements.

2.1.2 Tests for asphalt binders

Asphaltic binders are generally classified/graded by their physical properties using a series of empirical or performance related tests. Historically, empirical tests such as Softening Point, Penetration and Fraass have been used to define the behaviour at high, intermediate and low temperatures. These have been used along with viscosity tests to define the relationship between binder

consistency and temperature.

Consistency and viscosity tests have been used in specifications for asphaltic materials throughout the World. However, it is important to recognize that many of the tests that exist can be approximated to tests carried out using different apparatus, test configurations and temperatures. The *Bitumen Test Data Chart* (BTDC) (Heukelom, 1969) provides an extremely useful means for doing this. The scales on this chart are selected so that a "straight run" unmodified binder will be represented by a straight line if, Fraass, Penetration at various temperatures, Softening Point (Ring and Ball) and viscosity at various temperatures are plotted. The slope of the line is a measure of the temperature susceptibility of the binder. Figure 2.2, shows the BTDC. A numerical value is often calculated to express the slope in the range covered by the penetration test referred to as the Penetration Index (or PI) (Pfeiffer and Van Doormaal, 1936) and is calculated as follows:

$$PI = \frac{20 \ (1 - 25A)}{1 + 50A} \tag{2.1}$$

where:

$$A = \frac{\log pen \ at \ T_1 - \log pen \ at \ T_2}{T_1 - T_2} \tag{2.2}$$

where: T_1 and T_2 are temperatures at which the penetration is measured.

Pfeiffer and Van Doormaal (1936) found that the Softening Point temperature was approximately equal to a penetration of approximated 800. Consequently,

-2.4-

Figure 2.2 : The Bitumen Test Data Chart

the Softening Point is often substituted into Equation 2.2, as follows:

$$A = \frac{\log pen \ at \ T_1 \ - \ \log 800}{T_1 \ - \ ASTM \ Softening \ Point} \qquad (2.3)$$

2.1.3 Rheological tests for asphalt binders

The rheological description of a material describes, fundamentally, the relationship between stress and strain. The nomenclature commonly used is given in Table 2.1.

When an asphaltic material is tested under sinusoidal loading, the resulting strain response is out of phase with the applied stress, Figure 2.3. This phase lag, δ, occurs due to a viscous component of the material behaviour and is related to viscous energy dissipation in the binder film. A material which behaves entirely in an elastic manner ($\delta=0°$) dissipates no energy. However, a purely viscous material dissipates all energy input ($\delta=90°$). The phase lag, δ, is used to define the storage and loss moduli by multiplying the complex stiffness modulus[1] by the cosine and sine of the angle respectively. The uniaxial complex stiffness modulus is as follows:

$$E^* = \frac{\hat{\sigma}}{\hat{\varepsilon}} \qquad (2.4)$$

where $\hat{\sigma}$ = Amplitude of axial stress

---

[1] The term complex modulus (E^* or G^*) is used to describe the relationship; maximum stress divided by maximum strain when a visco-elastic material is tested with sinusoidal loading.

	Stiffness Modulus	Compliance
Uniaxial	E	D
Shear	G	J
Bulk	K	M

Note: Stiffness modulus is defined as a stress divided by a strain whereas the compliances are defined by a strain divided by a stress.

Table 2.1 :   Definition of Moduli and Compliances
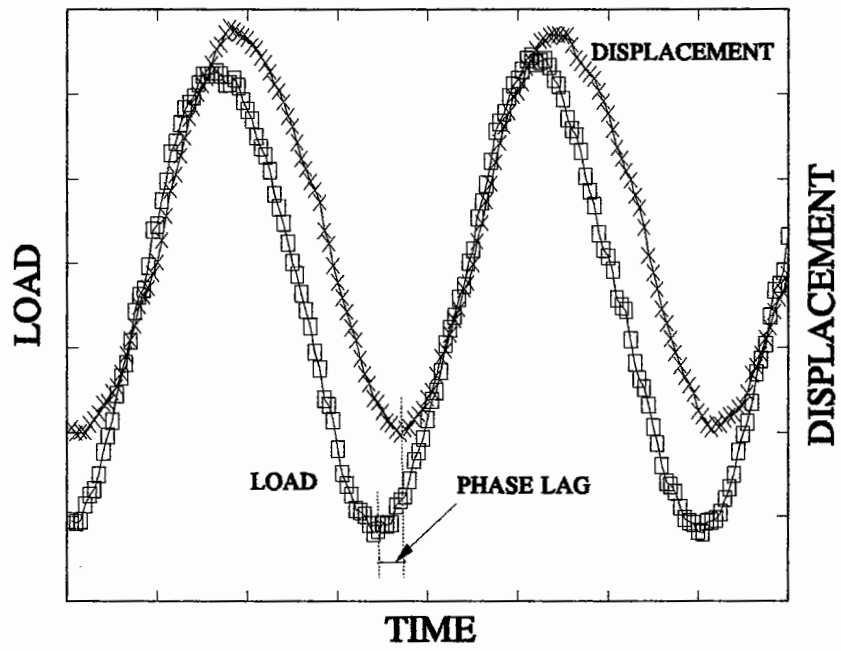
Figure 2.3 : Stress-Strain Response Measured in a Bituminous Material

$$\varepsilon \quad = \text{ Amplitude of axial strain}$$

The phase lag is used to calculate the storage (E') and loss (E'') complex stiffness modulus, as follows:-

$$E' = E^* \cos\delta \tag{2.5}$$

and

$$E'' = E^* \sin\delta \tag{2.6}$$

Another parameter often used to describe the energy dissipation is tan δ, which is the ratio of E'' over E'. Tests conducted on asphalt binders are normally done in a shear mode and, consequently, either the complex, storage and loss shear stiffness moduli (G^*, G' and G'') or the compliances (J^*, J' and J'') are measured.

The applicability and method of the measurement depend to a large extent on the properties of the material being tested and its end use. Two methods involving the *Dynamic Shear Rheometer* (DSR) (AASHTO TP5) and the *Bending Beam Rheometer* (BBR)[1] are now being routinely used with asphalt binders (AASHTO TP1). The DSR uses a 1 mm or 2 mm film of binder sandwiched between two parallel plates (8 mm or 25 mm in diameters). The unit assembly is housed in a temperature controlled environment and a torque is applied to the system to generate a displacement. The resulting stress and strain amplitudes are recorded and the complex shear modulus calculated using Equation 2.7.

---

[1] Developed as part of the by SHRP A-002 contract.

$$G^* = \frac{\hat{\tau}}{\hat{\gamma}} \qquad\qquad (2.7)$$

where $\hat{\tau}$ = Amplitude of Shear Stress

$\hat{\gamma}$ = Amplitude of Shear Strain

The phase lag, δ, is also measured (as illustrated in Figure 2.3) and this enables the storage and loss shear moduli to be obtained.

where

$$G' = G^* \cos\delta \qquad\qquad (2.8)$$

and

$$G'' = G^* \sin\delta \qquad\qquad (2.9)$$

The BBR was specifically developed to overcome testing problems[1] that can occur with DSR's when testing stiff binders at cold temperatures. The testing mode of this equipment is illustrated schematically in Figure 2.4. A slender beam of asphalt binder (125 × 6.25 mm) which is simply supported is loaded with a constant force at mid span. The deflection is monitored with time and this is used for calculation of bending stiffness (using bending theory for a simply supported beam) as a function of time using Equation 2.10.

---

[1] The ability of some DSR's to apply sufficient load to generate a given strain is often difficult and the cost of equipment can be prohibitive for routine testing.

LOAD

DEFLECTION
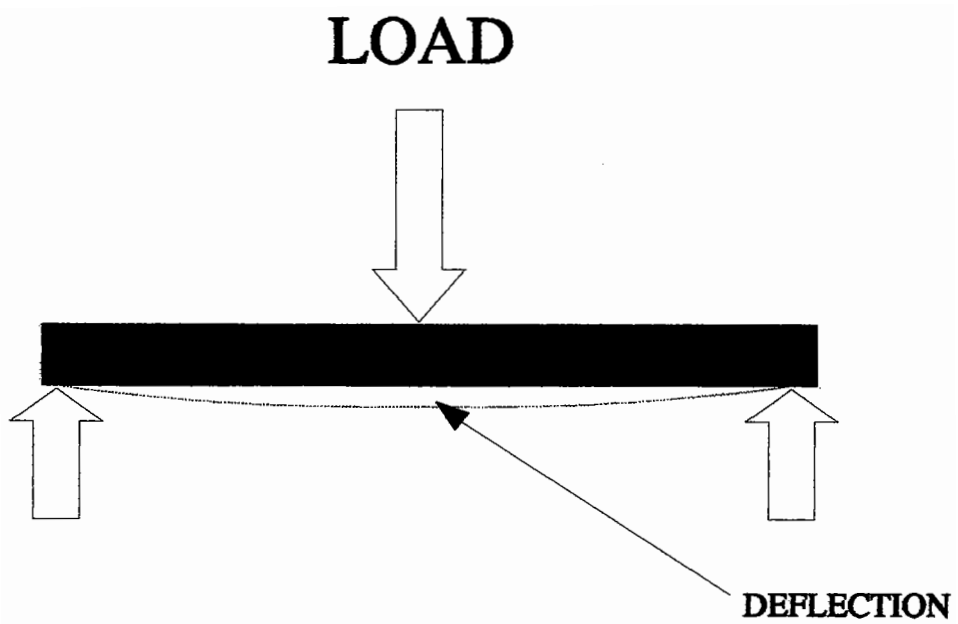
Figure 2.4 : The Bending Beam Rheometer

$$S(t) = \frac{PL^3}{4bh^3 \, \Delta(t)} \tag{2.10}$$

where:

$S(t)$ = Creep stiffness modulus at time, t

(t = 60 seconds is used as standard)

P = Applied constant load, normally 100 g

L = Distance between beam supports, 102 mm

b = Beam width, 12.5 mm

h = beam thickness, 6.25 mm

$\Delta(t)$ = Deflection at time, t

(t = 60 seconds used as standard)

The stiffness modulus $S(t)$ can be considered to be essentially equal to the uniaxial modulus $E(t)$ and can be converted to a shear modulus (assuming a Poisson's ratio of 0.5) by Equation 2.11.

$$G(t) = \frac{E(t)}{3} \tag{2.11}$$

2.1.4 Relationships between stiffness, temperature and loading time

The stiffness modulus of an asphaltic binder is dependent upon both time and temperature. At very cold temperatures it becomes "glassy" and is very stiff with an uniaxial stiffness modulus of approximately 3 GPa (Van der Poel, 1954). This "limiting" stiffness is similar for most binders. As the

temperature is increased, the stiffness decreases until the asphaltic binder exhibits entirely viscous behaviour and then the stiffness is inversely proportional to the loading time. Figure 2.5 illustrates this behaviour. It should be noted, that interchange of loading time and temperature produce the same effect. Short (fast) loading times will result in high stiffnesses whereas long (slow) loading times produces low stiffness results as illustrated in Figure 2.6.

The results from testing binder are normally plotted as log complex stiffness versus the test frequency. Typical data for a 60/70 penetration grade binder is presented in Figure 2.7. This data was obtained over a range of frequencies (7.8 to 250 Hertz) and temperatures (-10 to 60°C). The data consists of a series of curves for the tests conducted at each temperature.

The data can be shifted horizontally to form a master curve at a common reference temperature. The steps required in order to perform this are as follows:-

1.   **Decide Reference Temperature** - A temperature of 20°C is commonly used. This is the temperature to which the stiffnesses obtained at other temperatures are shifted along the frequency axis. This is done by determining at what frequency they would have had to be tested to give the same result as at the reference temperature.

2.   **Determine Shift Factors, *a(T)*** - This can be done by trial and error or
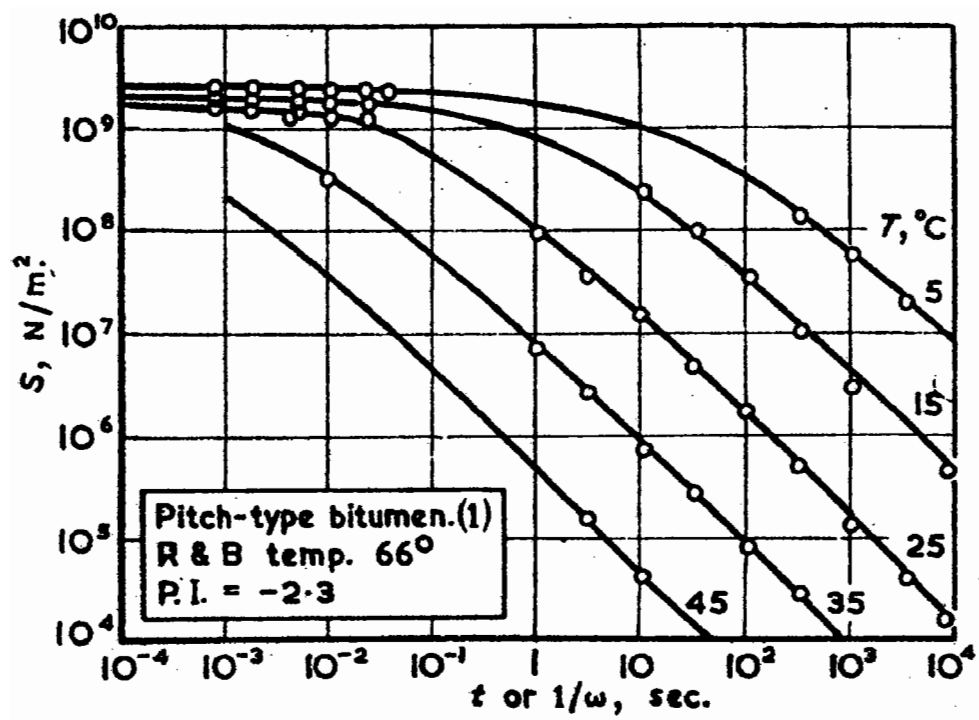
Figure 2.5 : Effect of Loading Time on Bitumen Stiffness at various Temperatures (after Van der Poel, 1954)
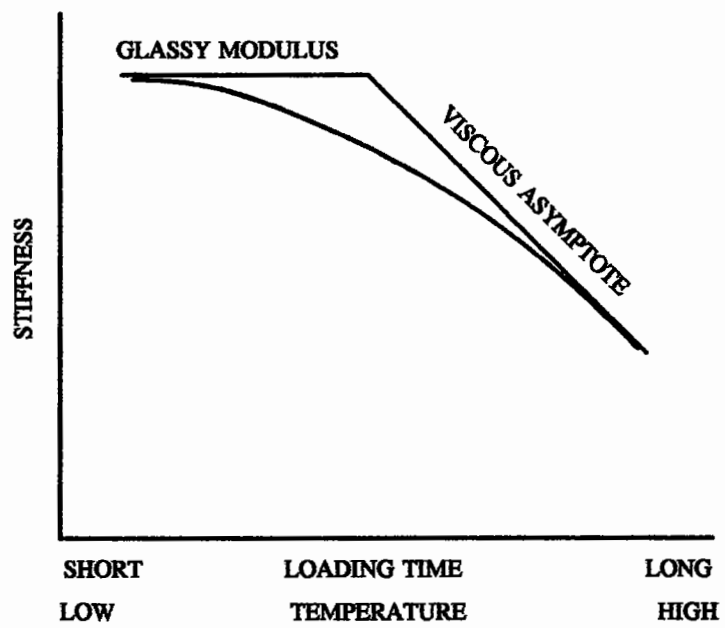
Figure 2.6 : Stiffness versus Loading Time and Temperature
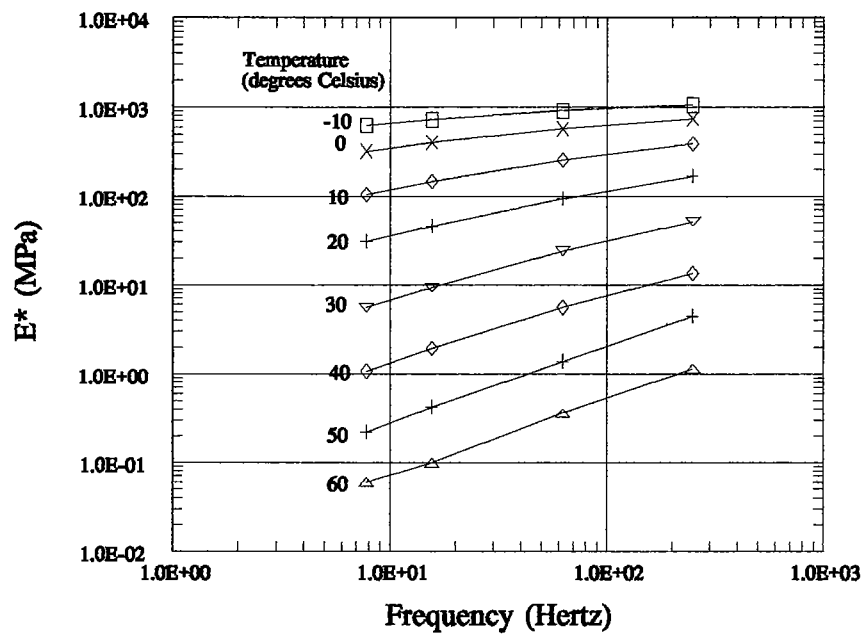
Figure 2.7 : Stiffness versus Frequency for a typical 60/70 Penetration Grade Binder at different temperatures

by sophisticated computer software. The shift factors are then generally plotted using either an Arhennius or Williams-Landel-Ferry (WLF)[1] (Ferry, 1980) relationship on a graph as illustrated in Figure 2.8. A relationship between the shift factor and temperature is then determined. The Arhennius or WLF relationships are defined by the equations as follows:-

Arhennius:-

$$\log a\ (T)\ =\ K\ [\frac{1}{T}-\frac{1}{T_{ref}}] \tag{2.12}$$

WLF:-

$$\log a(T)\ =\ \frac{-C_1\ (T-T_{ref})}{(C_2+T-T_{ref})} \tag{2.13}$$

where: $a(T)$ =   The shift factor relative to the reference temperature.

K, C_1, C_2 =   Constants.

Regression analysis can be used to determine the constants in the equations.

---

[1]Generally the Arhennius shift is used for colder temperatures whereas the WLF shift is used at higher temperatures. Often the glass transition temperature is used as the defining temperature for the choice of the shifting procedure. However, in asphaltic binders and materials the glass transition temperature is poorly defined and different researchers use different defining temperatures (Christensen et al., 1992).
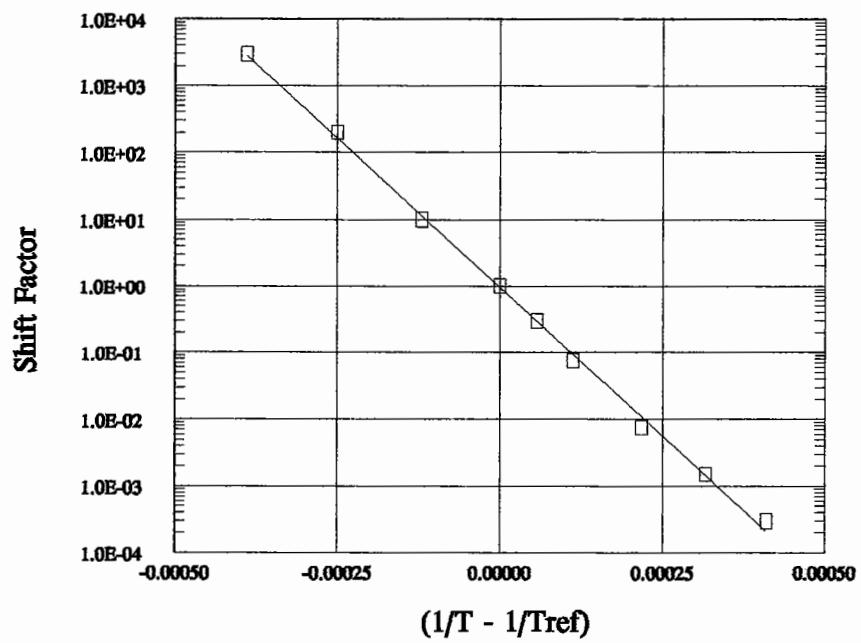
Figure 2.8 : Arhennius Shift Factor for 60/70 Penetration Grade Binder

However, if a suitable reference temperature is used various researches (Dobson, 1969; and Christensen et al., 1992) have proposed that single values can be assigned to the constants in the above Equations 2.12 and 2.13.

3.   Once the shift factor $a(T)$ has been obtained, the frequencies for the measurements at temperatures other than the reference temperature are shifted, as indicated in Figure 2.9, to produce a single curve. A similar shift can also be made to the other properties e.g. phase angle, loss and storage stiffness modulus.

This form of presenting data, as master curves, is very useful because it allows the prediction of the moduli at any loading frequency or temperature and the comparison of data on an equal basis.

Using the principal of time and temperature superposition for simple thermo-rheological materials with linear visco-elastic behaviour, the results from both the BBR and DSR can used to produce "master curves" (either for $G(t)$ or G^*). These relationships can be established for the majority of bituminous binders. It should be noted that if large strains are used in the testing, then non-linear visco-elastic behaviour may be encountered, and, consequently, time and temperature superposition will cease to be a reliable method (Collins, 1991).

2.1.5   Relationships between rheology and consistency

Before routine methods became available for measuring the rheology of
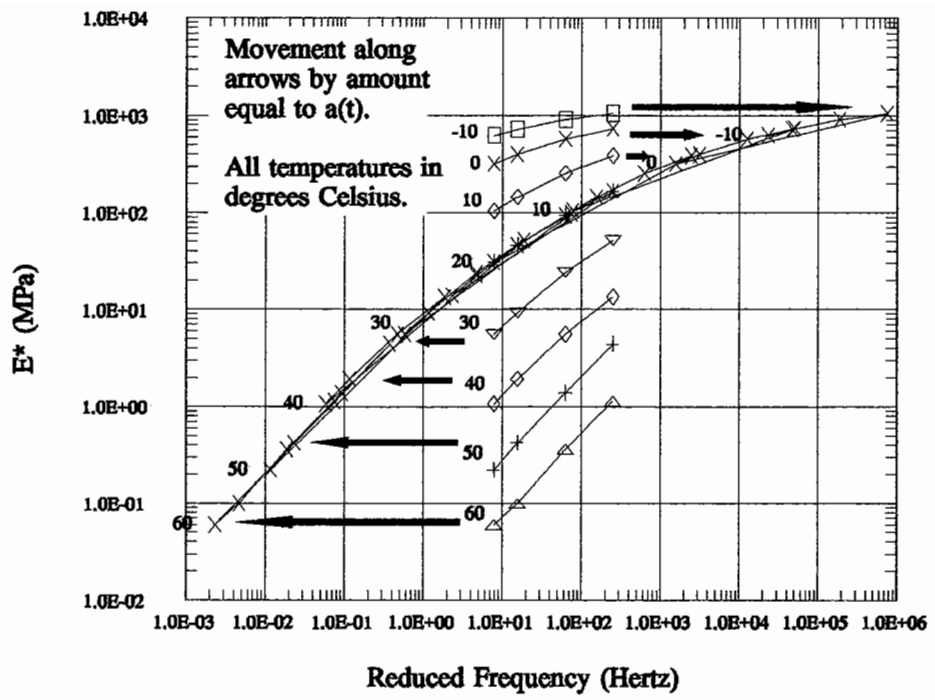
Figure 2.9 : Master Curve for a 60/70 Penetration Grade Binder

asphaltic binders, procedures were developed to estimate stiffness as a function of simple consistency tests. The most widely used and accepted method is that developed by Van der Poel (1954). His method involved use of the Softening Point (as an estimation of the temperature when the Penetration would be 800 mm^{-1}), the Penetration (25°C, 100 grammes) and loading time or frequency to obtain the binder stiffness (see Figure 2.10). However, the use of this prediction method does have a large associated error (up to 100%) and, consequently, the results need always to be used with caution in the context of a well researched and calibrated design method.

2.2   ASPHALTIC MIXTURES

2.2.1   Asphaltic Concrete

There is a wide range of asphaltic mixtures available. However, probably the most widely used mix in the world is a material called **Asphaltic Concrete** which is made up from a well graded aggregate together with 4-6% bitumen by mass. The mixture is applied hot and compacted by rolling with the temperature being dependent upon the viscosity of the bitumen. The composition is designed to give a air low void content after compaction. The term Asphaltic Concrete has now been adopted throughout Europe with the British name Dense Bitumen Macadam being dropped. The work presented later in this thesis was carried out with this type of material.

An asphaltic mixture must have certain key structural properties which are
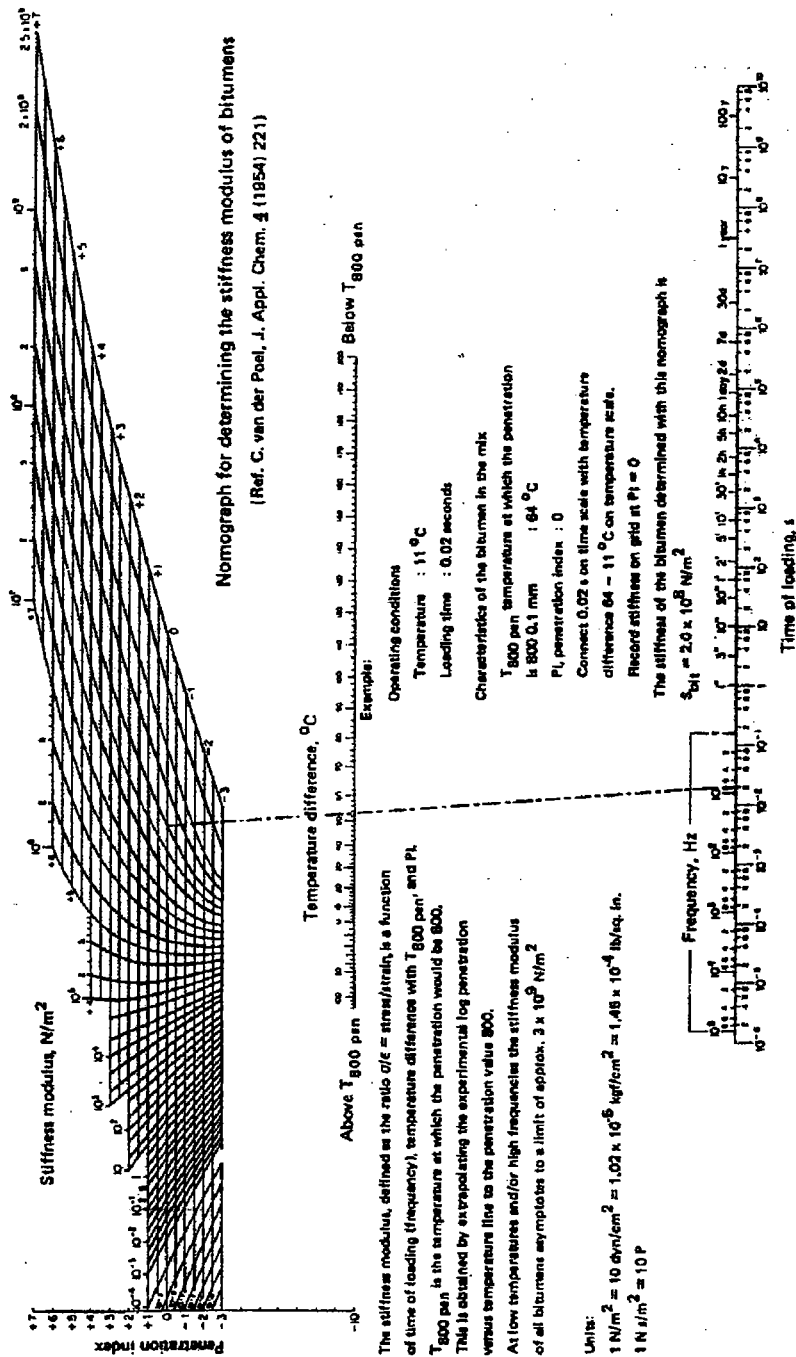
Figure 2.10 : Van der Poel's Nomograph

used to control the level of strains in the pavement. The important strains (Brown et al., 1985) related to the life of an asphaltic pavement are illustrated in Figure 2.11. The material properties which effect the pavement life with traffic loading are as follows:-

Stiffness - this parameter influences the level of stresses and, hence, strains within the pavement structure which, in turn, effects the tensile strain (controlling fatigue life) and the vertical compressive strain in the formation which has been used as an index of pavement rutting.

Fatigue Strength - this parameter indicates the material's ability to withstand the repeated application of loads without cracking at a certain level of tensile strain.

Permanent Deformation - this characterizes the material's ability to withstand rutting in the wheel tracks in the asphaltic layer.

The first two of the above criteria can be estimated from a knowledge of the composition (with a limited degree of accuracy for conventional materials) since both stiffness and fatigue are dominated by the performance of the binder. However, the third criterion depends on many variables (particularly aggregate properties) and always needs to be assessed by testing. Other material properties (such as skid resistance, roughness and durability) need to be considered when selecting asphaltic materials to ensure that quality pavements are constructed.
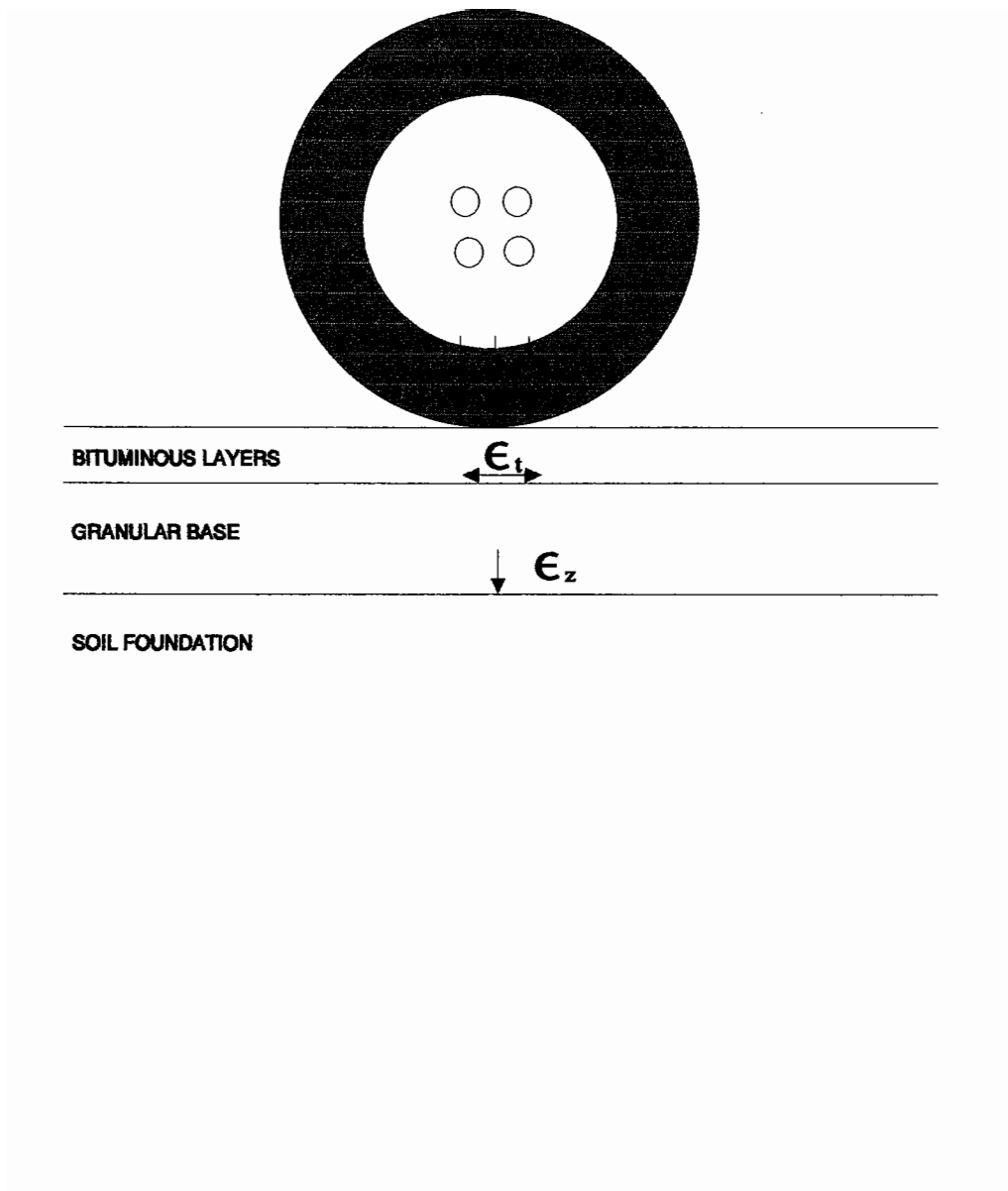
Figure 2.11 : Important Strains Related to the Life of an Asphaltic Pavement, Vertical Compressive Subgrade Strain and Tensile Strain at Underside of Bituminous Layers

2.2.2 Mixture stiffness

The range of stiffnesses for asphaltic materials is very large and is a function of both loading time and temperature. At low service temperatures and short loading times the stiffness is generally a function of the mixture volumetrics and the binder properties whereas at high service temperatures and long loading times the aggregate properties are very significant. The stiffness of the mixture can be treated as elastic at very low temperatures/short loading times, moving to linear visco-elastic behaviour as the temperature/loading times increase, and finally to a mixture of visco-elastic-plastic behaviour at high temperatures/long loading times (Francken et al., 1974; Van der Poel, 1954; and Perl et. al., 1981). If strain levels are kept low, the material generally exhibits linear elastic or linear visco-elastic behaviour at temperatures less than 25°C and at loading times associated with moving traffic. However, as the strain level is increased, non-linear behaviour results. At high temperatures it is difficult to test materials at lower strain levels and consequently most stiffness measurements incorporate non-linear behaviour.

The stiffness of asphaltic mixtures can be measured by a variety of techniques which can generally be considered as either; i) applying a bending stress and measuring a deflection or strain to compute the stiffness, or ii) applying a direct stress (axial or shear) to a specimen and measuring the resulting strain to compute the stiffness. Generally, bending methods are used at lower temperatures in order to increase strain resolution whereas the direct methods tend to be more popular for work conducted at higher temperatures.

For the higher loading rates and lower temperatures, stiffness properties may be considered in a similar manner to that outlined above for bituminous binders. Hence, if plotted as a function of loading frequency, tests conducted at different temperatures can be combined using an Arhennius fitting procedure to define a master curve of stiffness and phase lag. From the master curve values can then be obtained at any loading frequency or temperature for pavement design calculations.

An alternate way of presenting mixture stiffness results in this range is to express them as a function of binder stiffness in order that the results are expressed in a form which is independent of binder type.

The assumptions regarding linear visco-elastic behaviour are generally valid when the binder stiffness is greater than 5 MPa (Bonnaure et al., 1977). Below this value, the aggregate structure plays a significant role in the stiffness result and the dependence of the mixture stiffness on binder stiffness can no longer be considered valid. However, it is still useful to construct plots of binder stiffness versus mixture stiffness so that the effect of aggregate structure can be demonstrated. Figure 2.12 illustrates this where the stiffness modulus of mixtures with similar mixture volumetrics are plotted against the binder stiffness. It can be observed that at the higher stiffness values, the moduli coincide while they diverge as lower values are reached. The mixture with the flatter line at the lower values of binder stiffness will tend to be more resistant to permanent deformation.
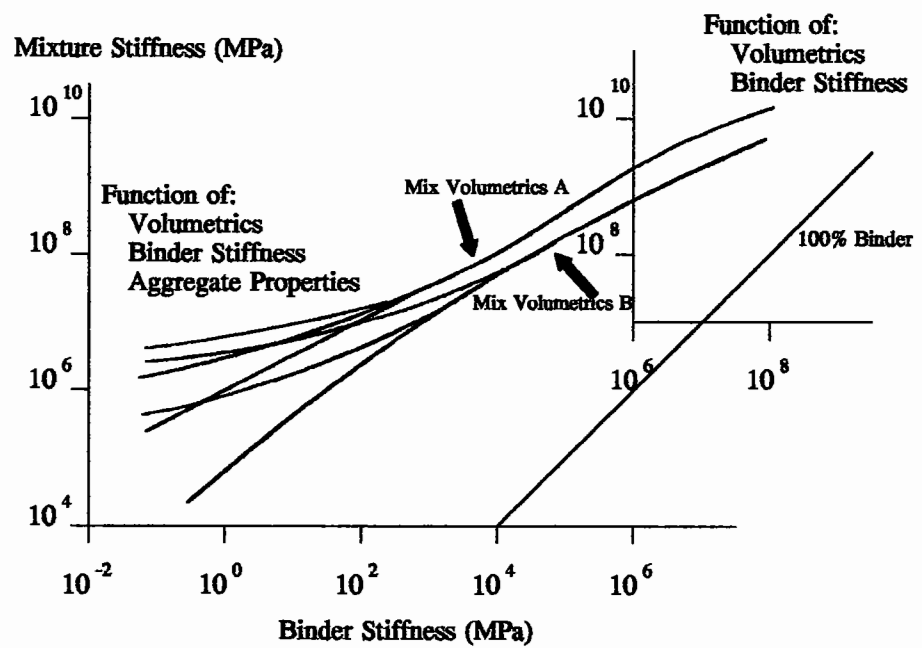
Figure 2.12 : The Effect of Aggregate Structure and Rate of Loading on the Stiffness of Bituminous Materials

For pavement design, stiffnesses are normally considered at both ends of the spectrum, ie. that associated with fast moving traffic at lower pavement temperatures for fatigue life calculations and with slow moving traffic at high pavement temperatures for the assessment of permanent deformation.

Pavement design for fatigue life relies on the computation of stresses and strains in the pavement structure and, since many methods use linear elastic layered analysis there is a requirement to determine a stiffness and Poisson's ratio to perform the calculations. Calculations of this kind are generally confined to the lower temperatures and faster speeds of loading where the material tends to behave more elastically (or in the linear visco-elastic range). Due to the past difficulty and cost in performing measurements of stiffness, several researchers have developed prediction methods (Brown, 1978; Kallas and Shook, 1969; Witczak, 1978; Miller et al., 1981; Bonnaure et al., 1977).

2.2.3 Permanent deformation behaviour

The measurement of stiffness for permanent deformation behaviour has been traditionally obtained from creep and repeated load, axial or triaxial tests on cylindrical specimens. Stiffness is considered to be a function of stress state and temperature and is often treated in a similar manner to that discussed above. However, the prediction of high temperature stiffness is not possible due the many controlling factors which include:-

Binder properties,

Mixture volumetric properties,

Aggregate properties such as shape, size and roughness.

The resistance of a mixture to permanent deformation is considered as arising from; (i) viscous resistance (associated with the binder properties), and (ii) frictional resistance associated with the internal frictional resistance of the mineral aggregate skeleton.

In order to avoid the difficulties in interpreting mixture properties at high pavement temperatures, several specifying authorities use wheel track tests to determine if materials are fit for a given role in the pavement structure with respect to permanent deformation.

2.2.4 Fatigue strength

Fatigue strength in asphaltic materials is defined as the ability of the material to resist cracking following repeated applications of load at a level generally below the ultimate tensile strength of the material. The measurement of fatigue strength, influencing factors and prediction of fatigue life are discussed in further detail in Chapter 3.

2.2.5 Other properties

Other properties which need to be considered in the selection of mixtures and which can significantly effect the properties discussed above are ageing

resistance and the damage caused by moisture, known together as durability.

2.3   SUMMARY

The visco-elastic properties of asphalt mixtures are influenced by the binder, aggregate and volumetrics. Since asphaltic mixtures are visco-elastic, energy will be dissipated when loading. To model the behaviour of the mixtures in pavement structures, visco-elastic material properties are required. These aspects are discussed in greater detail later in this thesis.

CHAPTER 3

Literature Review

3.0   INTRODUCTION

Fatigue strength can be defined as the ability of a material to withstand repeated applications of stress, generally at a level below the tensile strength of the material, without fracture.

The importance of testing asphalt mixtures for fatigue performance was first recognized in the 1950's (Hveem, 1955) due to increasing concern with pavement cracking. Since that time significant progress has been made with regard to the understanding of fatigue behaviour of asphaltic mixtures. Fatigue cracking can generally be considered as occurring in two stages; 1) the formation of cracks (crack initiation), and 2) the growth of cracks (crack propagation). This literature review covers the significant developments that have been made over the past forty years providing an introduction to the research presented in this thesis.

3.1   TEST CONFIGURATIONS

The fatigue performance of asphaltic mixtures is generally evaluated with repeated load tests on prepared specimens either using a constant applied load (controlled stress) or deflection (controlled strain). Figure 3.1 shows various
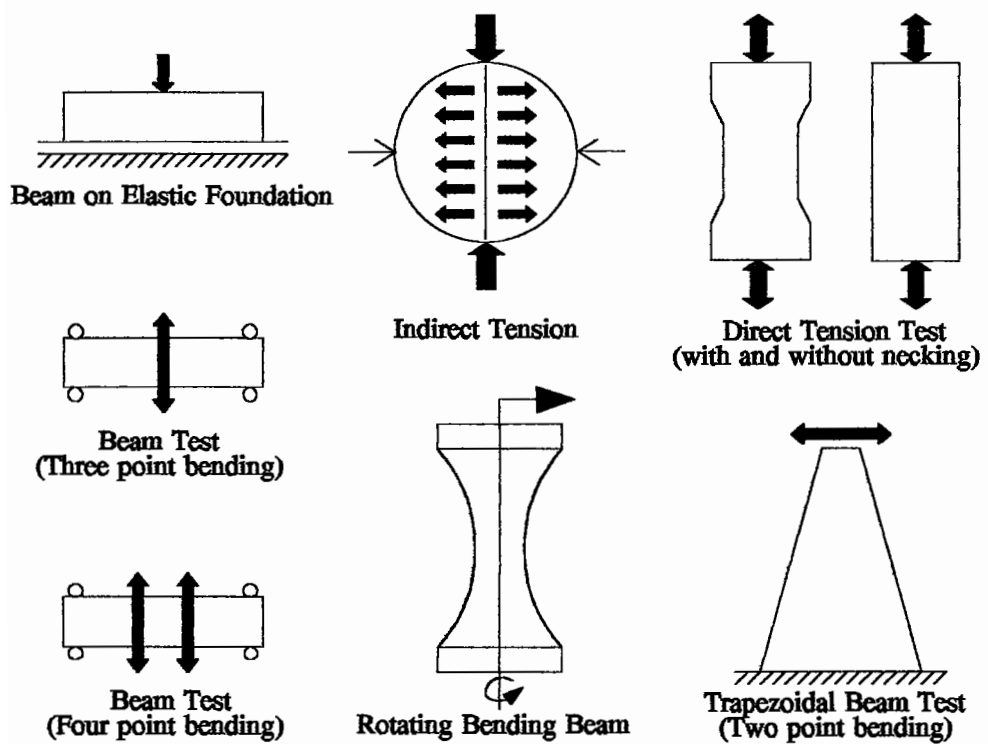
Figure 3.1 : Tests for Measuring Fatigue Performance

configurations of tests employed. These are described below:-

Three or Four Point Bending Tests are conducted on prismoidal specimens which are held horizontally and dynamically loaded. The four point bending test has the advantage of a zero shear force over the middle third of the specimen where the bending stress is uniform and at its highest value. The three point bending test has a maximum bending stress at the mid span of the beam, at a single point which is coincidental with the point of applied load.

The **Two Point Bending Test** uses a trapezoidal shaped cantilever beam specimen which is fixed at its base with the top of the beam being cyclically loaded. The bending stress varies continually along the length of the beam with the maximum bending stress located towards the centre of the beam, its position being dependent upon the chosen geometry. Unlike the three or four point bending tests, the maximum bending stress occurs away from the loading/fixing points.

The **Rotating Bending Beam Test** uses a cylindrical necked specimen to which a static cantilever load is applied. The specimens are held in the chuck of a motor which is then rotated rapidly. The rotation of the beam results in a sinusoidal load being applied to the specimen which varies between tension and compression. The maximum bending stress occurs away from the points of loading/fixing in a similar manner to that obtained with the two point bending test.

The **Beam on Elastic Foundation Test** provides a more simulative test than the other bending tests but calculation of bending stress/strain is more difficult. In addition stress reversal is not possible with this type of test.

Other tests are used to evaluate performance which apply a direct axial force to the specimen. Two typical configurations of the **Direct Tension Compression Test** are illustrated in Figure 3.1. One of the two illustrations shows a necked specimen in order to reduce the possibility of cracking near the fixing points. In a direct stress test, the stress is uniform across the cross sectional area which is different from the bending tests where the maximum stress only occurs at the extreme fibres.

A further test which has been used to evaluate fatigue performance is the **Indirect Tensile Test** for which the test configuration is also illustrated in Figure 3.1. This test, however, suffers from a very complex bi-axial stress/strain distribution in the specimen (Hadley et al., 1970; and Sousa et al., 1991) and, consequently, the results from this type of test have to be used with caution. In addition, the test configuration does not permit stress reversal.

3.2   STRAIN CRITERIA

The above tests are often used to obtain data which can be plotted as a graph of log life versus log stress or strain (see example in Figure 3.2) giving a straight line relationship. Pell (1962) showed that data from bending beam and axial tests could be plotted in this format. However, as with most fatigue

Figure 3.2 : Stress versus Life Relationship

testing, they also noted a relatively large amount of scatter existed with data of this form as shown in Figure 3.2. This data was obtained with a sand asphalt mixture in a rotating bending beam test (controlled stress). This results in a relatively large number of test specimens being necessary in order to define a fatigue relationship.

Figure 3.2 shows the results plotted as the logarithm of tensile stress plotted against the logarithm of number of load applications. However, the relationships obtained in this form are very dependent upon the test conditions. For example, if the tests are conducted at different temperatures different relationships are obtained for individual mixtures (see Figure 3.3). If tests are conducted at different frequencies a similar effect occurs with fatigue life increasing as the strain decreases, as shown in Figure 3.4. Pell et al. (1961) plotted the data as log strain versus log life for a series of test results obtained at different loading frequencies and test temperatures. He observed that the resulting fatigue relationships were so close that they could be described by a single relationships of log strain versus log life, as illustrated in Figure 3.5. Pell et al. (1961) concluded that different temperatures and speeds of loading can be accounted for by their effect on stiffness and the behaviour is controlled by the magnitude of strain. This type of relationship became known as the strain criterion (Equation 3.1) and is was found to be valid for the controlled stress mode of loading with mixtures which exhibit a relatively high stiffness.
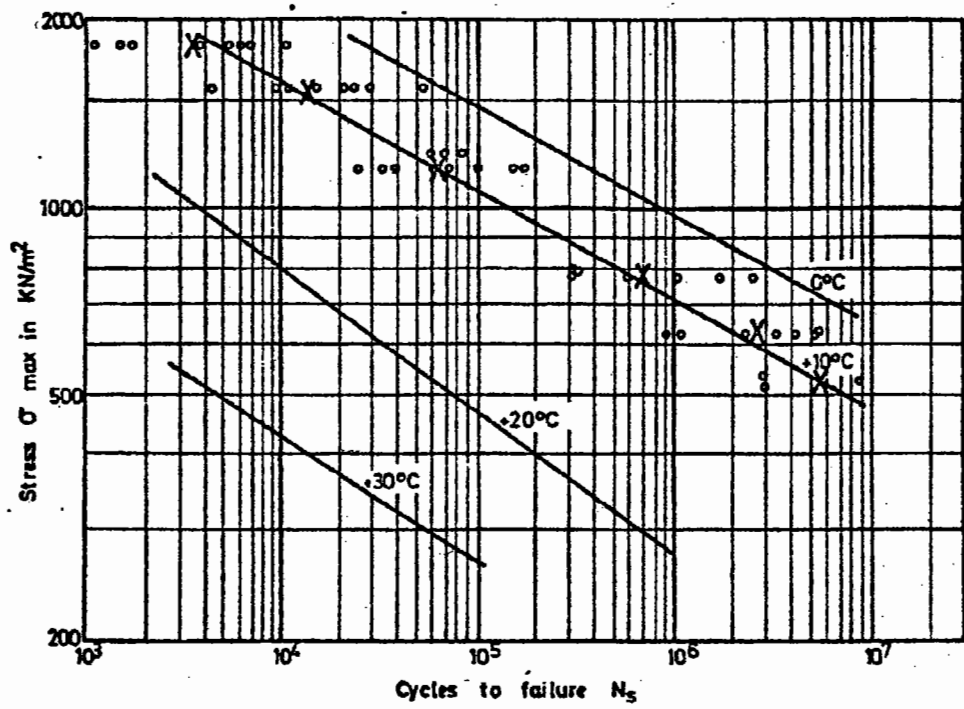
Figure 3.3 : The Effect of Temperature on Stress versus Life Relationships
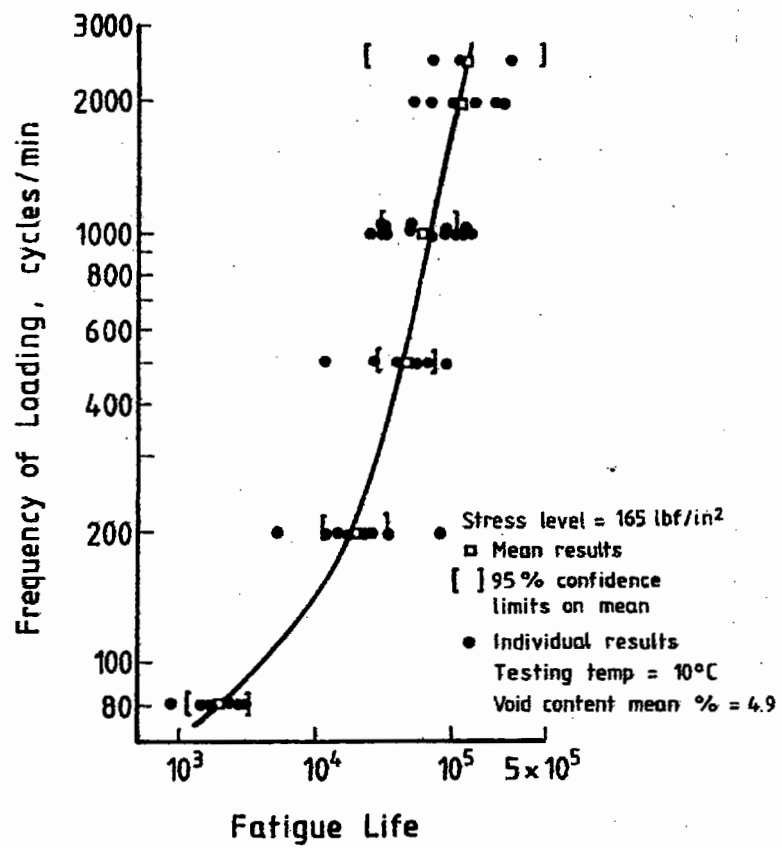
Figure 3.4 : The Effect of Frequency on Fatigue Life

TEMP °C	+ 25	+ 20	+ 7	− 0·5	− 0·5	− 0·5	− 9·5	−13·5
SPEED R.P.M.	3000	3000	2300	1000	2300	3000	3000	1000
KEY	●	◻	x	·◦·	○	✛	+	△
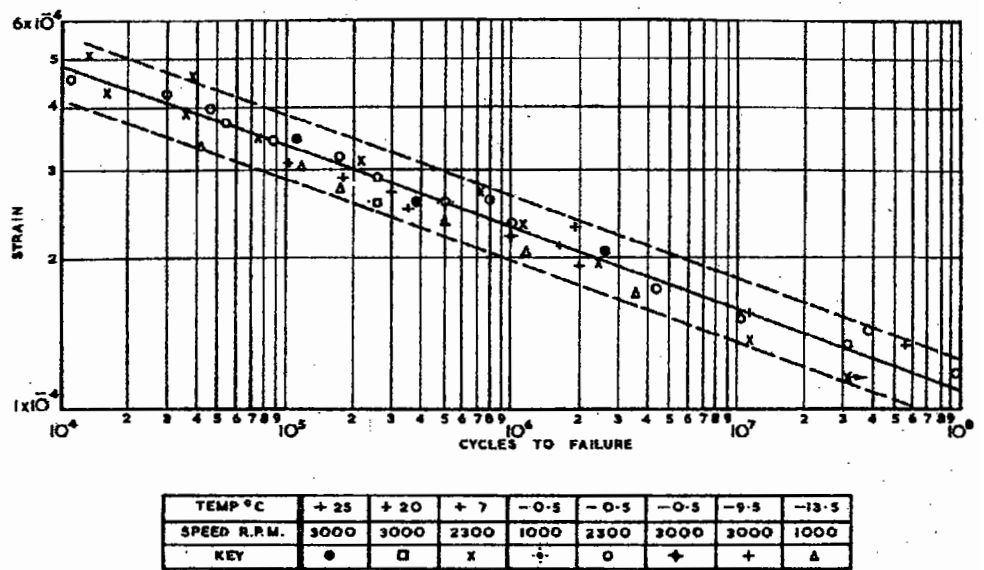
Figure 3.5 : The Strain Criteria

-3.9-

$$N_f = c \left(\frac{1}{\varepsilon_t} \right)^m \qquad\qquad (3.1)$$

where;

N_f = number of load repetitions for fatigue life

ε_t = tensile strain

c, m = constants

3.3 FAILURE CRITERIA

The failure criteria used with controlled stress and strain tests are different. Generally they are as follows:-

Controlled strain fatigue tests are normally considered to have reached a terminal condition when the stiffness has dropped to 50% of its initial value. This results in a test which can be completed in a reasonable time scale. In addition, the 50% value is used since this stiffness modulus is considered to be representative of a pavement in a condition when fatigue cracking is becoming evident (Raithby et al., 1972).

Controlled stress fatigue tests are normally considered to have reached terminal condition when either the specimen has fractured or when the stiffness reduces to less than 10% of its initial value.

The above definitions result in specimens being relatively intact when removed
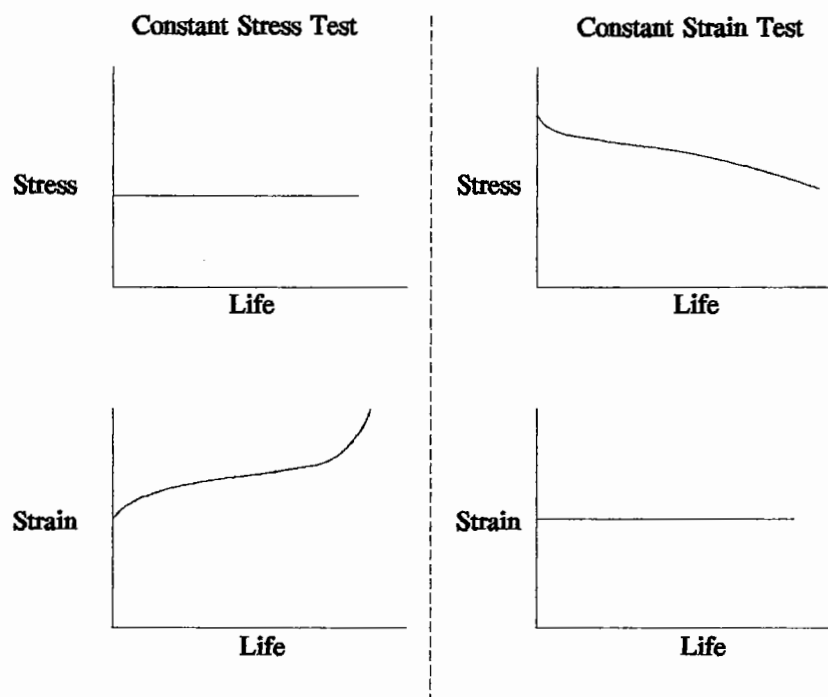
Figure 3.6 : Variation of Stress and Strain in Constant Stress and Strain Fatigue Tests

from a controlled strain test in contrast to being significantly fractured in a controlled stress test. In addition, the relative increase/decrease in stress during the two tests results in the life of a controlled strain fatigue test being greater than that obtained in a controlled stress test. This is illustrated in Figure 3.6.

A modification to Equation 3.1 was proposed by Finn et al. (1977) and Monismith et al. (1985) as given in Equation 3.2 for mixtures tested in either controlled stress or strain fatigue tests.

$$Nf = a \left(\frac{1}{\varepsilon_t}\right)^b \left(\frac{1}{S_{mix}}\right)^c \qquad (3.2)$$

where;

N_f = number of load repetitions for fatigue life

ε_t = tensile strain

S_{mix} = stiffness modulus

a, b, c = constants

This indicates that the mixture stiffness plays a key role in fatigue performance of pavements because as well as being directly related to the life it also controls the level of tensile strain.

3.4   MODE OF LOADING

Monismith and Deacon (1969) proposed the use of a mode factor, **MF**, to

fatigue tests have been used for thin asphalt layers whereas controlled stress

tests have been favoured for use with thick layers.

3.5   EFFECT OF MIXTURE VARIABLES

The performance of a mixture in fatigue is significantly effected by the

volumetric properties of the mixture and the type of binder. Other aspects,

such as type of aggregate, play a smaller role. The volumetric composition of

the mixture is considered in terms of the binder volume (V_b), aggregate/stone

volume (V_s), the air volume (V_a) or any combinations of these. The

combinations which have been of most interest have been the voids in mineral

aggregate $(VMA = V_b + V_a)$, the volume of binder (V_b) and the voids filled

with binder $(VFB = V_b / VMA)$.

For a laboratory test, fatigue life increases non-linearly with increasing volume

of binder (V_b), as follows:-

$$N_f = Functon \left(V_b{}^n \right) \qquad\qquad (3.4)$$

where;

n =   a constant normally between 4 and 6.

Figure 3.7 shows a typical relationship reported by Pell and Cooper (1975).
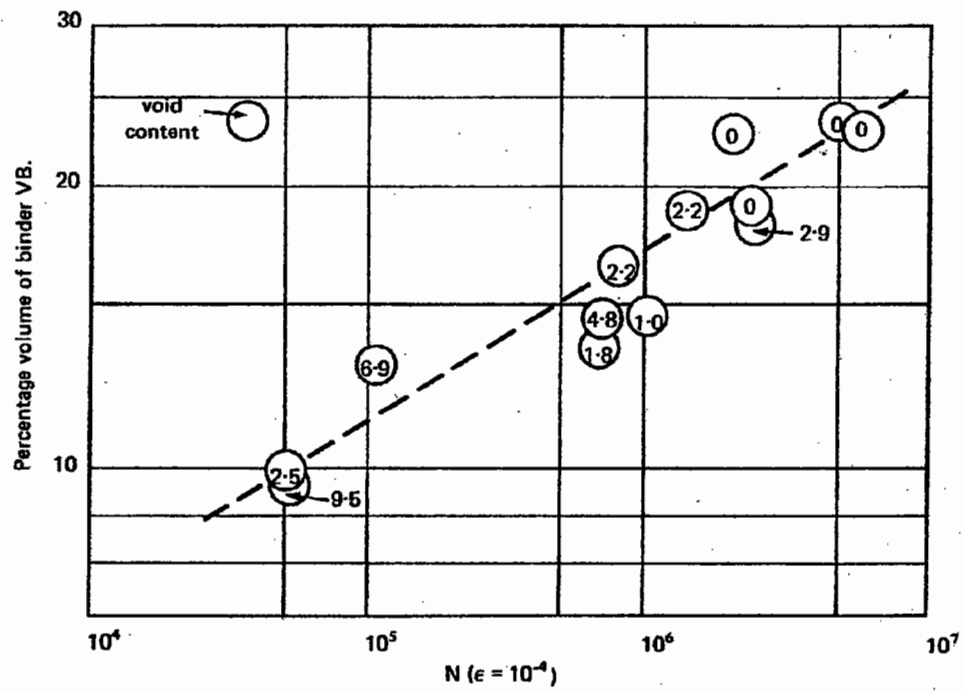
Figure 3.7 : Volume of Binder versus Fatigue Life at $\varepsilon = 10^{-4}$

The effect of aggregate type is important in that an aggregate which packs together more efficiently giving a lower *VMA* will give a better fatigue performance compared to an aggregate that does not readily compact. However, if the volumetric relationships are considered, the majority of the variability can be explained, suggesting that the mineral nature of the aggregate surfaces has only a small influence. This is consistent with the fatigue process taking place in the binder film. Cooper (1976) tested aggregates including slags, gravels, granites, limestones and basalts finding this to hold true. Other researchers (Bonnaure et al., 1980; and Francken et al. 1987) have also found that the type of aggregate and gradation play only a minor role compared to mixture volumetrics.

Binder properties have been shown to effect the performance of asphaltic materials very significantly. Various researchers have proposed different binder properties which correlate to fatigue performance. Pell and Copper (1975) demonstrated the effect of Softening Point on the performance of a mixture at a level of 100 $\mu\mathcal{E}$ (Figure 3.8) with a higher value giving better fatigue performance at that level of strain in controlled stress testing.

Francken et al. (1987) also showed that the type of binder is important in the assessment of fatigue life where a parameter "Λ" (which is related to the asphaltene content of the bitumen) is directly related to the permissable tensile strain (Figure 3.9). It should, however be noted that as the asphaltene content increases, the viscosity increases (Whiteoak, 1990) so in some ways this effect may be similar to that reported by Pell and Cooper (1975).
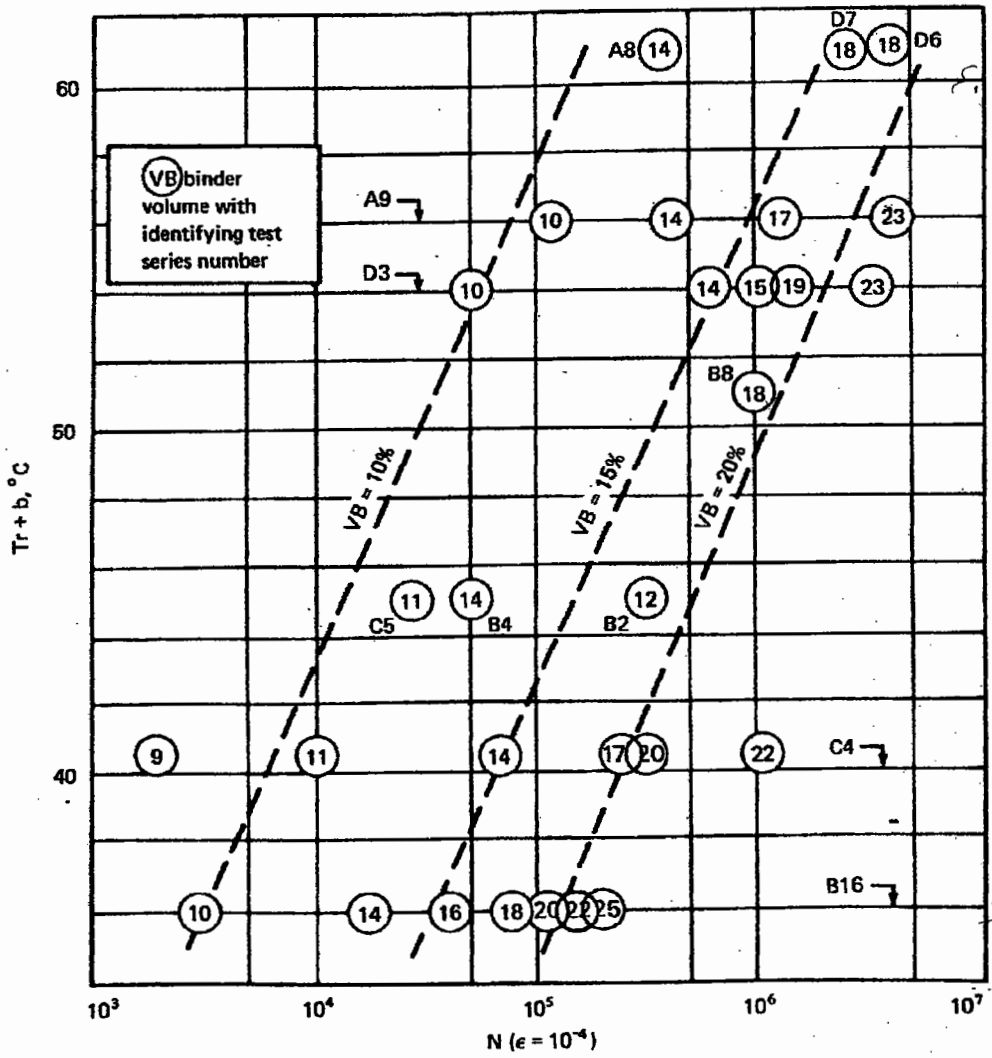
Figure 3.8 : Ring and Ball Softening Point Temperature versus Fatigue Life at ε = 10⁻⁴ for Various Gradings and Binder Contents
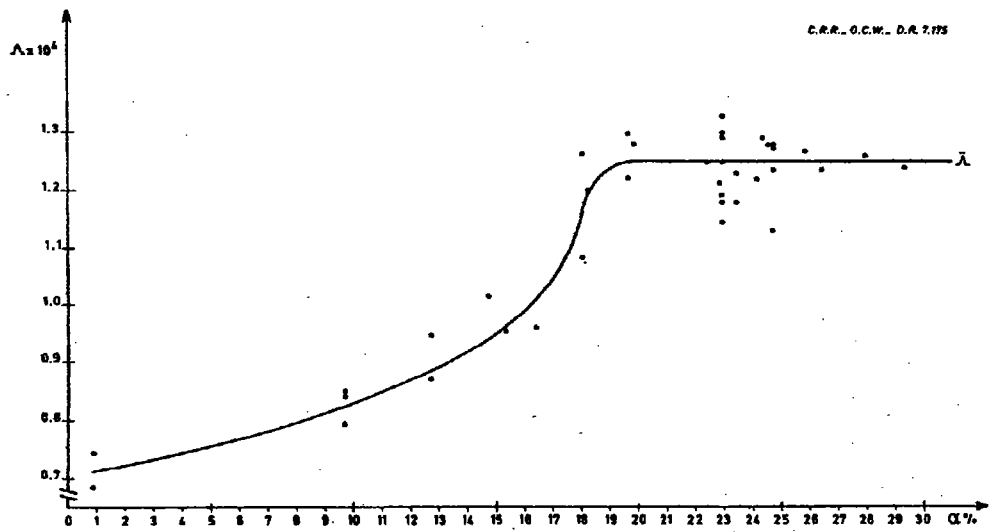
Figure 3.9 : Variation of Λ versus the Percentage of Asphaltenes ($\alpha\%$) in the Binder

The importance that mixture stiffness plays with regard to fatigue performance has been demonstrated by Bonnaure et al., (1980). Mixture stiffness can be related to the binder properties since it is significantly effected by the binder stiffness which in turn correlates with Softening Point and viscosity for conventional binders.

More recently, SHRP has specified the shear loss stiffness (G'' or $G^* \sin\delta$) of the binder as a fatigue parameter. This rheological measure is a more fundamental parameter but it can be correlated to many of the previous parameters used for conventional binders. For example, if the data presented by Christensen et al. (1992) is analyzed (Softening Point versus log G'') a correlation with a regression coefficient (r^2) of 0.875 results. In addition, the shear loss modulus is directly related to the ability of the binder to dissipate energy.

3.6   DISSIPATED ENERGY

Energy is dissipated in asphalt mixtures during loading and relaxation because the material behaves substantially in a visco-elastic manner at ambient temperatures. The dissipation of energy is demonstrated in Figure 3.10 were a linear elastic material is compared to a visco-elastic material. With an elastic material, the energy stored in the system (when loaded) is equal to the area under the load-deflection curve and, during unloading, all the energy is recovered. By contrast, a visco-elastic material, when unloaded, traces a different path to that when loaded. This phenomena is commonly known as
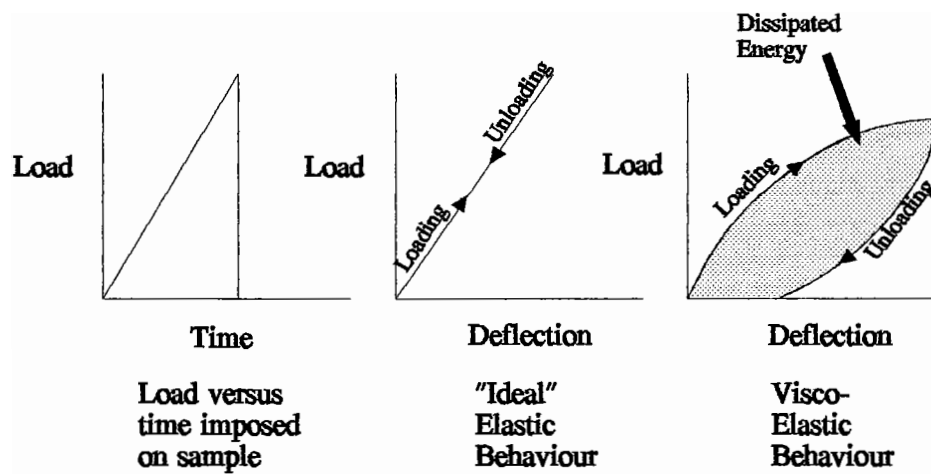
Figure 3.10 : Linear Elastic versus Visco-Elastic Behaviour

"Hysteresis" and the energy dissipated is equivalent to the area within the loop (Figure 3.10).

When a visco-elastic material, is sinusoidally loaded about a zero position, as in a bending beam fatigue test, a phase lag is observed between the load and measured deflection. If the load is plotted against the deflection, a hysteresis loop is obtained (see Figure 3.11). The area of the loop can be calculated and if the load/deflection relationship is expressed as stress/strain, the dissipated energy per loading cycle is obtained as follows:-

$$w_i = \pi \ \sigma_i \ \varepsilon_i \ \sin \ \phi_i \qquad (3.5)$$

where;

w_i =   dissipated energy in cycle i

σ_i =   stress amplitude in cycle i

ε_i =   strain amplitude in cycle i

ϕ_i =   phase lag in cycle i

If non-sinusoidal loading is applied, then the area within the loop can be calculated by numerical integration.

The dissipation of energy is largely associated with viscous flow of the binder which dissipates the energy as heat. The dissipation of energy, more importantly, also relates to the formation of micro-cracks/crack surfaces (Little, 1995).
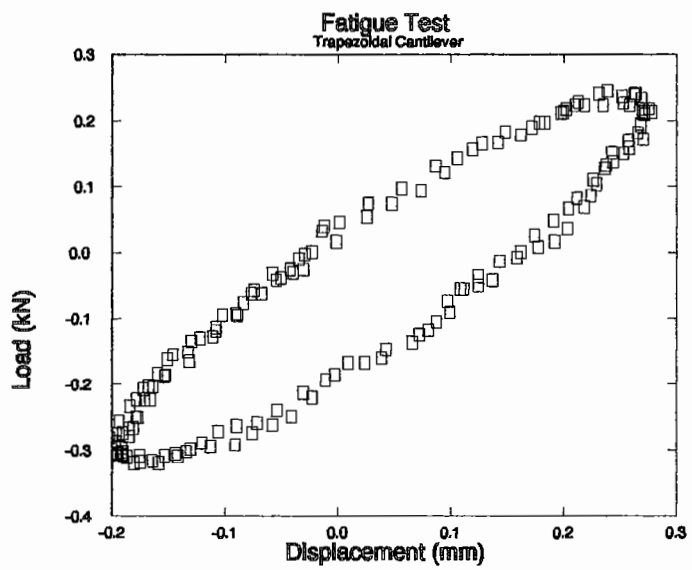
Figure 3.11 : Hysteresis Loop Obtained from Plotting Load versus Deflection

The amount of energy dissipated per loading cycle changes throughout a fatigue test. In a controlled stress test, the dissipated energy per loading cycle increases whereas in a controlled strain test it decreases, as illustrated in Figure 3.12. This is consistent with the reduction in the stiffness of the specimen and the change in dimensions of the hysteresis loop.

The earliest work using dissipated energy with asphaltic materials was reported by Chomton and Valayer (1972) and van Dijk et al. (1972). Chomton and Valayer (1972) presented a relationship in terms of "cumulative dissipated energy" versus number of loading cycles, as follows[1]:-

$$W = A\ N^z \qquad (3.6)$$

The cumulative dissipated energy is calculated by summing the dissipated energy throughout a fatigue test, as follows:-

$$W = \pi \sum_{i=0}^{i=N} \sigma_i\ \varepsilon_i\ \sin \phi_i \qquad (3.7)$$

Chomton and Valayer presented the results for three materials (two wearing courses and one base course) and suggested that the parameters A and z could be **"independent of the mix formulation"**.

---

[1]   Chomton and Valayer used the terms **absorbed energy, E,** and k in place of W and A, and they gave a value for z of 0.66. However, subsequently W (cumulative dissipated energy), A and z have become the norm in the literature for the expression of the relationship and to avoid confusion they are used throughout this thesis.
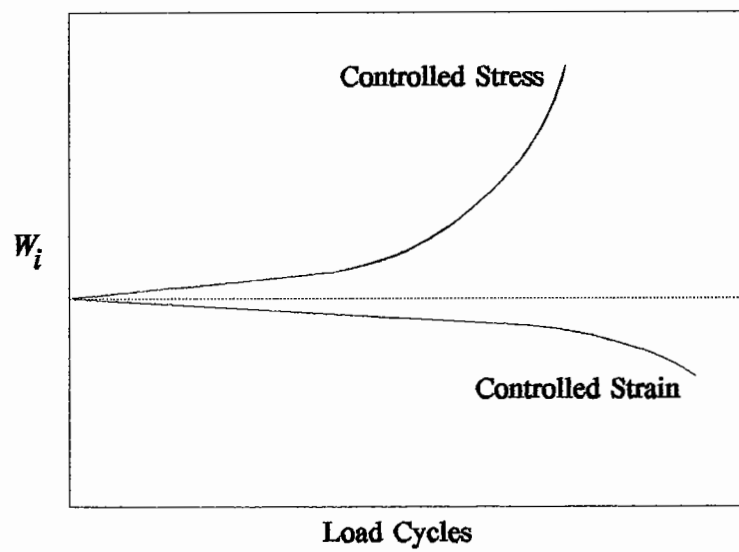
Figure 3.12 : Variation of Dissipated Energy per Load Cycle during Controlled Stress and Strain Fatigue Tests

Van Dijk et al. (1972) reported results in a similar form to Equation 3.6 with an exponent of 0.625 but no allowance was made for change of stiffness and phase angle in these calculations. In addition, they observed that the percentage retained bending strength of an asphaltic specimen was related to the total energy dissipated, as shown in Figure 3.13.

Van Dijk (1975) and van Dijk et al. (1977) reported further work which demonstrated several important aspects. It was clear that a single relationship could not be used for all materials (see Table 3.1 for mix details used), Figure 3.14. In addition, a ratio, Equation 3.8, was developed which takes values which are related to the mixture stiffness.

$$\psi = \frac{W_{initial}}{W} \qquad (3.8)$$

where;

$$W_{initial} = \pi \times N \times \sigma_0 \times \epsilon_0 \times \sin \phi_0 \qquad (3.9)$$

This ratio was found to be above unity for controlled strain tests and below unity for controlled stress tests (see Figure 3.15). This is a result of decreasing dissipated energy per cycle in a controlled strain test compared to increasing dissipated energy per cycle in a controlled stress test. It can be seen from Figure 3.15 that as the materials get stiffer, the ratio tends to approach unity. This is probably related to the increasing rate of crack growth that occurs with stiffer materials. Clearly, ψ is a function of the mode of testing and the mixture stiffness.
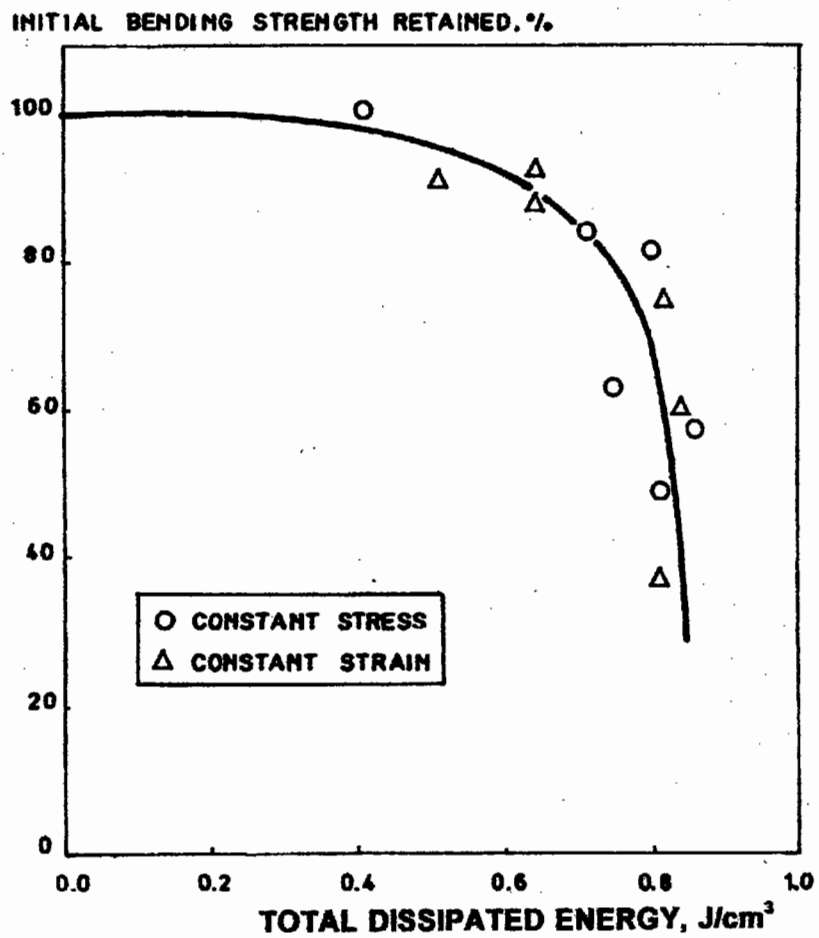
Figure 3.13 : Percentage Retained Bending Strength versus Total Dissipated Energy for Constant Stress and Strain Tests

Mix Number	1	2	3	4	5	6	7	8	9	10	11	12	13
Mix Type	Asphaltic Concrete (California)	Lean Sand Asphalt	Dense Bitumen Macadam	Gravel Sand Asphalt (Dutch)	Lean Bitumen Macadam	Dense Asphaltic Concrete	Dense Bitumen Macadam	Rolled Asphalt Base Course	Grave Bitume (French)	Asphalt Base Course (German)	Rich Sand Asphalt	Gravel Sand Asphalt (Dutch)	Bitumen Sand Base Course
Mix Volumetrics													
Aggregate Volume, (%)	84.1	81.1	85.6	78.0	61.9	86.7	85.4	83.7	81.4	88.1	72.9	79.1	70.8
Binder Volume, (%)	14.2	10.5	11.0	11.0	4.9	11.4	11.0	14.1	9.3	9.3	19.3	13.3	8.9
Air Void Volume, (%)	1.7	8.4	3.4	11.0	33.2	1.9	3.6	2.2	9.3	2.6	7.8	6.6	20.3
Binder Properties													
Softening Point, (oC)	61	52	52	64	51	59	60.5	62.5	60	52	53.5	60	67
Penetration, mm/10	38	61	59	26	68	36	40	34	27	58	60	40	20

Note: Additional information on mixture properties are given in the reference.

Table 3.1 : Mixture Properties (after van Dijk and Visser, 1977)
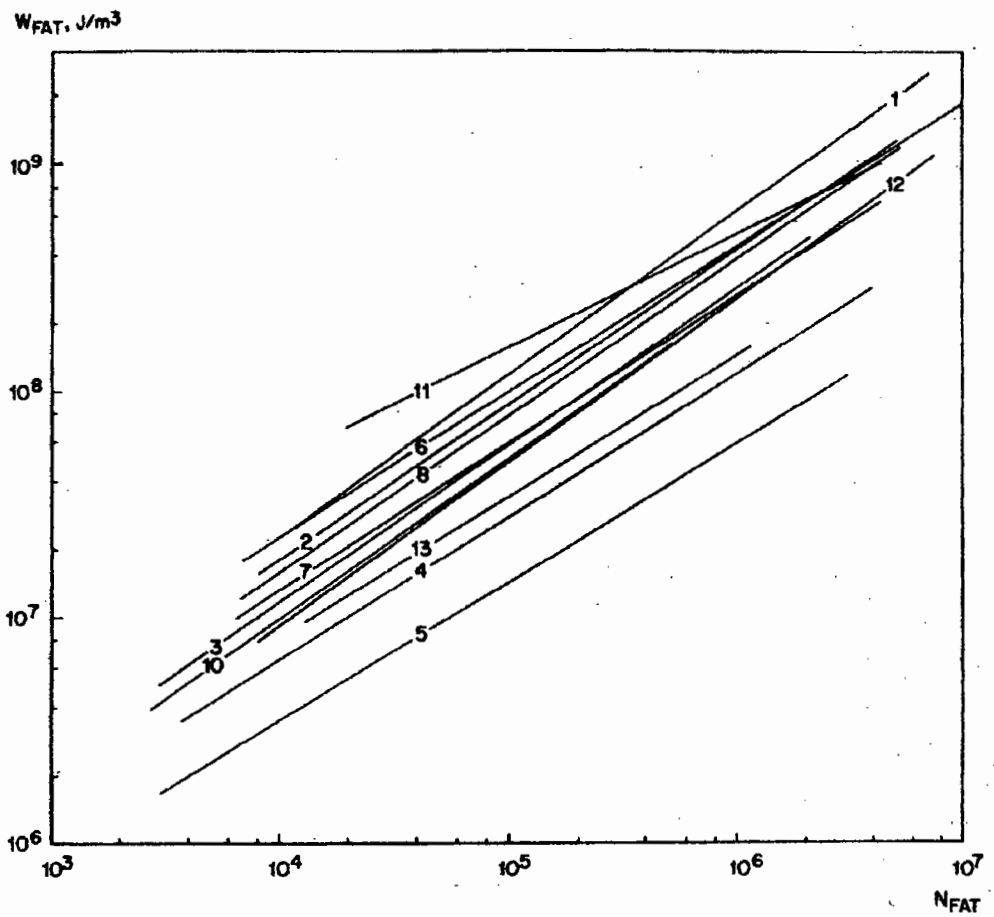
**Figure 3.14 : The Cumulative Dissipated Energy versus
Fatigue Life for a Series of Mixtures
(Vb = 4.9 to 19.3% and VMA = 11.9 to 38.1%, see Table 3.1)**
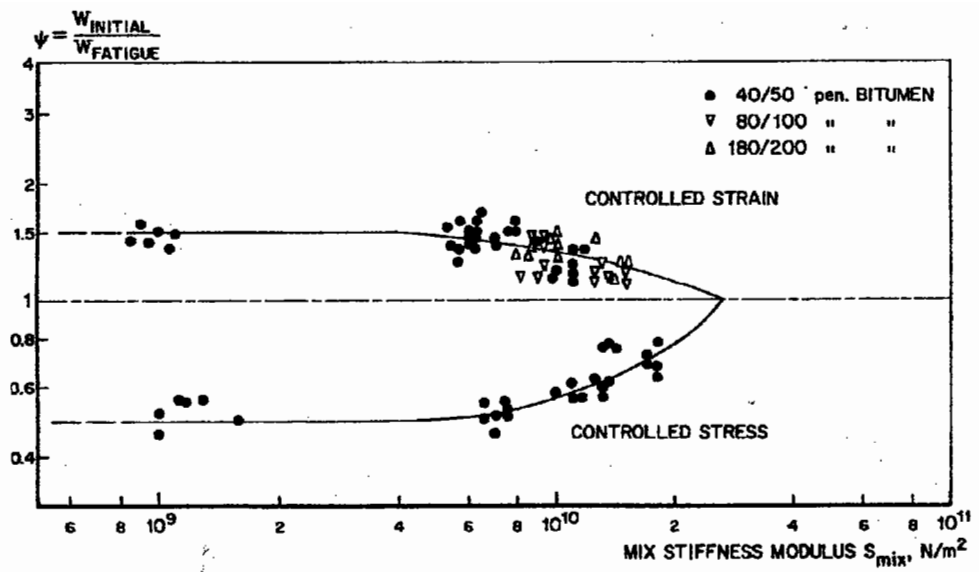
Figure 3.15 : Stiffness versus Ratio ψ

3.7   PREDICTION OF FATIGUE CRACKING

Fatigue life prediction can be considered in two distinct steps; i) the prediction of the fatigue life of a laboratory specimen, and ii) the prediction of pavement performance.

The prediction of fatigue life of laboratory specimens is less complicated than the prediction of life in a road pavement because a single loading scheme is often used with one temperature and generally with no rest periods[1]. Several methods for fatigue life prediction have been developed and these are discussed below.

The Dissipated Energy Method - a simplified method developed by Van Dijk et al. (1977). They gave constant values (the mean obtained from experiments) to the parameters ψ, Z and A of 1.22, 0.66 and 4.0×10^4 J/m^3 respectively. The ψ factor of 1.22 resulted in the prediction method being more appropriate for controlled strain tests. This gave a relationship between the permissable tensile strain, mixture stiffness, phase lag and the fatigue life as follows:-

$$N_{fat} = \left[\frac{1.55 \times 10^4}{\epsilon_t \, S_{mix} \, \sin \delta} \right]^{2.9412} \tag{3.10}$$

The Nottingham Method - developed by Cooper (1976), relies upon a linear

---

[1]   Rest periods occur when a time interval exist between the load applications.

relationship between the slope of the fatigue line and the log of the intercept, as follows:

$$m = a - b \log c \qquad \text{(3.11)}$$

This form of relationship results in a focus point for the fatigue lines which was obtained as $N = 4 \times 10^3$ and $\varepsilon_t = 6.3 \times 10^{-4}$. A relationship between the life at 100 $\mu\varepsilon$ using the Ring and Ball Softening Point and Volume of Binder (V_b) was developed as follows:

$$\log N \, (\epsilon = 10^{-4}) = 4.13 \log V_b + 6.95 \log SP_i - 11.13 \qquad \text{(3.12)}$$

By combination of the two above equations, a relationship can be deduced to predict the life in a controlled stress test. The method is also available in the form of a nomograph, Figure 3.16.

$$\log N_{fat} = 15.9125 \log \epsilon_t + 52.52 - (\, 5.1625 \log \epsilon_t + 16.52 \,) \log V_b - (\, 8.6875 \log \epsilon_t + 27.8 \,) \log SP_i \qquad \text{(3.13)}$$

The results used to develop this method were obtained from controlled stress rotating cantilever fatigue tests.

The Belgium Method - developed by Francken et al. (1987) uses a temperature susceptibility parameter Λ which is closely related to the asphaltene content of the material. They defined the fatigue life (based upon analysis of controlled stress test results) using the form of relationship in Equation 3.14.
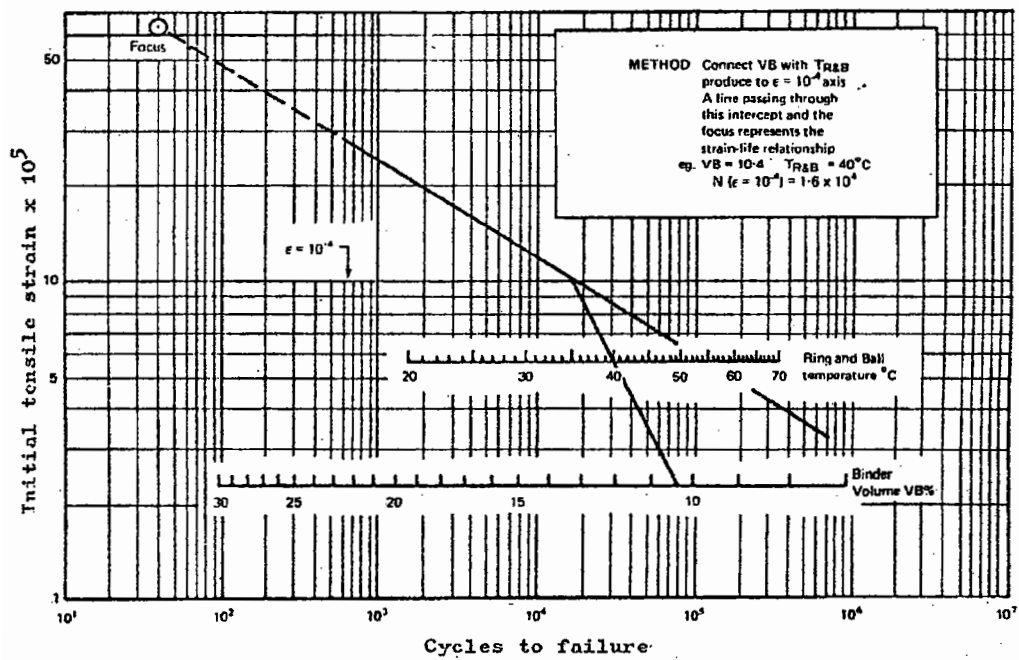
Figure 3.16 : Nomograph to Predict Fatigue Life from Tensile Strain, Ring and Ball Softening Point and Volume of Binder

$$\epsilon = K \cdot N_{fat}^{(-a)} \qquad or \qquad N_{fat} = \left[\frac{\epsilon}{K} \right]^{\left(\frac{1}{-a}\right)} \qquad (3.14)$$

where;

$$K = G \times \frac{V_b}{(V_b + V_a)} \times \exp\left(-5 \times \frac{V_s}{100} \right) \qquad (3.15)$$

where for $\Lambda \leq 0.43$

$$G = 75.3 \cdot 10^{-4} \qquad (3.16)$$

and for $\Lambda > 0.43$

$$G = 0.874 \, \Lambda^2 - 0.86 \, \Lambda + 0.216 \qquad (3.17)$$

The temperature susceptibility parameter Λ is related to the asphaltene content as discussed earlier (see Figure 3.9).

The Bonnaure Method - was developed from the statistical analysis of data from several research institutions (Bonnaure et al., 1980). Fatigue strength can be predicted from the volumetric composition of the mixture and the mixture stiffness for either controlled stress or controlled strain test conditions. A nomograph has also been developed which is shown in Figure 3.17, or alternatively, the fatigue life can be calculated from the following equations:-

For controlled strain conditions [with S_{mix} in Pa]:-
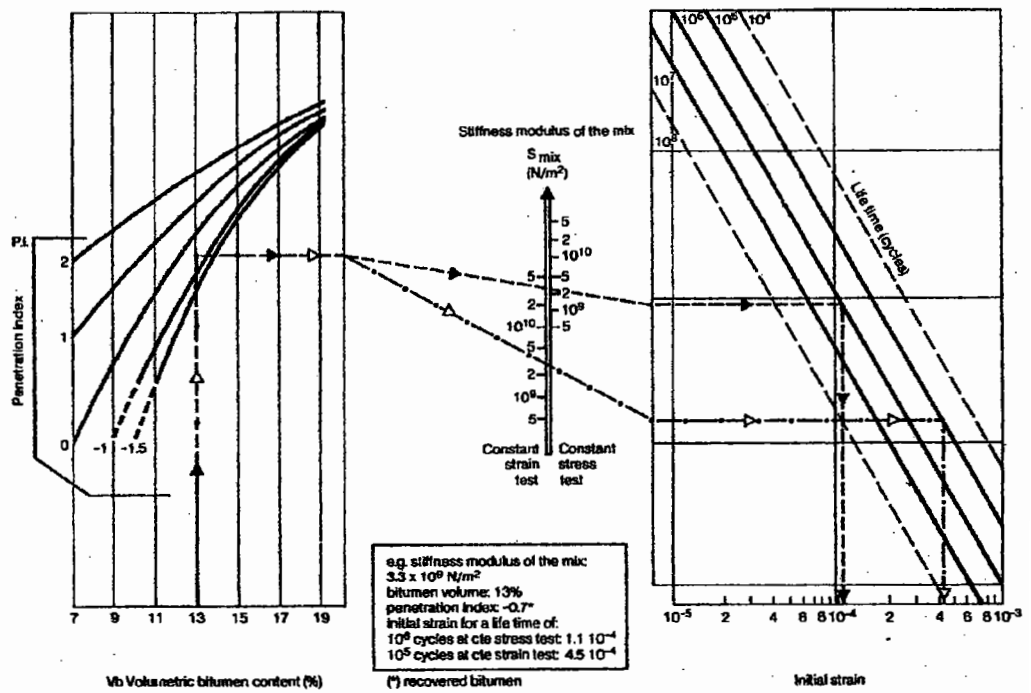
Figure 3.17 : Nomograph to Predict Fatigue Life from Tensile Strain, Mixture Stiffness, Penetration Index and Volume of Binder

$$N_{fat} = [(\ 4.102 \ \times \ PI \ ) \ - \ (\ 0.205 \ \times \ PI \ \times \ V_b \ )$$
$$+ \ (\ 1.094 \ \times \ V_b \ ) \ - \ 2.707 \ ] \ \times \ S_{mix}^{\ -0.36} \ \times \ N^{-0.2} \qquad (3.18)$$

For controlled stress conditions [with S_{mix} in Pa]:-

$$N_{fat} = [\ (\ 0.300 \ \times \ PI \ ) \ - \ (\ 0.015 \ \times \ PI \ \times \ V_b \ )$$
$$- \ 0.198 \ ] \ \times \ S_{mix}^{\ -0.28} \ \times \ N^{-0.2} \qquad (3.19)$$

where;

PI = binder Penetration Index

V_b = volume of binder in mixture

N_{fat} = number of load applications

S_{mix} = mixture stiffness

The Asphalt Institute Method (1982) - involves the stiffness modulus of the mixture along with an adjustment for the volumetrics of the mixture, as follows:-

$$N_{fat} = 18.4 \ \times \ C \left[\ 4.32 \ \times \ 10^{-3} \ \times \ \epsilon_t^{\ -3.29} \ \times \ E^{*\ -0.854} \ \right] \qquad (3.20)$$

where;

N = number of 80 kN ESAL's

ϵ_t = tensile strain in asphalt layer

E^* = complex stiffness modulus

C = a function of voids and binder volume, defined as follows:-

$$C = 10^M \qquad (3.21)$$

and

$$M = 4.84 \left[\frac{V_b}{V_a + V_b} - 0.69 \right] \qquad (3.22)$$

where;

V_a =   volume of air voids

The above equations have been adjusted to allow for the differences that occur between field and laboratory specimens and predict a life associated with 20% or greater cracking based upon analysis of the AASHO road test data.

A NCHRP - study resulted in an equation to predict fatigue that relied only on the mixture stiffness and the tensile strain (Finn et al., 1977). The equation for predicting the life of a laboratory specimen is as follows:-

$$N_{fat} = 660.7 \times 10^9 \times \mu\epsilon_t \times E^{* \; -0.854}$$

where;

N =   number of 80 kN ESAL's

$\mu\epsilon_t$ =   tensile microstrain in asphalt layer

E^* =   complex stiffness modulus

This is a special case of the Asphalt Institute equation where the volume of binder and air voids are set to values consistent with standard asphaltic concrete paving mixtures.

SHRP A-003A (Deacon et al., 1994) - project developed a relationship which

used the loss stiffness modulus. This parameter is directly related to the energy dissipated in an asphaltic mixture. The relationship developed (with an r^2 of 0.79) is as follows:-

$$N_{supply} = 2.738 \times 10^5 \times e^{(0.077 \times VFB)} \times \epsilon_0^{-3.624} \times S_0''^{2.720} \qquad (3.24)$$

where;

N_{supply} = the number of load repetitions to a 50% reduction in stiffness.

e = base of the natural logarithm.

ε_0 = flexural strain.

S_0'' = the initial flexural loss stiffness modulus estimated from shear testing (psi).

VFB = voids in the mineral aggregate filled with binder $[V_b/(V_a+V_b)]$.

The predicted fatigue life (N_{supply}) is compared, in a probabilistic manner, to the fatigue life required. Thus for a mix to be satisfactory:-

$$N_{supply} \geq M . N_{demand} \qquad (3.25)$$

where;

M = a multiplier whose value depends on the design reliability and on the variabilities of the estimates of N_{supply} and N_{demand}.

N_{demand} = design ESAL's (equivalent single axle loads) adjusted to a constant temperature of 20°C divided by an empirically determined shift factor which takes a value

of 10 and 14 for 10% and 45% cracking allowed in the wheel paths respectively.

The reliability multiplier is estimated from the following:-

$$\ln (M) = Z_R \left[Var\{\ln(N_{supply})\} + Var\{\ln(N_{demand})\} \right]^{0.5} \qquad (3.26)$$

where;

Z_R =   a function of the reliability level which assumes values of 0.253, 0.841, 1.280 and 1.640 for reliability levels of 60, 80, 90 and 95 percent.

$Var\{\ln(N_{supply})\}$ =   the variance of the natural logarithm of N_{supply}.

$Var\{\ln(N_{demand})\}$ =   the variance of the natural logarithm of N_{demand}.

3.8   FRACTURE MECHANICS

The basic concepts of fracture mechanics as introduced by Griffith (1921) in the 1920's provide an alternate approach to define the fatigue properties of asphaltic mixtures using fracture mechanics. The classical approach for linear elastic materials is to define the rate of crack growth in the material as a

function of a stress intensity parameter K[1]. As the crack grows, the intensity of stress at the crack tip increases until a stage is reached where rapid unstable crack growth and the critical condition of K_{IC} occurs. The relationship between crack growth and the parameter K is defined by the Paris Erdogan equation (Paris et al., 1963), as follows:-

$$\frac{dc}{dN} = A \ (\Delta K)^n \tag{3.27}$$

where;

dc/dN = rate of crack growth

c = crack length

N = number of load applications

A, n = material constants

K = stress intensity factor

The use of fracture mechanics principles with asphaltic material was introduced by Majidzadeh et al., (1971) who concluded that the general form of Paris' crack growth law was applicable to asphalt mixtures. For stiff foundations, the exponent "n" was found to be equal to 4 and was independent of mixture

---

[1]This parameter allows the calculation of stress at the crack tip for linear elastic materials. Although this parameter is often used for asphaltic materials, the assumption of linear elastic behaviour is not valid except for very cold temperatures and small strains. For non-linear materials exhibiting viscous and plastic properties, alternate approaches are available which make use of analogous parameters termed the J integral and C* (Sadananda et al., 1980 and Jenq et al., 1990).

variables, whereas the parameter "*A*" was affected by mixture variables such as binder content, binder grade and mixture density.

Later work (Majidzadeh et al., 1976; Majidzadeh, Dat and Madisi-Ilyas 1976; and Majidzadeh et al., 1977) indicated that the relationship proposed by Paris et al, (1963) was not sufficient and more terms were required to describe the data, as follows:

$$\frac{dc}{dN} = A_1.K_I + A_2.K^2 + A_3.K^4 + A_4.K^6 \qquad (3.28)$$

It was further concluded that, if the Paris Erdogan equation was used, the exponent "*n*" would lie between 2 and 8 depending upon the type of loading, whereas "*A*" could be estimated, as follows:

$$A\ (\times10^9) = 0.231 + 2.613\left[\frac{1000\ \sigma_t}{E^*}\right] + \left[\frac{3.233\ K_{IC}}{10,000}\right] \qquad (3.29)$$

where;

σ_t = tensile strength (stress rate equals 1200 psi/second).

E^* = complex stiffness modulus (psi) (10 Hz)

K_{IC} = fracture toughness (lbs/in$^{1.5}$) (stress rate 1200 psi/second)

Since the exponent "*n*" was effected by loading, Majidzadeh presented a further crack growth law which had two terms with constant exponents of 2 and 4, as follows:

$$\frac{dc}{dN} = A_1.K^2 + A_2.K^4 \qquad\qquad (3.30)$$

where;

$$A_1(\times\ 10^{10}) = 7.02\ +\ 77.9 \left[\frac{1000\ \sigma_t}{E^*}\right]^2 -\ 6.09\ \times\ \left[\frac{K_{IC}}{1000}\right]^3 \qquad (3.31)$$

and

$$A_2\ (\times\ 10^{16}) = 31.36\ -\ 1132.4 \left[\frac{1000\ \sigma_t}{E^*}\right]^3 -\ 43.32 \left[\frac{K_{IC}}{1000}\right]^3 \qquad (3.32)$$

The above equations could be used to cover all loading conditions, but it should be noted that the form of the equation is different from the Paris Erdogan equation. Paris et al., (1963) had based their results on elastic materials. However, asphaltic materials contain a significant viscous contribution to their behaviour. This can be considered by using the analysis conducted by Schapery (1973). He developed an equation which has the same form as the Paris Erdogan equation, as follows:

$$\frac{dc}{dN} = AK^n \qquad\qquad (3.33)$$

where;

$$A = \frac{\pi}{6\,\sigma_t^2\,I_1^2} \cdot \left[\frac{(1-\mu^2)\,D_2}{2\Gamma}\right]^{\frac{1}{m}} \cdot \int_0^{\Delta t} w(t)^{2\left[1+\frac{1}{m}\right]} dt \qquad (3.34)$$

I_1	=	a factor dependent upon: the stress conditions at the crack tip, the failure stress and length of failure zone
D_2	=	Compliance at $t=1$ second
μ	=	Poisson's ratio
Γ	=	energy required to produce a unit area of crack surface
$w(t)$	=	the pulse shape of the stress intensity factor
m	=	the slope of the tensile creep compliance curve.
σ_t	=	maximum tensile strength

The parameter A in Schapery's equation is dependent upon the temperature and load level (unlike the A is Majidzadeh's equation) since as stress level and temperature increase, then the slope of the creep compliance curve will change.

Molenaar (1983) conducted an analysis of various specimen geometrics and conducted tests to develop a procedure for the estimation of A from routine test methods, as follows:-

$$\log A = 4.389 - 2.52 \log (E\,\sigma_t\,n) \qquad (3.35)$$

where; E = mixture stiffness modulus (kPa)

σ = tensile strength (kPa)

Experiments conducted by Lytton et al., (1983) led to the Equation 3.44, where *A* is expressed as a function of *n*.

$$\log A = \frac{-n + 0.69}{0.511} \tag{3.36}$$

and

$$n = 0.8 \left(1 - \frac{1}{m}\right) \tag{3.37}$$

In Lytton's work, *A* is directly related to *n*, whereas Molenaar introduced the stiffness modulus and tensile strength. These parameters act as surrogates for fracture energy and the shape of stress intensity factor. However, Molenaar (1983) reports a correlation coefficient of 0.96, which he concluded predicts the *A* value with reasonable accuracy.

Lytton et al., (1993) extended his analysis to incorporate field effects to produce the relationships:

$$\log A = 4.389 - 2.52 \log (K \cdot \sigma \cdot n) \tag{3.38}$$

where, K = coefficient determined through field calibration (10,000)

    σ = tensile strength (psi)

This relationship is used in the SHRP SuperPave™ (Lytton et al., 1993) software to describe the fatigue crack growth.

3.9 REST PERIODS AND HEALING

In road pavements, a period of time occurs between the applications of stress by vehicular traffic. This rest period can be very long (eg. that between vehicles spaced out on a highway) or relatively short (eg. between successive wheels on a vehicle).

Two different types of studies have been performed by researchers in this subject area; i) Experiments which have a rest period between individual load applications, and ii) Experiments where a series of load pulses are applied followed by a period of rest. These experiments have been termed as those with "*intermittent loading*" and those with "*storage periods*" (Bonnaure et al., 1982).

McElvaney and Pell, (1973) conducted tests with *storage periods* and found that *storage periods* increased the fatigue life, however, no limit on the increase in performance was found.

Raithby et al., (1970) used a uniaxial mode of testing with *intermittent loading* and conducted tests in the temperature range 10 to 40°C at a frequency of 25 Hz. He demonstrated that the increase in fatigue life due to *intermittent loading* was related to the length of the rest period and the temperature.

Francken (1979) and Verstraeten et al., (1982) expresses the life increase due to *intermittent loading* (see Figure 3.18) using a relationship as follows:-
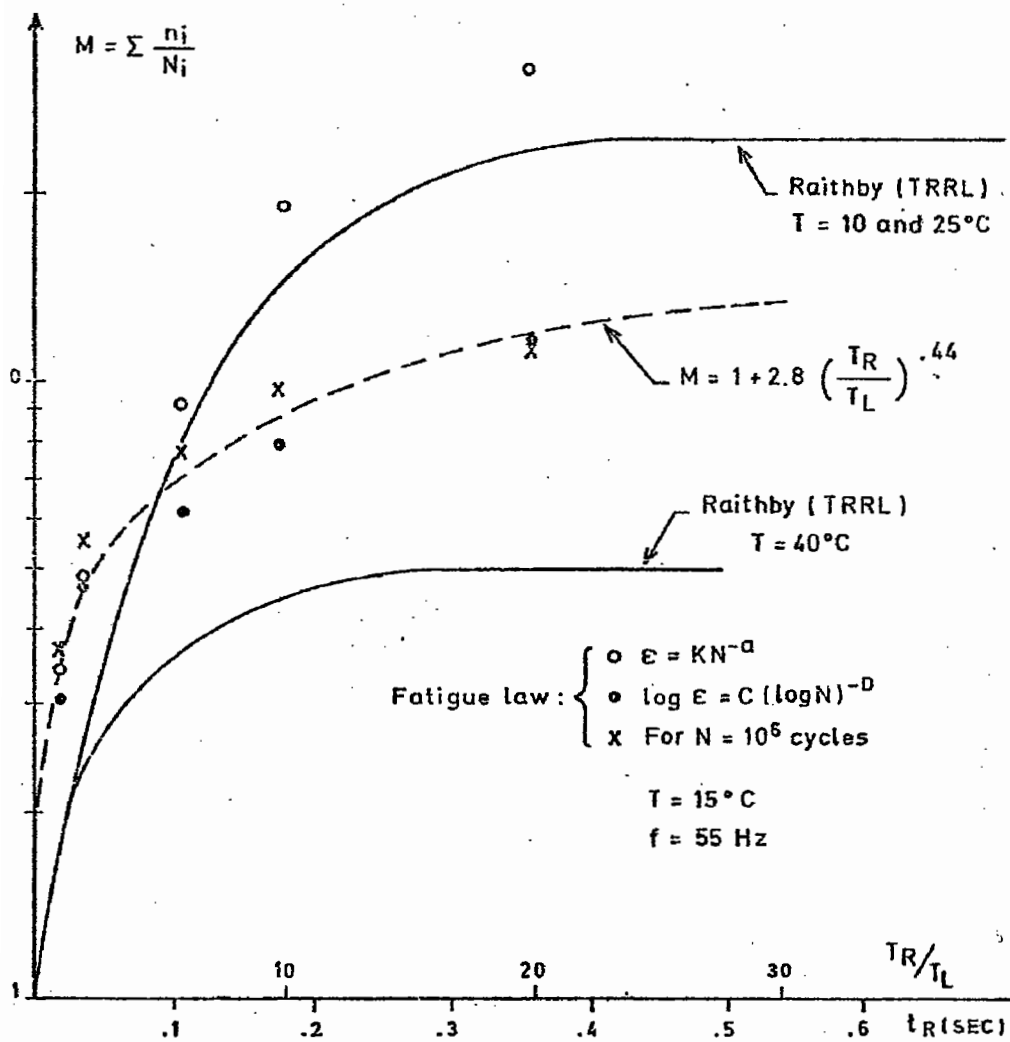
Figure 3.18 : The Effect of Rest Periods on Fatigue Life (after Francken, 1979)

$$M(j) = 1 + C_1 (j)^{C_2} \qquad (3.39)$$

where;

j = rest period/loading period

Rest periods were varied between 1 and 20 times the loading period for three mixture types. The increase in fatigue life appeared to be highly dependent upon mixture composition, particulary the binder content (Figure 3.19). Lytton et al. (1993) adopted a similar shift factor for healing, as in Equation 3.40.

$$SF_h = 1 + a (t_r)^b \qquad (3.40)$$

where;

t_r = the rest period, commonly recorded in seconds

a, b = the healing coefficient and exponent, respectively

The coefficients and exponent have been calibrated to the field for both back-calculated layer moduli (obtained from the analysis of pavement deflection data) and also from the analysis of laboratory testing. Lytton et al. (1993) noted the similarity in the results and considered that this supported their validity. The results are presented in Table 3.2 for the four climatic zones considered in Superpave.

3.10   CUMULATIVE LOADING

Unlike loading in fatigue tests, the traffic loads applied to a pavement structure
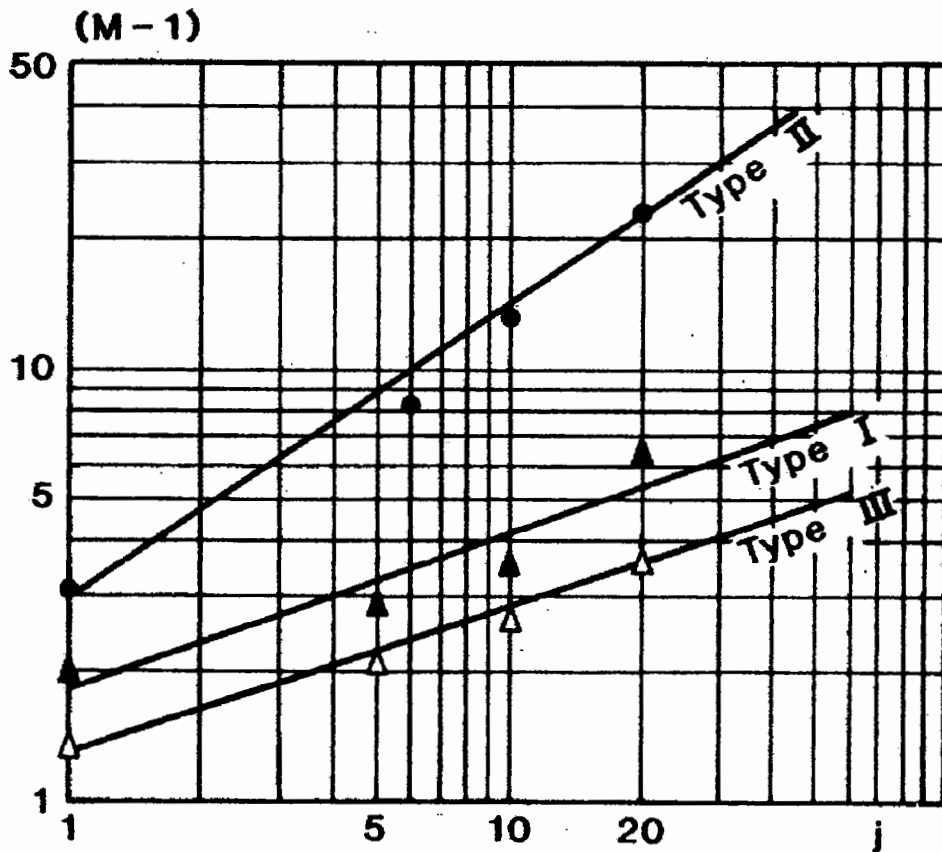
Type	Description	Volumes (%)			Binder Properties	
		Binder	Aggregate	Voids	Penetration (mm 10^{-1})	Ring and Ball softening Point (°C)
I	Dense Bituminous Concrete	13.1	82.8	4.1	58	50
II	Stone Filled Sand Sheet - similar to Hot Rolled Asphalt	17.7	79.4	2.9	47	54.5
III	Base Course Asphalt Concrete	10.7	81.7	7.6	57	54.6

Figure 3.19 : Influence of Rest Periods on Fatigue Life for Three Different Mixtures (after Francken et al., 1987)

Climatic Zone	From Pavement Deflection Data		From Laboratory Test Data	
	a	b	a	b
Wet - Freeze	0.037	0.261	0.037	0.261
Wet - No Freeze	0.097	0.843	0.128	1.075
Dry - Freeze	0.056	0.642	0.071	0.762
Dry - No Freeze	0.051	0.466	0.057	0.492

Table 3.2 : Healing Parameters "a" and "b" Used in Superpave

(see Equation 3.40)

vary in magnitude. The approach used to consider compound loading which is generally applied to with asphaltic materials is that developed by Miner (1954). Work conducted by Monismith and Deacon (1969) and McElvaney (1972) showed that this approach, known as "Miner's Law" or "Linear Summation of Cycle Ratio's Criterion," is applicable to asphaltic materials subjected to compound loading. The relationship at failure is expressed as follows:-

$$\sum_{i=1}^{j} \frac{n_i}{N_i} = 1 \qquad (3.41)$$

where;

n_i = the number of load applications at a level i

N_i = the number of load applications at a level i that will result in fracture

j = number of load levels

The amount of damage at a single load level is calculated as follows:-

$$D = \frac{n_i}{N_i} \qquad (3.42)$$

Thus, a compound load fatigue life can be predicted by considering the proportion of loading at a given load level required to give failure at that load level and summing these to obtain the number of load applications associated with compound loading, N_c, as follows:-

$$N_c = \frac{100}{\sum\limits_{i=1}^{j} \left(\dfrac{P_i}{N_i} \right)}$$ (3.43)

where;

P_i = percentage of load condition i

Hopman et al., (1989) evaluated Miner's Law with consideration of dissipated energy and suggested a modified damage rule, as follows:-

$$D = \left[\frac{n_i}{N_i} \right]^x$$ (3.44)

where;

x = an exponent obtained from laboratory test data

He suggested mean values of x ranging between 0.82 and 0.92 from results obtained from four point bending tests to a point which he considered was consistent with crack initiation. Hopman et al. (1989) also suggested two other fatigue stages. In the second stage the "hair cracks are growing and a network of cracks are formed" whereas the third stage was considered to occur as "the material is assumed to break down". In these stages x varies between 0.04 and 0.28 (2nd stage) and takes the value of 1 for the third stage.

3.11   PAVEMENT DESIGN ADJUSTMENTS

Historically, the results from laboratory fatigue testing have been found to be

significantly different from pavement performance. This has necessitated the use of "shift factors". These "shift factors", which have been used to account for healing, crack propagation, differences in stress states and lateral wheel distribution, differ between researchers. Generally, the factors have been developed for a particular method of pavement design and caution is necessary when applying one researcher's factors to a different method of testing and/or pavement design. For example, Brown et al. (1985) adopted total shift factors of 77 and 440 for critical and failure conditions. The 77 factor includes ×3.5 for crack propagation, ×20 for rest periods and ×1.1 for lateral wheel distribution whereas the 440 factor includes ×20 for crack propagation, ×20 for rest periods and ×1.1 for lateral wheel distribution. Critical is defined as the "first appearance of wheel path cracking" and failure is taken "to represent the fully cracked state". These factors are used in conjunction with a characteristic design temperature which considerers the variation of asphalt stiffness with temperature during the day at different depths weighted according to the percentage of traffic at the time. The consideration of different climates would result in the use of different traffic weighted design temperatures and other shift factors more appropriate to the climatic conditions.

3.12 SUMMARY

The fatigue process in asphaltic materials is extremely complicated and needs consideration of many aspects as discussed. Early work points to the importance of strain and stiffness. Later in the 1970's work with the dissipated energy approach demonstrated the potential to overcome the differences found

between different test types (eg. controlled strain versus controlled stress).

-3.52-

Dissipated energy involves two additional parameters (stress and phase lag). The dissipated energy approach captures the visco-elastic material property effects such as rate and time of loading as well as temperature.

The effect of mixture variables, particulary the volumetric proportions, have been shown to be important. Consequently, careful attention has to be paid to accurate measurement and quantification of mixture constituents.

The work presented in the following chapters expand upon those concepts presented above, particulary in section 3.6, with regard to dissipated energy.

CHAPTER 4

Experimental

4.0   INTRODUCTION

The experimental work consisted of several test programmes with distinct objectives as follows:

1.   **Test Development :** In this programme two fatigue test procedures, uniaxial tension-compression and trapezoidal cantilever beam were evaluated as possible candidate test methods for a fundamental test procedure. This work formed part of the University of California's evaluation of different test methods in which they made use of a bending beam fatigue test and North Carolina State University contributed results obtained from the Indirect Tensile Fatigue Test. The statistical comparison of the test methods was undertaken by the University of California and is reported in the literature (Tayabli et al., 1992). The work reported in this thesis is concerned with the development of the two test methods for performing fatigue tests and the modification to software and the analysis of the test results in terms of dissipated energy.

2.   **Assessment of Modified Binders :**   Several modifiers were evaluated using the trapezoidal cantilever beam fatigue test. This piece of work was conducted in order to extend the testing described above to modifiers.

3. **Wheel Tracking Validation :** These experiments were performed in order to relate the element tests to results from a pilot scale facility which simulates traffic loading more realistically. This part of the testing is also used to assist with determination of "shift factors" between laboratory measured fatigue life and pavement performance.

4. **Assessment of Simplified Test Procedures :** The indirect tensile test procedure was used to determine the stiffness modulus and the strength of a limited number of the materials tested. In addition some work was performed with a repeated load axial test and frequency sweep data to obtain mixture rheology which could be combined with analysis techniques to obtain fatigue life estimation. These procedures are considered useful for application in specifications if a correlation could be established with the more fundamental tests, since these methods are considered simpler in their execution compared with beam fatigue tests.

The results from the various test programmes were used in the analysis work that was performed. The analysis consisted of two principle parts; 1) assessment of fatigue test results and 2) comparison to pavement performance. The latter part made use of various modelling techniques including Finite Element analysis.

In order to accomplish the above test programmes, experimental work was conducted as described in the following sections.

4.1   FATIGUE ELEMENT TESTS

The experimental work to evaluate the test methods, uniaxial tension-compression and trapezoidal, consisted of a one half factorial experimental design. The experimental design varied the binder content, binder type, temperature, void content, and aggregate type.

The two binders selected for the work were from the Boscan (SHRP ref. AAK) and California Valley (SHRP ref. AAG) sources and are indicated in the mixture code by the letter "B" and "V" respectively. These binders were selected to represent different temperature susceptibility. In terms of the Penetration Index (PI) the California Valley is around -0.5 whereas the Boscan is about 0. Empirical test data for these binders is presented in Table 4.1.

The two aggregates selected, Watsonville (SHRP ref RB) and Texas Chert (SHRP ref RL) represented two extremes, a "good quality" granite and a "low quality" river gravel. The choice of the two aggregates for this test program was effected by the needs of the A-003A research program. This involved evaluation of five distress types; permanent deformation, fatigue damage, ageing, stripping (loss of binder adhesion to the aggregate) and thermal cracking. While the mineral nature of the aggregate is known to have little effect on fatigue and thermal cracking performance, the two aggregates selected for this work represent the extremes for all distresses. The granite has crushed faces and is regarded as a high quality aggregate whereas the river gravel has rounded particles (which increases the deformation susceptibility)

Binder Ref.	Treatment	Penetration at 25°C (0.1 mm)	Absolute Viscosity 60°C (poise)	Kinematic Viscosity 135°C (cSt)	Softening Point (ASTM) (°C)
AAG-1	Tank	53	1,950	246	50
	TFOT	34	3,490	--	52
	PAV	18	8,140	--	56
AAK-1	Tank	70	3,320	582	49
	TFOT	41	10,240	--	58
	PAV	27	27,300	--	63

Table 4.1 : Empirical Properties of SHRP AAG and AAK Grades.

and exhibits poor adhesion qualities. These were referred to in the mixture code by the letters "W" and "T" respectively.

The binder contents selected represented the Hveem and Marshall optimums. The Marshall optimum was approximately one half of one percent higher than the Hveem design. The high and low conditions were referred to by "0" or "1" as the second digit of the mixture reference. In addition, the volumetrics of the mixtures were varied by changing the compaction level to achieve void contents of approximately 4 and 8%.

The experimental design for the one half factorial is shown in Table 4.2. The initial plan called for controlled stress testing using both test types to be conducted according to the design. However, as the work proceeded it became apparent that the uniaxial mode of testing was resulting in failures close to the loading platens (this aspect is discussed under test procedures). Consequently, this mode of testing was abandoned and in place a limited amount of fatigue testing was conducted in the controlled strain mode using the trapezoidal cantilever fatigue test in addition to the planned controlled stress testing. This consisted of testing sixteen specimens all with the Watsonville granite with the Marshall design binder content and both temperatures and void contents. These are indicated by the italic type/shaded blocks in Table 4.2. Additional testing was used to investigate other aspects but the specimens were referred to by the SHRP mixture code where possible. This additional work involved testing at 30°C in order to extend the data set to include higher temperatures, evaluation of modified materials and testing of specimens from the LCPC test

A	B	C	D	E	F
0	0	0	0	0	0
0	0	0	0	0	1
1	0	0	0	1	0
1	0	0	0	1	1
1	1	0	0	0	0
1	1	0	0	0	1
0	*0*	*1*	*0*	*1*	*0*
0	*0*	*1*	*0*	*1*	*1*
1	0	1	0	0	0
1	0	1	0	0	1
0	1	1	0	0	0
0	1	1	0	0	1
1	1	1	0	1	0
1	1	1	0	1	1
0	0	0	1	1	0
0	0	0	1	1	1
1	0	0	1	0	0
1	0	0	1	0	1
0	*1*	*0*	*1*	*0*	*0*
0	*1*	*0*	*1*	*0*	*1*
1	1	0	1	1	0
1	1	0	1	1	1
0	*0*	*1*	*1*	*0*	*0*
0	*0*	*1*	*1*	*0*	*1*
1	0	1	1	1	0
1	0	1	1	1	1
0	*1*	*1*	*1*	*1*	*0*
0	*1*	*1*	*1*	*1*	*1*
1	1	1	1	0	0
1	1	1	1	0	1

Notes:
A = Aggregate Stripping Potential, (0 = RB, 1 = RL)
B = Asphalt Temperature Susceptibility, (0 = AAK, 1 - AAG)
C = Asphalt Content,, (0 = Hveem, 1 = Marshall)
D = Compaction Level, 0 = Target 4% Voids, 1 = Target 8% Voids)
E = Temperature, (0 = 0°C, 1 = 20°C)

For Controlled Stress Tests
 F = Stress, (0 = Low, 1 = High)

For Controlled Strain Tests
F = Strain, (0 = Low, 1 = High)
Italic numbers/shaded blocks indicate cells used for controlled strain experiment.

Table 4.2 : Experimental Design for Test Development

track at Nantes.

The experimental work with modifiers made use of a different aggregate source and binder grades. The source of the aggregate was Mesquite, Nevada whereas the binder used was from the Shell Martinez source (a California Valley Crude) and consisted of either an AR1000 or AR4000 grade[1] and these were used with modifiers to make a total of nine different binders, (seven modified with two controls) used with a standard asphaltic concrete mixture. The modifiers used were; Styrene-Butadiene Rubber (SBR), Styrene-Butadiene-Styrene copolymer (SBS); Styrene-Ethylene-Butadiene-Styrene copolymer (SEBS) and an Ethylene Vinyl Acetate copolymer (EVA). These were used in different percentages as indicated in Table 4.3. Since the binders were supplied by Shell they are referred to by a "S" followed by one or two characters. The first character a "1" or "4" indicates the AR1000 or AR4000 grade respectively. These modified binders have a further alphabetic character to refer to the polymer as indicated in Table 4.3.

The testing of materials from LCPC was initially conducted to allow the University of California to compare the different test methods under evaluation. However, it also provided the scope for including more modifiers and

---

[1] The AR binder grading system is a method adopted by some US states, mainly those in the west. The system used **A**sphalt **R**ecovered after rolling thin film ageing, hence **AR**. The word "asphalt" is used in the USA in place of "bitumen". The final four numbers refer to the viscosity of the binder at 60°C (140°F).

Mixture Ref.	Description
S1	AR1000
S4	AR4000
S1A	AR1000 + 3% SBS
S1B	AR1000 + 1.7 % SBS[1]
S1C	AR1000 + 2% SBS[1]
S1D	AR1000 + 3% SEBS[1]
S1F	AR1000 + 2.5 % SBR[1]
S1G	AR1000 + 3% SBR
S1H	AR1000 + 3% EVA

Notes:

1.   All mixtures binders were from the Martinez crude.

2.   Aggregate source was from Mesquite, Nevada.

Table 4.3 : Reference System used with Modified Binders

aggregate types in the test programme. The geometry adopted from this testing was that used by LCPC since this enabled LCPC to manufacture specimens using their normal procedures. The mixture references used are given in Table 4.4 along with other information relating to each mixture.

4.2   WHEEL TRACKING VALIDATION

The wheel tracking validation work was conducted in order to provide an accelerated validation of the fatigue tests investigated. In order to accomplish this, two test programmes were considered involving tests with modified and conventional materials. The testing was carried out in the Nottingham Slab Testing Facility (STF) which loads a slab of material in a manner which simulates traffic loading more realistically. The experimental plan for this work is given in Table 4.5.

The aggregates selected for the work were the Watsonville granite (SHRP ref RB) and a low absorbtion limestone (SHRP ref RD). The binder grade was varied with six unmodified and three modified binders being evaluated in the test programme. The composition of the modified binders was not known so they were given an arbitrary reference as illustrated in Figure 4.1.

4.3   SIMPLIFIED TEST PROCEDURES

The highway industry has traditionally tested cylindrical specimens, for example Marshall specimens or cores, to obtain properties for mixture design

Mixture Ref.	Binder Content (%)	Binder Pen Grade (mm × 10⁻¹)	Air Voids (%)	LCPC Section
1675	5.4	60/70 (asphalt A)	4.3	II
1676	4.6	60/70 (asphalt A)	4.3	IV
1685	5.4	60/70 (asphalt B)	3.5	I
1695	6.2	10/20	1.8%	III

Notes:

1. Mixture 1695 is referred to as a high modulus mixture.

2. Asphalt B is more "structured" than asphalt A.

3. Asphalt B is less temperature susceptible that asphalt A.

4. Each section had a different construction thickness.

5. The aggregate was a hard igneous rock.

Table 4.4 : Mixtures evaluated from the LCPC Test Track

| Aggregate | | Binder/Modified Binder Reference | | | | | | | | |

		Binder/Modified Binder Reference								
		AAA-1	AAC-1	AAF-1	AAG-1	AAK-1	AAM-1	M406G	M415G	M416G
Aggregate	RB				**3**			**3**	**3**	**3**
	RD	*1*	*1*	*1*	*1*	*1*	*1*			

Notes:

1. "**3**" number in bold indicate A-004 test matrix

2. "*1*" number in italic indicate A-003A test matrix

3. Binder references beginning with the letter M indicate the use of a modifier

4. Modifier codes used by the SHRP A-001 contractor are:-

    i.   M 405 G   M-MF-002-001

    ii.   M 415 G   M-MF-001-002

    iii.   M 416 G   M-TH-003-001

Table 4.5 : Wheel Tracking Simulative Testing Test Matrix

Typical code   M 414 K ◄─────────────── indicates non-modified
                                ↗ ↑ ↖   binder

indicates ─────╱   ╲───── indicates modifier
modified   reference number
binder
                    indicates contract A004
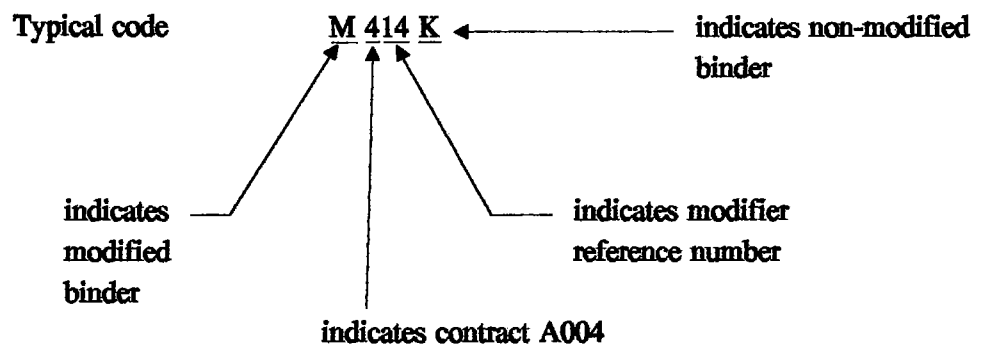
Figure 4.1 : Reference System for Modified Binders

-4.12-

or compliance testing. Thus, there is considerable interest to make use of this geometry and to avoid the preparation time and expenses of diamond sawing beams as required by the Trapezoidal Cantilever Beam fatigue test. Consequently, two different types of tests were investigated, an Indirect Tensile Test to determine stiffness modulus and Tensile strength. Tests were conducted on specimens removed from Trapezoidal beams and wheel tracking slabs at the end of the testing. It was assumed that these specimens were undamaged when tested and that they could provide a comparison with the test data generated from the more fundamental test procedure.

4.4 SPECIMEN PRODUCTION

The **Uniaxial Tension-Compression test** utilised cylindrical specimens of asphalt-aggregate mixture measuring 82 mm diameter by 220 mm long. These were made by coring slabs (measuring 404 mm × 280 mm × 127 mm) of mixture which had been made in the Nottingham Roller Compactor. These specimens used Watsonville granite aggregate (reference RB) and the California Valley and Boscan binders (references AAK and AAG).

Trapezoidal Fatigue test specimens were manufactured in a similar manner but instead of coring, the slabs were sliced using two specially designed jigs in order to achieve trapezoidal shaped specimens. The binders, modified asphalts, and aggregates used in the mixtures were supplied either from the SHRP Materials Reference Library (MRL) or by Shell Development Company of Houston, Texas.

The **STF Fatigue Wheel Tracking test** utilised rectangular shaped slabs measuring 1000 mm x 500 mm x 50 mm. The specimens were made by compacting slabs of mixture in a steel mould using a single drum vibrating roller. The aggregates and binders used in these tests are indicated in Table 4.5. The work involved two combined test programs; an evaluation of mixtures with conventional binders (SHRP project ref A-003A) and an evaluation of mixtures with modified binders. The nature of the binder modifiers was not made available and the references used (see Table 4.5) were those dictated by the A-001 and A-004 contractors (see Table 1.1).

4.4.1 Mixing

Prior to use, all the aggregate was screened into individual size fractions, and batches were then reconstituted in accordance with pre-determined grading and asphalt contents. The grading and asphalt contents used for the mixtures are given in Table 4.6 and are illustrated in Figure 4.2 (also included for information is the grading of the mixture in the specimens supplied by LCPC).

Mixing followed similar procedures to that contained in the Asphalt Institute (TAI) MS-2 Manual (The Asphalt Institute, 1984). This defines mixing temperature as being equivalent to 170 +/- 20 centistokes (approximately 1.6 poises) based upon the unaged asphalt properties, see Table 4.7. In the case of modified asphalt the same temperature was used as for the unmodified asphalt of the same grade. Viscosity versus temperature information was not available which would have enabled assessment of equi-viscous mixing

Sieve Size		Aggregate			
(USA)	(Metric)	RB used for Fatigue Wheel Tracking	RL, RB used for uniaxial and Trapezoidal Fatigue Testing and RD used for Fatigue Wheel Tracking	Mesquite (Nevada) Aggregate used for Trapezoidal Fatigue Testing (Supplied by Shell Development Co.)	LCPC specimens prepared in Nantes
1"	25 mm	100	100	100	100
3/4"	19 mm	95	95	99.4	-
-	14 mm	-	-	-	99
1/2"	12 mm	81	80	-	-
-	10 mm	-	-	-	76
3/8"	9.8 mm	69	68	73.6	-
-	6.3 mm	-	-	-	55
No. 4	4.76 mm	49	48	54.3	-
-	4 mm	-	-	-	44
No. 8	2.36 mm	35	35	-	-
No. 10	2 mm	-	-	38	33
No. 16	1.18 mm	24	25	-	-
	1 mm	-	-	-	23
No. 30	600 μm	17	17	-	-
No. 40	425 μm	-	-	21	-
-	315 μm	-	-	-	13
No. 50	300 μm	12	12	-	-
No. 100	150 μm	8	8	-	-
-	80 μm	-	-	-	7.4
No. 200	75 μm	5.5	5.5	5	-
Binder Content by weight of mixture (%)		5.1	4.31	4.5	See Table 4.4

Table 4.6 : Asphalt Contents and Aggregate Gradings
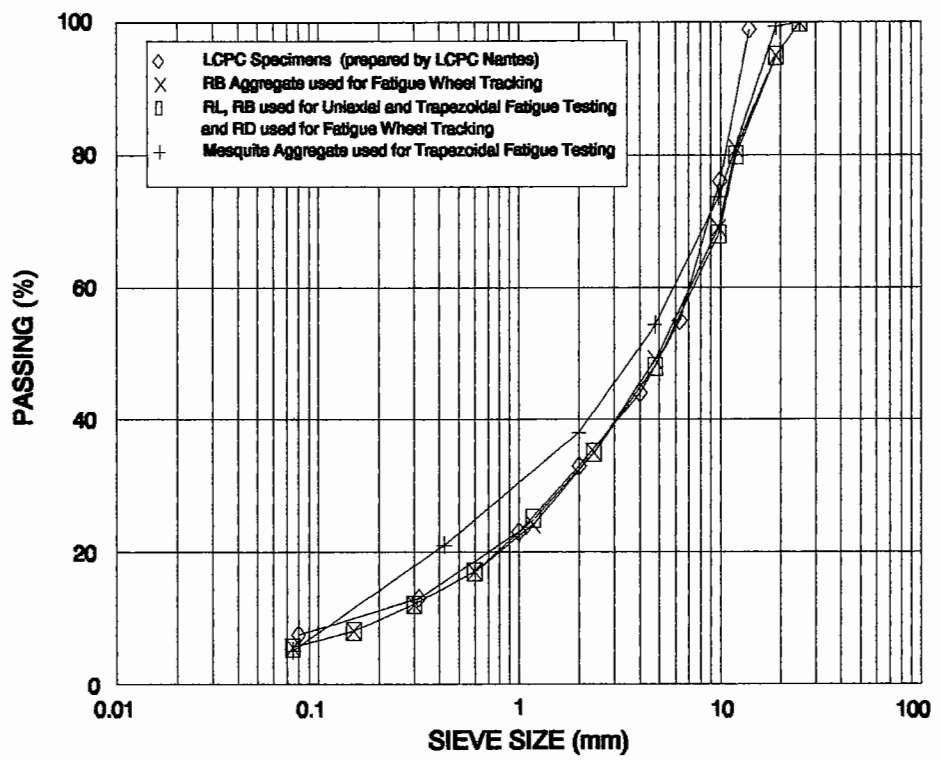
Figure 4.2 : Grading Curves for Mixtures used in Test Program

Asphalt	Mixing Temperature (°C)	Compaction Temperatures (°C)
AAA-1	151	140
AAC-1	147	135
AAF-1	149	138
AAG-1	142	133
AAK-1	159.5	148.5
AAM-1	167	155

Table 4.7 : Target Compaction and Mixing Temperatures

temperatures. The detailed mixing procedure was as follows:-

i) The required batch weights were prepared and heated in a thermostatically controlled oven to the mixing temperature +/- 5°C. This involved heating the aggregate for about three hours.

ii) Asphalt/modified asphalt was heated at the same time as the aggregate in air jacketed containers to a temperature within +/- 5°C of the target mixing temperature.

iii) The aggregate was then placed in a Sun and Plant type mixer, Figure 4.3. A heated oil jacket around the mixing pan enabled the correct mixing temperature to be maintained. A small hollow was then formed in the centre to receive the asphalt/modified asphalt, which was weighed into the mixture in accordance with the required batch weights, after which the mixing commenced.

iv) The asphalt/modified asphalt-aggregate mixture was mixed for 180 seconds, after which the mixture was transferred to metal trays, which were then placed in ovens at 60°C for a fifteen hour conditioning period.

4.4.2 Compaction

The ability of a material to be compacted under a rolling wheel load is sensitive to the consistency of the asphalt at the time of compaction. It was
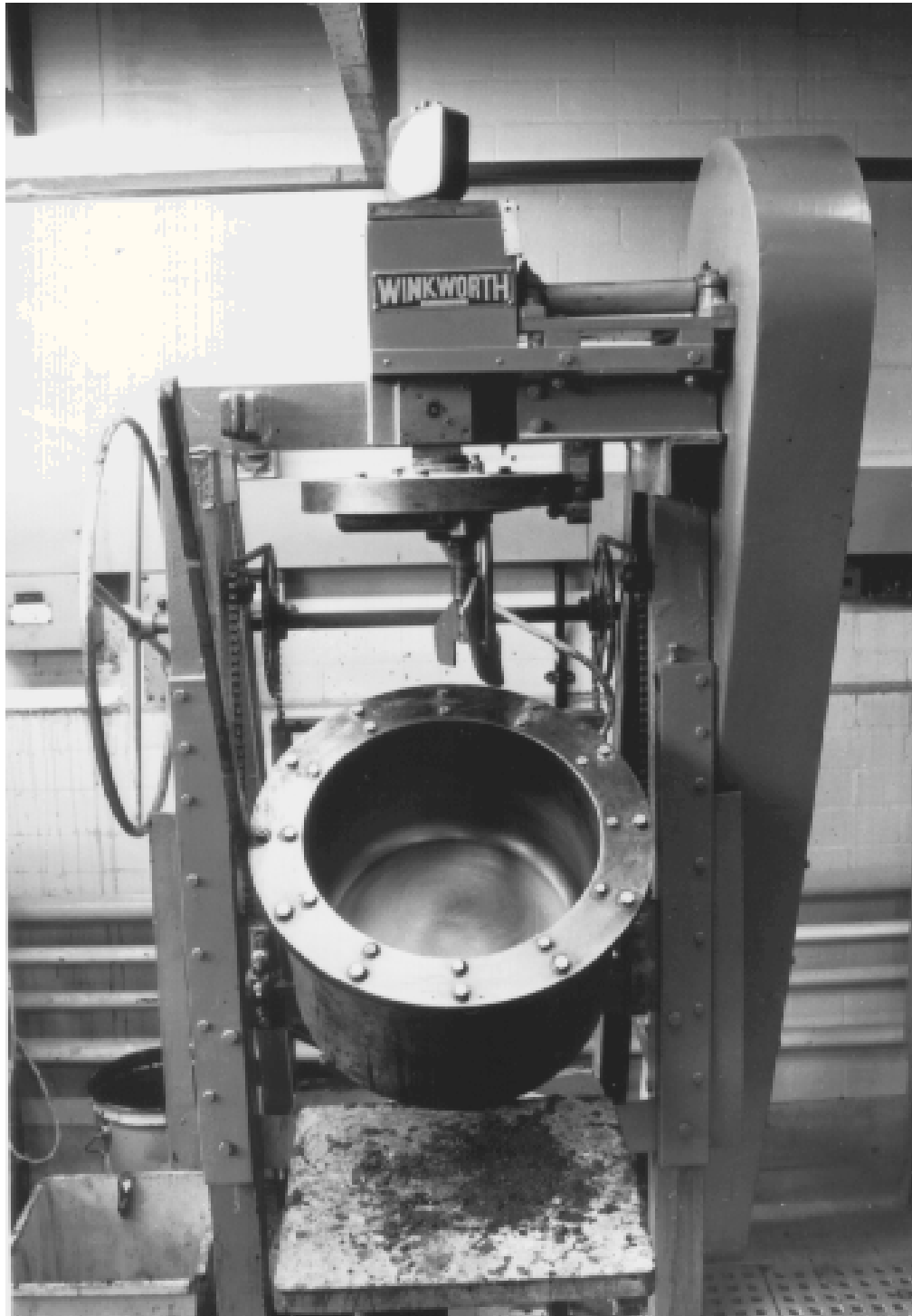
Figure 4.1 : Sun and Planet Mixer

found that the desired level of compaction could be achieved by using a temperature consistent with a viscosity in the unaged binder equivalent to 280 +/- 30 centistokes (approximately 2.65 poises), see Table 4.7

As indicated earlier for the **Uniaxial Tension-Compression and Trapezoidal Fatigue test** slabs were manufactured in moulds measuring 404 mm in length, 280 mm wide and 127 mm high. The detailed procedure is given below:

a)   Ten trays of mixed material were placed in two layers through five guide slots, Figure 4.4, (two trays per slot) to obtain equal amounts of material in each segment of the mould. After the fifth tray was placed, the guide was raised to the top of the layer and the material was tamped ten times per slot using a heated steel ball fixed to a steel rod (diameter approximately 50 mm) pre-heated to the mixture temperature. Five further trays of material making a second layer were added and the guide raised again following which each segment was tamped a further ten times. The guide was then removed from the mould.

b)   The material was then rolled to the required depth using a segment of a roller. This apparatus is shown in Figure 4.5.

The slabs of asphalt aggregate mixture were allowed to cool to room temperature after which they were stripped from their moulds and cored to produce specimens for testing.
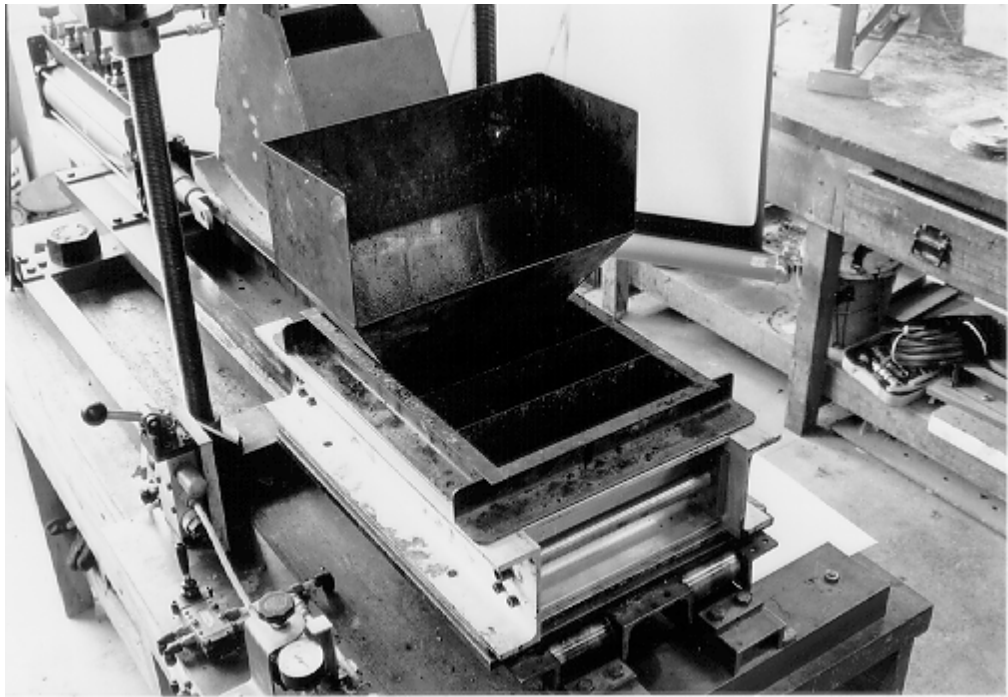
Figure 4.4 : Placing Material Through Guide Slots
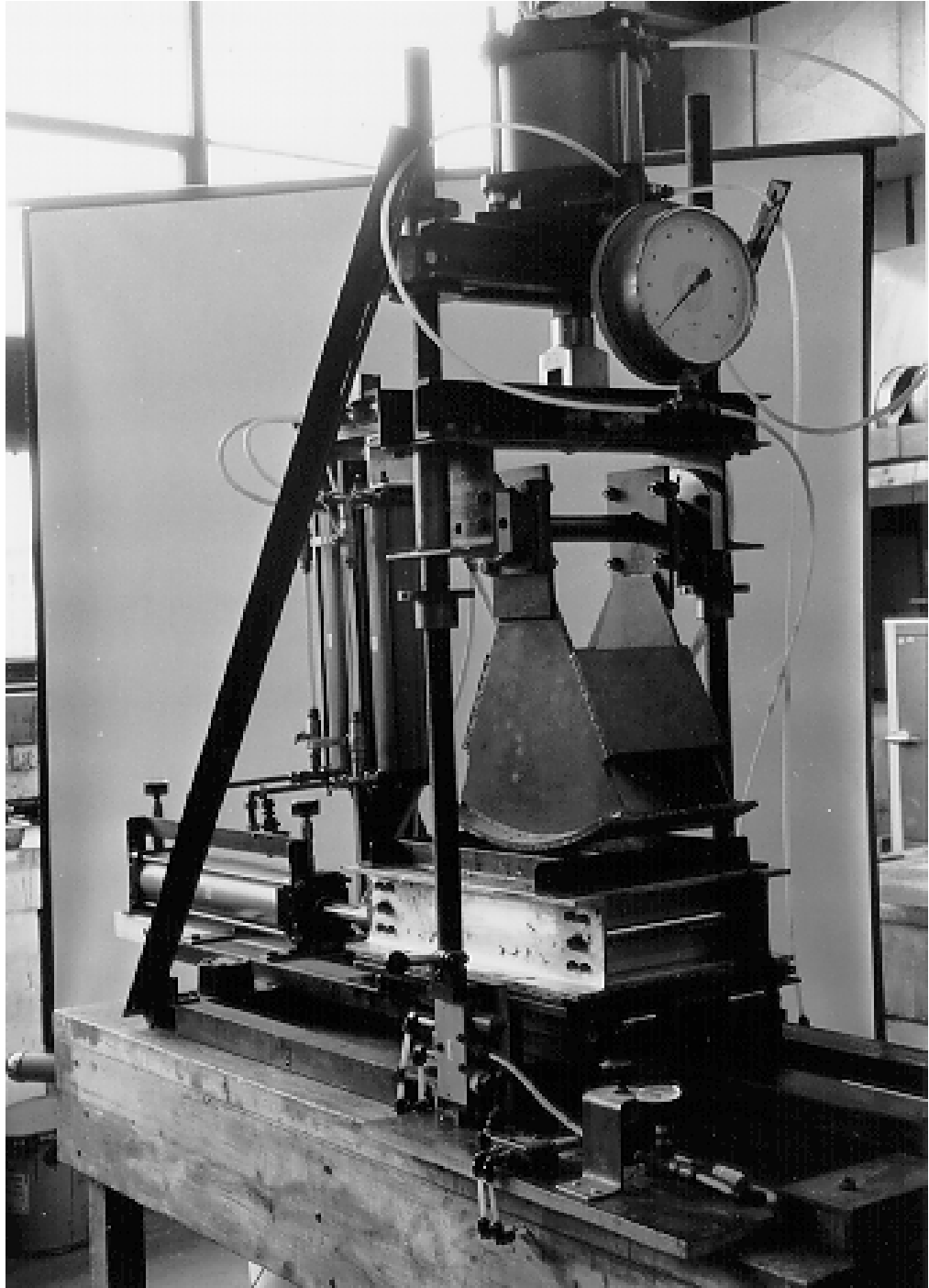
Figure 4.5 : Roller Compactor

To obtain specimens for **Uniaxial Tension-Compression Fatigue** testing four cores were taken from each slab. The direction of coring was horizontal so that the direction of the axial stress was parallel to the surface, simulating horizontal stresses occurring in a pavement. This also allowed cores of appropriate length to be obtained. A typical cored slab is shown in Figure 4.6.

The cores cut from the slab were 280 mm long and 82 mm in diameter. These were trimmed to a length of approximately 220 mm using a masonry saw.

The dried specimens were then bonded to end caps using 'Araldite' epoxy resin. The jig used for fixing end caps is shown in Figure 4.7. The resin was allowed to harden for a minimum of 24 hours prior to testing. 'Pips' were glued onto the specimen to enable measurement of axial strain over an effective gauge length of 100 mm in the centre of the specimen. Thus strain measurement is remote from the ends and not effected by spurious strains near the end caps.

For the **Trapezoidal Fatigue Testing** the specimens were sawn along the longitudinal vertical axis using a masonry saw to produce slices 40 mm thick. These slices were then trimmed to produce rectangular specimens measuring 380 mm x 125 mm (Figure 4.8). The trapezoidal shape was then sawn using the jig shown in Figure 4.9.

After the specimens were trimmed they were placed upon absorbent paper and allowed to dry out at room temperature until a constant mass was obtained.

To obtain specimens for **Uniaxial Tension-Compression Fatigue** testing four cores were taken from each slab and the direction of coring was horizontal so that the direction of the axial stress was parallel to the surface, simulating horizontal stresses occurring in a pavement. This also allowed cores of appropriate length to be obtained. A typical cored slab is shown in Figure 4.6.

The cores cut from the slab were 280 mm long and 82 mm in diameter. These were trimmed to a length of approximately 220 mm using a masonry saw.

The dried specimens were then bonded to end caps using 'Araldite' epoxy resin. The jig used for fixing end caps is shown in Figure 4.7. The resin was allowed to harden for a minimum of 24 hours prior to testing. 'Pips' were glued onto the specimen to enable measurement of axial strain over an effective gauge length of 100 mm in the centre of the specimen. Thus strain measurement is remote from the ends and not effected by spurious strains near the end caps.

For the **Trapezoidal Fatigue Testing** the specimens were sawn along the longitudinal vertical axis using a masonry saw to produce slices 40 mm thick. These slices were then trimmed to produce rectangular specimens measuring 380 mm x 125 mm (Figure 4.8). The trapezoidal shape was then sawn using the jig shown in Figure 4.9.

After the specimens were trimmed they were placed upon absorbent paper and

Figure 4.6 : A Slab after coring and Prepared Specimens
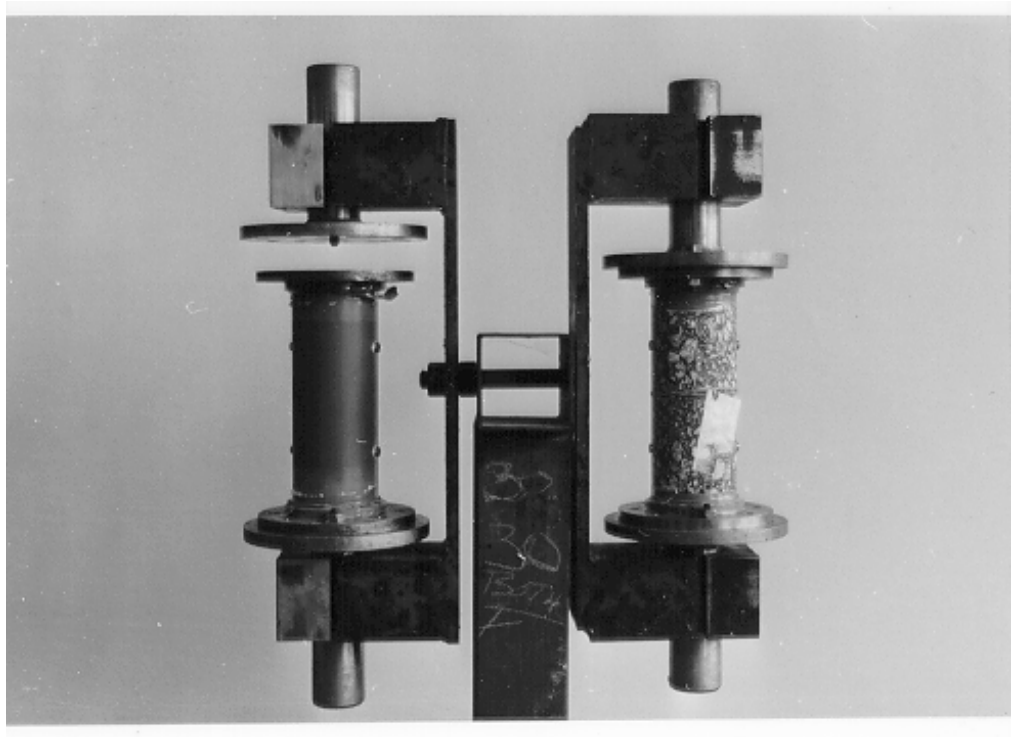
Figure 4.7 : Jig for Gluing End Caps onto Cylindrical Specimens

Figure 4.8 : Jig for Producing 40 mm Slices

Figure 4.9 : Jig for Sawing Trapezoidal Specimen

This usually took two to four days. The specimens were then sealed using a foil tape and weighed in air and water to enable the calculation of mixture density.

The dried specimens were then bonded to end plates using epoxy resin. The jig used for fixing the plates is shown in Figure 4.10. The resin was allowed to harden for a minimum period of 24 hours prior to testing.

For the **STF Fatigue Wheel Tracking test** slabs of mixture were manufactured in a steel mould with plan dimensions of 100 mm x 500 mm. To ensure consistency, the degree of compaction, air void content was specified in the experimental plan as 5%. The batch weights were calculated so that a slab compacted to a final thickness of 50 mm would have the required void content. However, this was difficult to achieve in a controlled manner due to the thickness of the slab being relatively small. This resulted in a small variation in compacted height resulting in a large variation in void content, eg. a 1 mm variation in depth results in approximately 2% difference in void content (for the same mass of material).

It is considered that changes in binder viscosity due to modification could have had some influence upon the time required for compaction. However, this aspect has not been assessed in a quantifiable manner, since viscosity measurements were not required as part of the experimental work. The detailed procedure used is as follows:-
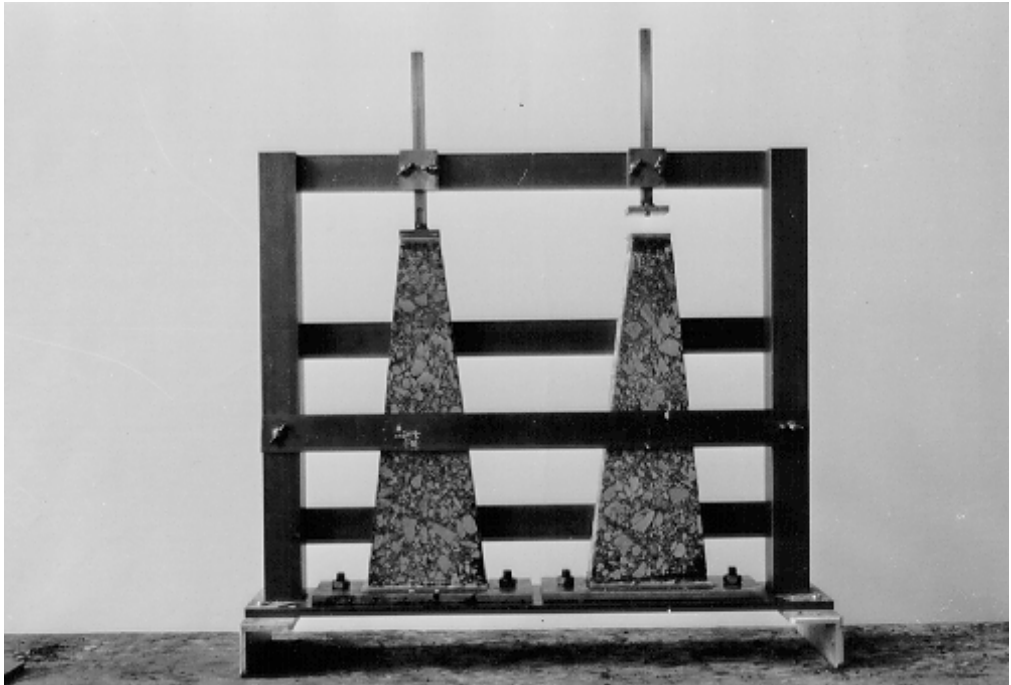
Figure 4.10 : Jig for Fixing End Plates to Trapezoidal Specimens

a)   The steel mould was heated using a gas flame to approximately 150°C. After which a piece of silicon backed paper was placed into the mould. The silicon side faced upwards and this ensured release of the asphalt/modified asphalt aggregate mixture from the mould.

b)   The sixteen trays of material were emptied onto the silicone paper (in the mould) and the top surface was raked to be approximately level. In the uncompacted state the level of the material was around 25 mm higher than the top of the mould.

c)   Using a single drum vibrating roller (in the non-vibratory mode) the material received an initial compaction of two passes. The vibration was then switched on and further passes were applied until no roller marks were evident in the material. This took approximately 10 passes in total to achieve. Figure 4.11 illustrates the compaction procedure.

After compaction, handles were attached to the side walls of the mould allowing transportation by fork lift. When cool, allen key bolts in the base were loosened, while the mould was held above the ground by the fork lift, allowing the steel base to fall off, Figure 4.12. A second set of side walls were then added to the base to facilitate the production of the next slab. The manufactured slabs, contained within the side walls (shear connector strips were welded onto the side walls of the mould to hold the slab in place in the mould and after removal of the base plate), were then placed upside down on a rubber mat to allow attachment of strain gauges to the underside.

Figure 4.9 : The Compaction Procedure - Fatigue Wheel Tracking Slabs
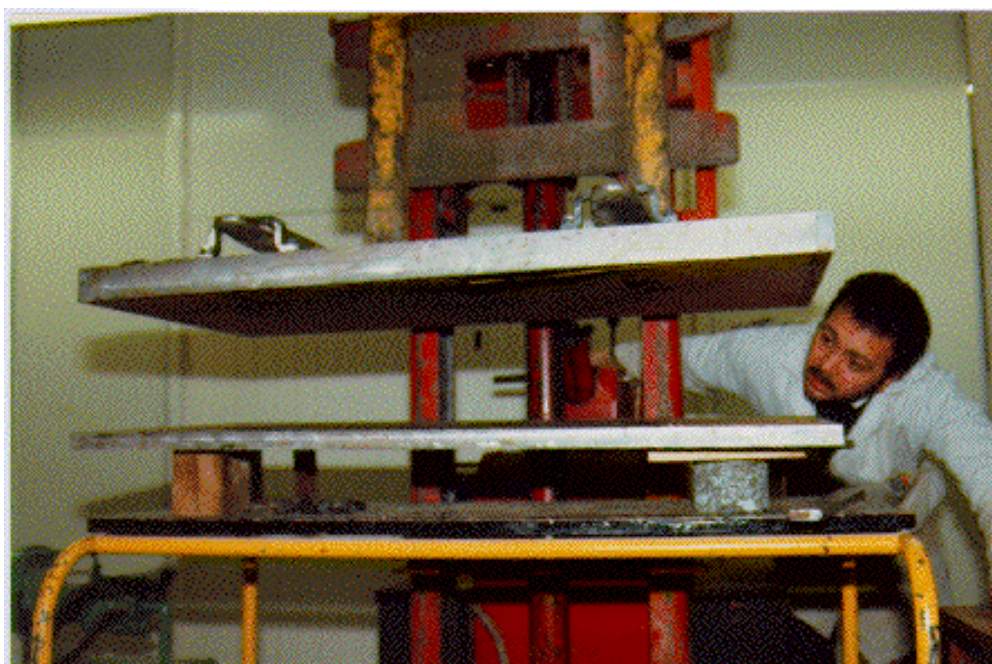
Figure 4.10 : Removal of the Base Plate from The Mould

4.4.3 *Specimen volumetric proportions*

The determination of mixture bulk density was carried out essentially as detailed in BS598 Part 3 (British Standards Institution, 1985) except that self adhesive foil tape was used to seal the cores instead of paraffin wax. The method was carried out as follows:-

i)   The specimen were weighed in air (W_1).

ii)   The specimens were then sealed using self adhesive aluminium foil and reweighed in air (W_2).

iii)   Each specimen was then weighed in water, (W_3).

iv)   The specimen bulk densities were calculated using the following equation.

$$G_{mb} = \frac{W_1}{W_2 - W_3 - \left[\dfrac{W_2 - W_1}{G_{sf}} \right]}$$
(4.1)

where; W_1 = mass of the specimen in air before sealing (g)

            W_2 = mass of the specimen in air after sealing (g)

            W_3 = mass of the sealed specimen in water (g)

            G_{sf} = relative density, aluminium foil tape (1.65 tonnes/m^3)

The use of this technique was considered necessary to truly measure the void content of specimens with cut faces and relatively high void contents of 8-12%. With this level of voids, if the specimen is not sealed, water will enter the specimen reducing the apparent volume obtained when weighed in air and water. This will result in a higher density and a lower measure of voids. If this is taken to the extreme case of a porous macadam where all the voids are essentially permeable to water a void content approaching zero would be obtained for an unsealed specimen. For dense asphaltic mixtures a void content of 8% unsealed compares to a sealed result of approximately 12% as illustrated in data presented in Figure 4.13 for both trapezoidal and uniaxial fatigue specimens.
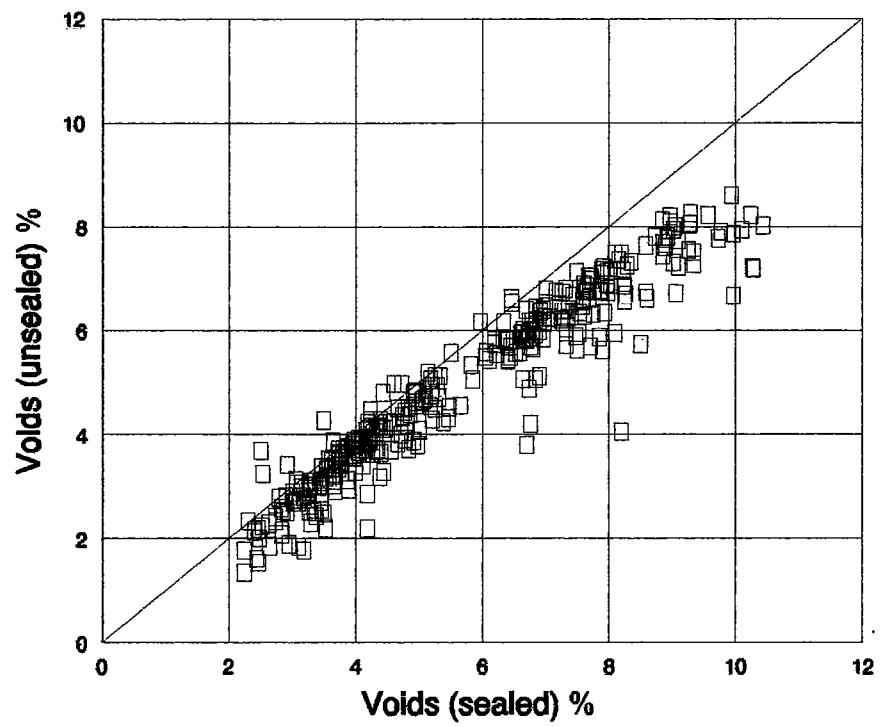
Figure 4.13 : Void Contents - Sealed versus Unsealed

-4.35-

Test Procedures

5.0   TEST DEVELOPMENT

Two fatigue test methods were used in the experimental work conducted at Nottingham, *Uniaxial Tension Compression* and *Trapezoidal Bending*. In addition two techniques were used to measure indirect tensile stiffness modulus and indirect tensile strength.

5.1   UNIAXIAL TENSION COMPRESSION FATIGUE TEST

The uniaxial tension-compression fatigue test was carried in a 'Mand' servo-hydraulic testing apparatus. Figures 5.1 and 5.2 show the apparatus and specimen ready for testing. A dummy specimen was used to monitor temperature throughout the tests. This consisted of a core of asphaltic material into which a thermocouple was embedded. The temperature of the sample under test was assumed to be consistent with the dummy specimen after a minimum period of twelve hours in the temperature control cabinet.

The specimens when tested were subjected to an axial load varying sinusoidally between tension and compression at a frequency of 20 Hz. The strain was determined by measuring the transient deformation on either side of
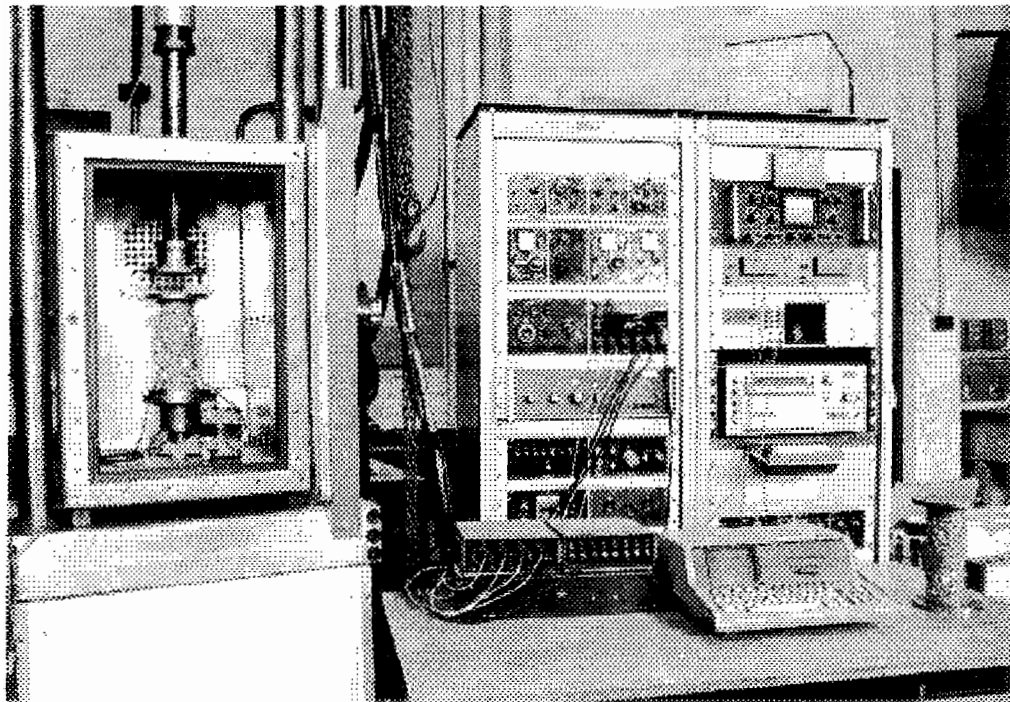
Figure 5.1 : General view of the Uniaxial Tension-Compression Fatigue Test Apparatus
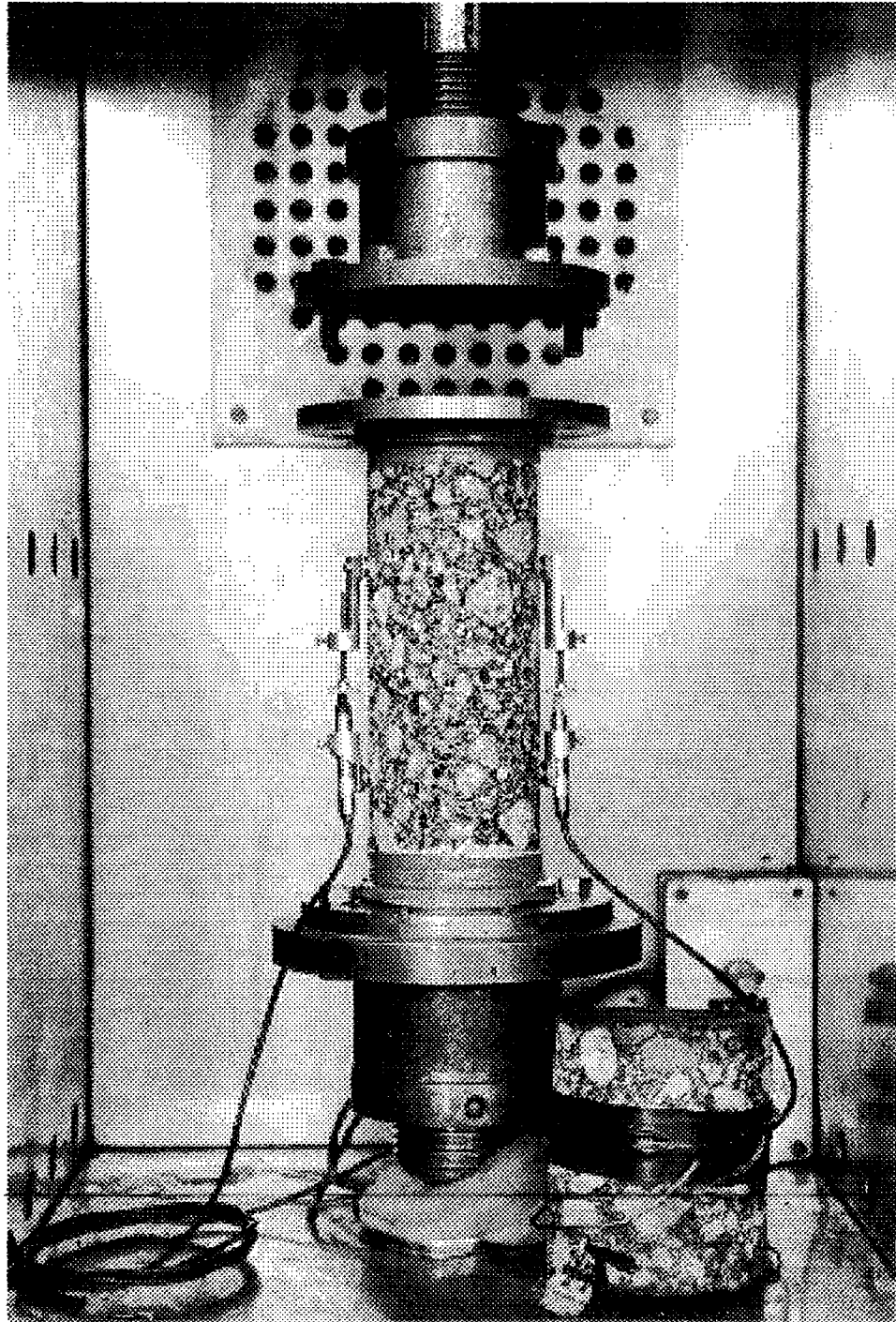
Figure 5.2 : A Cylindrical Specimen Fixed in Position Ready for Fatigue Testing

the specimen using LVDT's. This deformation was then divided by the gauge length of 100 mm to give the value of peak to peak (tension-compression) strain. Typical load and deformation readings obtained are shown in Figure 5.3. The mean load was controlled to keep the mean gauge length constant at 100 mm and because of the nature of the material, this was always compressive. The mean stress level was anticipated to effect the fatigue performance. Mudock et al. (1958) showed that the ratio of compressive to tensile stress would enable the effect of a variable mean stress level to be quantified.

The control and data acquisition system was analogue but digital interfaces were used to couple this to a Hewlett Packard HP85-B micro computer enabling long term tests to be run with control and data acquired at pre-determined intervals.

The need to keep a constant gauge length required some adaption of the computer software. It was found during the initial tests that the mean length of the specimen was fluctuating by an amount which was in excess of 2,500 $\mu\varepsilon$. This fluctuation took place over a period of a few minutes and was essentially a flow of the material under the influence of the mean stress level of the specimen. Initially, the software was set up to keep the mean gauge length constant by adjusting the load level by a fixed amount if the gauge length was outside a certain tolerance. However, as the specimen started to correct itself it was noted that the correction was always overshooting by a large error. It was considered that since this material was behaving in essentially an visco-elastic manner that the rate of change of mean load was

-5.4-
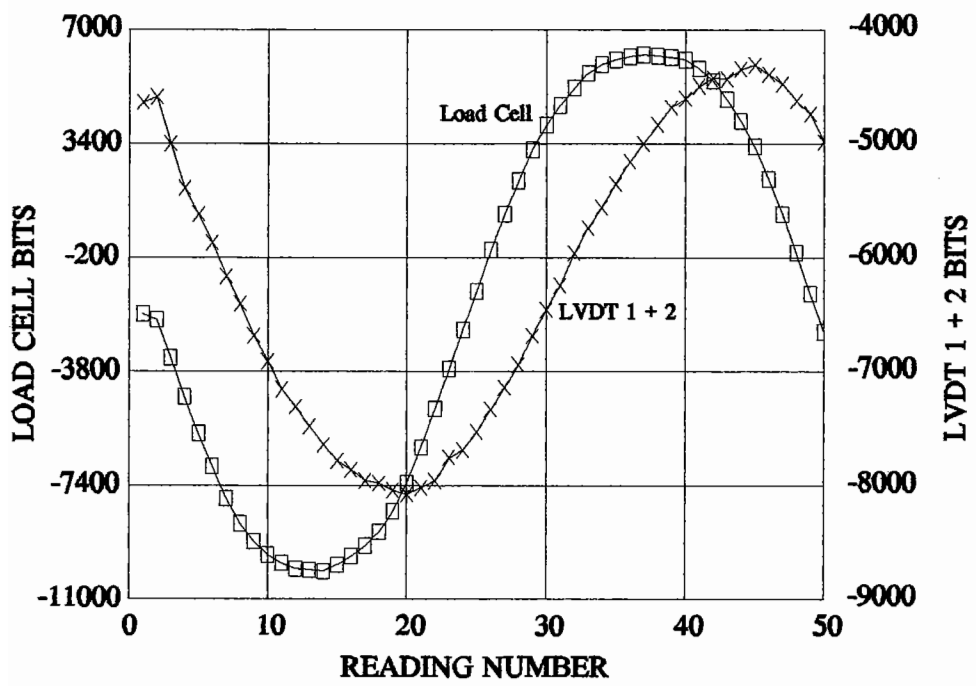
Figure 5.3 : Typical Load and Deformation Readings Obtained from the Uniaxial Tension-Compression Fatigue Test

important. Thus, considerable modifications where made to the control software in order to achieve a constant gauge length during the test. The result of this modification was that it was found important to control the **rate of change** of mean load level versus the error in gauge length and the **rate of change** of the gauge length. Thus, the scheme adopted was to; 1) read the mean position of the LVDT's, 2) calculate the rate of change of the mean position from the last observed position, 3) dependent upon the actual position and the current rate of change, adjust the load bits sent to the digital to analog converter (D-A), 4) repeat. A correction to adjust the load bits was made during approximately every five seconds of testing which was equivalent to 100 load cycles at the test frequency of 20 Hertz (this was the time that the computer took to read and process the signal, store the data and to send new information to the D-A and varied depending upon what data had to be stored). When the mean length was close to the actual desired gauge length this correction was very small. Figure 5.4 shows a typical example of poor control versus what was considered acceptable.

The total stress applied to the specimen was calculated by first estimating the mixture stiffness from the method developed by Brown, 1978 (see equations 2.11 to 2.13). In some conditions the above procedure resulted in an overestimation of mixture stiffness. To avoid excessive loads being applied to the specimens, values of stiffness were adjusted where it was evident from experience that the estimated value was incorrect.

From the estimation of mixture stiffness the tensile strain corresponding to

EXTENSION vs LOAD CYCLES
TEST REF. VOW1001

Good control

Notes :
1.   LVDT range is approximately +/- 0.6mm.
2.   LVDT is out of range for sample with poor control. This indicates a visco-plastic strain greater than 0.6% (6000 micro strain).

longer = +ve
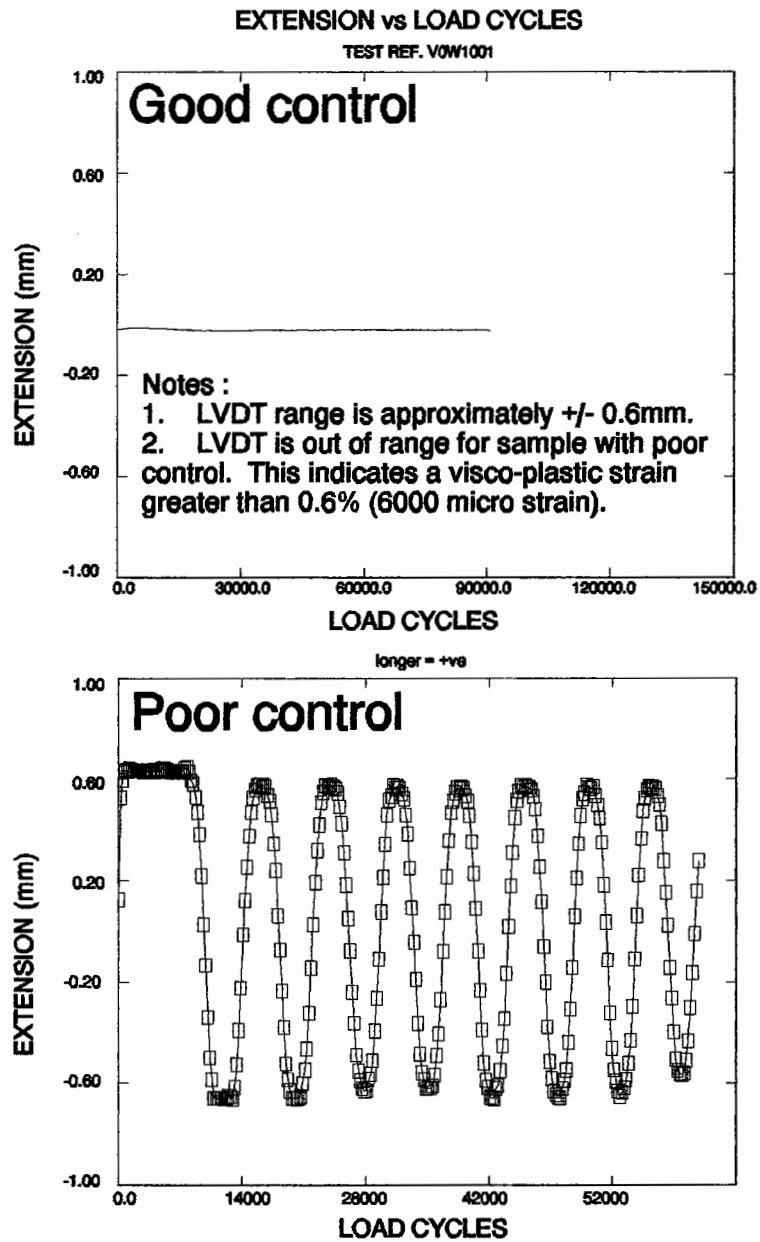
Poor control

Figure 5.4 : "Good" versus "Poor" Gauge Length Control in the
Uniaxial Tension-Compression Fatigue Test

fatigue lives of 10^4 and 10^5 cycles were calculated from the following expression developed during earlier testing at the University of Nottingham (Cooper, 1976) on moulded samples in rotating bending.

$$Log\ \epsilon_t = \frac{52.52\ -\ 16.52\ log\ V_b\ -27.8\ log\ SP_i\ -\ log\ N}{5.1625\ log\ V_b\ +\ 8.6875\ log\ SP_i\ -\ 15.9125} \quad (5.1)$$

where; ε_t = tensile strain

           V_b = binder volume (%)

           SP_i = initial softening point of binder (°C)

From the tensile strain the required tensile stress (σ_t) and peak to peak load (2W) were calculated as follows:-

$$\sigma_t = S_{me}\ \epsilon_t \quad\quad\quad (5.2)$$

$$2W = 2\ A\ \sigma_t \quad\quad\quad (5.3)$$

where; A = cross sectional area of the specimen

The reported results are normalized initial testing strain, target strain, target stress level amplitude and life to failure. The first strain value was normalized to account for the changes during the time taken for the stress to stabilize to the target value. The normalized initial tensile strain was calculated as follows:

$$\epsilon_{t,\ int} = \frac{\epsilon_A\ \sigma_T}{2\ \sigma_A} \quad\quad\quad (5.4)$$

where; $\varepsilon_{t,\ int}$ = Normalized initial tensile strain.

$$\sigma_T \quad = \quad \text{Target peak to peak stress}$$

$$\sigma_A \quad = \quad \text{actual peak to peak stress at first measurement.}$$

$$\varepsilon_A \quad = \quad \text{Peak to peak strain measurement at first measured load application.}$$

Life to failure was defined as the point at which the specimen could no longer withstand a tensile load, ie. the specimen fractured.

Following completion of tests, data was transferred to ASCII files and these were then used to produce graphical representation of the results. A typical example of the plot generated is given in Figure 5.5. In addition to the above, an estimation was made of the mean stress level used in each individual test to keep the specimen length constant.

The failure position of each specimen was noted in all instances to be outside the 100 mm gauge length of the specimen and in the majority of instances to be very close to one of the two end fixing positions. Figure 5.6 shows a typical failed specimen with the crack occurring close to the top end cap in this instance.

Due to the occurrence of failure near the fixing positions, an analysis of the test configuration was performed. This was done using a finite element program 'FEPS' (Sharrock, 1983) which uses 8-node parabolic isoparametric Finite Elements. For this study the specimen was considered to be axisymmetric and the end caps perfectly rigid. This last assumption although not strictly
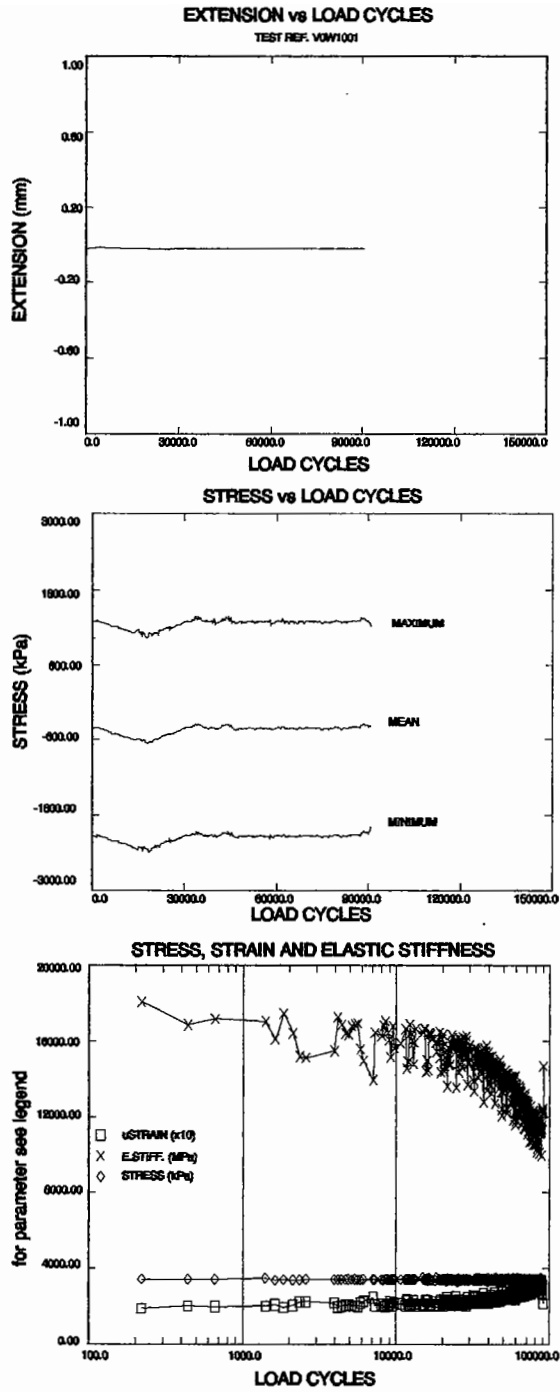
Figure 5.5 : Typical Result from the Uniaxial Tension-Compression Fatigue Test

Figure 5.6 : Failed Specimen - Uniaxial Tension-Compression Fatigue Test

correct was considered to be indicative of the expected behaviour with the stiffness of the end cap and loading platen on the Mand effectively behaving in a rigid manner. Figure 5.7 and 5.8 show the deflected specimen shape (in tension) and principal stress vectors respectively. These indicate that the highest stress will occur near the end cap at the point which has greatest curvature on the deflected shape of the specimen (element no 80). The stress at this location estimated from the contour plot of the Major Principal stress (P1), Figure 5.9, to be approximately 150 to 250% greater than the stress at the centre of the specimen. It would, therefore, be logical to expect failures to occur at this location. As a direct consequence, this test program was curtailed and the available resources used for conducting more tests in the trapezoidal fatigue apparatus.

5.2   TRAPEZOIDAL FATIGUE TESTING

Two sizes of trapezoidal specimens were evaluated as indicated in Figure 5.10. The larger of these was the size adopted by the University of Nottingham while the smaller has been adopted by Laboratoire Central des Ponts et Chaussées (LCPC), Nantes, France. Forty of these specimens were shipped to Nottingham from LCPC. These specimens were obtained from a circular test track and had base and top widths of 56 and 25 mm respectively. The height of these specimens was 250 mm with a thickness of 25 mm.

The testing was carried out in two modes, "controlled strain" and "controlled stress", using an electro-magnetic apparatus (Figure 5.11).

73	74	75	76	77	78	79	80
65	66	67	68	69	70	71	72
57	58	59	60	61	62	63	64
49	50	51	52	53	54	55	56
41	42	43	44	45	46	47	48
33	34	35	36	37	38	39	40
25	26	27	28	29	30	31	32
17	18	19	20	21	22	23	24
9	10	11	12	13	14	15	16
1	2	3	4	5	6	7	8

Notes:

1. This figure represents one quarter of the specimen shape.

2. Deflections have been magnified by × 20.

Figure 5.7 : Deflected Specimen Shape - Uniaxial Tension-Compression Fatigue Test
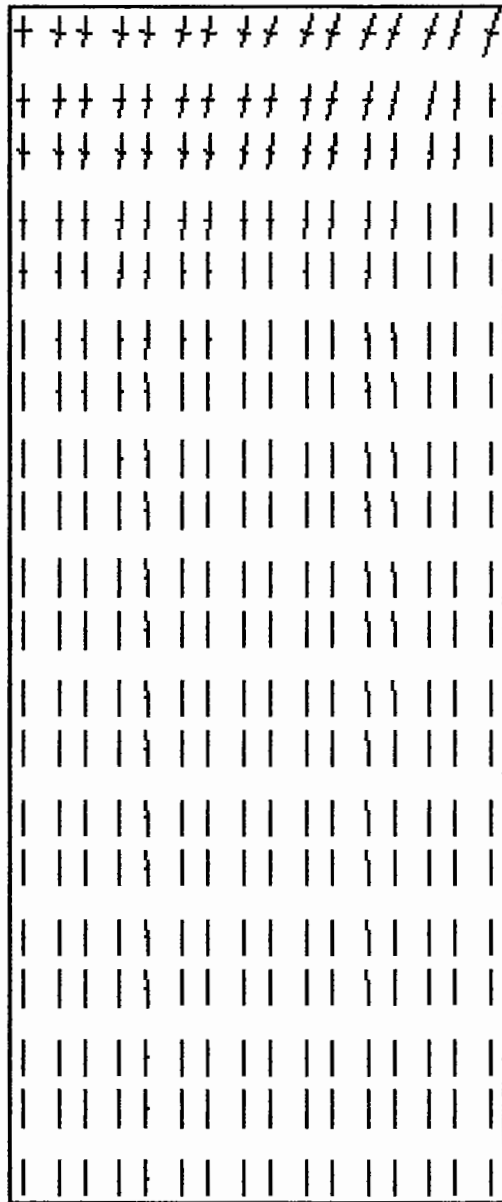
Notes:

1.   This figure represents one quarter of the specimen shape.

Figure 5.8 : Principal Stress Vectors - Uniaxial Tension-Compression Fatigue Tests

Outside Edge

**Top
Flange**

This represents one
quarter of the specimen
shape.

A = 70   B = 80   C = 90   D = 100   E = 110   F = 120   G = 130   H = 140   I = 150
J = 160   K = 170   L = 180   M = 190

2 mm DISPLACEMENT TO TOP FLANGE   INTERVAL = 10
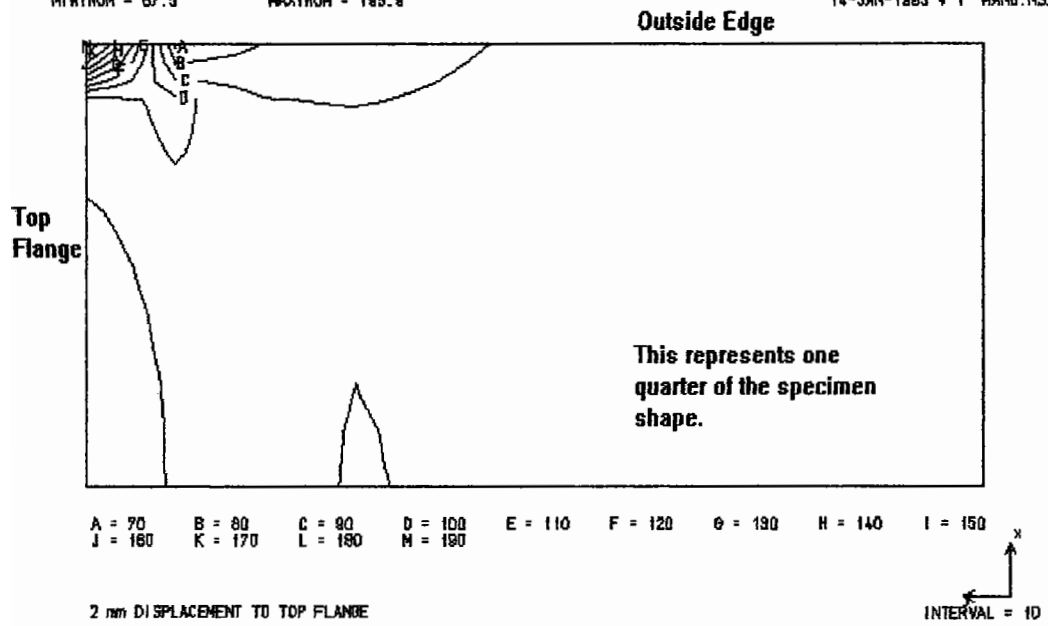
**Figure 5.9 : Maximum Principle Stress Contour from Axi-Symmetric
Finite Element Analysis**

Figure 5.10 : Relative Size of Nottingham and LCPC Specimens
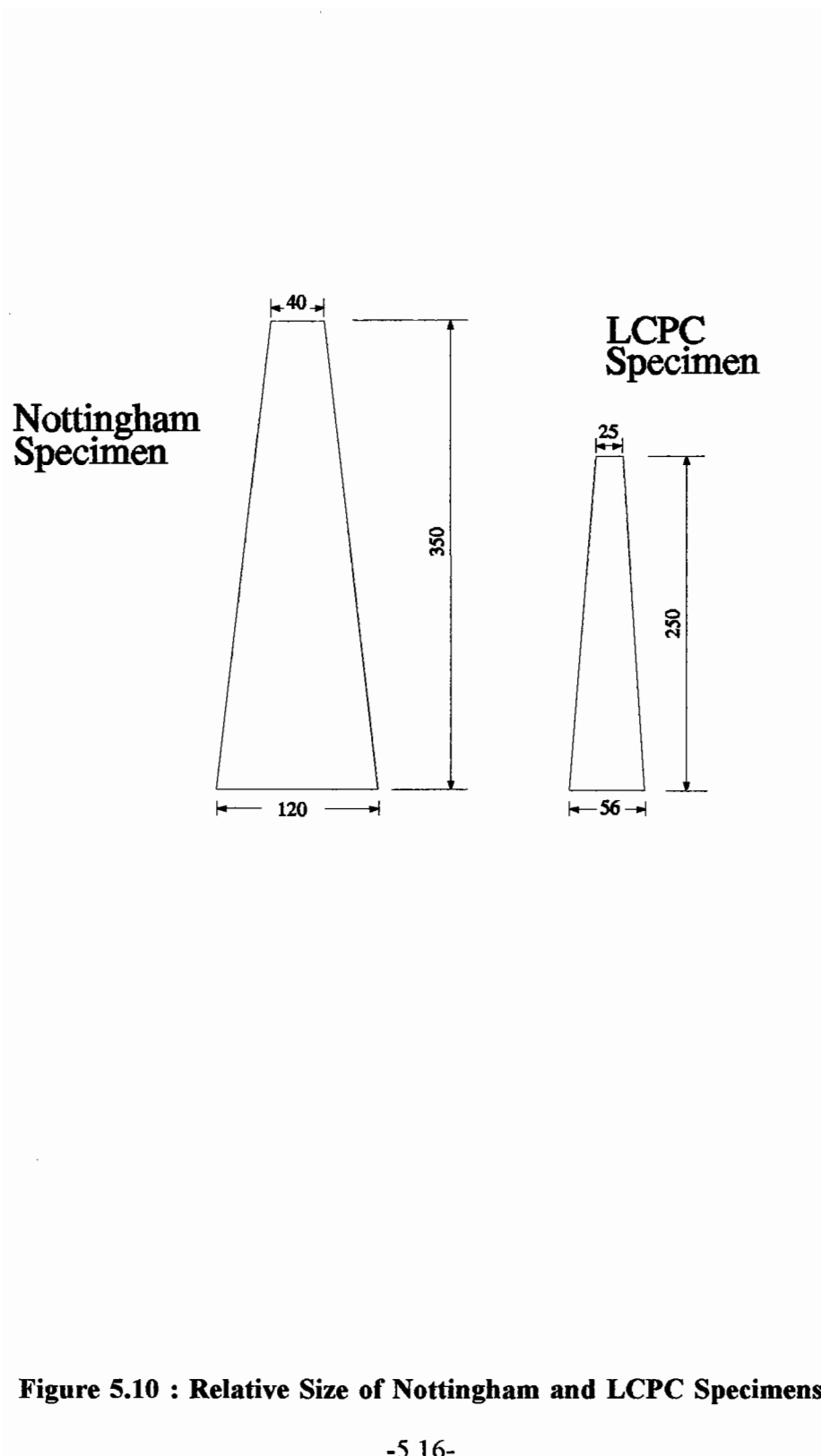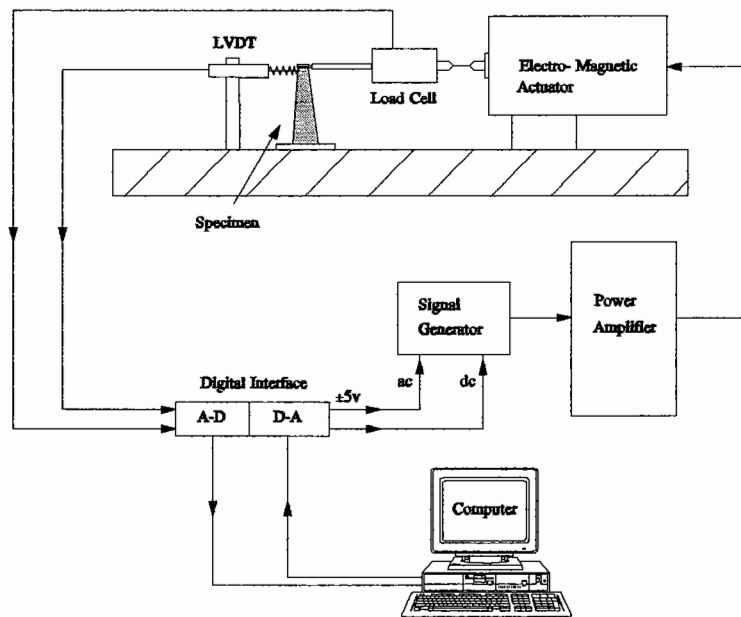
Figure 5.11 : Trapezoidal Cantilever Fatigue Test Apparatus

Temperature was monitored using a dummy specimen placed in a temperature controlled cabinet. This consisted of a core of asphaltic material into which a thermocouple was embedded. The temperature of the sample under test was assumed to be the same as the dummy specimen after a minimum period of twelve hours in the temperature controlled cabinet. In addition, later in the test program, the test software and electronics were modified to enable up to six temperature readings to be taken automatically during the test. These modifications were made to enable quantification of any change in specimen temperature during testing.

Each individual test was conducted at a constant temperature with a total of five different temperatures being used during the programme of tests (0, 4, 10, 20 and 30 °C).

When tested, the specimens were subjected to a bending stress/strain varying sinusoidally between tension and compression at a constant frequency. The deflection at the top of the specimen was measured by a displacement transducer (LVDT) whereas load was measured by a load-cell situated between the specimen and the actuator. The load amplitude was kept constant for the controlled stress tests, but was adjusted for the controlled strain tests to keep the deflection amplitude at the top of the specimen constant.

An analogue control and data acquisition system was used, with digital interfaces added to couple this to a PC, enabling long term tests to be run, with control being maintained and data acquired at pre-determined intervals.

The software for the system enabled control of peak values of either stress or strain along with control of mean stress level/mean deflected position. The development of this software enabled the acquisition and storage of significantly more data than previous studies conducted at the University of Nottingham.

As for the uniaxial testing, it was considered important that the specimen be loaded about a mean position. The necessary modifications were made to the software to allow the mean deflected position to be monitored. It was found that the mean load could be adjusted based simply upon the mean position. This algorithm was simpler than that used for the uniaxial testing and it was considered that the reason why this worked with the beam was a result of; 1) the overall lower load levels applied to the specimen (only the extreme fibre had the maximum stress) and 2) the use of a faster computer (80286 CPU) which effectively enabled control every second (about 20 loading cycles).

Two stress levels were used to test each type of material. The stress level was chosen to give an estimated life of 10^4 and 10^5 cycles for the high and low stress conditions respectively as for the uniaxial testing described above. Binder stiffness, mixture stiffness and the tensile strain required for a given fatigue life (corresponding to fatigue lives of 10^4 and 10^5) were estimated. The required tensile stress (σ_t) and peak to peak load (2P) were then calculated as follows:-

$$\sigma_t = S_m \cdot \epsilon_t \qquad\qquad (5.5)$$

$$2P = \frac{8\ bd^2\ \sigma_t}{3L} \qquad\qquad (5.6)$$

Where b, d, P and L are as defined in Figure 5.12.

During each test, either two or three ASCII files were created on the hard disk of the computer. The first contained a summary of the results, i.e. cycle number, load, complex modulus. The second contained raw wave forms for load and displacement, stored at pre-defined periods during the test. The third, when collected, contained records from thermocouples attached to the specimens or located elsewhere in the temperature control cabinet. Tables 5.1 to 5.3 illustrate typical examples of the data collected in the three ASCII files.

By recording the detail of results as illustrated in Table 5.1 it is possible to observe the mean deflected position versus the mean load applied to ensure that the specimen remains vertical with a mean deflected position of approximately zero. This was considered a quality control check to ensure that failure had occurred by fatigue rather than by creep deformation.

Figure 5.13 shows typical output from the load cell and the LVDT versus reading number, whereas Figure 5.14 shows the hysteresis loop obtained by plotting load cell output versus LVDT output.

BENDING STRESS
TRAPEZOIDAL CANTILEVER

Bending Stress

$$\sigma_t = \frac{K\,PL}{bd^2}$$

Where:-

$$K = \frac{6 \times L}{(L + 2x)^2}$$

Max Bending Stress

$$\sigma_t = \frac{3PL}{4\,bd^2}$$
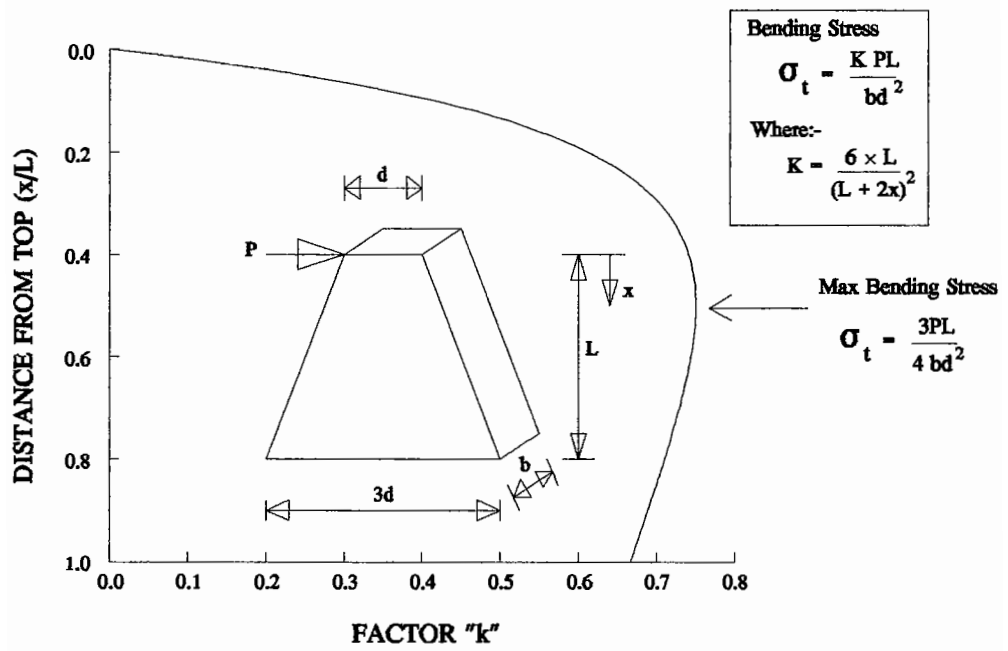
Figure 5.12 : Geometry of the Trapezoidal Fatigue Specimen and Definition of *b*, *d*, *P* and *L*

TRAPEZOIDAL CANTILEVER CONTROLLED STRESS FATIGUE TEST
Summary of Fatigue Test Data
b0w0-5-17   {specimen ref.}
170590   {date}
20Celsius   {title information}
specimen ht=350mm
width of top=40mm
specimen thickness=42mm
Frequency=20Hertz
peak to peak stress=3000Pascals   {stress or strain}
****
Cycles static-Load p-p-Load mean-Defl p-p-Defl. Stiff   {order of results}
     100 -0.05 0.75   617 -72.0 6071
     200 -0.04 0.76   642-160.0 5950   Cycles = No of load cycles.
     300 -0.04 0.77   661-112.0 5831   Static-Load = Load required to stop specimen
     400 -0.04 0.76   682 -70.0 5620   from bending over
     500 -0.04 0.76   684 -23.0 5605   p-p-Load = Peak to peak load.
     600 -0.04 0.77   692 -3.0 5545   mean-Defl = Mean deflection from
     700 -0.04 0.77   713 27.0 5417   centre in microns -
     800 -0.04 0.77   716 39.0 5385   ideally this should be
     900 -0.04 0.77   729 30.0 5273   close to zero.
    1000 -0.04 0.77   730 -23.0 5268   Stiff = Complex modulus of beam.
       .
       .
       .
{results continue, note stiffness is reducing}

       .
    3600 -0.04 0.76 1043 23.0 3676
    3700 -0.04 0.77 1085 24.0 3544
    3800 -0.04 0.76 1173   8.0 3262
    3900 -0.04 0.77 1300   8.0 2961
    4000 -0.04 0.75 1633   7.0 2302
    4100 -0.03 0.65 2858 12.0 1147
    4200 -0.06 0.15 4969 276.0   149

**Table 5.1 : Example of Data Contained in Summary Format from the
Trapezoidal Fatigue Test Apparatus**

TRAPEZOIDAL CANTILEVER CONTROLLED STRESS FATIGUE TEST
Load Cell and lvdt output

		{specimen ref.}
V0W1_1_22		{specimen ref.}
220292		{date}
0Celsius		{temperature}

specimen ht=350mm
width of top=40mm
specimen thickness=42mm
Frequency=20Hertz
peak to peak stress=5000Pascals   {stress or strain}
****

Reading Load lvdt   {order of results}
Cycle No.=114   {cycle no. in fatigue test}

1	3548	568	
2	3289	553	
3	3088	532	Reading - one hundred and sixty
4	2818	507	readings were taken each time a
5	2416	492	signal was read from the digital
6	2071	462	interface. At a frequency of
7	1780	439	20 Hertz this represents approx.
8	1380	383	2.5 periods.
9	916	379	Load = Load cell bits
10	555	369	lvdt = LVDT bits
11	166	345	
12	-276	275	Note: bits converted to load and
13	-676	247	displacement using calibration
14	-977	217	factor used in software.

.
.
.

(continued)

.
.
.

159	-2814	72
160	-3129	34

Cycle No.=1016

1	3742	552
2	3942	576
3	4185	607

.
.

(continued)

Table 5.2 : Example of Raw Data from Digital Interface (load cell and LVDT output) from the Trapezoidal Fatigue Test Apparatus

TRAPEZOIDAL_CANTILEVER_CONTROLLED_STRAIN_FATIGUE_TEST
Summary_of_Fatigue_Test_Temperature_Data
V1W1-5-93
300191   (specimen reference information)
20Celsius
specimen_ht=350mm
width_of_top=40mm
specimen_thickness=44mm
Frequency=20Hertz
strain200
****

Cycles	temp1	temp2	temp3	temp4	temp5	temp6	(records from six
17	20.0	20.3	20.4	20.4	20.5	20.5	thermocouples)
53	19.9	20.3	20.4	20.4	20.5	20.4	
90	19.9	20.2	20.4	20.4	20.4	20.4	
125	19.9	20.2	20.4	20.3	20.4	20.4	
174	19.9	20.3	20.4	20.4	20.5	20.4	
211	19.8	20.2	20.4	20.3	20.4	20.4	
246	19.8	20.2	20.4	20.3	20.4	20.5	
281	19.8	20.1	20.4	20.2	20.4	20.3	
316	19.8	20.3	20.3	20.3	20.5	20.5	
351	19.8	20.2	20.4	20.2	20.4	20.4	
385	19.8	20.0	20.3	20.0	20.4	20.4	

.

. (Continued)

.

Cycles	temp1	temp2	temp3	temp4	temp5	temp6
9403	20.2	20.3	20.3	20.3	20.7	20.6
9511	20.2	20.2	20.3	20.3	20.7	20.6
9618	20.2	20.2	20.4	20.3	20.6	20.4
9707	20.1	20.1	20.2	20.2	20.6	20.4
9815	20.1	20.2	20.3	20.2	20.6	20.4
9905	19.9	20.1	20.3	20.2	20.5	20.5
10011	20.0	20.1	20.2	20.1	20.4	20.6
10115	20.0	20.1	20.0	20.0	20.6	20.3
10205	19.8	20.0	20.2	20.1	20.4	20.4
10311	19.8	20.1	20.1	20.0	20.4	20.4
10401	19.7	20.1	20.2	20.0	20.4	20.6
10509	19.8	20.1	20.1	20.0	20.4	20.3
10616	19.8	20.1	20.2	20.0	20.4	20.4
10706	19.6	20.0	20.1	20.0	20.3	20.3
10813	19.8	20.1	20.1	20.0	20.2	20.2

(Temperature records cease at end of test)

Table 5.3 : Example of Temperature Data from Digital Interface (six thermocouples generally located on specimen surface) from the Trapezoidal Fatigue Test Apparatus
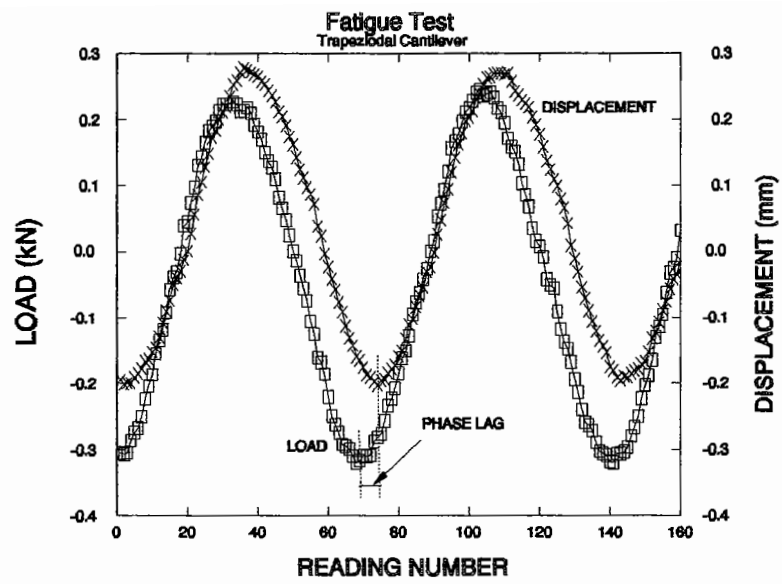
Figure 5.13 : Typical Load and Displacement Signals versus Time (reading Number) Obtained from the Trapezoidal Fatigue Test Apparatus
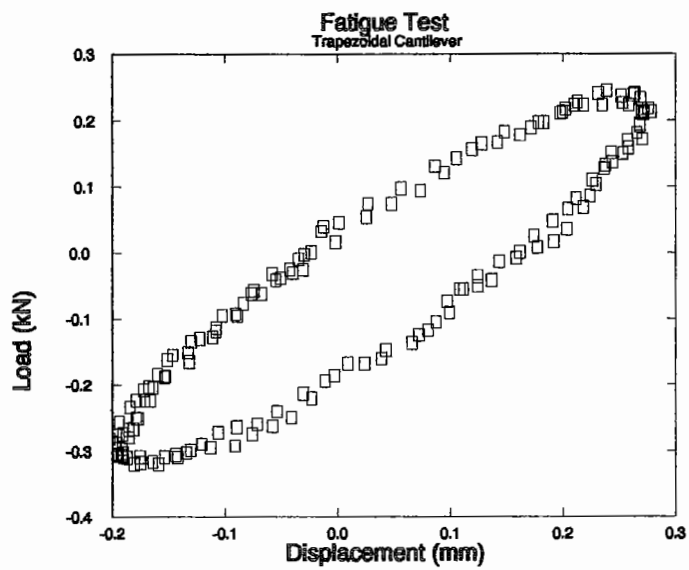
**Figure 5.14 : Typical Hysteresis Loop Obtained from the Trapezoidal
Fatigue Test Apparatus**

Analysis of the data files after completion of testing enabled calculation of the phase angle between the load and displacement signals. The deflection and load amplitudes were used in both test modes to calculate the complex stiffness modulus, E^*.

The values of E^* quoted have been calculated from deflections due to both bending and shear stress. The deflection due to shear was approximately 6% of the total deflection, dependent upon specimen geometry and this was calculated assuming a Poisson's ratio of 0.35 using the procedures described below.

An analysis of the trapezoidal cantilever beam has been carried out by two different methods; 1) using conventional bending theory and, 2) using finite element analysis.

The simple theory of bending states:-

$$\frac{M}{I} = \frac{\sigma}{y} = \frac{E}{R}$$ (5.7)

Where M =   bending moment

           I =   moment of inertia

           σ =   stress at distance y from the neutral axis

           E =   elastic modulus

           R =   radius of curvature

The following symbols are used:-

           δ =   deflection at top of beam

θ =   slope of beam centerline (1/R)

l =   length of beam

D =   depth of beam at any point

d =   smallest depth of beam

b =   breadth of beam

w =   load applied to beam perpendicular to the neutral

                             axis

x =   distance from point of loading where D = d

G =   shear modulus

μ =   Poisson's ratio

γ =   shear stress

τ =   shear strain

The analysis is performed for the beam with variable base top width, ie.

$$D \; max = jd \qquad\qquad (5.8)$$

$$Therefore \quad D = d + (j-1)\frac{dx}{l} \qquad\qquad (5.9)$$

$$and \; I = \frac{bd^3(l+(j-1))^3}{12l^3} \qquad\qquad (5.10)$$

Firstly a general equation for slope between two points x = A and x = B is derived, and then an equation for deflection due to bending. Finally, calculation of shear deflection is carried out. The calculation of slope is performed as follows:-

$$\text{Considering } \theta_{AB} = \int_{x=A}^{x=B} \frac{M}{EI} dx \quad \text{where } M = wx \qquad (5.11)$$

$$\text{let } K = \frac{Ebd^3}{12l^3} \qquad (5.12)$$

$$\text{and } Q = j-1 \qquad (5.13)$$

$$\text{then } K\,\theta_{AB} = \int - \frac{wx}{(l+Qx)^3} \, dx \qquad (5.14)$$

Substituting $u = l + Qx$, gives;

$$\frac{du}{dx} = Q, \quad dx = \frac{du}{Q}, \quad x = \frac{u-l}{Q} \qquad (5.15)$$

Integrating and substituting limits, $\theta_{AB} = 0$ when $x = l$, gives;

$$\theta_{AB} = \frac{W}{KQ^2} \left[\frac{1}{1+Qx} - \frac{l}{2(l+Qx)^2} - \left(\frac{1}{(1+Q)} - \frac{1}{2(1+Q)^2} \right) \frac{1}{l} \right] \qquad (5.16)$$

The calculation of bending deflection is as follows:-

$$\int_A^B \theta = \delta_{AB} \qquad (5.17)$$

$$\text{let } u = l + Qx \text{ and } K = \frac{Ebd^3}{12l^3} \quad (as\ above) \qquad (5.18)$$

$$\textit{Also,} \quad R = \left[\frac{1}{(1+Q)} - \frac{1}{2(1+Q)^2} \right] \qquad (5.19)$$

$$\textit{then} \; K \, \delta_{AB} = \frac{-w}{Q^2} \int -\frac{1}{(l+Qx)} + \frac{l}{2(l+Qx)^2} + \frac{R}{l} dx \qquad (5.20)$$

Integrating and substituting limits; $\delta_{AB} = 0$ when x = 1, gives;

$$\delta_{AB} = \frac{12wl^3}{2QEbd^3} \left[\begin{array}{c} (\ln(l+Qx) + \dfrac{l}{2(l+Qx)} - \dfrac{R(l+Qx)}{l} + \\[3mm] R\,(1+Q) - \dfrac{1}{2(1+Q)} - \ln\,(1+Q)l \end{array} \right] \qquad (5.21)$$

When $x = 0$ (ie deflection at point of loading), we obtain;

with $j = 3$ (Nottingham specimen)

$$\delta = 0.31458 \, \frac{wl^3}{Ebd^3} \qquad (5.22)$$

with $j = 2.24$ (LCPC specimen)

$$\delta = 0.38898 \, \frac{wl^3}{Ebd^3} \qquad (5.23)$$

The deflection of a beam occurs due to both bending stresses and shear stresses. The calculation of deflection resulting from shear is as follows:-

$$G = \frac{E}{2(1+\mu)} \qquad (5.24)$$

-5.30-

$$\tau = \frac{w}{bd\left[1+\frac{(j-1)x}{l}\right]} \qquad (5.25)$$

$$\gamma = \frac{w}{bd\left[1+\frac{(j-1)}{l}\right]} \cdot \frac{2(1+\mu)}{E} \, dx \qquad (5.26)$$

$$shear\ deflection\ \delta_{AB} = \int_A^B \frac{\dfrac{w}{bd(1+\frac{(j-1)x}{l})}}{} \cdot \frac{2(1+\mu)}{E} \, dx \qquad (5.27)$$

Integrating and substituting limits, when x = 0 δ = 0, gives;

$$\delta = \ln j \left[\frac{2(1+\mu)w}{Ebd(j-1)}\right] \qquad (5.28)$$

$$for\ j = 3\delta = 1.09861\ (1+\mu)\ \frac{wl}{Ebd} \qquad (5.29)$$

$$and\ j = 2.24 \quad \delta = 1.30077\ (1+\mu)\ \frac{wl}{Ebd} \qquad (5.30)$$

The total deflection is equal to the shear deflection plus the bending deflection and is calculated as follows:-

with $j = 3$ (Nottingham specimen)

$$\delta = \frac{wL}{Ebd}\left[1.09861(1+\mu) + 0.31458\frac{L^2}{d^2}\right] \qquad (5.31)$$

with $j = 2.24$ (LCPC specimen)

$$\delta = \frac{wL}{Ebd}\left[1.30077(1+\mu) + 0.38898\frac{L^2}{d^2}\right] \qquad (5.32)$$

Assuming $\mu = 0.35$ then shear deflection equals 5.8% of total deflection for a beam with $j = 3$.

The dimensions of the Nottingham specimen *Dmax* $= 3d$ ($j = 3$) were chosen to achieve the maximum value of tensile stress at half height (when x equals $0.5l$) of the specimen. The analysis for this configuration is as follows:-

$$using \ \sigma = \frac{My}{I} \qquad (5.33)$$

$$\sigma = \frac{6wl^2}{b} \cdot \frac{x}{(ld+2xd)^2} \qquad (5.34)$$

$$when \ \frac{d\sigma}{dx} = 0 \ then \ \sigma = max \qquad (5.35)$$

Differentiating gives;

$$\frac{d\sigma}{dx} = \frac{6wl^2}{b} \cdot \frac{(ld+2xd)-4dx}{(ld+2xd)^3} \qquad (5.36)$$

$$\text{let } \frac{d\sigma}{dx} = 0 \qquad\qquad (5.37)$$

$$\text{therefore } ld = 2xd \qquad\qquad (5.38)$$

$$\text{and } x = \frac{l}{2} \text{ when } \sigma = \text{max} \qquad\qquad (5.39)$$

A second analysis was conducted using the Finite Element program FEPS (Sharrock, 1983). This approach consists of a finite element analysis using 8 node parabolic isoparametric elements. For this study the Nottingham specimen was considered to be in a plane stress situation with both end plates behaving in a perfectly rigid manner. Rotation of the top plate was allowed. These assumptions, although not strictly correct, were considered to be indicative of the expected behaviour. Assuming an Elastic Modulus = 10000 MPa and Load = 2 kN, the finite element analysis gave a deflection (δ) of 1.11172 mm. This compares to a computed value of 1.11186 mm for a beam with the same dimensions.

Graphical representations of the analysis are given in Figures 5.15 to 5.21 for; mesh and deflected shape, major principal stress (P1), minor principal stress (P2), angle between P1 and x axis, normal stress component in plane perpendicular to x (Sx), normal stress component in plane perpendicular to y(Sy) and shear stress component on planes perpendicular to x & y (Sxy) respectively. The units of stress given are in the figures are MPa × 10.
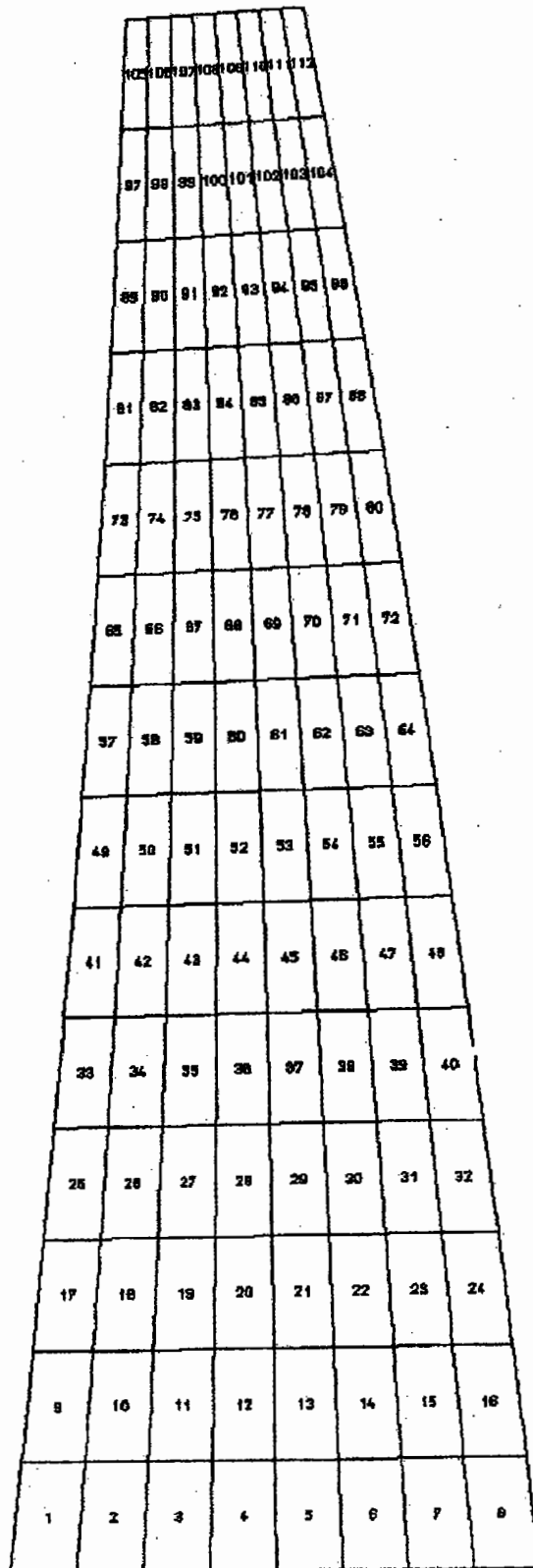
Figure 5.15 : Mesh and Deflected Shape

TRAPEZOIDAL CANTILEVER BEAM

MINIMUM = -13.6   MAXIMUM = 83.2

```
A = -10
B = 0
C = 10
D = 20
E = 30
F = 40
G = 50
H = 60
I = 70
J = 80
```

y

x

2 kN HORIZONTAL LOAD
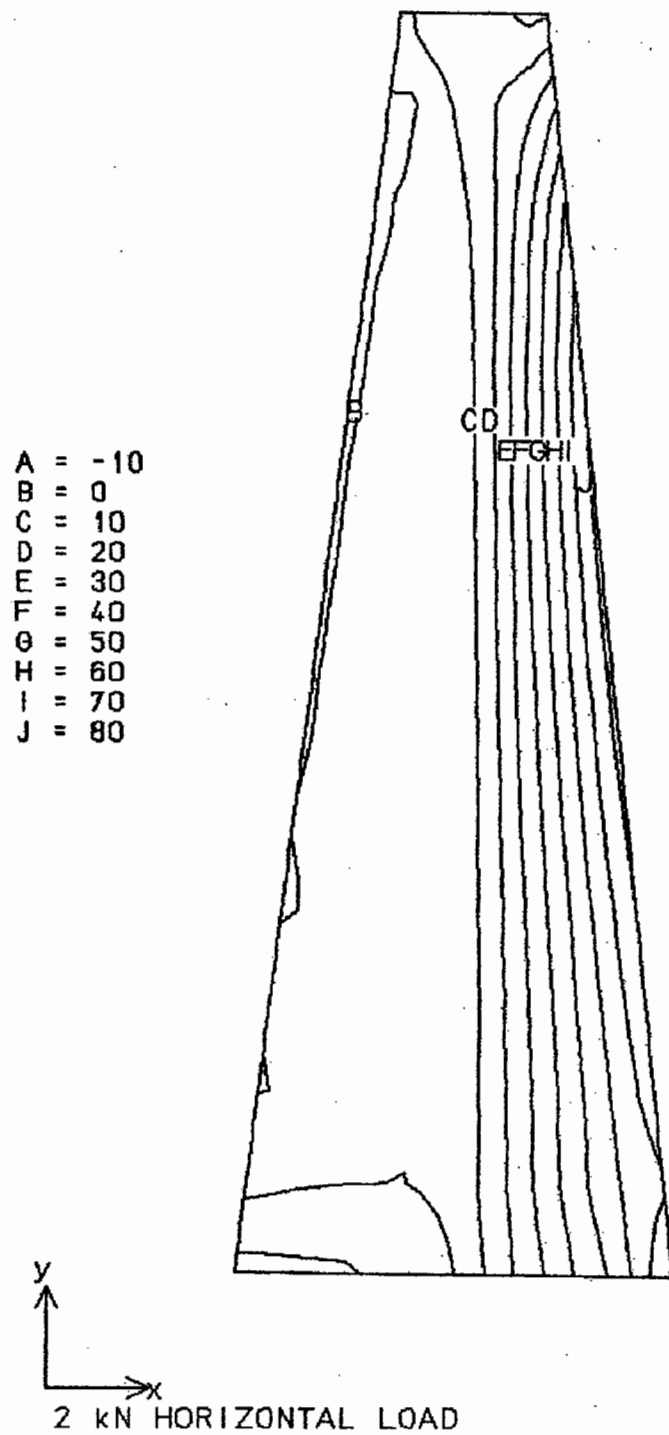
Figure 5.16 : Major Principal Stress (P1)

-5.35-

TRAPEZOIDAL CANTILEVER BEAM

MINIMUM = -83.2   MAXIMUM = 13.6

A = -80
B = -70
C = -60
D = -50
E = -40
F = -30
G = -20
H = -10
I = 0
J = 10

y

x

2 kN HORIZONTAL LOAD
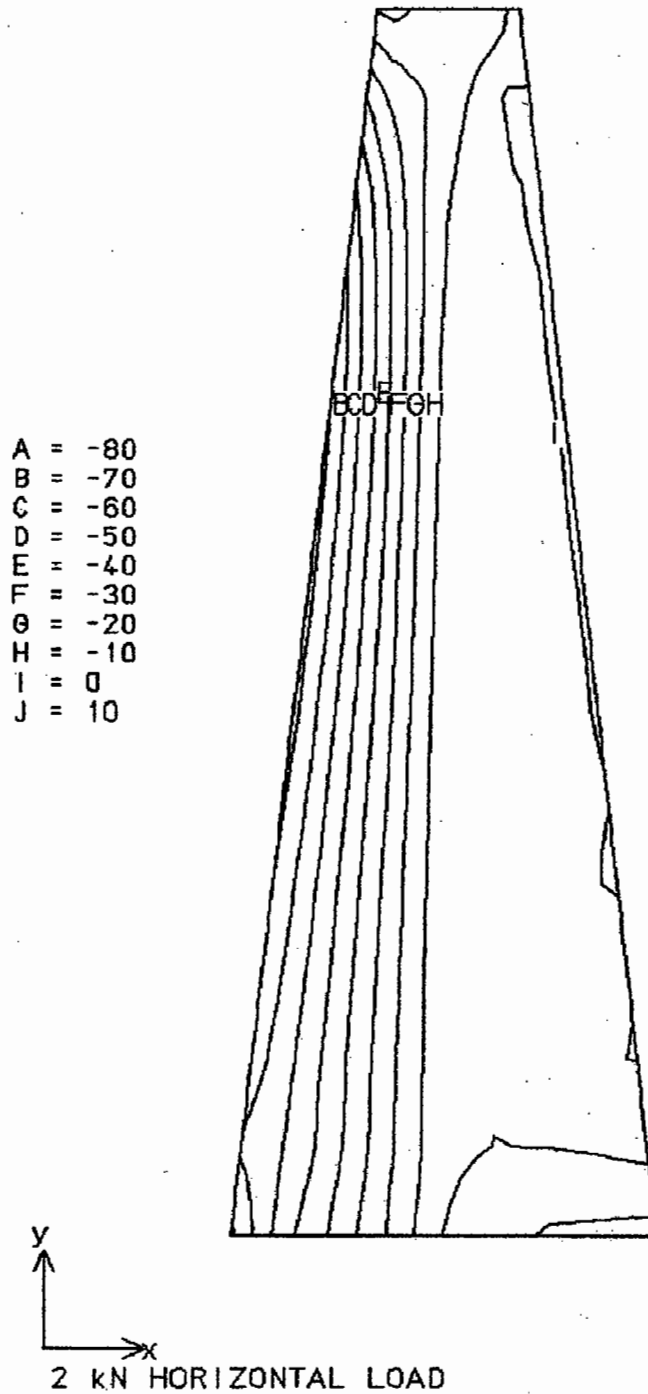
Figure 5.17 : Minor Principal Stress (P2)

-5.36-
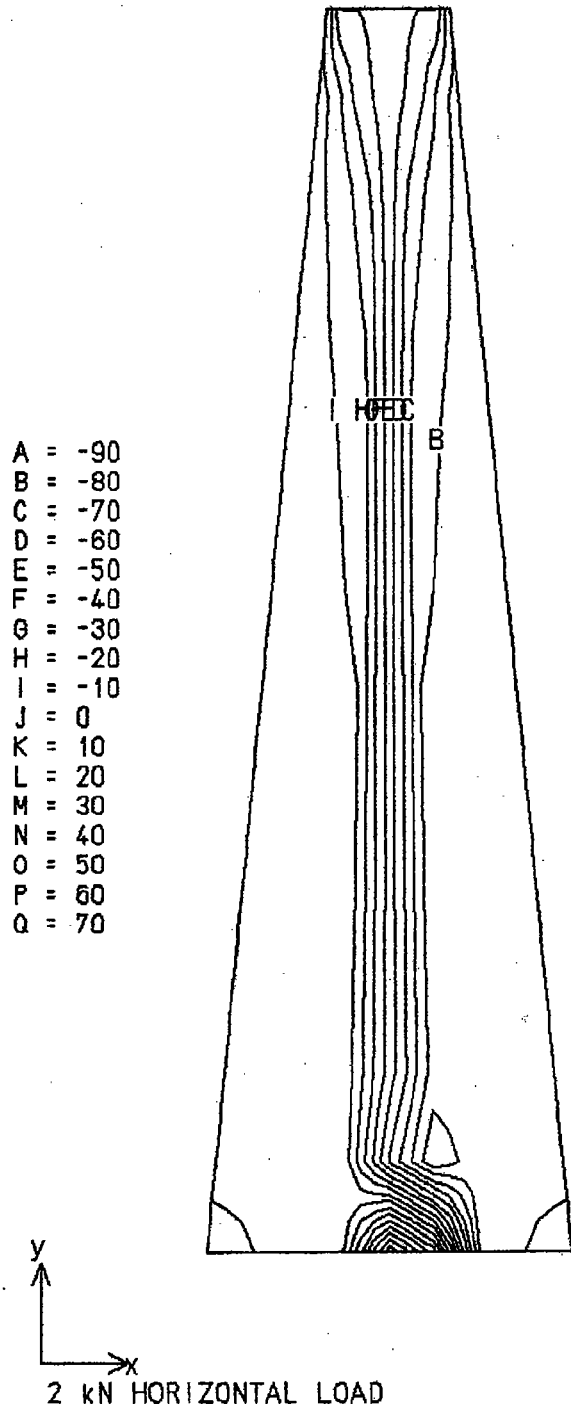
Figure 5.18 : Angle between Major Principal Stress (P1) and x axis

TRAPEZOIDAL CANTILEVER BEAM

MINIMUM = -18.8   MAXIMUM = 18.8

A = -18
B = -15
C = -12
D = -9
E = -6
F = -3
G = 0
H = 3
I = 6
J = 9
K = 12
L = 15
M = 18

2 kN HORIZONTAL LOAD
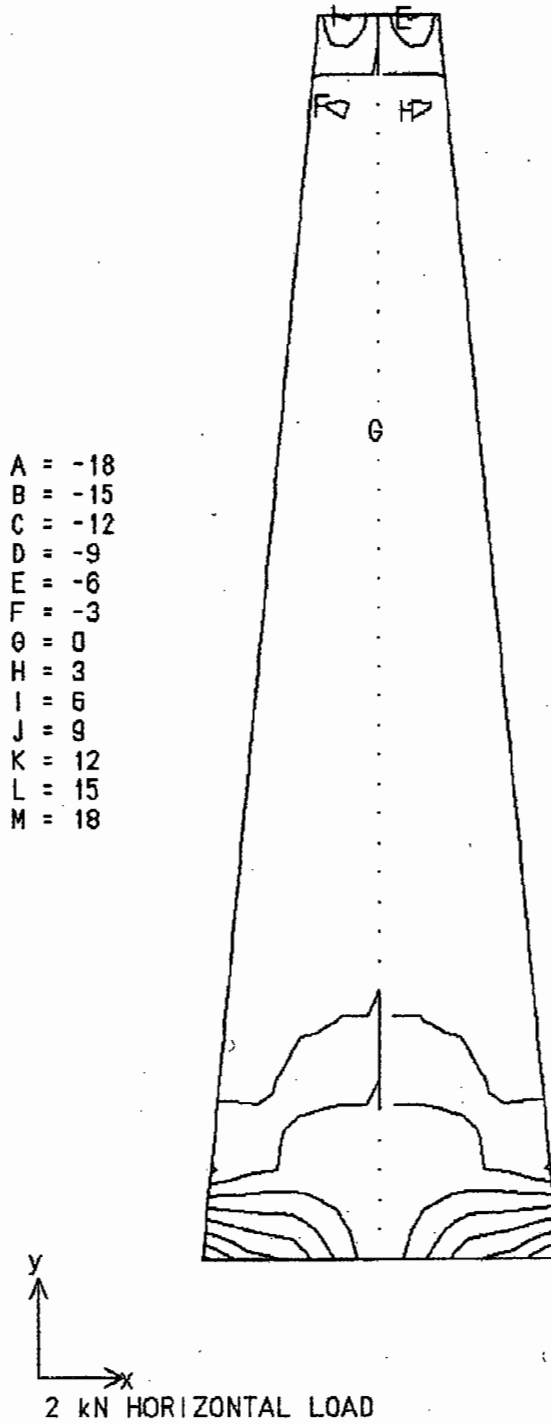
Figure 5.19 : Normal Stress Component in Plane Perpendicular to x (Sx)

-5.38-

TRAPEZOIDAL CANTILEVER BEAM

MINIMUM = -82.1   MAXIMUM = 82.1

A = -80
B = -70
C = -60
D = -50
E = -40
F = -30
G = -20
H = -10
I = 0
J = 10
K = 20
L = 30
M = 40
N = 50
O = 60
P = 70
Q = 80

2 kN HORIZONTAL LOAD
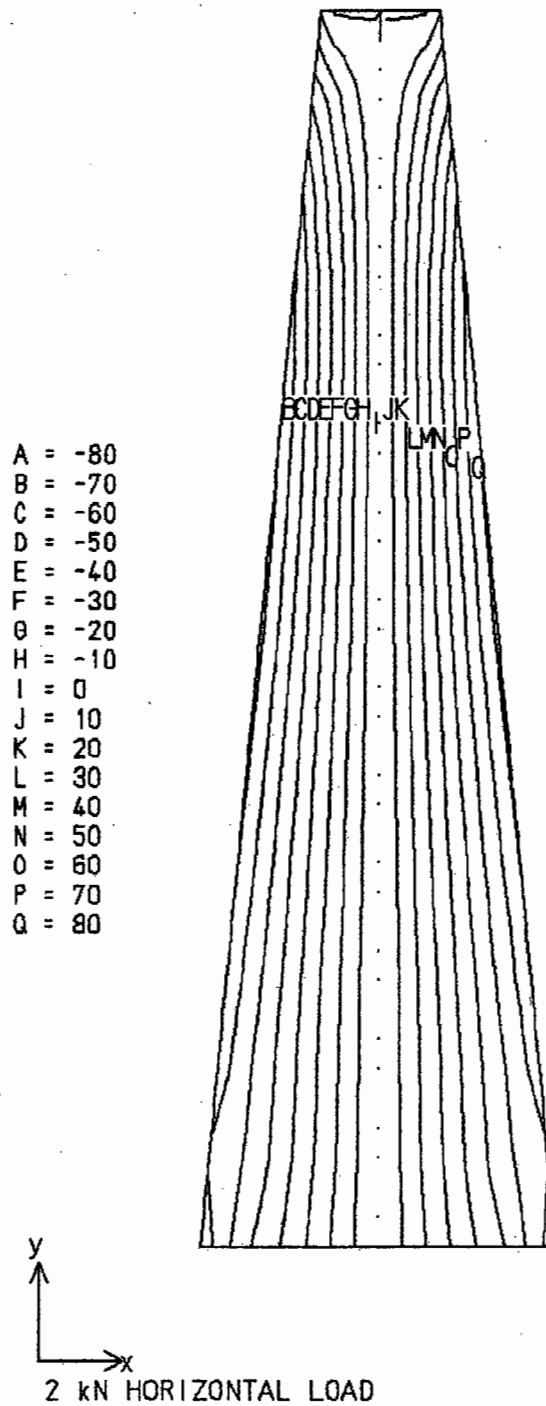
Figure 5.20 : Normal Stress Component in Plane Perpendicular to y (Sy)

-5.39-

TRAPEZOIDAL CANTILEVER BEAM

MINIMUM = -20.2   MAXIMUM = 2.2

A = -20
B = -18
C = -16
D = -14
E = -12
F = -10
G = -8
H = -6
I = -4
J = -2
K = 0
L = 2

y

2 kN HORIZONTAL LOAD
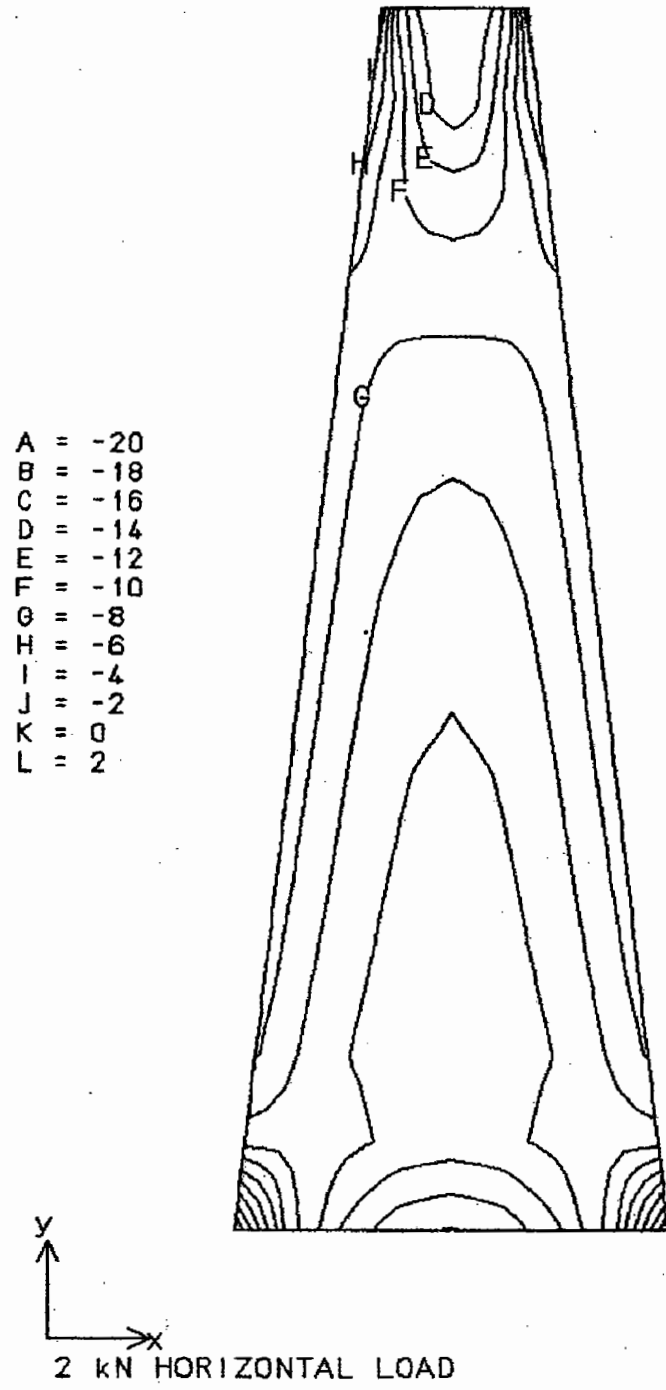
**Figure 5.21 : Shear Stress Component on Planes
Perpendicular to x & y (Sxy)**

-5.40-

In summary the complex stiffness modulus can be calculated as follows:-

$$S = \frac{PL}{bd\delta}\left[C1\ \frac{L^2}{d^2} + C2\ (1+\mu)\right] \qquad (5.40)$$

where; $C1$ = 0.31458 and $C2$ = 1.09861 for the Nottingham specimen

and $C1$ = 0.38898 and $C2$ = 1.30077 for the LCPC specimen.

The testing mode, frequency, temperature and compaction level (void content) are included in the tables containing the test results.

The definition of failure adopted generally is dependent upon the mode of testing. A reduction of specimen complex modulus to 50% of the initial value is used to define the number of cycles to failure, Nf, for the controlled strain testing whereas a value of 10% is used for the controlled stress testing. At 10% of the initial complex modulus the specimens contained large cracks. In the controlled strain test the specimens were generally "visually" intact at 50% reduction in complex modulus. However, if the controlled strain tests were continued to 10% of the initial complex modulus a large crack was evident in the specimens.

Note: Crack length was not quantified during the testing.

Figure 5.22 illustrates the above definitions of Nf for the two modes of loading used in the fatigue tests. Generally, the controlled strain tests were stopped after a 80% reduction in stiffness. This level of stiffness reduction was chosen
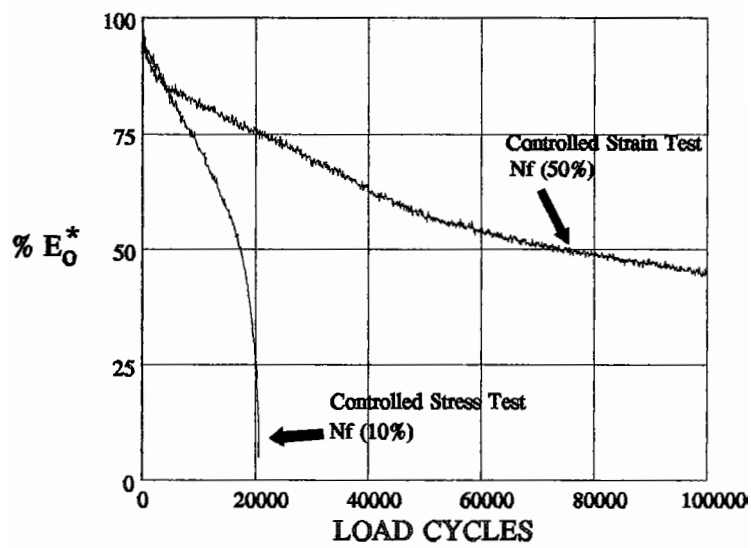
Figure 5.22 : Definition of Failures in Controlled Strain and Stress Tests

to enable investigation of the crack initiation using an energy ratio concept (see Chapter 6). It was considered from a preliminary analysis that the cracks should form at around 50% stiffness reduction and if the tests where stopped at this level of stiffness it would not have been possible to investigate this aspect.

5.3   FATIGUE WHEEL TRACK TESTING

The testing consisted of applying a moving wheel load to asphalt slabs (instrument with strain gauges) and monitoring the strain induced on the underside of the slab. The tests were stopped at the onset of longitudinal wheel-path cracking on the top surface of the slab.

Two strain gauges on the underside of each slab measured the transverse tensile strain, considered to be associated with fatigue. Evaluation of the mixture performance was made by considering the level of this tensile strain (ε_t) versus the number of wheel applications required to produce a pre-defined degree of damage, (fatigue life *N1*). Where three tests were carried out per cell different initial strain levels were targeted in order that a relationship of log ε_t versus log *N1* would be produced. This type of relationship is illustrated in Figure 5.23. In all cases a slope for the fatigue line has been estimated enabling comparisons to be made on an equal basis.

The Slab Test Facility (STF) is a moving wheel loading apparatus in which
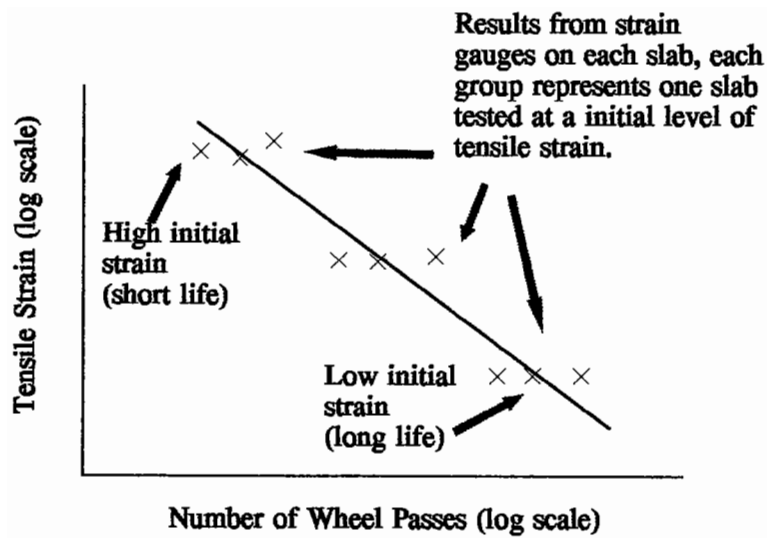
Figure 5.23 : Typical Fatigue Relationship

asphalt slabs can be subjected to simulated vehicle loading under controlled conditions. The loading system is a linear tracking, servo controlled hydraulic apparatus.

A side view of the STF is illustrated diagrammatically in Figure 5.24. The carriage supporting the wheel is driven by means of a wire rope tensioned around a drum, which is axially coupled to a servo controlled motor. A feedback displacement transducer produces a voltage proportional to wheel position and, when differentiated, a signal proportional to velocity. This is compared to the command velocity signal set by an electronic control unit and any difference is minimised by sending a signal to a servo valve which rapidly corrects the motor speed. Once over the slab, trigger voltages at each end, representing position, are used to stop the carriage and a circuit to detect zero speed then commands reversal. The result is a controlled reciprocation of the carriage at a constant speed over the slab.

The loading arrangement is by means of twin beams acting as a lever on the moving carriage. Constant wheel load over the slab can only be achieved by applying an increasing actuator load of the correct "slope" as the wheel approaches the actuator. This is conveniently obtained by using the carriage position voltage as a command signal which increases as the carriage approaches the actuator. An in-line load cell attached to the actuator shaft provides feedback voltage proportional to the actuator load. This is compared to the signal level representing the required load set at the electronic control unit, which operates the hydraulic actuator through a servo valve so that it
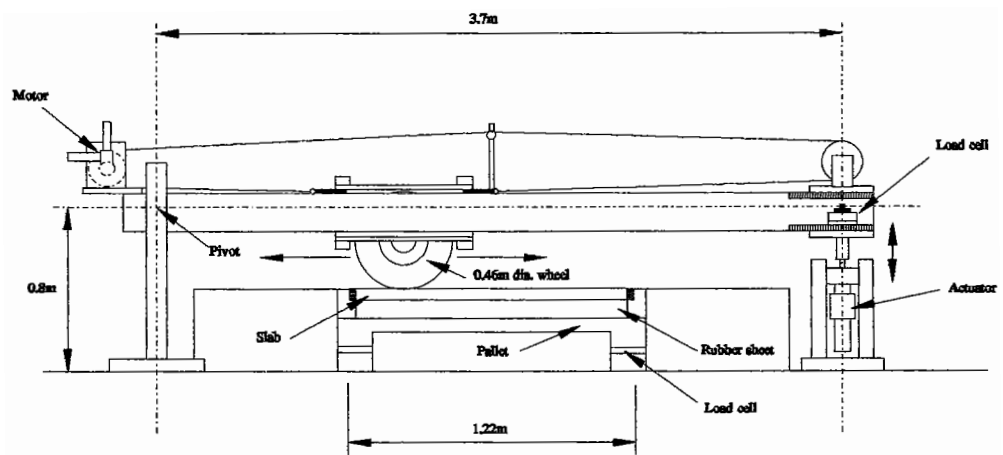
Figure 5.24 : The Slab Test Facility

maintains a constant wheel load during carriage movement over the slab. Actuator displacement has to be responsive as it has to react to the lever deflection, tyre, slab and support compression during loading. Slab load is also measured by load cells placed under each corner of a steel pallet. The upper plate of the pallet is detached so that different reinforcement can be inserted between it and its supporting frame, thus enabling different support conditions to be obtained. Figure 5.25 shows the general experimental arrangement for this programme testing using the Slab Test Facility. Bidirectional tracking was employed, with no transversing (lateral wander). The loading wheel was fitted with a pneumatic tyre which could be inflated to give a maximum contact pressure of around 650 kPa. Pavement temperature could be cycled or maintained constant anywhere within the range 15°C to 30°C. For this programme a tyre pressure of 380 kPa and a constant temperature of 20°C was used.

Slabs were manufactured in a steel mould measuring 1.0 m in length, 0.5 m in width and 0.05 m in depth. Following instrumentation, the slab was lifted into position, being supported on a rubber mat 92 mm thick. The complex modulus of the rubber was obtained by conducting cyclic loading tests on a specimen in compression at a temperature of 20°C (see Table 5.4). The results obtained indicated that in the range of frequencies 1 to 10 Hertz, the complex modulus was approximately 10 MPa. The thickness of the mat was chosen in order to achieve a level of tensile strain in the approximate range 50 to 500 micro-strain at the underside of the asphalt slabs. The rubber mat was supplied in sheets 11.5 mm in thickness and 8 individual sheets were glued together to
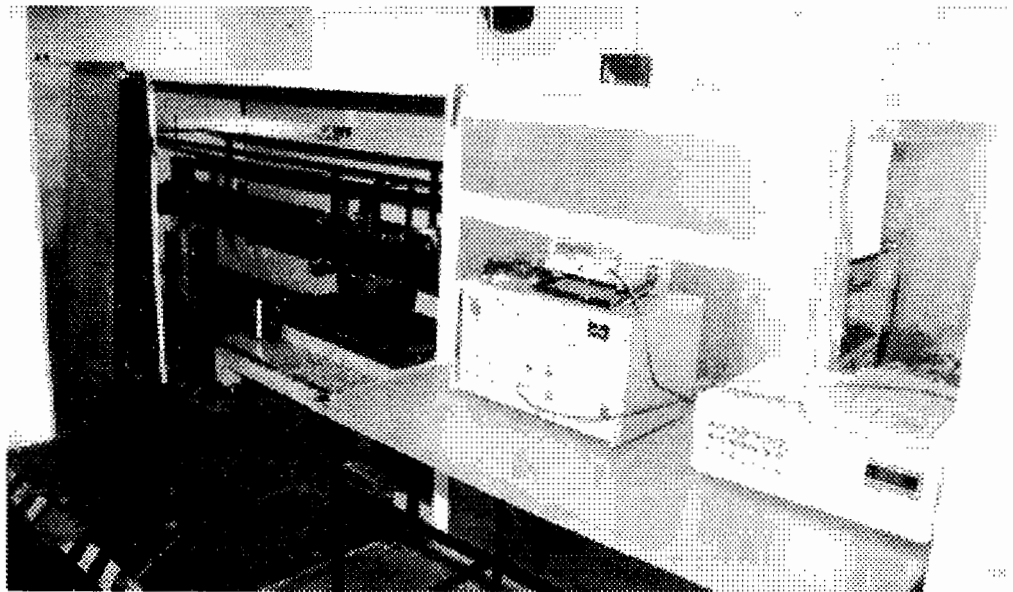
Figure 5.25 : General Experimental Arrangement for the Fatigue Wheel Tracking Apparatus

produce the 92 mm support mat.

A structural analysis (using elastic layer analysis) of the slab test facility was then performed to determine the "mode factor" (Monismith and Deacon, 1969) which is defined as:

$$MF = \frac{A - B}{A + B} \qquad (5.41)$$

where: A = the percentage change in stress due to a stiffness decrement of "C" percent.

B = the percentage change in strain due to a stiffness decrement of "C" percent.

The mode factor has been used to assess the mode of fatigue testing, (ie. controlled stress or strain) which best simulates actual pavement conditions. The mode factor assumes a value of -1 for controlled stress conditions and +1 for controlled strain conditions.

The analysis of stress and strain for the pavement structure in the slab test facility indicated that the MF would be in the range -0.70 to -0.77. Thus, the conditions simulated are closer to those obtained in controlled stress. If similar calculations are carried out for typical full scale pavement structures a mode factor range of -0.70 to -0.77 would be associated with a thick (eg. greater than 150 mm) structural layer. Thus, laboratory scaling results in the thin asphaltic layer (50 mm depth) in the STF representing a relatively thick (> 150 mm

Frequency (Htz)	E* (MPa)	No. of Tests
1	9.0	2
4	9.3	4
10	10.1	9

Table 5.4 : Complex Modulus Test Results Obtained with Rubber Support Material

depth) full scale pavement structure.

5.3.1 Instrumentation and test procedure

The manufactured slabs, contained within the side walls, were placed upside down on a rubber mat to allow attachment of strain gauges with epoxy resin. The underside of most slabs were instrumented with eight 60 mm 120 ohm strain gauges and subsequently painted white using an emulsion paint, after which they were carefully placed upon the rubber mat which was positioned on a steel pallet within the test apparatus (see Figure 5.26). The position of the strain gauges is indicated in Figure 5.27. Slabs 1 to 3 (A-004 test programme) were only instrumented with 7 gauges, gauge number. 8 being omitted. Gauge 8 was found to be necessary to monitor large residual/delayed elastic-visco-plastic transverse strain.

At this stage the slabs were left for a minimum period of two hours to allow any accumulated residual stress associated with moving the slab to relax before starting the tests.

The strain was measured using a quarter bridge arrangement with strain gauge amplifiers and output was monitored using a digital oscilloscope. The detailed test procedure was as follows:-

i) The equipment was switched on with the wheel position off the slab, zero load and speed.
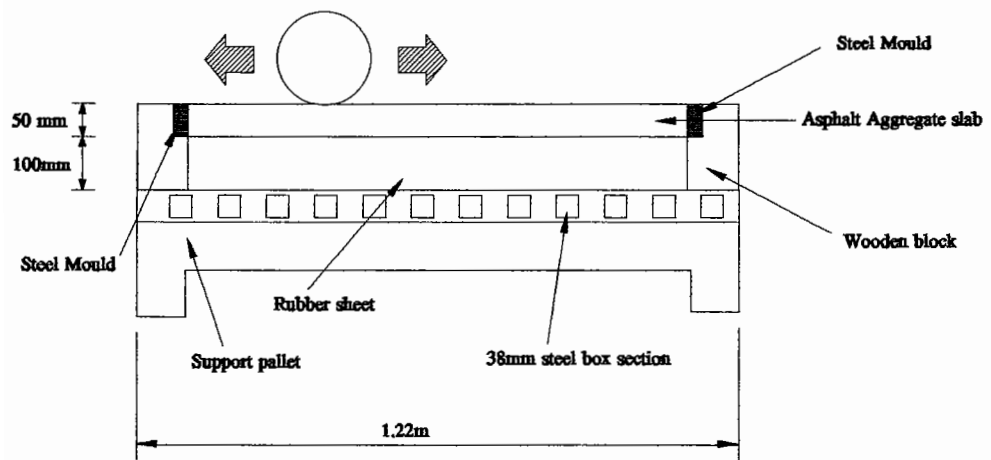
Figure 5.26 : Slab Details for Fatigue Wheel Tracking Tests
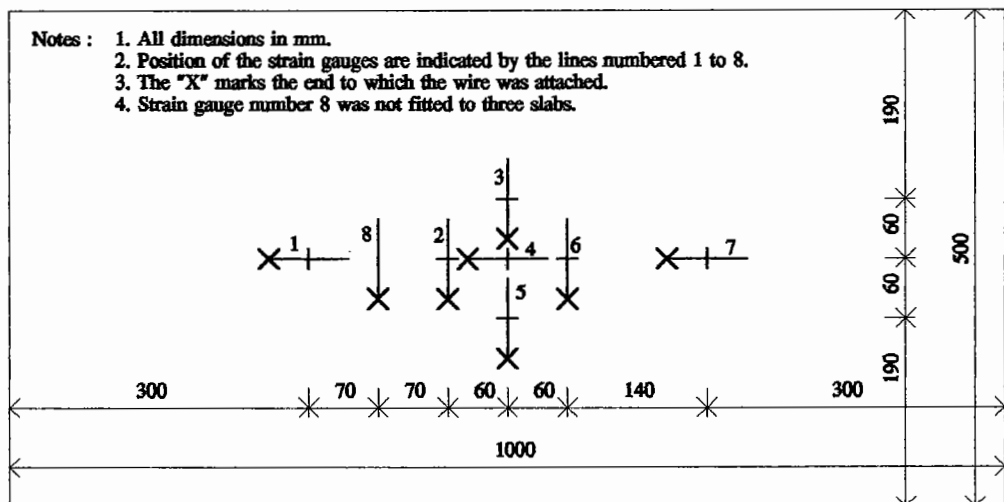
Figure 5.27 : Location of Strain Gauges on Underside of Fatigue Wheel Tracking Slabs

ii) The speed control was used to increase the speed to 30 passes per minute with zero load. The equipment was allowed to run in this mode to "warm up" until smooth passage to and fro was established.

iii) The cycle counter was reset to zero and load applied by turning the load control until the desired strain was achieved from gauge 4. Gauge 4 was always used as the "target gauge" for obtaining the applied load. The reading on the "load control" was noted and a plot of all gauges output taken. It took approximately 5 load cycles to achieve the correct load level and the first plot of the results was normally obtained at approximately cycle number twenty.

Plots of voltage output from the strain gauge amplifiers were obtained periodically (on approximately a logarithmic basis) during the running of the test. Tests were continued until cracking was apparent in the slabs or until an excess of two hundred and fifty thousand wheel passes had been applied. After testing, the slabs were photographed to record the extent of cracking and eight cores were taken to determine density and stiffness. After the cores were abstracted the remaining parts of the slab were discarded.

The testing work commenced in June 1991 with a trial slab tested in order to gain familiarity with the equipment and continued until October 1992 with the completion of all the laboratory tests.

The time required for each test (including instrumentation) was approximately one month.

5.3.2 *Strain gauges*

Four different types of strain were measured during the testing work as follows:-

i)   Transient longitudinal strain under the centre line of the loaded strip.

ii)   Transient transverse strain under the centre line of the loaded strip.

iii)   Transient transverse strain at a 300 mm offset distance from the centre line of the loaded strip.

iv)   Residual/delayed elastic, visco-plastic transverse strain under the centre line of the loaded strip.

A typical example of each strain gauge output is presented in Figures 5.28 to 5.31. It should be noted that in the longitudinal direction (gauges 1, 4 and 7) both compressive and tensile strains occur whereas in the transverse direction (gauges 2, 3, 5, 6 and 8) there is only tensile strain which is not completely recovered during each wheel pass. The residual/delayed elastic-visco-plastic transverse strain was specifically measured with gauge 8 (Figure 5.30). Figure 5.31 shows an example of the typical magnitude of this strain increase with increasing number of load applications. The shape of the transverse strain measured off the centre line (gauges 3 and 5) was similar to that under the centre line (gauges 2 and 6) but of a lower magnitude. Gauges 3 and 5 were
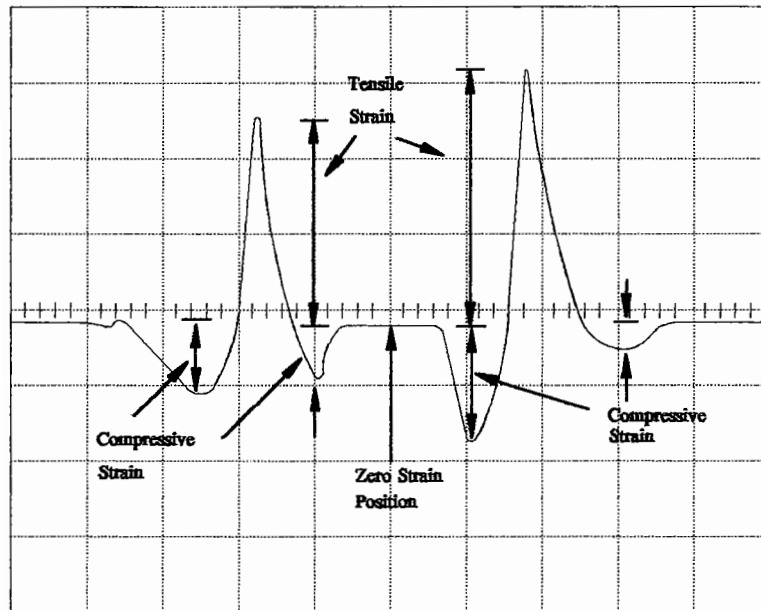
Figure 5.28 : Longitudinal Strain Gauge Output

Peak Height Of
Transient Strain

Residual/Delayed
Elastic-Visco-Plastic
Transverse Strain
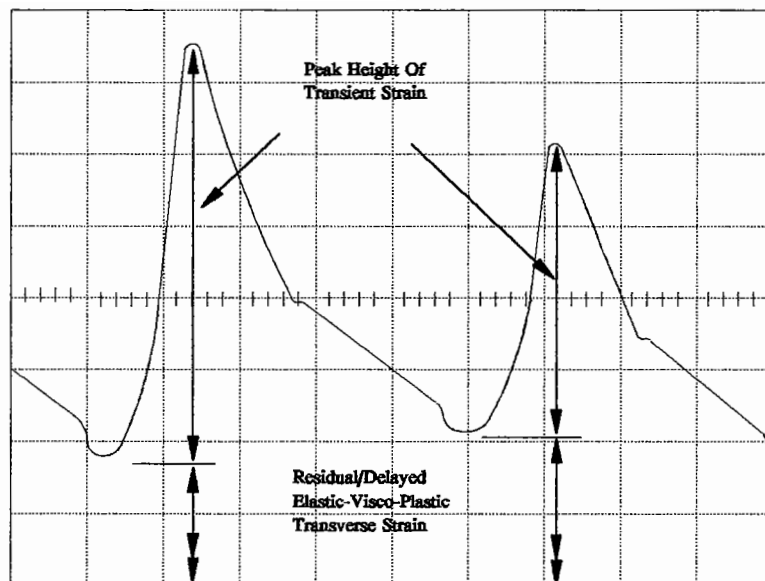
For position of zero strain see
Figure 5.30.

Figure 5.29 : Transverse Strain Gauge Output (Dynamic)
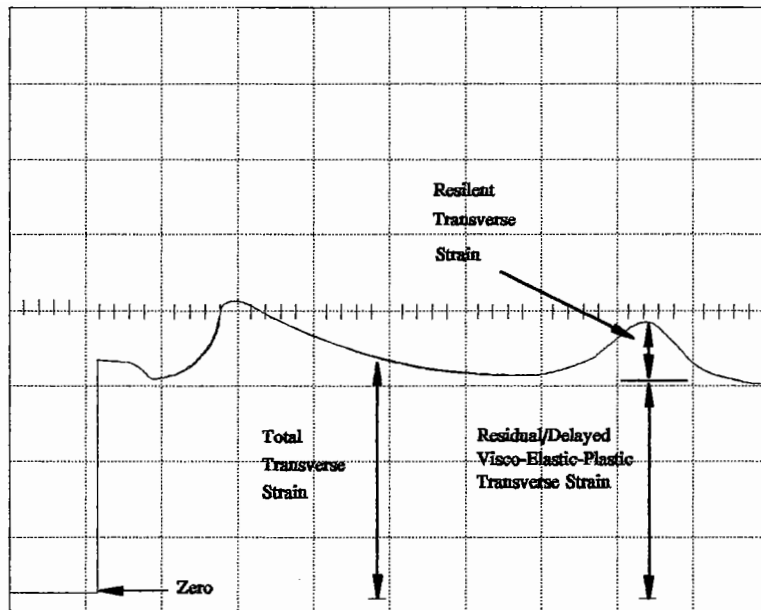
Figure 5.30 : Transverse Strain Gauge Output (Residual)
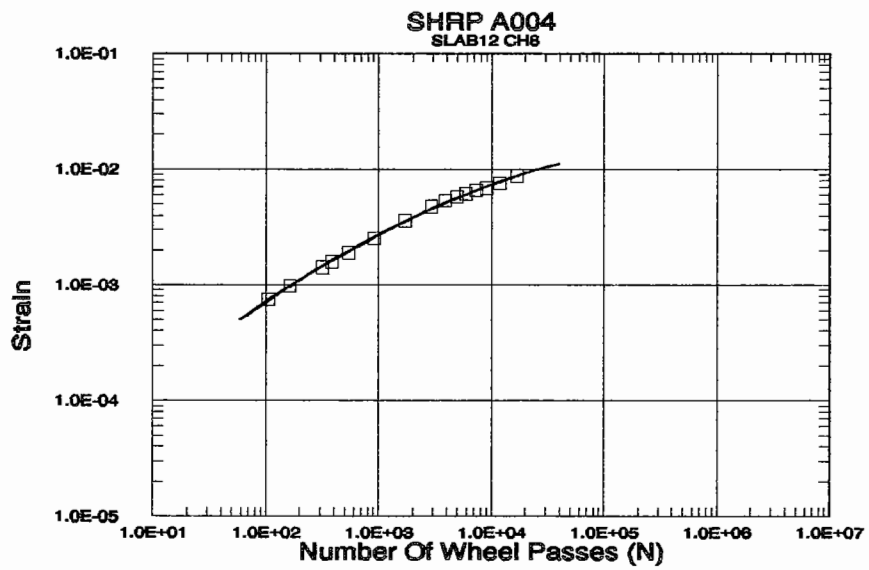
Figure 5.31 : Typical Increase in Magnitude of Residual/Delayed Elastic-Visco-Plastic Strain

of little benefit in establishing relative performance. The initial tensile strains, measured under the centre line were of similar magnitude in both longitudinal and transverse directions.

5.4 SIMPLIFIED TEST PROCEDURES

Two additional physical tests, Indirect Tensile Stiffness and Strength, were performed on the specimens both as a quality control measure to ensure that the fatigue wheel tracking slabs were uniform and also in an attempt to see if any simple relationships could be established between fundamental fatigue measurements and more simplistic test procedures. These experiments are described below.

5.4.1 Indirect tensile stiffness measurement

The stiffnesses of the core specimens taken from fatigue specimens (trapezoidal and slabs) were measured using the Indirect Tensile Test (ITT) in the Nottingham Asphalt Tester (Cooper and Brown, 1989). In this test the core specimens were subjected to a transient load pulse across their vertical diametral axis and the resultant transient deformations along the horizontal diametral axis were measured. The relationship used to calculate stiffness (Schmit, 1972) was as follows:-

$$S_m = \frac{(0.273 + \upsilon)\ P}{\Delta\ h\ t} \tag{5.42}$$

where; S_m = Stiffness of mixture

v = Poisson's ratio (assumed to be 0.35)

P = Peak vertical load

Δh = Peak transient deformation along the horizontal diametrical axis

t = Thickness of specimen

The ITT stiffness was measured at three temperatures, 0, 10 and 20 degrees Celsius with a loading time of approximately 0.14 seconds.

5.4.2 *Fracture strength*

Fracture strength was also measured in the indirect tensile mode of loading but using a slower speed of loading[1] of 50.8 mm/minute. The apparatus consisted of a modified Marshall loading frame to which a load cell and data acquisition were added. The tests were carried out over a range of temperatures between -10 and 20 degrees Celsius. From the data, the maximum tensile strength at failure was calculated for each specimen as follows:-

$$S_T = \frac{2\ P_{ult}}{\pi\ t\ D} \tag{5.43}$$

---

[1]The speed of loading used is that of the Marshall test procedure (2 inches per minute). This was the sole capability of the apparatus used.

where; P_{ult} = Vertical load which induces failure

              D = Diameter of specimen

              t = Thickness of specimen

In addition, a continuous plot of load and horizontal displacement versus time (which gives vertical displacement) was obtained for further analysis. This included the determination of Poisson's ratio (see Equation 5.44), stiffness of the mixture and the calculation of energy required to fracture the specimen.

$$v = 3.59 \frac{\Delta h}{\Delta v} - 0.27 \qquad (5.44)$$

The energy to failure was calculated using a similar method as that developed by Ruth et al. (1974), as follows:-

$$Energy = \int P_t \, v_t \, dt \qquad (5.45)$$

where; P_t = Vertical load at time t

              v_t = Vertical deformation at time t

The "failure energy" could be taken as either the energy at the peak load or that which corresponds to a particular deformation. In order to investigate this aspect several different times where used to calculate this energy, in particular the energy associated with; 1) the time to peak load, 2) the time to achieve a horizontal deformation of 1 mm and 2 mm, 3) the time at which the horizontal deformation starts to increase rapidly. Figure 5.32 shows a typical example of
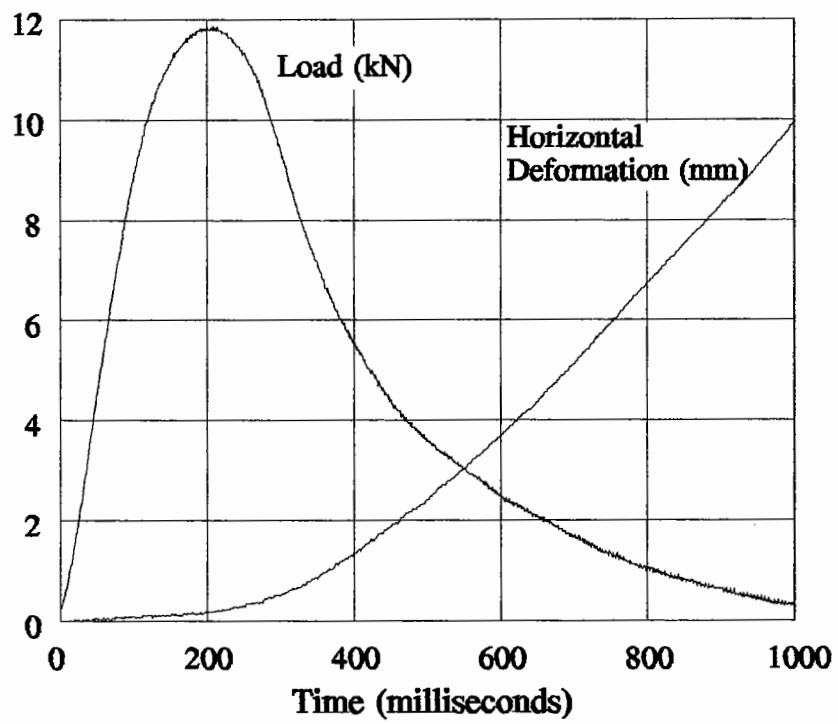
Figure 5.32 : Typical Example of Data Collected from the Indirect Tensile Fracture Test

the data collected during this test.

-5.64-

CHAPTER 6

Fatigue Element Test Results

6.0   INTRODUCTION

This chapter presents and provides an analysis of the fatigue test results obtained for the fatigue element test. The main part of the text concentrates on the analysis of the results from the trapezoidal fatigue test. In addition some discussion is given on the results obtained from the uniaxial fatigue test but this is limited due to the curtailment of this test program because of the problems discussed in Chapter 5.

6.1   UNIAXIAL TENSION COMPRESSION

The results obtained for this test programme are summarised in Table 6.1. The thirty nine results presented contain samples at the target densities, corresponding to 4 and 8% voids, and also at other densities. The results have been plotted in Figure 6.1 and 6.2 for AAK and AAG asphalt respectively using all densities/volumes of binders (aggregate RB). Insufficient reliable data exists to draw any firm conclusions. However, the number of results available for all the AAK asphalt samples (ignoring the effect of air voids) enable approximate values of *c* and *m* as defined by Equation 3.1 to be established (see Table 6.2). The results indicate that mixes made with the

Mix Ref.	Temp (°C)	Spec. Ref.	Spec. Density (t/m³)	Max. Density (t/m³)	Voids (%)	Date Made	Date Tested	Strs Amp (kPa)	Mean Strs (kPa)	Tensile Strain Amp.($\mu\varepsilon_t$)	Complex Modulus (GPa)	Fatigue Life (cycles)
B0W	0	2/19/9	2.374	2.552	7.0	22/1/90	2/5/90	1635	-459	125.1	13.1	13160
B0W	0	3/19/8	2.383	2.552	6.6	9/4/90	2/5/90	1635	-308	104.5	15.6	17080
B0W	0	2/1/*	2.463	2.552	3.5	4/12/90	26/1/90	1150	-	66.0	17.4	511990
B0W	0	3/1/*	2.468	2.552	3.3	4/12/90	26/1/90	1150	-	57.0	20.2	527450
B0W	0	2/15/5	2.468	2.552	3.3	29/3/90	18/4/90	1725	-643	79.0	21.8	102480
B0W	0	3/14/6	2.469	2.552	3.3	29/3/90	18/4/90	1725	-405	87.5	19.7	70540
B0W	20	2/37/15	2.361	2.552	7.5	3/5/90	30/5/90	600	-23	90.9	6.6	83760
B0W	20	4/2/*	2.378	2.552	6.8	4/12/90	25/1/90	1500	-	188.0	8.0	4180
B0W	20	2/2/*	2.467	2.552	3.3	4/12/90	25/1/90	1500	-	156.0	9.6	6050
B0W	20	3/2/*	2.467	2.552	3.3	4/12/90	25/1/90	1500	-	206.0	7.3	5330
B1W	0	1/3/*	2.378	2.522	5.7	6/12/90	29/1/90	2750	-	177.0	15.5	1810
B1W	0	1/10/*	2.286	2.522	9.4	24/1/90	16/2/90	1100	-	147.1	7.5	5830
B1W	0	2/25/12	2.351	2.522	6.8	26/4/90	22/5/90	1000	-136	74.0	13.5	632880
B1W	0	2/3/*	2.467	2.522	2.2	6/12/89	25/1/90	2750	-	173.0	15.9	5390
B1W	0	3/3/*	2.444	2.522	3.1	6/12/89	29/1/90	2750	-	166.5	16.5	4070
B1W	20	4/4/*	2.381	2.522	5.6	6/12/90	15/1/90	750	-	552.5	1.4	1650
B1W	20	3/34/16	2.444	2.522	3.1	2/5/90	30/5/90	1100	-77	140.1	7.9	17100
B1W	20	2/34/20	2.435	2.522	3.4	2/5/90	10/6/90	1100	-23	69.7	15.8	646060
B1W	20	2/4/*	2.447	2.522	3.0	6/12/90	12/2/90	750	-	110.9	6.8	58350
B1W	20	3/4/*	2.431	2.522	3.6	6/12/90	30/1/90	1150	-	165.0	7.0	10890
B1W	20	4/48/22	2.328	2.522	7.7	29/5/90	28/6/90	800	-10	177.1	4.5	15580
B1W	20	1/48/23	2.346	2.522	7.0	29/5/90	28/6/90	800	-54	107.4	7.4	34480
B1W	20	4/3/*	2.431	2.522	3.6	6/12/90	12/2/90	750	-	209.2	3.6	9790
B1W	20	1/4/*	2.393	2.522	5.1	6/12/90	15/1/90	750	-	290.3	2.6	26970
V0W	0	4/7/3	2.381	2.545	6.4	18/1/90	17/4/90	1710	-504	81.1	21.1	127400
V0W	0	1/6/4	2.372	2.545	6.8	18/1/90	17/4/90	1710	-414	94.5	18.1	90920
V0W	0	2/23/10	2.482	2.545	2.5	17/4/90	3/5/90	2000	-831	83.0	24.1	42500
V0W	0	1/24/11	2.488	2.545	2.2	17/4/90	11/5/90	2000	-471	77.8	25.7	97180
V0W	20	1/7/1	2.382	2.545	6.4	18/1/90	11/4/90	1175	-187	107.0	11.0	7280
V0W	20	4/6/2	2.376	2.545	6.6	18/1/90	11/4/90	1175	-175	129.5	9.1	7300
V1W	0	3/13/*	2.277	2.529	10.0	6/2/90	22/2/90	1250	-	85.4	14.6	157850
V1W	0	4/8/7	2.337	2.529	7.6	22/1/90	1/5/90	1535	-309	108.1	14.2	114460
V1W	0	3/33/14	2.457	2.529	2.8	1/5/90	25/5/90	1600	-382	63.2	25.3	109440
V1W	0	2/13/*	2.300	2.529	9.1	6/2/90	22/2/90	1250	-	77.1	16.2	68420
V1W	0	2/33/13	2.449	2.529	3.2	1/5/90	25/5/90	1600	-501	59.6	26.8	152860
V1W	20	2/43/19	2.357	2.529	6.8	17/5/90	11/6/90	500	-19	163.3	3.1	145640
V1W	20	3/41/18	2.446	2.529	3.3	15/5/90	31/5/90	2000	-519	84.7	23.6	2120
V1W	20	2/27/17	2.354	2.529	6.9	27/4/90	31/5/90	500	-33	62.1	8.1	143970
V1W	20	3/43/21	2.357	2.529	6.8	17/5/90	11/6/90	500	-21	49.5	10.1	127420

*   Indicates no ascii data file and no mean stress level recorded

Table 6.1 : Summary of Test Results from the Uniaxial Tension-Compression Fatigue Test
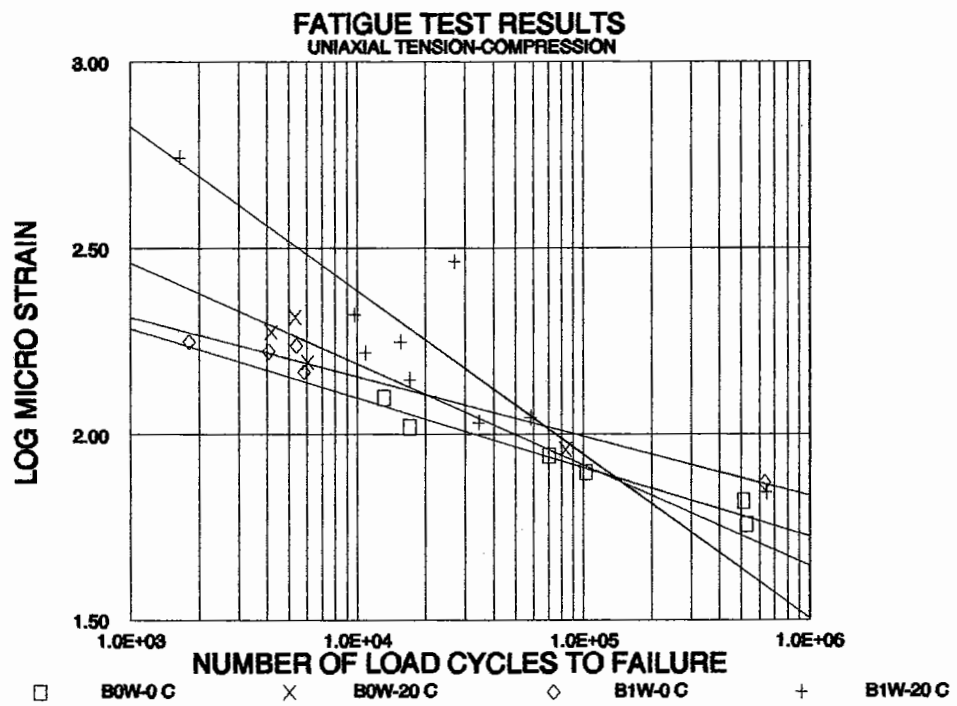
Figure 6.1 : Fatigue Test Results for Boscan Asphalt/Watsonville Aggregate Mixture for the Uniaxial Tension-Compression Test

-6.3-

FATIGUE TEST RESULTS
UNIAXIAL TENSION-COMPRESSION
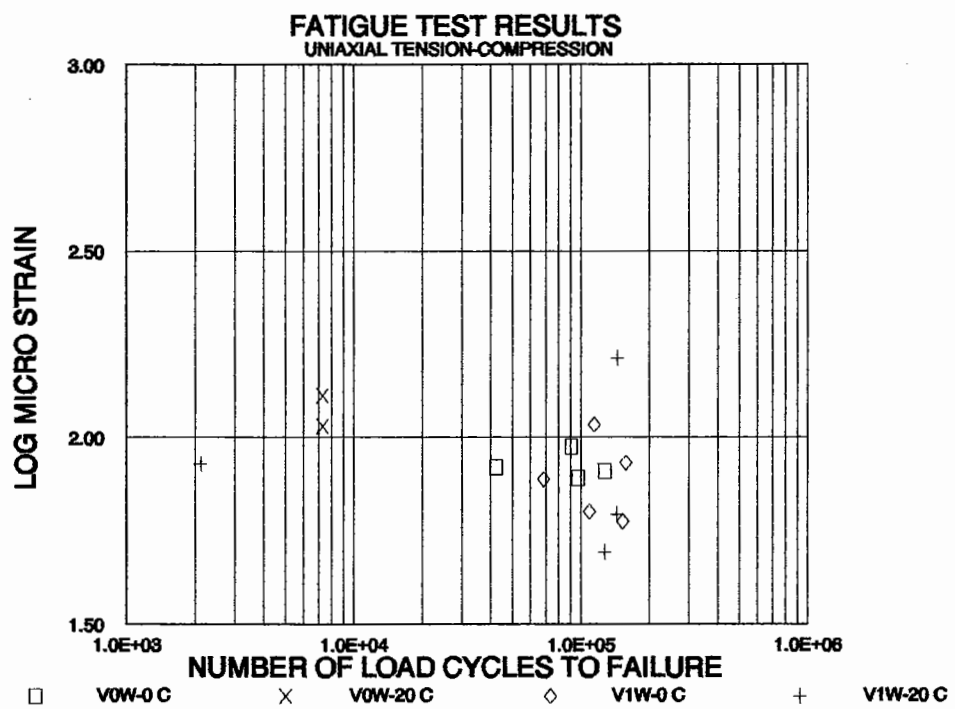
Figure 6.2 : Fatigue Test Results for Valley Asphalt/Watsonville Aggregate Mixture for the Uniaxial Tension-Compression Test

Mixture Ref.	Test Temp. (°C)	No. of Tests	Constant "c"	Exponent "m"	r^2
B0W	0	6	1.76036×10^{15}	-5.36198	0.953
B0W	20	4	1.16784×10^{12}	-3.68625	0.923
B1W	0	5	2.77245×10^{17}	-6.24038	0.972
B1W	20	9	2.61789×10^{9}	-2.27081	0.736

Table 6.2 : Coefficient "c" and exponent "m" of Fatigue Relationships Obtained from Uniaxial Tension-Compression Fatigue Testing

higher binder contents have longer lives at most equivalent strain levels. The results from the testing at 20°C had steeper slopes than those tested at 0°C.

Use of the method developed by Cooper (1976) proved quite robust in predicting the fatigue life of the specimens, as illustrated in Figure 6.3. This figure also shows five results obtained with a mixture used for testing the apparatus which was made with a local aggregate (Bardon Hill Tuff) and a 100 penetration grade binder. The relationship between measured and predicted fatigue performance (with a r^2 value of 0.881) was as follows:-

$$\log Nf_{measured} = 1.003995 \log Nf_{predicted} + 0.214514 \qquad (6.1)$$

As stated earlier because of the limited testing carried out no firm conclusions could be drawn with regard to the fatigue behaviour of the materials from this mode of testing. However, some trends are apparent as follows:

i)   Mixes referenced B1W (ie. higher asphalt content) had longer lives at equivalent strain levels than mixes B0W.

ii)   The fatigue relationship for mixes tested at 20°C (Asphalt AAK) indicated that the slope of these lines (m) are steeper than those obtained at 0°C.

The F.E. analysis, assuming the material to be isotropic and homogeneous,

ACTUAL VS PREDICTED LIFE
Uniaxial tension-compresion tests
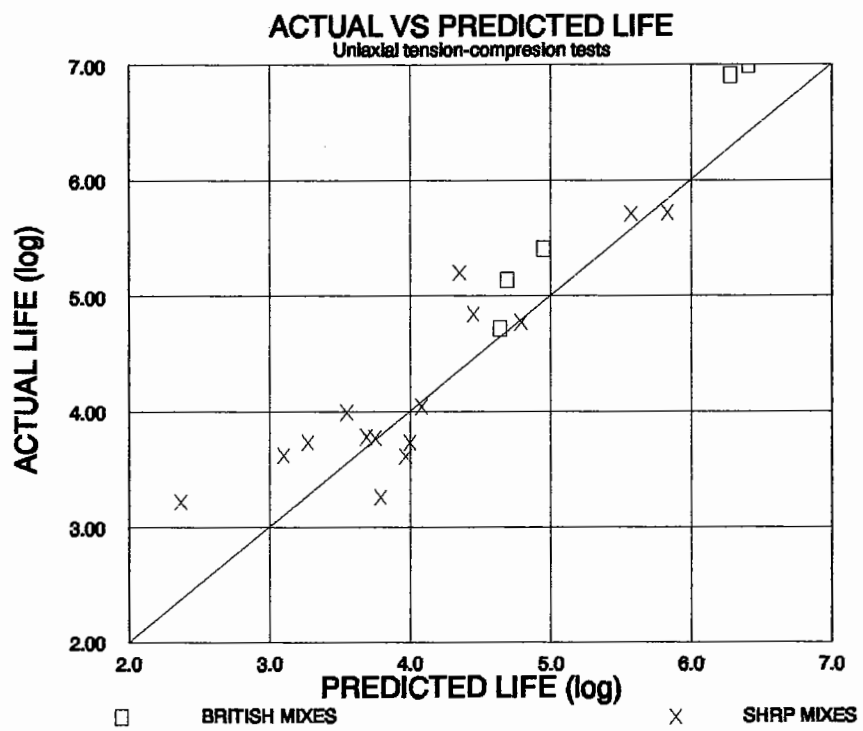
Figure 6.3 : Actual versus Predicted Fatigue Life for the Uniaxial
Tension-Compression Fatigue Test

indicated that a stress concentration exists near the end caps. This is a direct result of fixing the specimen to the end caps with epoxy resin. The stress concentration is consistent with the failure position obtained with the specimens.

The stress concentration results in the estimation of stress and strain at the failure position being difficult. These values could change by up to 100% if the failure position moved by 10 mm. This is considered unacceptable for a standard fatigue test to define the strain-life relationship of an asphalt-aggregate mixture.

6.1.1 Uniaxial tension-compression stiffness

One of the necessary features of the uniaxial testing was maintaining a compressive load, which varied in magnitude depending upon the nature of the material under test, in order to prevent the specimen from increasing in length. Thus, from a knowledge of this mean value of stress and the peak-to-peak stress levels it is possible to deduce a compressive and tensile stiffness modulus independently for each specimen tested. It was found that the relative difference obtained for the two values got larger as the stiffness increased. This is a function of the larger mean load level required to keep the specimen length constant. A relationship has been obtained for the ratio of the stiffness moduli versus the tension-compression complex modulus, illustrated in Figure 6.4 (with an r^2 value of 0.686), as follows:-
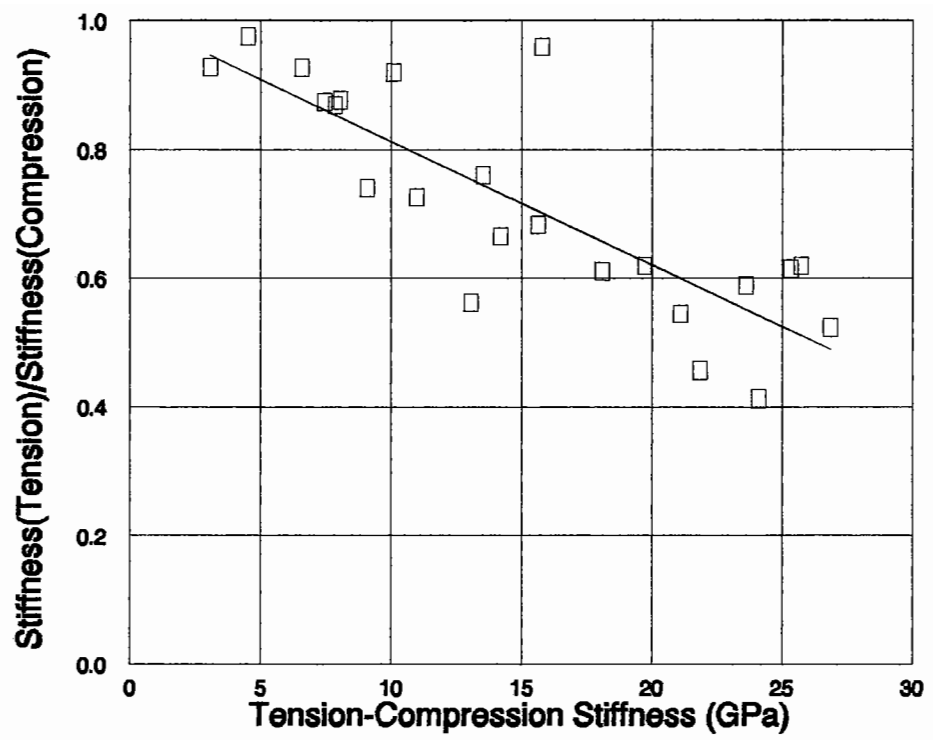
Figure 6.4 : Tension-Compression Stiffness versus the Ratio of Stiffness in Tension to Compression

$$\frac{E^*_{tension}}{E^*_{compression}} = 1.00 - 0.01919 \ E^*_{tension-compression} \qquad (6.2)$$

The mean stress level can also be considered as a function of the stress amplitude used for the fatigue testing, as illustrated in Figure 6.5, (valid in range 500 to 2,000 kPa with a r^2 value of 0.86) as follows:-

$$\overline{\sigma}_{compressive} = -16.2948 + 0.1345 \ \sigma_{amplitude} - 2.2525 \times 10^{-4} \ \sigma^2_{amplitude} \qquad (6.3)$$

This form of relationship could be useful for establishing the mean stress level in future tests in the Uniaxial Tension-Compression device. However, problems associated with stress concentrations will need careful assessment. A possible way forward with this type of test would be to make use of a necked specimen, as illustrated in Figure 3.1.

6.2   TRAPEZOIDAL FATIGUE TESTING

The analysis of the fatigue results obtained from the testing of trapezoidal specimens was performed in different stages in order to investigate aspects of behaviour, as follows:-

i)   Change in stiffness and phase angle during the fatigue process.

ii)   The definition of crack formation and the adoption of a more uniform failure criterion from controlled stress and strain fatigue tests.
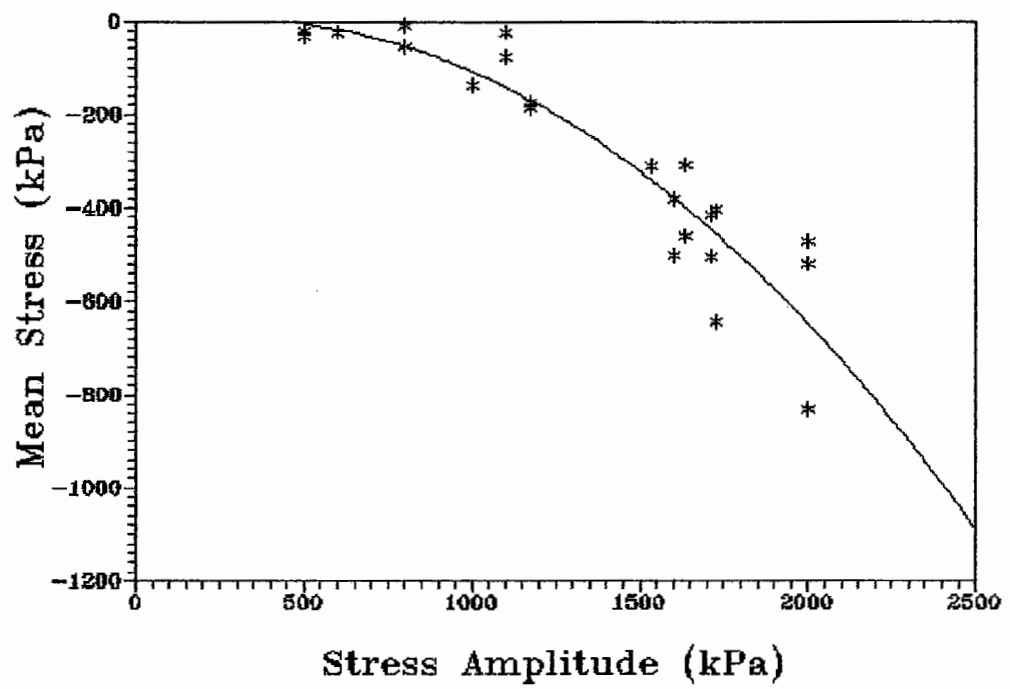
Figure 6.5 : Mean Stress Level versus the Amplitude of Stress

iii)   The calculation of dissipated energy.

iv)   Predictive method development for fatigue crack prediction in the trapezoidal fatigue test.

6.2.1   Stiffness reduction

Stiffness reduction in fatigue testing has traditionally been considered by plotting the stiffness reduction versus the number of load cycles using logarithmic scales, eg. Figure 6.6. A plot of this form illustrates a change in behaviour as the slope of the line increases in the late stages of the test. However, logarithmic plots can often produce a misleading illustration of the data if not used with caution. Figure 6.7 illustrates a similar effect to that obtained in Figure 6.6 but in this case the data plotted is that of a straight line.

The test method developed by SHRP contractors (Harrigan et al., 1994) for fatigue testing (designation M-009) recommends plotting the log of stiffness versus the log of the number of load repetitions and fitting an exponential relationship of the form:-

$$Stiffness = A \, e^{\, bN} \qquad\qquad (6.4)$$

where; e =   natural logarithm to the base e

A =   constant

b =   constant
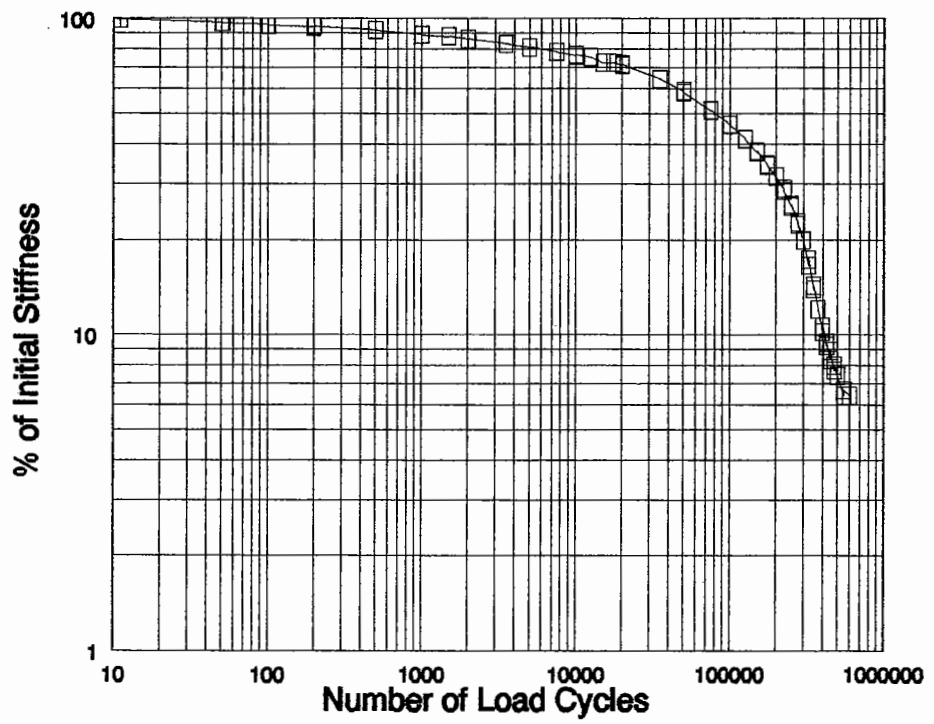
Figure 6.6 : Data from Test Specimen AACRH100 Plotted on Log-Log Scales
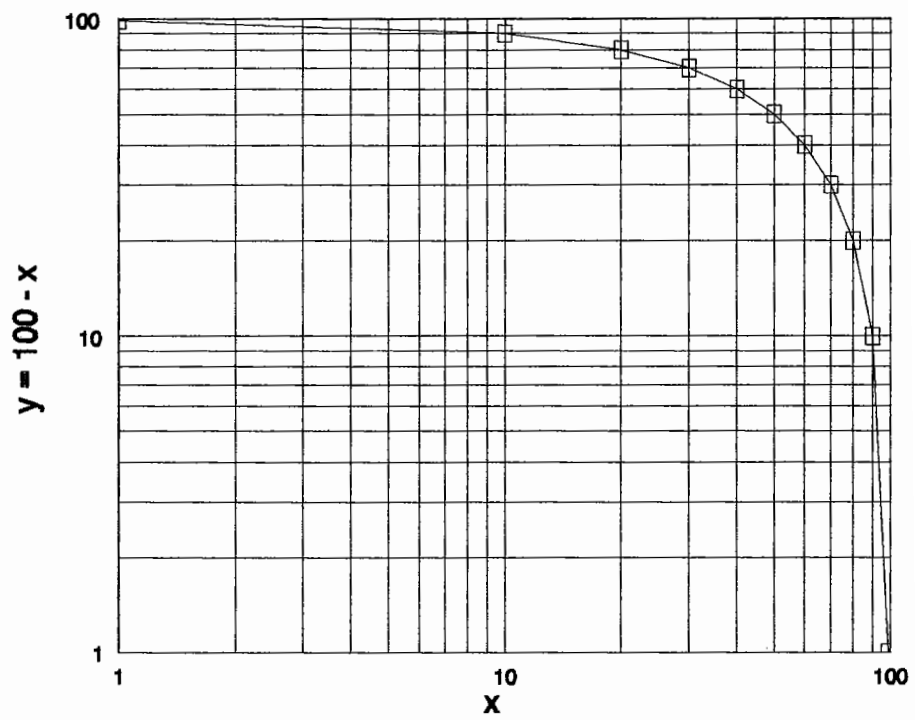
Figure 6.7 : A Straight Line Plotted on Log Scales
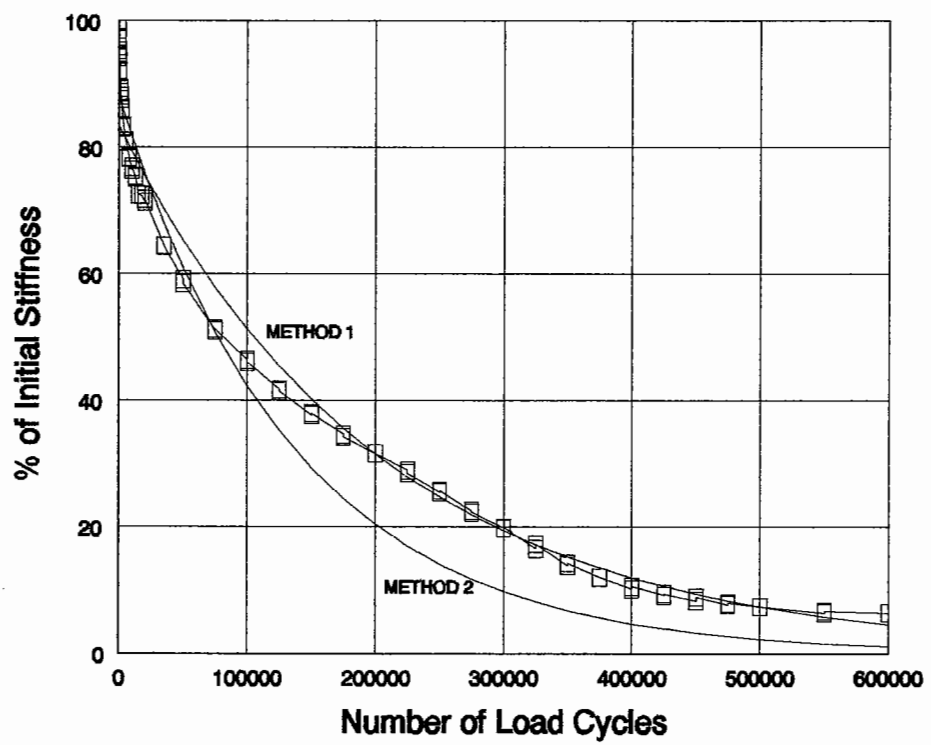
Figure 6.8 : Data from Test Specimen AACRH100 Plotted on Linear Scales

The data plotted in Figure 6.6 [test specimen ref. AACRH100 obtained form the SHRP A-003A contractor (Tayebali, 1991)] has been analyzed using the above equation with two procedures; 1) considering all the data, and 2) considering only data collected before the stiffness has reduced to half of the stiffness obtained at load cycle 50 (recommended method). The values obtained for A and b are as follows:-

	Method 1	Method 2
A	36,5485 psi	-4.84956e-06
b	38.5918 psi	-7.31253e-06

These curves along with the initial data are plotted in Figure 6.8 but this time using linear scales. It can be seen that the shape of this curve appears very different to that plotted in Figure 6.6. The stiffness drops quite sharply during the initial stage of the test followed by a relatively linear decrease during the middle portion of the test and finally a flattening out of the stiffness curve towards the end of the test. The two lines (method 1 and method 2) discussed above are also plotted. It can be observed that these relationships, while not producing large errors, do not match the physical behaviour of the stiffness reduction with number of load cycles. In addition, errors are produced in the initial stiffness estimation of 14% and 8.4% respectively for method 1 and 2. The initial stiffness was 439,212 psi and reduced to that defined by method 2 (the recommended method) after 1,500 loading cycles.

Similar plots of stiffness reduction were obtained from results of the controlled

stress tests but after the linear stage, instead of flattening out, the stiffness began to decrease more rapidly until the specimen fractured.

A direct consequence of this was the decision that the stiffness reduction over the middle portion of the fatigue test should be considered to be related linearly to the number of load cycles and not by a function which is related to the logarithm of load cycles. A similar result was obtained by Raithby (1972) who compared tests with continuous loading to those with rest periods. The consequence of this was a decision to change the sequence for data collection from logarithmic to linear. This was implemented by measuring the initial stiffness and setting this to 100%. As stiffness dropped data was acquired at each 5% reduction in stiffness.

6.2.2   Stiffness versus phase angle

During the trapezoidal fatigue test, the load and displacement signals were stored periodically. These were subsequently analyzed to obtain the phase lag, δ. Figures 6.9a to 6.9c show a typical example of sine waves from one data set. The solid lines are regression fits of the sinusoidal load and displacement signals. One of the regression analyses resulted in a gross error for this data set (bottom right, Figure 6.9a) and data was excluded. In the later stages of the test when the specimen had a significant crack, the shape of the curve from the load cell became very irregular and could no longer be considered as sinusoidal. This irregular behaviour started when the stiffness was reduced to approximately 50% of its initial value.
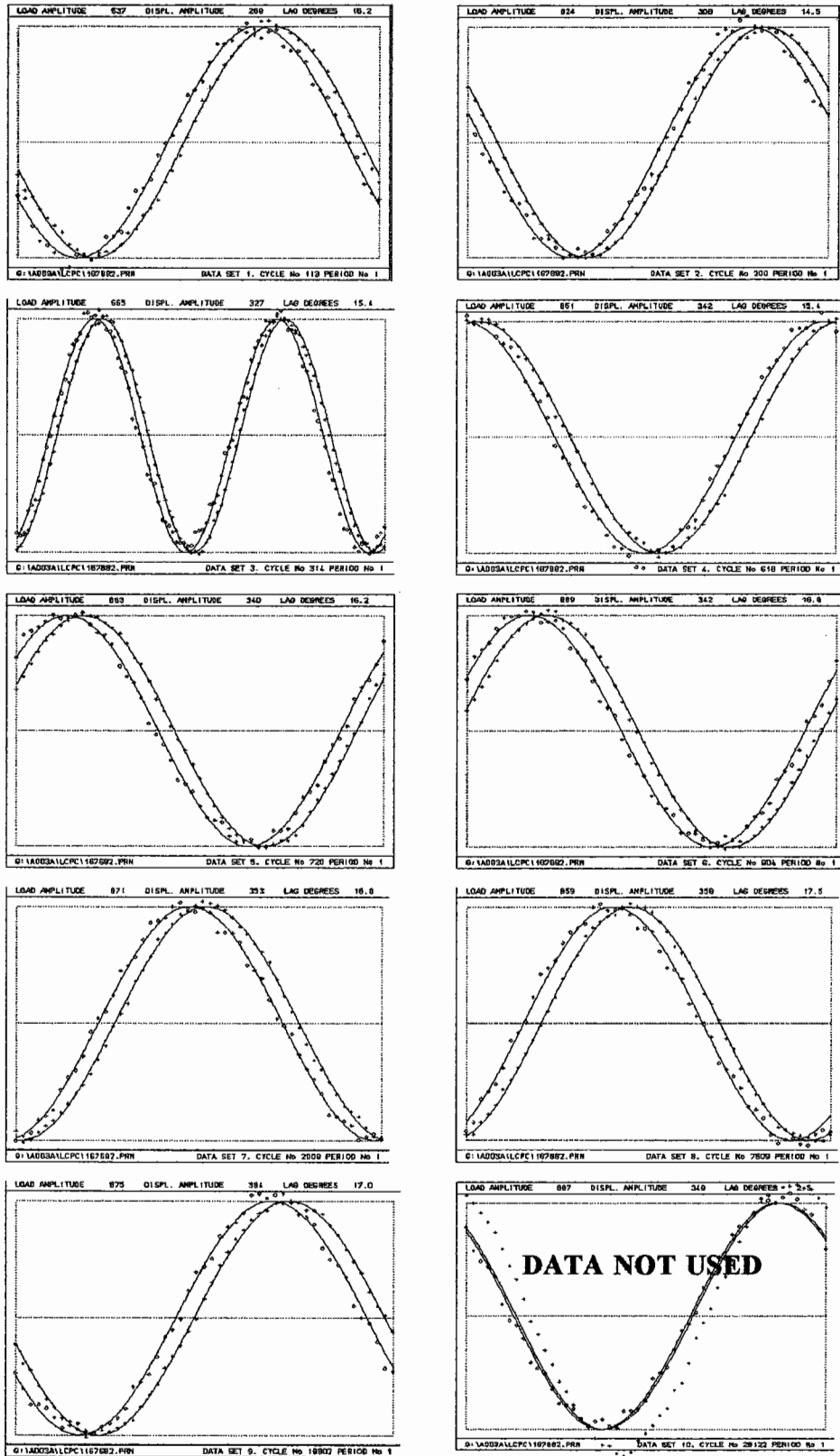
Figure 6.9a: Change in the Phase Angle During the Trapezoidal Fatigue Test
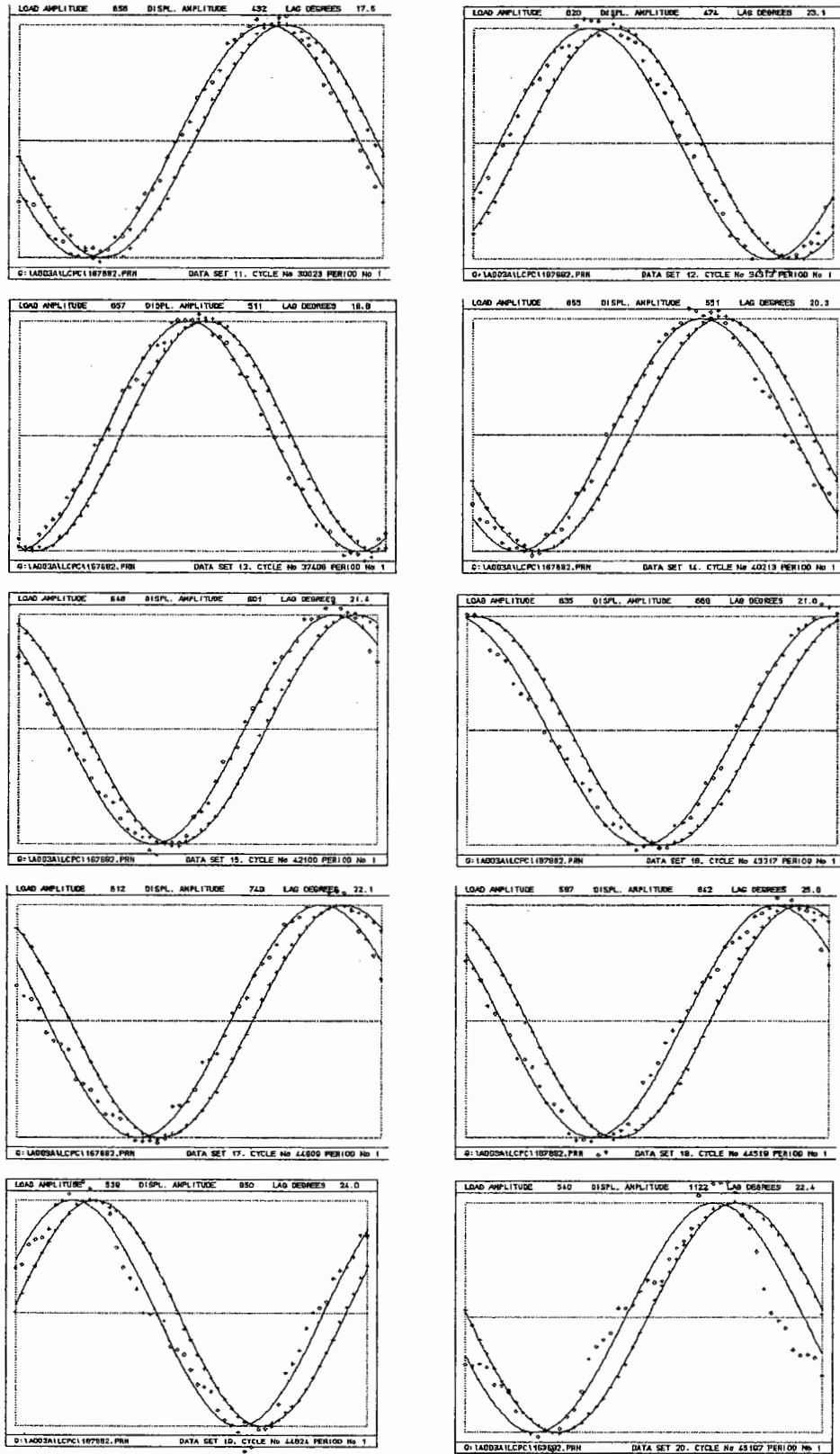
Figure 6.9b: Change in the Phase Angle During the Trapezoidal Fatigue Test
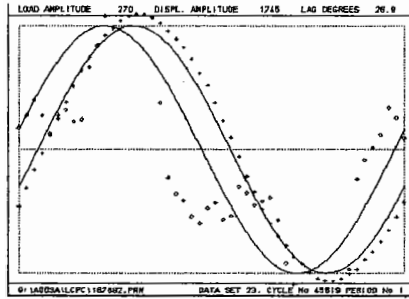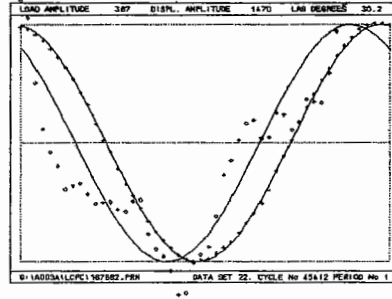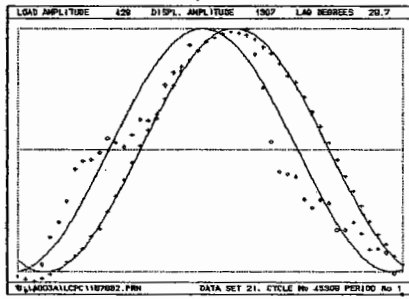
END OF TEST

**Figure 6.9c : Change in the Phase Angle During the Trapezoidal
Fatigue Test**

In order to analyze the fatigue data in terms of dissipated energy it was considered desirable to fit a relationship between stiffness and phase angle. This was particulary important for the earlier set of data since phase angle information was only collected on a logarithmic basis. Figure 6.10 shows the same data from the same test as presented in Figures 6.9a to 6.9c but plotted against the complex stiffness modulus. As can be observed from this figure, a relationship can be established for each mixture at a given temperature and loading frequency, between the complex stiffness modulus and phase angle, of the form:

$$\delta = a \ E^{*b} \tag{6.5}$$

where; $a \ \& \ b$ = constants

E^* is in units of MPa in Figure 6.1

[The above relationship does not hold true after a large crack has formed in the specimen and is only considered valid to a condition defined as "crack initiation". The definition of crack initiation is discussed later in this chapter.]

It was also found that when "$log \ a$" was plotted against "b", for all the mixtures tested, a linear relationship was obtained, as shown in Figure 6.11. This relationship may be expressed as:-

$$b = 0.224 - 0.222 \ log \ a \tag{6.6}$$

Thus, by combining Equations 6.5 and 6.6 we obtain:-

$$PHASE\ ANGLE = 741.641\ E^{*\ -0.418569}$$
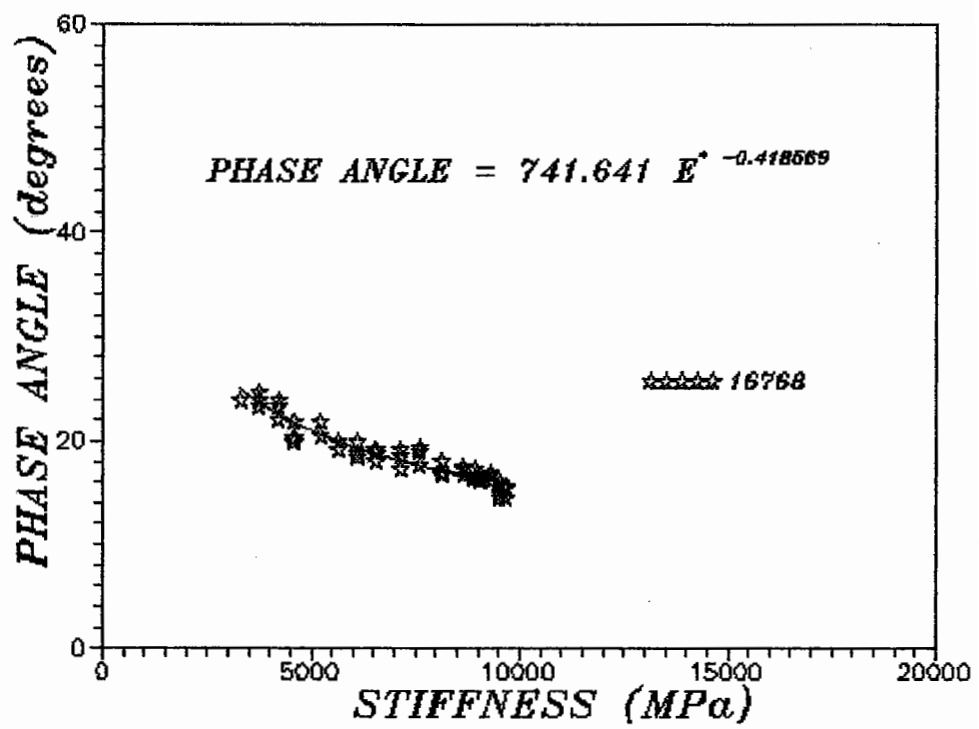
**Figure 6.10 : Typical Relationship Obtained Between
Stiffness and Phase Angle**
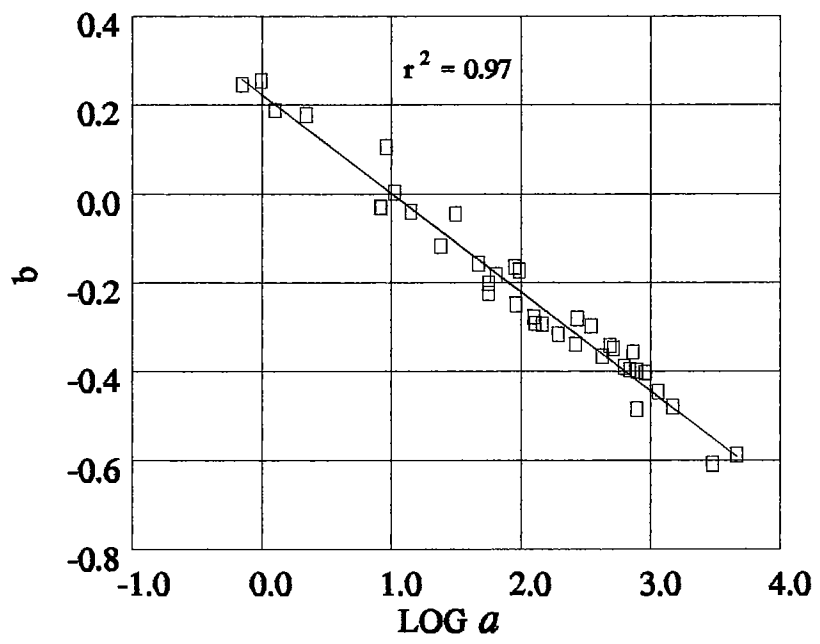
Figure 6.11 : "Log *a*" versus "*b*"

$$\delta = a \left[E^* \right]^{(\, 0.224 \, - \, 0.222 \, \log \, a \,)} \qquad\qquad \text{(6.7)}$$

The significance given to "a" in Equation 6.7 is that it is dependant upon the rheological properties of the mixture and it describes the damage to the mixture in terms of the relationship between the phase angle and extensional complex modulus during an individual fatigue test. The relationships obtained from the fatigue testing can be considered to have a common "focus", and given an initial complex modulus and phase angle, the value for "a" is determined, as follows:-

$$\log a = \frac{\log \delta \, - \, 0.224 \, \log \left[E^* \right]}{1 \, - \, 0.222 \, \log \left[E^* \right]} \qquad\qquad \text{(6.8)}$$

The relationship presented in the above equations is illustrated in Figure 6.12 along with typical examples of data obtained from the testing.

6.2.3   Crack initiation

The number of cycles to failure, as discussed earlier, is normally defined differently depending upon the mode of loading. Alternatively, Hopman et al. (1989) proposed the use of an "Energy Ratio" to define the number of cycles ($N1$) in a controlled strain test, to a point where cracks are considered to initiate (defined as the merging of micro-cracks to form a sharp crack, which then propagates), Figure 6.13. "The Energy Ratio" is defined as follows:
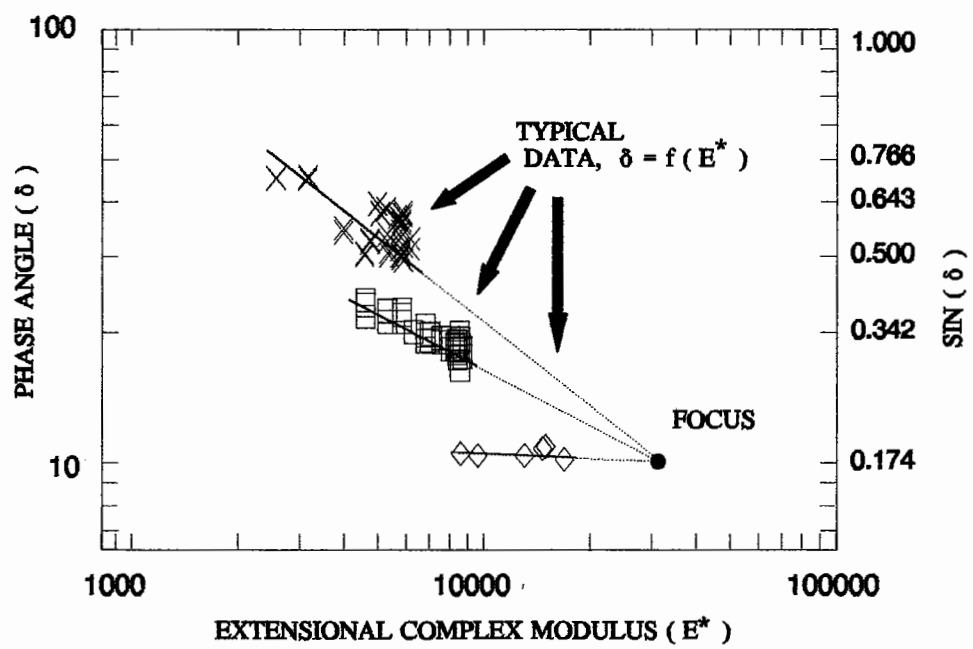
Figure 6.12 : Typical Relationships Between Complex Stiffness Modulus and Phase Angle Illustrating "Focus" Position

(Not to scale)

ENERGY RATIO

N1 POINT

NUMBER OF LOAD CYCLES
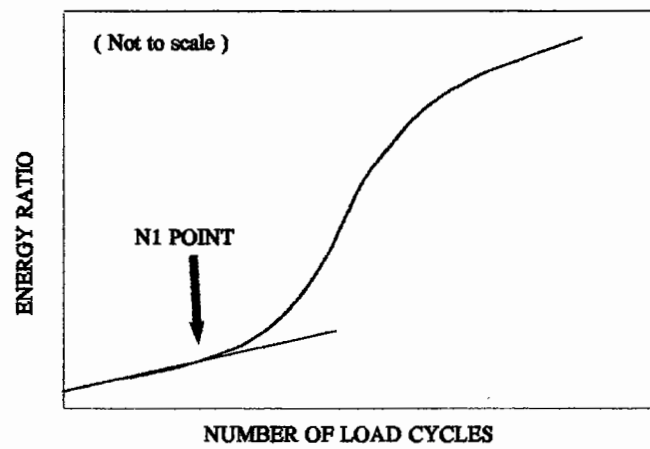
Figure 6.13 : Illustration of Energy Ration versus Number of Cycles, Controlled Strain Fatigue Test

$$Energy \; Ratio \; = \; \frac{n \; w_o}{w_i} \qquad\qquad (6.9)$$

where; n = cycle number

w_o = dissipated energy in first cycle

w_i = dissipated energy in cycle i

The "Energy Ratio" plotted against number of cycles reveals a change in behaviour at a number of cycles, $N1$. This approximately corresponds to a 40% reduction in extensional complex modulus. This point was considered to be the formation of a sharp crack. However, the "Energy Ratio" can be written as:-

$$Energy \; Ratio \; = \; \frac{n \; (\; \pi \; \sigma_o \; \varepsilon_o \; \sin \; \delta_o \;)}{(\; \pi \; \sigma_i \; \varepsilon_i \; \sin \; \delta_i \;)} \qquad\qquad (6.10)$$

where; n = cycle number

σ_o = stress in cycle i

ε_i = strain in cycle i

δ_i = phase lag in cycle i

If the stress term is replaced by the product of strain and complex stiffness modulus and considering that the strain level (for a controlled strain test) remains constant then Equation 6.10 can be written as follows:-

$$\text{Energy Ratio} = \frac{n \, (\, \pi \, \varepsilon_o^2 \, E_o^* \, \sin \, \delta_o \,)}{(\, \pi \, \varepsilon_o^2 \, E_i^* \, \sin \, \delta_i \,)} \qquad (6.11)$$

It can be observed that the above equation has several constant terms that can be removed without changing the shape of the curve in Figure 6.13 and thus the equivalent ratio, "R_ε", is reduced to the following form:

$$R_\varepsilon = \frac{n}{E_i^* \, \sin \, \delta_i} \qquad \text{or} \qquad \frac{n}{E_i^{''}} \qquad (6.12)$$

where; $E_i^{''}$ is the extensional loss modulus at any cycle "i".

It should also be noted that the change in $\sin \, \delta$ is small compared to the change in E^* (see Figure 6.12) and does not significantly alter the shape of the curve shown in Figure 6.13. Thus the equation for defining $N1$ can be simplified to:

$$R_\varepsilon \approx \frac{n}{E_i^*} \qquad (6.13)$$

For a controlled stress test using the same basis for simplifying the equation, "R_σ" is as follows:

$$R_\sigma \approx n \, E_i^* \qquad (6.14)$$

For controlled strain test data $N1$ is defined as the point at which the slope of the energy ratio versus number of load cycles deviates from a straight line (see Figure 6.14b). The evidence for "crack initiation" at this point was confirmed

CONTROLLED STRAIN FATIGUE TEST
COMPLEX MODULUS VERSUS LOAD CYCLES

E^* (MPa)

a)

R_ϵ

b)

w_i (J/m^3)

c)
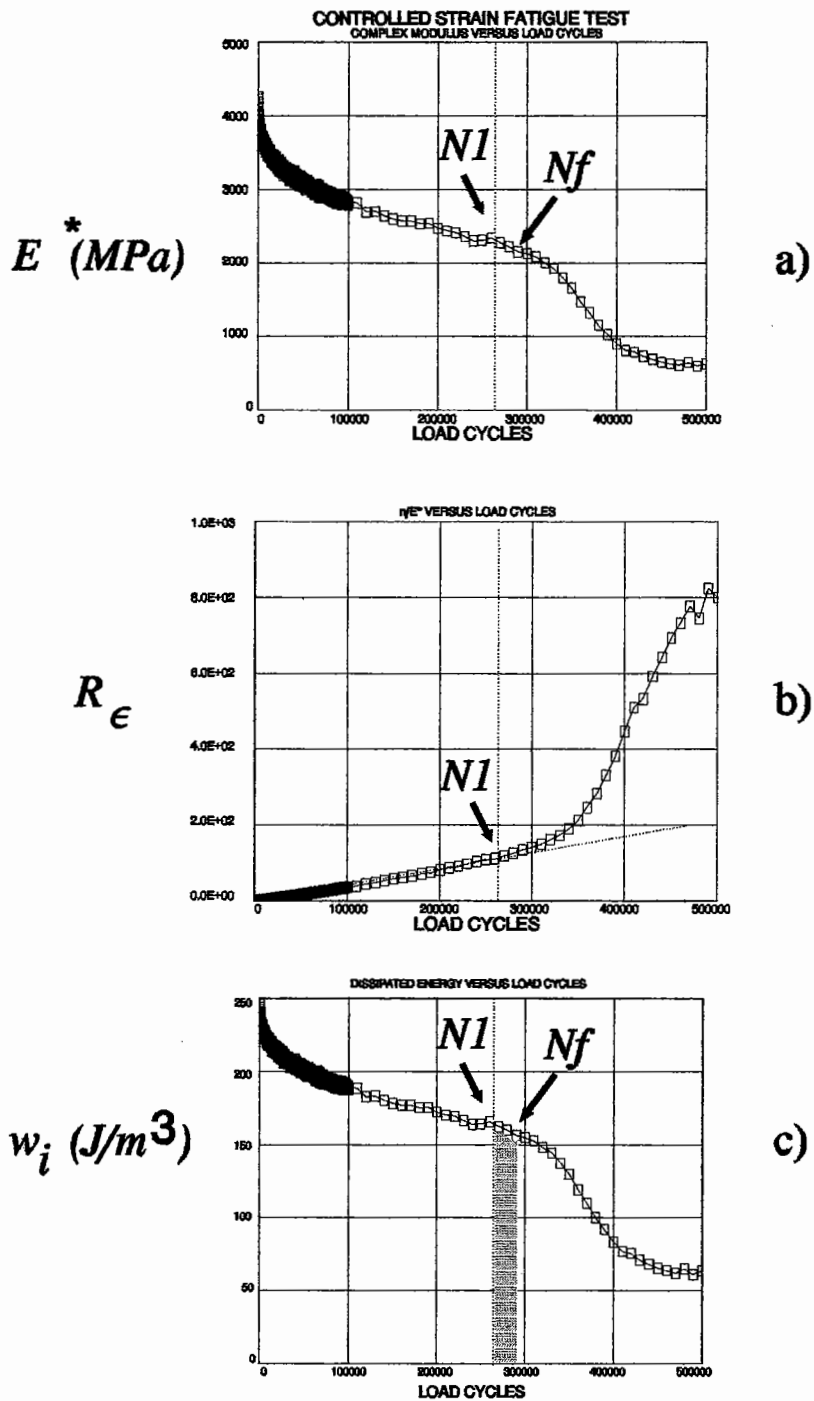
Figure 6.14 : E^*, R_ε, and w_i versus Load Cycles; Trapezoidal
Controlled Strain Fatigue Test

by visual observations and earlier work at Nottingham (McCarthy, 1960) where similar reductions in stiffness modulus occurred prior to observed crack propagation.

In a controlled stress test the load amplitude remains constant and after crack initiation the stress at the crack tip increases rapidly. Consequently $N1$ can be easily determined from the peak of R_σ (see Figure 6.15b). The concept of defining fatigue life to the $N1$ point is very attractive since the data obtained from either test type represents material in the same state of damage rather than the less meaningful reduction in extensional complex modulus of either 50% or 90% which are arbitrary values and difficult to define in their initial condition, ie., it is very difficult to determine the initial value of E^* (see Figures 6.14 and 6.15).

It should be noted that the $N1$ condition is very much harder to define for controlled strain tests compared to controlled stress tests. This is a result of a reduction of stress at the crack tip as the crack progresses, resulting in a reducing rate of crack propagation.

In the remainder of this thesis, results are presented to two lives, $N1$ and Nf, corresponding to "crack initiation" and "failure" (as defined earlier).

In both types of fatigue test, controlled stress and controlled strain, the cumulative dissipated energy measured is largely that associated with the initiation of a crack. The $N1$ point occurs generally in a range between 40%
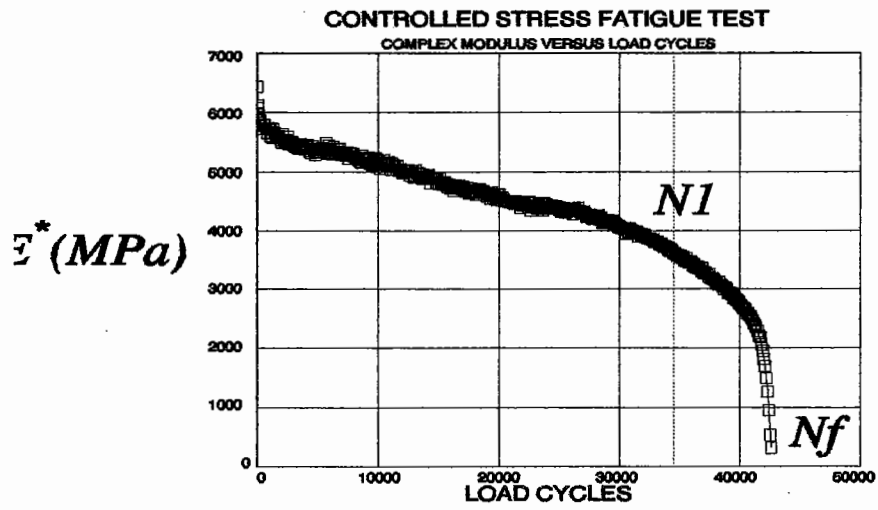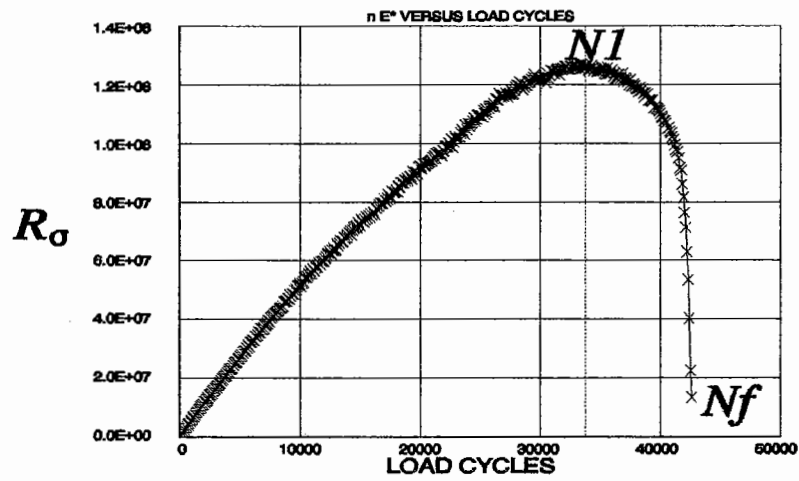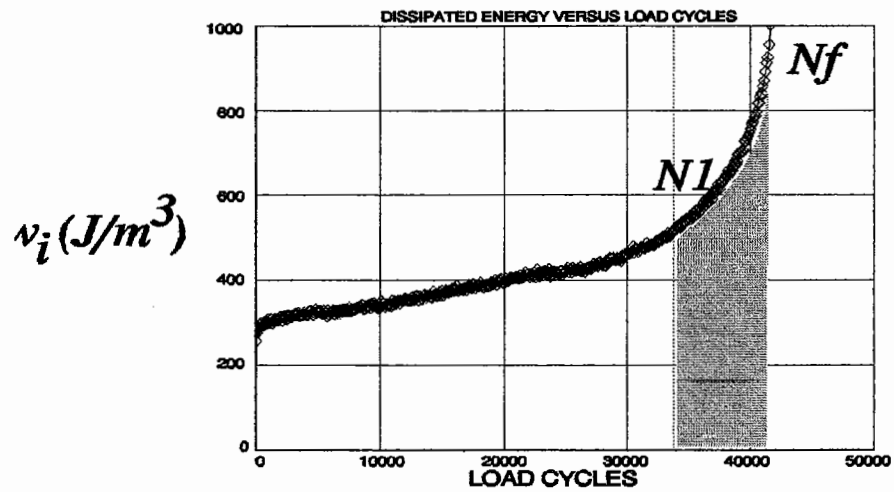
Figure 6.15 : E^*, R_σ, and w_i versus Load Cycles; Trapezoidal Controlled Stress Fatigue Test

and 50% reduction in the initial extensional complex modulus. Therefore, in a controlled strain test which is stopped after a 50% reduction in complex modulus the energy dissipated, which is associated with crack propagation is usually small. In a controlled stress test, the crack growth accelerates rapidly after initiation so life associated with crack propagation is also relatively small. This is illustrated in Figures 6.14 and 6.15 (the shaded area in Figures 6.14 and 6.15 is the amount of dissipated energy associated with crack propagation). Thus, both fatigue tests give similar relationships for "$N1$" and "Nf", largely associated with crack initiation only. In addition the assumptions regarding specimen geometry are no longer valid after crack initiation and, therefore, the dissipated energy after the $N1$ stage should only be considered as an apparent energy. Consequently, the $N1$ point is considered to be the preferred failure criterion, since the energy computed to the Nf criterion will contain a certain amount of error.

6.2.4 Cumulative dissipated energy

Cumulative dissipated energy is calculated from the relationship given in Equation 6.15. The change in the phase angle, δ, is considered by use of the parameters a and b as described in Equation 6.5.

$$W = \sum_{i=1}^{i=N1 \text{ or } Nf} \pi \, \varepsilon_i^2 \, E_i^* \sin \delta_i \qquad (6.15)$$

The cumulative dissipated energy is the summation of the areas contained within all the hysteresis loops experienced by the material during the fatigue

test.

The parameters *A* and *Z* to *N1* and *Nf* conditions (see Equation 3.6) were then determined and these values along with the other experimental parameters discussed above are presented in Tables 6.3a and 6.3b. In addition Table 6.3a contains, for information, the complex stiffness modulus and phase angle of the unaged binder for the condition evaluated (Christensen et al., 1992). [The number of samples used to determine each fatigue line was relatively low in most cases. Consequently the slopes (Z_{Nf} and Z_{N1}) given in the table of results potentially contain experimental variability larger than is desirable for testing of this type].

6.3 ANALYSIS OF FATIGUE TEST RESULTS

The individual data points (see Table 6.4) for cumulative dissipated energy versus life to *N1* and *Nf*, for individual specimens are shown in Figure 6.16. It can be seen that although the data points all lie in a similar band the scatter is relatively large. As shown in Table 6.3 individual data sets have different values of "*A*" and "*Z*". In order to predict fatigue life of a particular mixture in the road pavement it is necessary to know these two parameters, since they describe the slope and position of the fatigue line.

As part of the study, relevant published data obtained by other workers (van Dijk et al., 1977; van Dijk, 1975; Gerritsen, 1987 and Gerritsen et al., 1987) was reviewed in order to extend the range of volumetric compositions

Mix. Ref.	VMA (%)	Vb (%)	Temp (°C)	Test Type	Freq (Htz)	No. of Tests	Binder Properties	
							E* (MPa)	δ (degrees)
B0T	14.5	10.3	20	Stress	20	5	8.2	45.9
B0T	18.0	9.8	0	Stress	20	5	180.1	23.2
B1T	16.2	11.5	0	Stress	20	5	180.1	23.2
B1T	19.3	11.1	20	Stress	20	4	8.2	45.9
V0T	15.6	9.5	0	Stress	20	4	450.8	13.1
V0T	17.2	9.3	20	Stress	20	3	42.1	44.7
V1T	15.5	10.9	20	Stress	20	4	42.1	44.7
V1T	18.9	10.4	0	Stress	20	6	450.8	13.1
B0W	14.3	11.3	0	Stress	20	5	180.1	23.2
B0W	18.4	10.8	20	Stress	20	4	8.2	45.9
B1W	16.2	12.8	20	Stress	20	4	8.2	45.9
B1W	19.4	12.3	0	Stress	20	5	180.1	23.2
V0W	14.0	11.5	20	Stress	20	4	42.1	44.7
V0W	17.6	10.9	0	Stress	20	5	450.8	13.1
V1W	15.8	12.5	0	Stress	20	4	450.8	13.1
V1W	19.8	11.9	20	Stress	20	6	42.1	44.7
V0W	15.1	11.5	30	Stress	20	5	22.5	59.2
B1W	16.7	12.7	0	Strain	20	2	180.1	23.2
B1W	16.6	12.8	20	Strain	20	2	8.2	45.9
B1W	20.4	12.2	0	Strain	20	3	180.1	23.2
B1W	20.2	12.2	20	Strain	20	3	8.2	45.9
V1W	16.6	12.3	0	Strain	20	5	450.8	13.1
V1W	16.9	12.3	20	Strain	20	4	42.1	44.7
V1W	20.2	11.8	0	Strain	20	3	450.8	13.1
V1W	20.2	11.8	20	Strain	20	2	42.1	44.7
S1	16.3	10.0	4	Strain	10	4	-	-
S4	15.2	10.1	4	Strain	10	5	-	-
S1A	14.7	10.1	4	Strain	10	5	-	-
S1B	15.2	10.1	4	Strain	10	4	-	-
S1C	15.3	10.0	4	Strain	10	5	-	-
S1D	14.3	10.1	4	Strain	10	5	-	-
S1F	15.2	10.1	4	Strain	10	5	-	-
S1G	15.1	10.1	4	Strain	10	5	-	-
S1H	14.2	10.2	4	Strain	10	4	-	-
1675	17.2	13.3	10	Stress	25	10	178.0	38.8
1676	16.1	11.3	10	Stress	25	10	162.0	37.8
1685	18.3	13.1	10	Stress	25	9	133.0	36.2
1695	16.5	15.5	10	Stress	25	8	399.0	25.0

Table 6.3a : Fatigue Test Results

Mix. Ref.	A_{NI} (kJ/m³)	Z_{NI}	A_{Nf} (kJ/m³)	Z_{Nf}	E^* (MPa)	a (MPa)	b
B0T	5.372	0.748	8.037	0.735	9071	4634.9	-0.588
B0T	0.955	0.801	0.933	0.816	11438	10.6	0.003
B1T	15.081	0.577	10.542	0.628	13259	2.2	0.178
B1T	10.174	0.650	16.049	0.634	4397	1145.9	-0.446
V0T	1.489	0.781	1.295	0.804	15619	0.7	0.246
V0T	4.150	0.646	2.303	0.739	8323	97.6	-0.173
V1T	58.515	0.447	59.735	0.468	11656	9.1	0.105
V1T	1.758	0.736	3.593	0.714	13571	780.8	-0.485
B0W	4.485	0.732	2.808	0.800	14228	46.6	-0.156
B0W	2.355	0.759	5.607	0.730	5169	515.7	-0.349
B1W	9.992	0.687	18.976	0.653	7002	349.4	-0.297
B1W	12.403	0.613	14.370	0.629	12147	64.2	-0.183
V0W	6.766	0.661	9.565	0.653	11333	89.3	-0.165
V0W	0.473	0.853	0.647	0.841	14621	1.3	0.188
V1W	0.650	0.854	0.526	0.842	20216	24.0	-0.117
V1W	5.307	0.634	4.026	0.694	8414	909.7	-0.403
V0W	29.357	0.512	67.666	0.479	5979	7735.2	-0.357
B1W	-	-	5.849	0.695	12434	8.3	-0.031
B1W	17.885	0.637	18.273	0.637	5928	780.7	-0.399
B1W	21.520	0.596	32.166	0.549	10698	264.0	-0.339
B1W	50.623	0.554	26.705	0.603	4539	487.4	-0.342
V1W	1502.930	0.298	11.576	0.638	18189	128.2	-0.291
V1W	37.320	0.486	32.371	0.496	8930	31.2	-0.045
V1W	-	-	37.422	0.710	11109	126.4	-0.277
V1W	1.041	0.835	0.843	0.859	6397	271.6	-0.281
S1	-	-	17459.5	-0.256	10176	91.1	-0.249
S4	-	-	1.1418	0.718	13659	8.2	-0.029
S1A	51.320	0.389	7.078	0.600	11530	1.0	-0.255
S1B	7.150	0.582	0.406	0.833	11725	14.1	-0.040
S1C	122.884	0.256	25.819	0.385	10247	56.2	-0.201
S1D	-	-	0.619	0.798	11122	56.2	-0.224
S1F	1.985	0.710	1.567	0.728	11768	2995.2	-0.608
S1G	97.266	0.389	5.974	0.634	12428	193.2	-0.316
S1H	-	-	4.659	0.663	15948	145.1	-0.293
1675	11.220	0.629	42.346	0.552	9213	693.5	-0.397
1676	9.086	0.650	164.338	0.458	10470	625.3	-0.390
1685	46.567	0.538	98.541	0.520	7261	1494.1	-0.480
1695	16.701	0.646	37.821	0.600	10839	425.3	-0.397

Note : The "a" value in this table was calculated using E^* value expressed in MPa.

Table 6.3b : Fatigue Test Results

No.	Ref.	T	Type	Va	VMA	Vfb	Vb	ε	σ	E*	δ	Nf	N1
2	B1W	0	Strain	4.1	16.8	75.6	12.7	200	2,425	12,124	11	74,015	120,012
3	B1W	20	Strain	3.8	16.6	77.1	12.8	200	1096	5480	25.9	190017	170004
4	B1W	20	Strain	3.8	16.5	77	12.7	300	1913	6375	24.3	14615	13515
5	B1W	0	Strain	9	21	57.1	12	200	1969	9845	12.3	90215	165319
7	B1W	0	Strain	7.6	19.9	61.8	12.3	300	3288	10959	14.3	12405	15015
8	B1W	20	Strain	7.7	19.9	61.3	12.2	100	479	4790	25.45	5060007	5550016
10	B1W	20	Strain	8.2	20.4	59.8	12.2	200	851	4253	27.1	310008	310008
11	V1W	0	Strain	4.1	16.4	75	12.3	100	2045	20453	7.45	1840010	1780003
15	V1W	0	Strain	4.2	16.5	74.5	12.3	200	4052	20261	7.45	238437	278436
16	V1W	20	Strain	4.8	17	71.8	12.2	100	795	7954	20.65	310001	330013
18	V1W	20	Strain	4.9	17.1	71.3	12.2	100	857	8570	19.3	190011	320014
19	V1W	20	Strain	4.3	16.6	74.1	12.3	200	1829	9147	20.85	11513	14706
23	V1W	20	Strain	9.1	20.8	56.2	11.7	200	1189	5943	26.3	15210	26109
24	V1W	20	Strain	7.6	19.5	61	11.9	200	1370	6850	22	4713	4312
25	B0T	20	Stress	3.5	13.9	74.8	10.4	136.4	1350	9899	21.5	59306	48660
26	B0T	20	Stress	4.2	14.5	71	10.3	147.1	1350	9178	20.65	37214	28472
27	B0T	20	Stress	4.8	15	68	10.2	205.7	1350	6564	29.15	2308	1805
28	B0T	20	Stress	4.4	14.7	70.1	10.3	266	2500	9400	24.6	1115	961
29	B0T	20	Stress	4.2	14.5	71	10.3	242.4	2500	10314	21.7	1306	1091
30	B0T	0	Stress	8.5	18.3	53.6	9.8	108.1	1000	9251	10.75	150012	129638
31	B0T	0	Stress	8.2	18.1	54.7	9.9	84.3	1000	11856	10.15	720004	596757
32	B0T	0	Stress	8.2	18.1	54.7	9.9	142.4	1700	11939	12.05	2201	2008
33	B0T	0	Stress	7.9	17.8	55.6	9.9	154.8	1700	10982	11.8	8801	7795
34	B0T	0	Stress	8	17.9	55.3	9.9	129.1	1700	13164	10.35	30701	25727
35	B1T	0	Stress	4.7	16.2	71	11.5	116.8	1600	13700	11	48911	39557
36	B1T	0	Stress	5	16.5	69.7	11.5	121.9	1600	13130	11.95	60600	49748
37	B1T	0	Stress	4.9	16.4	70.1	11.5	186.4	2500	13414	12	7301	6568
38	B1T	0	Stress	4.4	16	72.5	11.6	202.1	2500	12373	10.85	6400	5910
39	B1T	0	Stress	4.5	16	71.9	11.5	182.8	2500	13676	11.35	3911	3687
40	B1T	20	Stress	8.6	19.7	56.3	11.1	113.7	500	4399	27.65	323943	263894
41	B1T	20	Stress	7.9	19	58.4	11.1	120.7	500	4143	28.25	365514	316360
42	B1T	20	Stress	7.9	19	58.4	11.1	202.6	900	4443	30.4	7510	6007
43	B1T	20	Stress	8.4	19.4	56.7	11	195.6	900	4602	28.3	13635	10811
44	V0T	0	Stress	6.5	15.9	59.1	9.4	96.7	1700	17588	7.05	470004	400023
45	V0T	0	Stress	6.3	15.8	60.1	9.5	115.9	1700	14668	7.6	75802	60972
46	V0T	0	Stress	5.2	14.8	64.9	9.6	170	2500	14707	7.45	3109	3042
47	V0T	0	Stress	6.4	15.9	59.7	9.5	161.1	2500	15514	8.05	15004	13408
48	V0T	20	Stress	7.7	17	54.7	9.3	70.6	600	8493	21.55	105375	83311
49	V0T	20	Stress	8	17.3	53.8	9.3	123.4	1000	8105	20.85	14211	11060
50	V0T	20	Stress	8.1	17.4	53.4	9.3	119.4	1000	8372	20.45	5611	4699
51	V1T	20	Stress	4.6	15.5	70.3	10.9	120.7	1300	10772	21.55	23100	18173
52	V1T	20	Stress	4.4	15.3	71.2	10.9	117.8	1300	11033	23	25413	21677
53	V1T	20	Stress	4.2	15.1	72.2	10.9	192.4	2400	12473	24.85	2816	2450
54	V1T	20	Stress	5.1	15.9	67.9	10.8	194.4	2400	12345	24.15	3802	3138
55	V1T	0	Stress	8.2	18.6	55.9	10.4	95.8	1000	10442	10.56	13000	7487
56	V1T	0	Stress	8	18.5	56.8	10.5	66.5	1000	15033	7.6	1049401	793517
57	V1T	0	Stress	8.8	19.2	54.2	10.4	110.1	1600	14531	9.25	140015	112032
58	V1T	0	Stress	8.4	18.8	55.3	10.4	108.5	1600	14742	7	84615	64858
59	V1T	0	Stress	8.6	19	54.7	10.4	113.5	1600	14091	6.9	120009	87671
60	V1T	0	Stress	9.1	19.4	53.1	10.3	158.9	2000	12584	7.35	837096	577721
61	B0W	0	Stress	2.8	14.1	80.1	11.3	112.1	1725	15390	10.9	130000	101543
62	B0W	0	Stress	2.9	14.3	79.7	11.4	100.8	1725	17115	10.45	180221	131038
63	B0W	0	Stress	3.2	14.5	77.9	11.3	295.4	3000	10157	10.45	29108	24849
64	B0W	0	Stress	2.8	14.2	80.3	11.4	208.1	3000	14413	11.8	6516	5803
65	B0W	0	Stress	3.4	14.6	76.7	11.2	213.3	3000	14065	10.55	1107	1020
66	B0W	20	Stress	7.5	18.3	59	10.8	105.8	600	5673	26.45	170000	131208
67	B0W	20	Stress	7.6	18.4	58.7	10.8	125.2	600	4793	24.8	9673	4922
68	B0W	20	Stress	7.6	18.4	58.7	10.8	192.8	900	4667	25.7	547	476
69	B0W	20	Stress	7.6	18.4	58.7	10.8	162.4	900	5541	27.9	86200	22611
70	B1W	20	Stress	3.7	16.5	77.6	12.8	161	1100	6832	24.25	42400	32705
71	B1W	20	Stress	3.1	15.9	80.5	12.8	164.3	1100	6695	25.6	42200	32149

Table 6.4 : Results from the Trapezoidal Fatigue Test

72	B1W	20	Stress	3.7	16.5	77.6	12.8	308.8	2000	6476	27.6	1913	1535
73	B1W	20	Stress	3.1	15.9	80.5	12.8	249.9	2000	8004	27.3	1300	942
74	B1W	0	Stress	6.7	19.1	64.9	12.4	76.5	1000	13076	11.6	522465	404005
75	B1W	0	Stress	6.7	19.1	64.9	12.4	86.5	1000	11562	12.6	480000	401508
76	B1W	0	Stress	7.3	19.6	62.8	12.3	84.7	1000	11803	11.25	1719342	1456086
77	B1W	0	Stress	6.9	19.2	64.1	12.3	145.5	1600	10993	12.35	48200	39351
78	B1W	0	Stress	7.7	20	61.5	12.3	120.3	1600	13299	11.7	28100	69411
79	V0W	20	Stress	2.6	14.1	81.6	11.5	113.3	1300	11474	18.95	29012	22936
80	V0W	20	Stress	2.2	13.7	83.9	11.5	124.5	1300	10442	18.75	35905	27605
81	V0W	20	Stress	2.4	13.9	82.7	11.5	183.1	2300	12561	19.5	2514	1995
82	V0W	20	Stress	2.8	14.2	80.3	11.4	211.9	2300	10856	27.3	1504	1173
83	V0W	0	Stress	7	17.9	60.9	10.9	61.8	1000	16192	7.05	336580	253529
84	V0W	0	Stress	6.8	17.8	61.8	11	81.1	1000	12324	7.7	4314053	3650214
85	V0W	0	Stress	6.3	17.3	63.6	11	106.3	1600	15055	8.2	290012	246923
86	V0W	0	Stress	6.8	17.7	61.6	10.9	106.3	1600	15057	8.3	68814	59673
87	V0W	0	Stress	6.4	17.4	63.2	11	110.5	1600	14478	8	920013	781953
88	V1W	0	Stress	2.7	15.2	82.2	12.5	78	1600	20515	7.1	1980000	1456449
89	V1W	0	Stress	3.4	15.8	78.5	12.4	75.7	1600	21141	7.3	449147	345674
90	V1W	0	Stress	3	15.5	80.6	12.5	150.8	2700	17904	9.95	807	43
91	V1W	0	Stress	4.2	16.5	74.5	12.3	126.7	2700	21303	8.55	136124	115685
92	V1W	20	Stress	7.8	19.6	60.2	11.8	59.5	500	8400	25.1	280000	225978
93	V1W	20	Stress	6.8	18.8	63.8	12	61.8	500	8092	22.7	520000	443826
94	V1W	20	Stress	7.5	19.4	61.3	11.9	99.1	800	8069	24.25	20800	14952
95	V1W	20	Stress	7.6	19.5	61	11.9	107.2	800	7461	27.05	28000	23747
96	V1W	20	Stress	6.8	18.8	63.8	12	85.9	800	9309	24	38800	30031
97	V1W	20	Stress	6.8	18.7	63.6	11.9	87.4	800	9155	22.5	43300	36127
98	S1	4	Strain	6.6	16.6	60.2	10	200	2075	10374	9.1	10558	15703
102	S1A	4	Strain	5	15.1	66.9	10.1	200	2748	13738	9.7	9853	8852
106	S1A	4	Strain	5.2	15.2	65.9	10	100	877	8770	11.6	200003	265008
107	S1B	4	Strain	5.7	15.7	63.8	10	200	2643	13217	9.8	5253	7650
109	S1B	4	Strain	5	15.1	66.9	10.1	100	1270	12702	10.4	135000	110006
111	S1C	4	Strain	5.3	15.4	65.5	10.1	200	2457	12285	8.1	4457	10305
114	S1C	4	Strain	5.1	15.2	66.4	10.1	100	536	5364	10.9	37958	235004
121	S1F	4	Strain	5.7	15.7	63.8	10	200	2206	11028	10.7	1752	2050
122	S1F	4	Strain	5.1	15.2	66.4	10.1	170	2303	13545	9.2	7406	7051
123	S1F	4	Strain	4.8	14.9	67.8	10.1	150	1900	12667	8.8	21605	18155
125	S1F	4	Strain	5	15.1	66.9	10.1	100	1008	10084	9.4	255022	215006
127	S1G	4	Strain	5	15.1	66.8	10.1	170	2219	13052	8.5	32100	48850
129	S1G	4	Strain	5.1	15.2	66.4	10.1	120	1550	12919	9.5	125003	115003
134	S1H	4	Strain	4.3	14.5	70.3	10.2	230	3530	15350	8.6	9300	11458
138	S4	4	Strain	5	15.1	68.9	10.1	100	1431	14308	6.3	96893	95005
139	1676	10	Stress	4.4	15.7	72.2	11.4	205.2	2000	9746	16.1	6207	5322
140	1676	10	Stress	4.5	15.9	71.5	11.3	183.4	2000	10903	17.3	9900	8448
141	1676	10	Stress	4.3	15.7	72.6	11.4	93.8	1000	10664	17.5	303539	259453
142	1676	10	Stress	3.3	14.7	78	11.5	65.4	750	11465	16.1	1844184	1583237
143	1676	10	Stress	5.9	17.1	65.4	11.2	66.1	750	11351	16.9	2031835	1849109
144	1676	10	Stress	4.7	16.1	70.5	11.3	95.3	1000	10491	16.3	482675	431792
145	1676	10	Stress	5	16.3	69.5	11.3	125	1250	10000	16.1	107427	89416
146	1676	10	Stress	4.7	16.1	70.5	11.3	128.4	1250	9736	15.7	45796	38388
147	1676	10	Stress	6	17.2	65.1	11.2	231.7	2500	10788	17.6	1355	912
148	1676	10	Stress	5.3	16.6	67.8	11.2	261.6	2500	9558	18.1	921	546
149	1685	10	Stress	5.4	18.4	70.8	13	140.4	1000	7120	20	107553	95637
150	1685	10	Stress	5.8	18.8	69.2	13	228.1	1500	6575	19.8	12495	10326
151	1685	10	Stress	5.2	18.3	71.3	13.1	269.4	1750	6497	21.3	6521	5072
152	1685	10	Stress	5	18.1	72.3	13.1	102.8	750	7295	19.8	429240	367217
153	1685	10	Stress	5.5	18.6	70.2	13	178.8	1250	6992	20.3	28023	23749
154	1685	10	Stress	5.4	18.4	70.8	13	227	1750	7709	20	10062	8203
155	1685	10	Stress	4.7	17.8	73.6	13.1	213.1	1500	7038	19.2	10516	8756
156	1685	10	Stress	5.3	18.4	71.1	13.1	120.1	1000	8324	20.7	115167	103812
157	1685	10	Stress	5.2	18.3	71.5	13.1	160.3	1250	7799	18.9	50673	42832
158	1695	10	Stress	1.2	16.7	92.8	15.5	178.3	1750	9814	13.7	98212	84464

Table 6.4 : Results from the Trapezoidal Fatigue Test (cont.)

159	1695	10	Stress	0.9	16.4	94.5	15.5	173	1750	10117	14.2	77866	66678
160	1695	10	Stress	0.7	16.2	95.9	15.5	201.1	2000	9945	14.5	36879	31440
161	1695	10	Stress	0.6	16.1	96.4	15.6	207.8	2250	10829	13.6	29009	25401
162	1695	10	Stress	1.1	16.6	93.2	15.5	231.5	2500	10800	13.8	17013	14566
163	1695	10	Stress	1.3	16.7	92.3	15.5	198.3	2250	11347	13.4	26908	22822
164	1695	10	Stress	0.5	16.1	96.8	15.6	104.3	1250	11989	13.1	1453302	1270190
165	1695	10	Stress	0.8	16.4	94.8	15.5	105.3	1250	11871	12.7	1136433	1012587
166	1675	10	Stress	3.5	16.8	79.2	13.3	83.3	750	9006	19.2	1417351	1277001
167	1675	10	Stress	3.5	16.8	79.2	13.3	103	1000	9713	16.3	111803	91832
168	1675	10	Stress	5.4	18.5	70.6	13	141.5	1250	8831	17.7	37600	31783
169	1675	10	Stress	4.7	17.8	73.7	13.1	169.3	1500	8858	16.8	13912	11779
170	1675	10	Stress	4.5	17.7	74.3	13.2	188.6	1750	9278	17	9894	7858
171	1675	10	Stress	4.1	17.3	76.4	13.2	79.9	750	9391	17.1	847350	728397
172	1675	10	Stress	4.5	17.6	74.7	13.2	107.7	1000	9283	17.8	102594	86296
173	1675	10	Stress	2.7	16.1	83.4	13.4	134	1250	9329	17.4	49659	42964
174	1675	10	Stress	3.3	16.6	80.3	13.3	163.1	1500	9199	18.4	30803	26390
175	1675	10	Stress	3.2	16.5	80.7	13.4	189.4	1750	9239	17.6	6661	5233
176	V0W	30	Strain	4.8	17	71.8	12.2	185.6	1000	5389	30.6	6976	4854
177	V0W	30	Strain	3.5	14.8	76.4	11.3	82.6	500	6053	37.5	109665	92477
178	V0W	30	Strain	3.3	14.6	77.4	11.3	50.1	300	5985	30.75	1484789	1245589
179	V0W	30	Strain	3.3	14.7	77.6	11.4	46.5	300	6454	30.05	641069	465167
180	V0W	30	Strain	3.3	14.6	77.4	11.3	83.1	500	6016	36.6	106628	85162
1	B1W	0	Strain	4	16.7	76	12.7	100	1274	12744	11.1	5180000	*******
6	B1W	0	Strain	8	20.2	60.4	12.2	200	2258	11290	11.2	*******	*******
9	B1W	20	Strain	7.9	20.1	60.7	12.2	100	457	4573	26.1	10100030	*******
12	V1W	0	Strain	4.3	16.6	74.1	12.3	100	1840	18401	6.25	1380017	*******
13	V1W	0	Strain	4.2	16.5	74.5	12.3	200	3199	15993	7.75	54501	*******
14	V1W	0	Strain	4.4	16.7	73.7	12.3	200	3168	15839	8.55	61412	*******
17	V1W	20	Strain	4.3	16.7	74.3	12.4	100	1005	10048	22.95	190014	*******
20	V1W	0	Strain	9.8	21.4	54.2	11.6	100	1310	13098	9.6	2690006	*******
21	V1W	0	Strain	8	19.8	59.6	11.8	200	2024	10118	10.05	38306	*******
22	V1W	0	Strain	7.4	19.3	61.7	11.9	200	2022	10111	11.25	72544	*******
99	V1W	4	Strain	6.3	16.3	61.3	10	170	1860	10941	9	13003	*******
100	V1W	4	Strain	6.2	16.2	61.7	10	150	1440	9603	8.4	20154	*******
101	V1W	4	Strain	6.1	16.1	62	10	100	979	9786	9.7	31601	*******
103	S1A	4	Strain	4.4	14.6	69.8	10.2	170	2175	12792	11.1	16106	*******
104	S1A	4	Strain	4	14.2	71.8	10.2	150	2025	13503	9.3	120008	*******
105	S1A	4	Strain	4.4	14.6	69.8	10.2	120	1061	8845	8.4	790006	*******
108	S1B	4	Strain	5.1	15.2	66.4	10.1	150	1324	8828	8.1	3006	*******
110	S1B	4	Strain	4.6	14.8	68.8	10.2	130	1580	12153	8.7	12350	*******
112	S1C	4	Strain	5.1	15.2	66.4	10.1	120	1473	12271	8.5	60007	*******
113	S1C	4	Strain	4.9	15	67.4	10.1	150	1593	10623	8.3	21950	*******
115	S1C	4	Strain	6.1	16	61.9	9.9	170	1818	10694	9.1	14005	*******
116	S1D	4	Strain	4.5	14.7	69.3	10.2	200	2046	10231	7.3	13900	*******
117	S1D	4	Strain	4	14.2	71.7	10.2	170	1942	11426	7.4	23401	*******
118	S1D	4	Strain	4.2	14.4	70.8	10.2	150	1667	11111	6.4	162029	*******
119	S1D	4	Strain	3.9	14.2	72.4	10.3	120	1322	11019	7	780003	*******
120	S1D	4	Strain	4.2	14.4	70.8	10.2	100	1183	11825	7.2	1280000	*******
124	S1F	4	Strain	4.9	15	67.4	10.1	120	1382	11515	8.7	14849	*******
126	S1G	4	Strain	5.4	15.4	65	10	200	2533	12663	9.6	10254	*******
128	S1G	4	Strain	4.7	14.8	68.2	10.1	150	2000	13331	9.3	60006	*******
130	S1G	4	Strain	5	15.1	66.9	10.1	100	1017	10174	8.4	935001	*******
131	S1H	4	Strain	4.2	14.3	70.7	10.1	100	1490	14904	8.3	585000	*******
132	S1H	4	Strain	3.9	14.2	72.4	10.3	150	2488	16586	8.3	8203	*******
133	S1H	4	Strain	3.6	13.9	74	10.3	200	3391	16953	8.7	12855	*******
135	S4	4	Strain	5.3	15.3	65.5	10	170	1594	9378	7.1	24608	*******
136	S4	4	Strain	4.6	14.7	64	10.1	200	3299	16494	6.7	6502	*******
137	S4	4	Strain	4.7	14.8	68.9	10.1	120	1735	14455	6.9	230004	*******
Max. Value		30		9.8	20.8	96.8	15.6	308.8	4052	21303	36.6	10100030	5550016
Min Value		0		0.5	13.7	53.1	9.3	46.5	300	4143	6.25	547	43

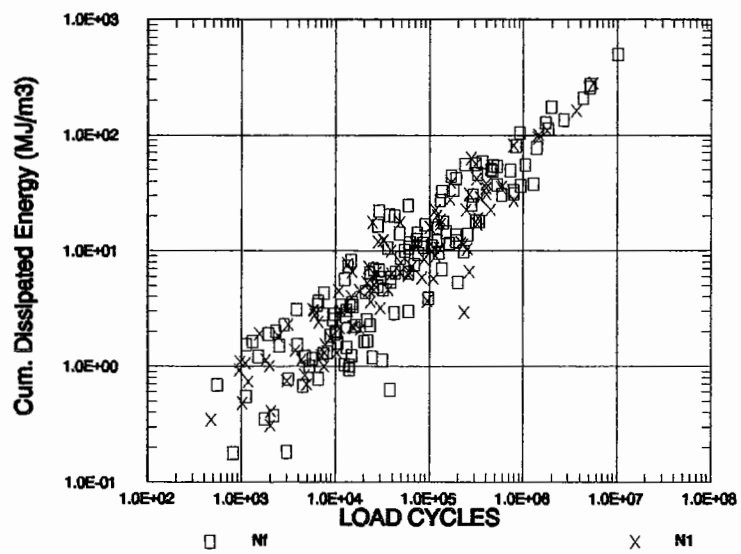**Table 6.4 : Results from the Trapezoidal Fatigue Test (cont.)**

Figure 6.16 : Fatigue Data Points, All Conditions and All Mixtures

considered.   Twenty-seven mixtures representing differing volumetric compositions were evaluated. The results are represented in Table 6.5.

The initial review of the data presented in Tables 6.3 and 6.5 shows that a relationship exists between the parameter A_{Nf} and volume of binder, Vb as illustrated in Figure 6.17.   This relationship, although not impressive, is conceptually similar to that found by Cooper (1976) in the analysis of their fatigue data and illustrates the importance of binder volume. This can be further demonstrated by reduction in the scatter of fatigue lines if the dissipated energy is considered only to occur in the binder film, as illustrated in Figure 6.18, from van Dijk et al. (1977). In this case the energy is considered to be dissipated in a unit volume of binder. The lines represented in Figure 6.18b are obtained by dividing the parameter A_{Nf} by the proportion of binder ($Vb/100$). Thus, the fatigue life is represented by the equation as follows:

$$W_{Nf} = \frac{100\ A_{Nf}}{Vb}\ N^{Z_{Nf}} \qquad\qquad (6.16)$$

The above relationship is used to demonstrate a conceptual interpretation regarding the significance of the binder volume. The "true" dissipated energy in the binder is considered impossible to determine.

On inspection of the data presented in Table 6.3b it appears that there is a linear relationship between log A and Z (for both the Nl and Nf condition) as shown in Figure 6.19. This relationship may be expressed as:-

Type of Mixture	VMA (%)	Vb (%)	A_{Nf} (kJ/m$_3$)	Z_{Nf}	Reference
Asphalt Concrete	15.9	14.2	30.2	0.718	1
Lean Sand Asphalt	18.9	10.5	31.3	0.691	1
Dense Bitumen Macadam	14.4	11.0	18.8	0.697	1
Gravel Sand Asphalt	22.0	11.0	18.1	0.637	1
Lean Bitumen Macadam	38.1	4.9	12.8	0.610	1
Dense Asphalt Concrete	13.3	11.4	64.6	0.630	1
Dense Bitumen Macadam	14.6	11.0	28.9	0.662	1
Rolled Asphalt Base course	16.3	14.1	24.8	0.699	1
Asphalt Basecourse	18.6	9.3	14.8	0.706	1
Rich Sand Sheet	27.1	19.3	468.0	0.503	1
Gravel Sand Asphalt	19.9	13.3	12.0	0.716	1
Bitumen Sand	29.2	8.9	21.4	0.642	1
Sand Asphalt	23.9	20.1	117.0	0.630	5
Asphalt Concrete	15.9	14.4	302.0	0.510	5
Asphalt Concrete	13.4	11.5	67.6	0.630	5
Asphalt Concrete	14.4	11.2	49.6	0.590	5
Macadam	38.9	4.9	10.8	0.680	5
Rolled Asphalt	17.4	14.1	87.3	0.580	5
Asphalt Wearing Course	15.0	12.3	53.8	0.600	6
Asphalt Wearing Course	18.1	*14.3	112.2	0.570	6
Asphalt Wearing Course	18.4	13.4	31.7	0.630	6
Asphalt Wearing Course	17.1	12.3	104.7	0.520	6
Asphalt Wearing Course	16.8	14.6	67.7	0.560	6
Asphalt Wearing Course	20.5	13.3	28.1	0.600	6
Dense Asphalt Concrete	18.6	13.5	29.7	0.634	7
Dense Asphalt Concrete	15.1	12.4	55.8	0.598	7
Dense Asphalt Concrete	20.7	13.5	28.8	0.598	7

Table 6.5 : Fatigue Test Results (after references van Dijk et al., 1975; van Dijk, 1977; Gerritsen, 1987 and Gerritsen et al., 1987)
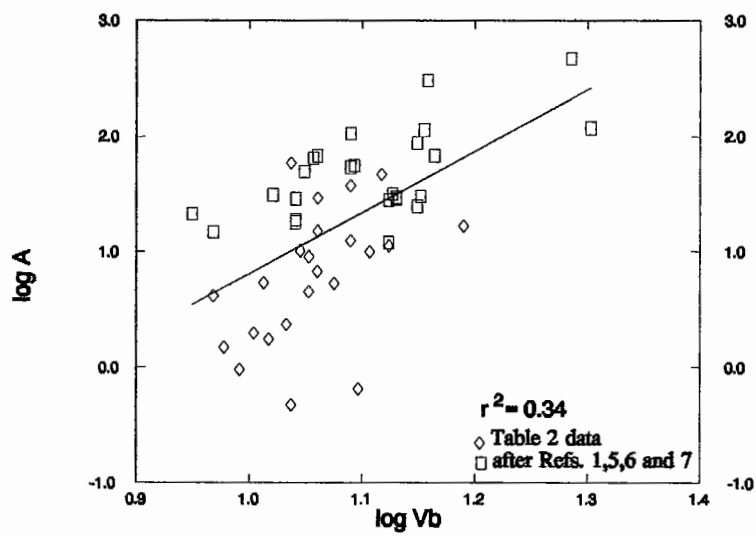
Figure 6.17 : Volume of Binder versus A (after van Dijk et al., 1977; van Dijk, 1975; Gerritsen, 1987 and Gerritsen et al., 1987)

-6.42-
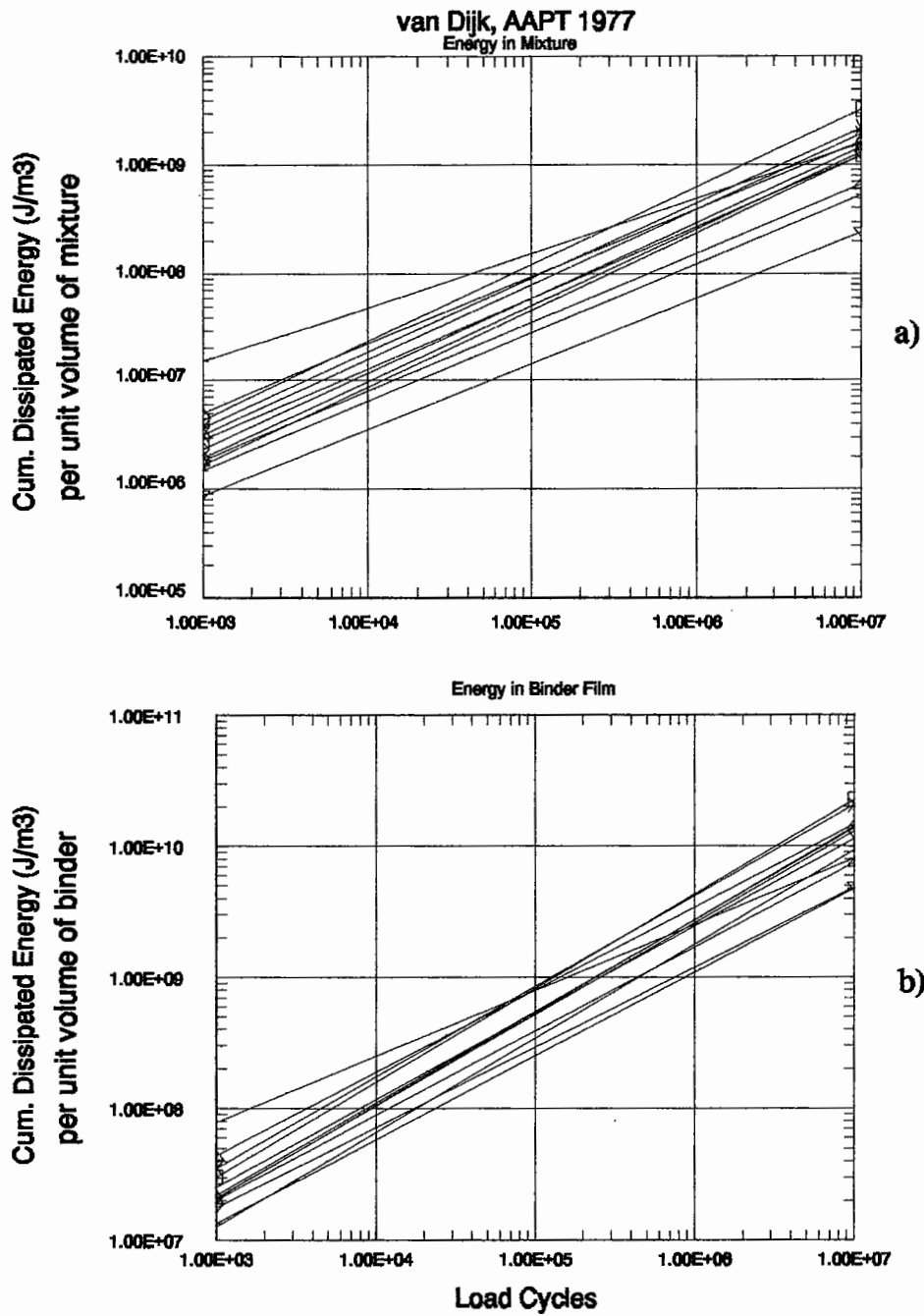
Figure 6.18 : Fatigue Lines Based upon Mixture Strain (a) and Binder
Strain (b), (after van Dijk et al., 1975)
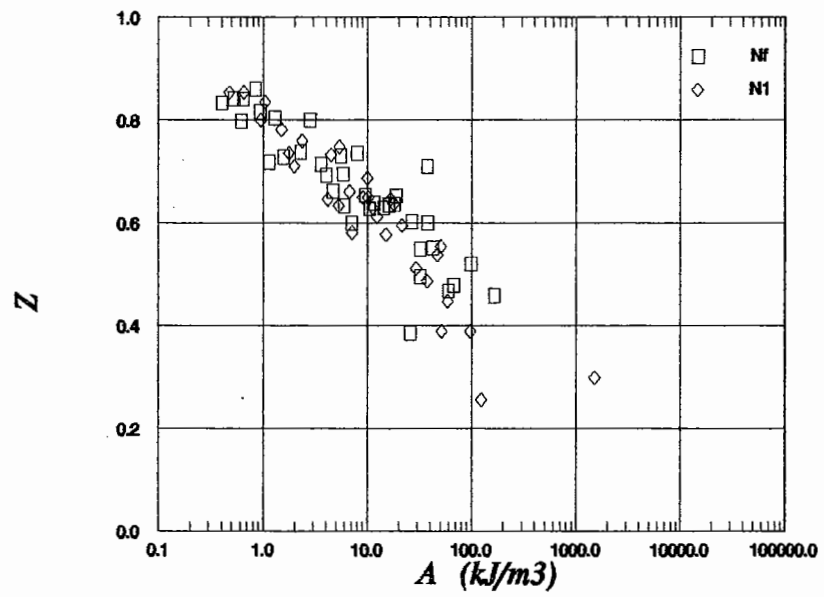
Figure 6.19 : Relationship Between Parameters *A* and *Z*
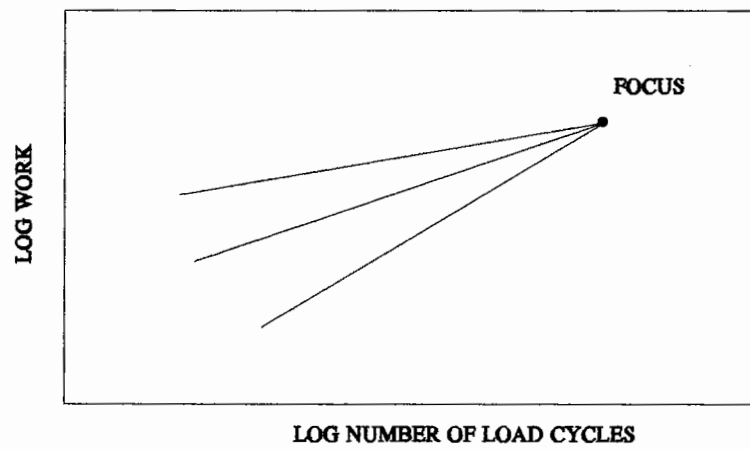
Figure 6.20 : Concept of a "Focus" Point

$$Z = c - d \log A \qquad\qquad (6.17)$$

Where c and d are constants having values of 0.809 and 0.188 respectively for the $N1$ condition. A certain amount of scatter exists. This scatter can be considered in one of two ways; either it is representative of typical scatter inherent in fatigue test results <u>or</u> Z is not dependent on A alone and other variables are involved. If the values of A and Z conform to Equation 6.17, then only the parameter A is required to define the fatigue life and this results in the log work - log life lines intersecting at a common point or "focus", Figure 6.20. The co-ordinates of the focus are obtained from $1/d$ for the life and by c/d for work. The position of the "focus" obtained by reviewing the results obtained from the data contained in Tables 6.3b and 6.5 are presented in Table 6.6 along with the appropriate regression coefficient.

In all instances, the position of the "focus" is at a number of cycles corresponding to a relatively high fatigue life. The results in Table 6.5 demonstrate the importance of considering a wide range of mixtures since the regression coefficient of the relationship appears to be a function of the number of mixture types evaluated by each researcher. This is to be expected due to the difficulty in accurately determining the slope of a fatigue line and the insufficient amount of data points generally used. In addition, some of the data sets, (van Dijk et al., 1977 and van Dijk 1975), contained data which has been obtained at several temperatures and loading frequencies. This aspect is undesirable since the effect of these parameters is then difficult to discern.

Researcher	No of Fatigue Lines	Position of Focus		Regression Coefficient
		log N	log W (kJ/m^3)	r^2
This work (N1)	32	5.309	4.306	0.87
This work (Nf)	38	5.618	4.539	0.85
van Dijk et al., 1975	12	9.365	7.635	0.56
van Dijk (1977)	6	9.841	7.779	0.71
Gerritsen (1987)	6	8.093	6.458	0.66
Gerritsen et al., (1987)	3	16.87	11.853	0.21
Tayebali et al., (1992)	21	5.135	4.097	0.90

Table 6.6 : Evaluation of the "Focus" Position From Different Researchers' Data

In order to develop a predictive method including possible variables which are not immediately apparent in the relationship between A and Z as shown in Figure 6.19 a statistical analysis was performed on all the data obtained from the fatigue testing. In fatigue prediction models developed by other researchers (Gerritsen, 1987; Pell and Cooper, 1975; Bonnaire et al., 1980 and The Asphalt Institute, 1982) the relevant parameters used have been the volumetric composition and a measure of the binder or mixture consistency (eg. softening point, viscosity at 60°C, or mixture stiffness). In the development of a new procedure associated with cumulative dissipated energy (work) it is important to remember that the energy dissipated is a function of the loss modulus (E^* $sin \ \delta$). This has been shown to relate to fatigue performance if the summation with respect to life is considered (Molenaar, 1990; Pronk, 1990; Hopman, 1990 and Rowe, 1991). An example of data obtained in this format during this research is shown in Figure 6.21. Consequently, parameters representing both mixture volumetrics and mixture visco-elastic behaviour were evaluated in the statistical analysis.

6.4   EVALUATION OF THE WORK RATIO, ψ_{N1}

In addition to visco-elastic and volumetric parameters the work ratio, ψ_{N1}, is an important parameter to obtain in order to predict the fatigue life. Van Dijk (1977) first introduced the ratio which is used to account for the reducing (strain test) or increasing (stress test) rate of energy dissipation during a fatigue test as illustrated in Figure 6.22. Van Dijk showed that this parameter was dependent on the mixture stiffness and the type of test, see Figure 6.23.
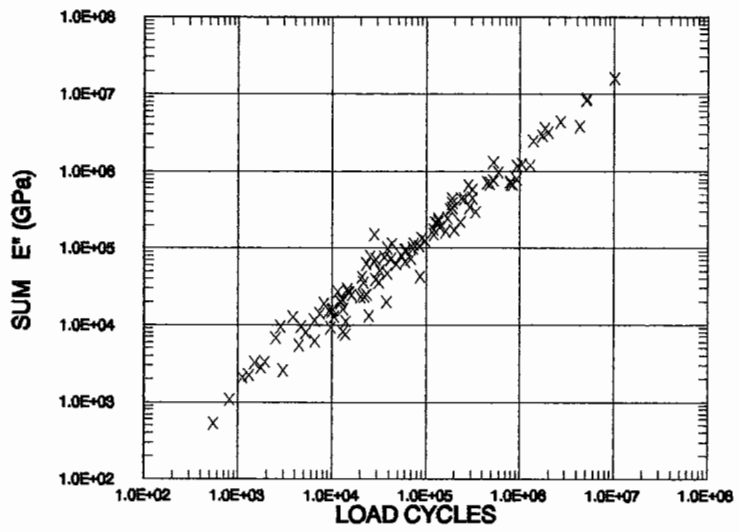
Figure 6.21 : Summation of the Loss Stiffness Modulus versus Number of Cycles to Failure
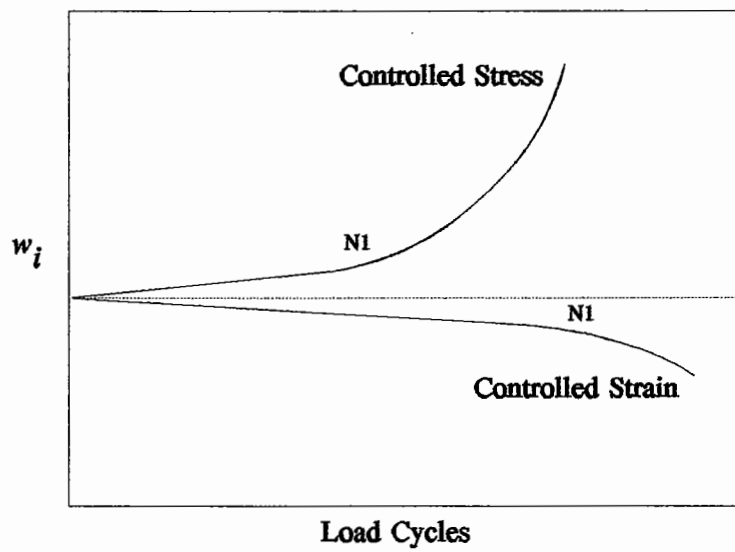
Figure 6.22 : Dissipated Energy per Cycle During Controlled Strain and Stress Fatigue Tests
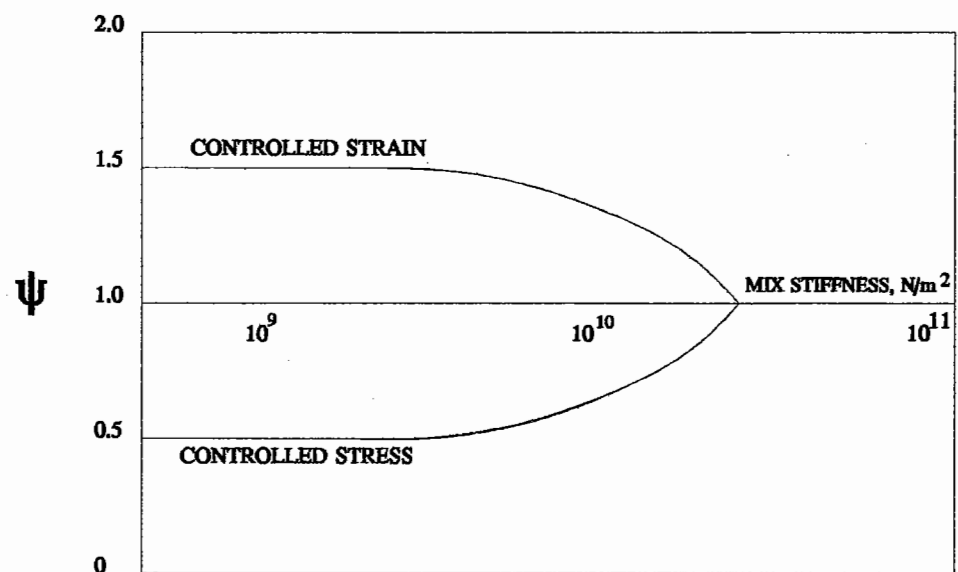
Figure 6.23 : Work Ratio as a Function of Mixture Stiffness and Test Type (after Van Dijk et al., 1975)

This parameter is defined as the ratio between the product of the initial dissipated energy in cycle 1 and *N1* divided by the cumulative dissipated energy, as follows:-

$$\psi_{N1} = \frac{w_o \, N1}{W_{N1}} \qquad (6.18)$$

The ratio can be shown to be dependent upon the initial rheology of the mixture. Expanding Equation 6.18 gives:-

$$\psi_{N1} = \frac{\pi \, \sigma_o \, \varepsilon_o \, \sin \delta_o \, N1}{\displaystyle\sum_{i=1}^{i=N1} w_i} \qquad (6.19)$$

By inspection of Figures 6.14 and 6.15 it can be observed that the rate of change in w_i is approximately linear up to *N1*, thus the summation term can be replaced by the mean value of dissipated energy multiplied by *N1*, as follows:-

$$\psi_{N1} = \frac{\pi \, \sigma_o \, \varepsilon_o \, \sin \delta_o \, N1}{\bar{w}_i \, N1} \qquad (6.20)$$

Considering a controlled strain test, Equation 6.20 can be reduced as follows:-

$$\psi_{N1} = \frac{\pi \, E_o^* \, \varepsilon_o^2 \, \sin \delta_o \, N1}{\pi \, \bar{E}'' \, \varepsilon_o^2 \, N1} = \frac{E_0''}{\bar{E}''} \qquad (6.21)$$

The mean value of extensional loss modulus may be deduced from Equations 6.7 and 6.8 as follows:-

i)   Determine the parameter **a**

$$a = 10^{\left[\frac{\log \delta_o - 0.224 \log \left[E_o^*\right]}{1 - 0.222 \log \left[E_o^*\right]}\right]} \qquad (6.22)$$

ii)   Determine the loss modulus at the *N1* condition, assuming that at *N1* the mixture has dropped to 60% of the original extensional complex modulus. [The choice of 60% of the original complex modulus for the definition of the *N1* criteria is based upon the observation that *N1* generally occurs at approximately this reduction, as illustrated in Figure 6.24]

$$E_{60}'' = 0.6 \, E_o^* \, \sin\left[a \, \left(0.6 \times E_o^*\right)^{(0.224 - 0.222 \log a)} \right] \qquad (6.23)$$

iii)   Determine the mean loss modulus.

$$\bar{E}'' = \frac{E_0'' + E_{60}''}{2} \qquad (6.24)$$

The combinations of Equations 6.22 to 6.24 can be written as Equation 6.25 for a controlled strain test:-

$$\Psi_{N1} = \left\{ \frac{2 \sin \delta_o}{\sin \delta_o + 0.6 \sin \left[a \left(E_{60}^*\right)^{(0.224 - 0.222 \log a)} \right]} \right\} \qquad (6.25)$$

Equation 6.25 is limited to controlled strain data. But it is possible to develop a similar relation for controlled stress data. However, if a mode of loading factor, Γ, is considered a relationship can be obtained which is applicable for both controlled stress and strain fatigue tests and any intermediate mode of
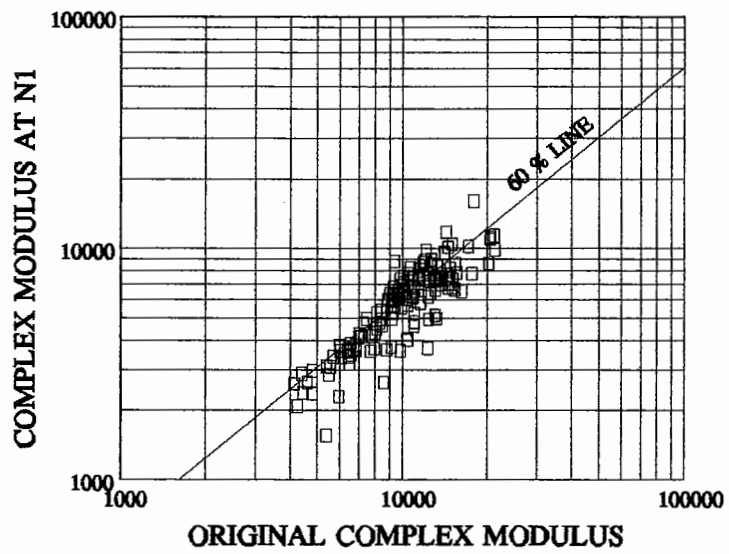
Figure 6.24 : Original Complex Stiffness Modulus versus Complex Stiffness Modulus at *N1*

loading. The mode of loading factor, which is similar to that developed by Monismith and Deacon (1969), is derived so that it varies either side of unity but is always positive. The mode of loading factor is defined as follows:-

$$\Gamma = [\frac{100 - A - B}{100}]$$ (6.26)

A = Percent change in strain defined as follows:-

$$[\frac{\varepsilon_o - \varepsilon_{60}}{\varepsilon_o}] \times 100$$ (6.27)

B = Percent change in stress defined as follows:-

$$[\frac{\sigma_o - \sigma_{60}}{\sigma_o}] \times 100$$ (6.28)

For a controlled stress test the mode of loading factor is greater than one whereas for a controlled strain test it is less than one.

Using the mode of loading factor, Γ, the general expression for the work ratio is as follows:-

$$\psi_{NI} = \left\{ \frac{2 \sin \delta_o}{\sin \delta_o + \Gamma \sin \left[a \left(E_{60}^*\right)^{(0.224 - 0.222 \log a)} \right]} \right\}$$ (6.29)

The work ratio, ψ_{NI}, has been calculated from the initial complex modulus and phase angle and input into the statistical analysis as a calculated parameter. Figure 6.25 illustrates the comparison between the predicted and measured ψ_{NI}
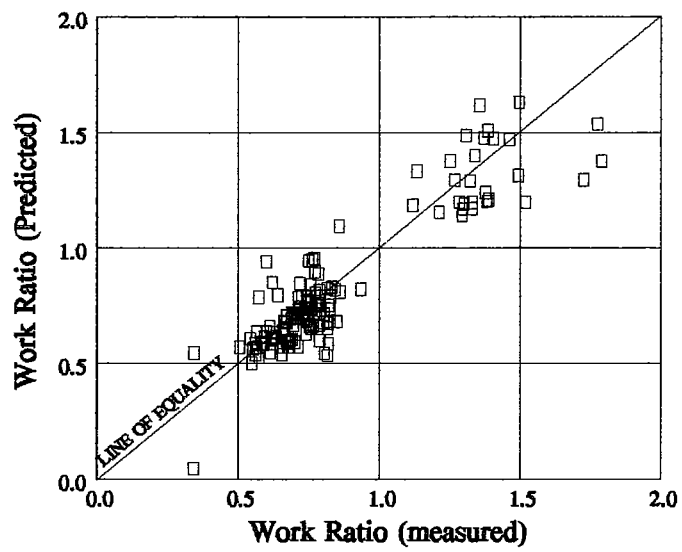
Figure 6.25 : Measured versus Predicted Work Ratio

-6.56-

6.5   STATISTICAL ANALYSIS

The SPSS/PC+ software package (SPSS UK Ltd., 1991) was used for the statistical analysis of the data presented in Table 6.4. Table 6.7 contains the correlation matrix obtained from the analysis and it can be observed that the single most significant parameter related to $N1$ is the logarithm of the initial dissipated energy, Log w_o. Single parameters also highly correlated are (in the order of significance); tensile strain, tensile stress, extensional loss modulus and VMA. It should be noted that although some parameters might be highly correlated they may not necessarily be the correct parameter to explain variance. In addition some parameters are related to more highly correlated parameters (eg. tensile strain and loss modulus are related to the initial dissipated energy). Thus, to investigate the interaction of these parameters multiple regression analysis (both forwards and backwards) was used. The analysis first considered all the parameters for which correlations are given in Table 6.7. This gave the following relationship:

$$N1 = 205 \times Vb^{6.44} \times w_o^{-2.01} \times \psi_{N1}^{1.64} \qquad (6.30)$$

[correlation coefficient, r = 0.84, units Vb (%) and w_o (J/m^3)]

Equation 6.30 demonstrates that w_o, Vb and ψ_{N1} are significant variables describing $N1$. Several terms that were found significantly correlated have not entered the equation (E'', σ_t, ε_t and VMA). In order to produce equations with these parameters the terms Vb and w_o were omitted from the analysis and this resulted in the following:

	Log Va	Log VMA	Log Vfb	Log Vb	Log ε_t	Log σ_t	Log E^*	Log w_o	sin ø	Log E''	ψ_{N1}	Log $(E'/\sin ø)$	N1
Log Va	1.0	0.537**	-0.923**	-0.637**	-0.160	-0.243*	-0.159	-0.243*	0.025	-0.270	0.138	0.063	0.009
Log VMA	0.537**	1.0	-0.558**	0.188	-0.093	-0.312**	-0.340**	-0.171	0.115	-0.268**	-0.109	0.234*	0.195*
Log Vfb	-0.923**	-0.558**	1.0	0.710**	0.185	0.233	0.118	0.303**	0.068	0.382**	-0.154	0.013	-0.029
Log Vb	-0.637**	0.188	0.710**	1.0	0.141	0.006	-0.150	0.216*	0.181	0.228*	-0.278**	0.216*	0.130
Log ε_t	-0.160	-0.093	0.185	0.141	1.0	0.705**	-0.136	0.932**	0.098	0.029	0.085	0.138	-0.715**
Log σ_t	-0.243*	-0.318	0.2326*	0.006	0.705**	1.0	0.606**	0.659**	-0.512**	0.023	0.290**	-0.565**	-0.521**
Log E'	-0.159	-0.340**	-0.118	-0.150	-0.136	0.606**	1.0	-0.125	-0.825**	<0.001	0.311**	-0.945**	0.074
Log w_o	-0.243*	-0.171	-0.303**	0.216*	0.932**	0.659**	-0.125	1.0	0.231*	0.318**	-0.087	0.222*	-0.757**
sin ø	0.0251	0.115	0.068	0.181	0.098	-0.512**	-0.825**	0.231*	1.0	0.531**	-0.491**	0.953**	-0.182
Log E''	-0.270**	-0.268**	0.382**	0.228*	0.029	0.023	<0.001	0.318**	0.531**	1.0	-0.521**	0.327**	-0.261**
ψ_{N1}	0.138	-0.109	-0.154	-0.278**	0.085	0.290**	0.311**	-0.087	-0.491**	-0.521**	1.0	-0.464**	0.180
Log$(E'/\sin ø)$	0.063	0.234*	0.013	0.216*	0.138	-0.565	-0.945**	0.222*	0.953**	0.327**	-0.464**	1.0	-0.155
N1	0.009	0.195*	-0.029	0.130	-0.715**	-0.521	0.074	-0.757**	-0.182	-0.261**	0.180	-0.155	1.0

Note: "*" indicates 1-tailed significance 0.01, "**" indicates 1-tailed significance 0.001

Table 6.7 : Correlation Matrix

Excluding *Vb*:

$$NI = 2.15e{-}11 \times Vfb^{\,6.37} \times VMA^{\,6.61} \times w_o^{-2.00} \times \psi_{NI}^{1.63} \quad (6.31)$$

[correlation coefficient, r = 0.84, units *Vfb* (%), *VMA* (%) and w_o (J/m³)]

Excluding w_o:

$$NI = 2.97e12 \times Vb^{\,6.20} \times \mu\varepsilon_t^{-4.08} \times E''^{\,-1.62} \times \psi_{NI}^{1.62} \quad (6.32)$$

[correlation coefficient, r = 0.83, units *Vb* (%) and *E''* (MPa)]

The two volumetric parameters (*Vfb* and *VMA*) in Equation 6.31 give a similar effect as *Vb* in Equation 6.30 (with exponents around 6.5). Thus, *Vb* ,which is a function of *Vfb* and *VMA*, appears to be an adequate volumetric parameter. Equation 6.32 gives the results of the analysis with the more traditional parameter tensile strain. The life in this equation now becomes a function of frequency and temperature since the loss modulus, which has also entered the equation, is effected by these parameters.

To use the cumulative dissipated energy concept to determine the fatigue performance of a mixture requires knowledge of coefficients *A* and *Z*. The above analysis indicates that, at the *NI* condition, *A* is dependent on binder volume whereas no relation is found for *Z* which is taken as a constant. These factors are accounted for in Equations 6.30 through 6.32 which are preferred due to their simplicity. Equation 6.30 has the highest correlation coefficient (at the forth decimal place) and less terms than Equations 6.31 and 6.32 and, therefore, is selected for the predictive equation.

6.6   PREDICTION METHOD

The prediction method discussed above is summarized in Figure 6.26 and Table 6.8 gives an example calculation where a predicted life of 30,710 load applications is obtained for a controlled stress test. If a controlled strain test is considered (with the same value of initial dissipated energy) the work ratio, ψ_{NI} becomes 1.03 resulting in a predicted fatigue life of 84,143 cycles.

The measured and predicted life (*NI*) using Equation 6.30 for all specimens tested is shown in Figure 6.27. This result is considered reasonable when considering the degree of scatter normally associated with individual test results.

6.7   SUMMARY

A parameter "*a*" has been defined in Equation 6.8 which is dependant upon the initial rheological properties of the mixture and describes the damage of the mixture in terms of the relationship between the phase angle and extensional complex modulus during an individual fatigue test. The relationships obtained from individual fatigue tests for extensional complex modulus versus phase angle can be considered to have a common "focus", which has enabled the development of a prediction procedure for "*a*".

A method is presented which allows the definition of a failure criterion based on a crack initiation point, *NI*, in a trapezoidal cantilever fatigue test. The *NI*

Input Data
===========

E^*
Vb
$\sin \delta$

Note : In addition to the listed items it is necessary to input the initial loading, eg. stress or strain. Also, the change of stress and strain at the N1 condition is required.
E and δ need to be established at conditions applicable to the test temperature and frequency of loading.

Calculate a from Equation 6.22

Calculate Γ from Equation 6.26

Calculate ψ_{N1} from Equation 6.29

Calculate $N1$ from Equation 6.30

Figure 6.26 : Prediction Method

Material Input	Example, E^* = 12345 MPa, Vb = 10.8%, δ_o = 24.15°
Mode of Loading	Controlled stress, 1000kPa, initial tensile stress. w_o = 104.1 J/m². Define increase in strain at failure = 67% (corresponding to a 40% reduction in E^*)
Equ. 6.22	a = 122 183.966
Equ. 6.26	Γ = 1.67
Equ. 6.29	ψ_{NI} = 0.551
Equ. 6.30	NI = 30,710

Table 6.8 : Example of Prediction
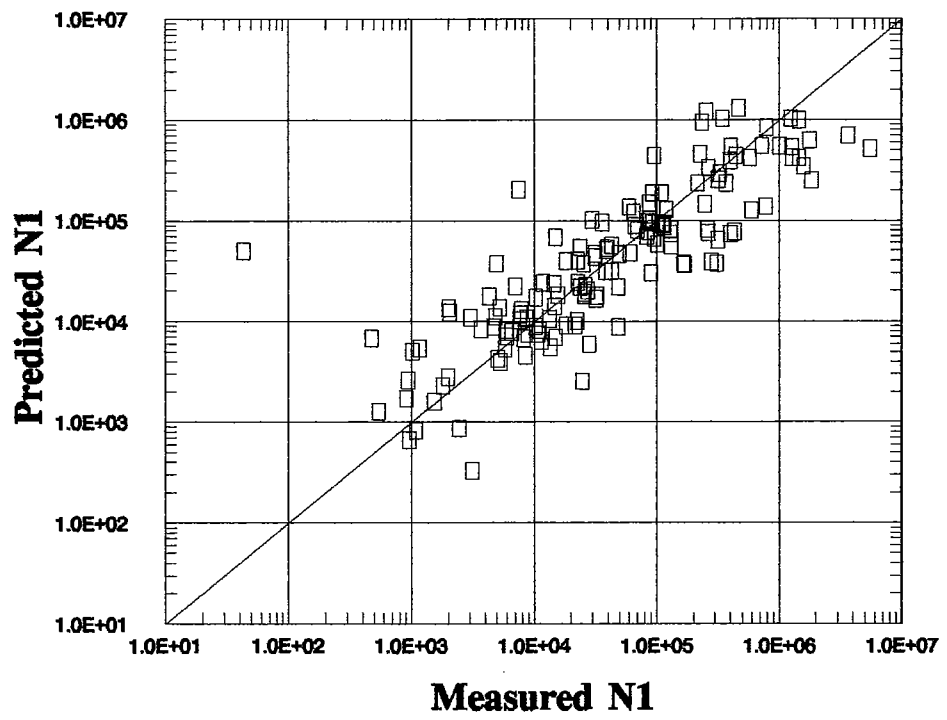
Figure 6.27 : Measured versus Predicted Fatigue Life, *N1*

criterion allows a comparison of materials at equal states of damage and avoids arbitrary definition of failure. It is concluded that this point is better defined in a controlled stress fatigue test.

The volume of binder has been shown to significantly effect the parameter "A" in the relationship $W = AN^Z$ and if a simple volumetric correction is applied then the scatter in fatigue lines can be shown to reduce considerably.

In the relationship between fatigue life and cumulative dissipated energy ($W = AN^Z$) the parameters $\log A_{Nf}$ and $\log A_{NI}$ lie on a straight line when plotted against Z_{Nf} and Z_{NI}. However, due to the low number of tests it is difficult to use this data due to the inherent scatter.

A procedure has been developed to define a work ratio, ψ_{NI}, which is based upon the rheology of the mixture and a mode of loading factor, Γ, which can be used for the prediction of fatigue life.

A method has been developed to enable fatigue life prediction to the NI criteria. Parameters which significantly affect the performance of a given mixture are the initial dissipated energy, w_o, volume of binder, Vb and the work ratio parameter, ψ_{NI}, as described in Equation 6.30.

In developing prediction methods emphasis must be placed upon the range of mixture variables considered. While the range in mixture variables is considered to represent most asphaltic concrete materials the extension of the

procedures to other mixtures should be verified by further testing.

CHAPTER 7

Wheel Tracking Experiments

7.0   INTRODUCTION

This work was conducted in order to provide validation for the results obtained from the Trapezoidal Fatigue Testing. Similar testing was conducted in the 1970's (Van Dijk, 1975) and was used as part of the justification for test selection and shift factors in the Shell Pavement Design Manual (SIPC, 1978) and the University of Nottingham method (Brown et al., 1985). Stages in the fatigue process were identified associated with the formation and widening of hair cracks followed by the formation of real cracks and finally failure of bottom or top surfaces. Strain was monitored through the testing and plots were obtained with the general shapes illustrated in Figure 7.1. The shape of the curve prior to the point "N_1" is inversely related to the stiffness of the slab as a single unit. After the "N_2" stage, cracks which are forming can extend around the strain gauges causing stress relief to the strain gauge and hence the strain can decrease. It is hypothesised that the point "N_1" is similar to that defined for the fatigue tests as *N1* which is considered to be the point when sharp crack initiates.

A preliminary experiment was conducted with local materials (Bardon Hill Aggregate and 100 Pen binder) in order to assess the functionality of the
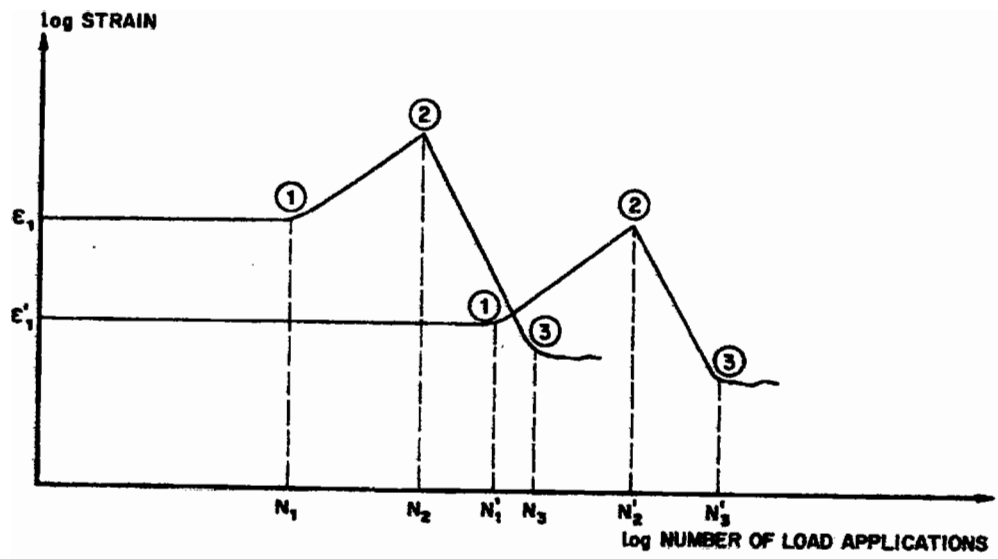
**Figure 7.1 : Strain Development in the Fatigue Wheel Tracking Test
(after Van Dijk, 1975)**

apparatus and to make necessary refinements to the test procedure prior to conducting the main test program. This preliminary work resulted in a few refinements such as the use of a silicon backed paper to line the mould and an improved method for moving the compacted sample into the testing location. The program commenced first with the series of tests at three strain levels for mixtures with modified binders (with a control unmodified mix) followed by further testing of conventional unmodified asphalt mixtures at a single strain level.

7.1   DATA FROM THE FATIGUE WHEEL TRACKING TESTS

With the large amount of data being generated, it was considered desirable to reduce this to a manageable format which could be used for the analysis. Thus, the recorded output from each gauge was reduced to the height of the transient tensile strain peak for gauges 1 to 7 and the residual/delayed elastic-visco-plastic tensile strain for gauge 8 (see Figures 5.28 to 5.31). These data are graphically presented in Appendix A. The wheel pressure was 380 kPa with a 3 kN load giving a contact area 0.011 m^2 which reduces to 0.007 m^2 if the area between the treads is deducted. The magnitude of load applied during each test is given in Table 7.1.

7.2   DEFINITION OF FATIGUE LIFE, *N1*

The definition of fatigue life, *N1*, was found to be very difficult. This was due to the lack of consistency in the crack pattern around the strain gauges,

Contract	Slab	Load Dial Setting	Mean Load Volts (mV)	Load (kN)
A-003A	1	8	437.7	4.512371
A-003A	2	3.02	200	2.061856
A-003A	3	3.02	211.3	2.178351
A-003A	4	1.19	79.2	0.816495
A-003A	5	3.02	193.5	1.995
A-003A	6	3.02	213.1	2.197
A-004	1	5.75	433.6	4.470
A-004	2	2.05	139.6	1.439
A-004	3	2.63	194.3	2.003
A-004	4	3.25	249.1	2.568
A-004	5	2.67	211.3	2.178
A-004	6	0.89	58.4	0.602
A-004	7	4.05	298.1	3.073
A-004	8	2.74	173.6	1.790
A-004	9	2.62	137.7	1.420
A-004	10	8.06	528.3	5.446
A-004	11	2.69	173.6	1.790
A-004	12	Lost reading	467.9	4.824

Table 7.1 : Load Levels used for Fatigue Wheel Tracking Experiments

partly due to the superior strength of the gauge and epoxy resin. Figure 7.2 shows typical output from two gauges annotated to explain the crack pattern. As a consequence of this the output from each gauge has been carefully reviewed and the $N1$ point estimated to be consistent with an observed change in behaviour of a particular gauge. The figures in Appendix A are annotated with the estimated positions for the $N1$ points whereas the data in Table 7.2 contains the $N1$ point versus the initial strain level for each gauge assessed.

7.3   VISUAL CRACKING OBSERVATION

Development of cracks on the top surface during the test were monitored in order to help with the definition of damage to the slab. In order to use a rational system to rank the degree of cracking, a classification system was used with a "Crack Index" value assigned to the top (CI_t) and bottom (CI_b) surfaces based upon the linear length of cracking in a 100 mm square area. The classification is illustrated in Figure 7.3.

To accomplish this at the end of each test the cracks on both the top and bottom surface were marked (to provide a contrast) and then photographed. The severity was ranked in accordance with the classification system. Figures 7.4 and 7.5 show a slab at the end of a test with cracks marked.

The Crack Indices are presented in Table 7.3 for both bottom (CI_b) and top (CI_t) surfaces.
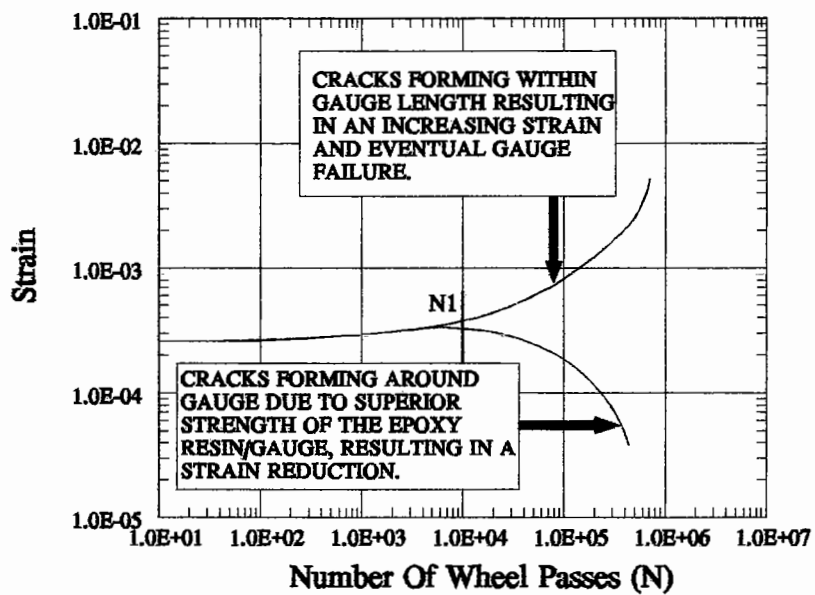
Figure 7.2 : Influence of the Crack Pattern on the Shape of Tensile Strain versus the Number of Load Applications

Contract	Slab No.	Gauge No.	log life to *N1*	log µε (initial)
A003A	1	1	2.85	2.41
A003A	1	2	3.00	2.44
A003A	1	3	2.91	2.10
A003A	1	4	2.56	2.57
A003A	1	5	2.68	2.29
A003A	1	6	2.94	2.43
A003A	1	7	2.82	2.48
A003A	2	1	4.47	2.41
A003A	2	3	4.12	2.25
A003A	2	4	4.44	2.44
A003A	2	5	4.24	2.13
A003A	2	6	4.21	2.38
A003A	2	7	3.82	2.48
A003A	3	1	3.82	2.48
A003A	3	2	3.88	2.44
A003A	3	3	3.62	2.16
A003A	3	4	3.65	2.57
A003A	3	5	3.62	2.13
A003A	3	6	3.82	2.41
A003A	3	7	3.71	2.44
A003A	4	1	3.88	2.50
A003A	4	2	4.09	2.77
A003A	4	3	4.00	2.41
A003A	4	4	4.15	2.63
A003A	4	5	3.88	2.44
A003A	4	6	3.88	2.76
A003A	4	7	4.00	2.51
A003A	5	1	2.65	2.57
A003A	5	2	3.12	2.83
A003A	5	3	3.85	2.60
A003A	5	4	3.97	2.64
A003A	5	5	3.85	2.54
A003A	5	6	3.26	2.86
A003A	5	7	2.82	2.57
A003A	6	1	4.29	2.16
A003A	6	2	5.06	2.16
A003A	6	3	4.76	2.01
A003A	6	4	4.68	2.20
A003A	6	5	3.94	1.95
A003A	6	6	3.95	2.17
A003A	6	7	4.41	2.22
A004	1	1	3.24	2.60
A004	1	2	3.12	2.51
A004	1	3	3.62	2.19
A004	1	4	3.05	2.63
A004	1	5	3.44	2.19
A004	1	6	3.12	2.51
A004	1	7	2.97	2.48
A004	2	1	4.26	2.22
A004	2	2	4.62	1.77
A004	2	3	4.88	1.50

Table 7.2: Summary Data, Tensile Strain versus *N1*

Contract	Slab No.	Gauge No.	log life to $N1$	log $\mu\varepsilon$ (initial)
A004	2	4	4.77	2.32
A004	2	5	4.82	1.48
A004	2	6	5.03	1.67
A004	2	7	4.76	2.19
A004	3	1	3.38	2.35
A004	3	2	3.26	2.25
A004	3	3	4.01	1.89
A004	3	4	3.53	2.44
A004	3	6	4.12	2.20
A004	3	7	3.76	2.22
A004	4	1	4.56	2.38
A004	4	2	3.74	2.54
A004	4	3	4.79	2.16
A004	4	4	3.54	2.63
A004	4	5	3.79	2.13
A004	4	6	3.09	2.54
A004	4	7	3.82	2.44
A004	5	1	3.56	2.32
A004	5	2	4.00	2.54
A004	5	3	3.12	2.31
A004	5	4	4.35	2.38
A004	5	5	4.45	2.38
A004	5	6	4.09	2.51
A004	5	7	3.88	2.41
A004	6	1	4.56	2.00
A004	6	2	4.60	2.18
A004	6	3	4.53	1.95
A004	6	4	4.65	2.37
A004	6	5	4.50	2.00
A004	6	6	4.56	2.32
A004	6	7	4.64	2.08
A004	7	1	3.48	2.70
A004	7	2	2.54	2.71
A004	7	3	3.12	2.41
A004	7	4	3.12	2.65
A004	7	5	3.24	2.44
A004	7	6	3.15	2.70
A004	7	7	3.24	2.75
A004	8	1	3.79	2.30
A004	8	2	4.82	2.25
A004	8	3	4.26	1.89
A004	8	4	4.35	2.43
A004	8	5	4.62	2.03
A004	8	6	4.38	2.31
A004	8	7	3.82	2.18
A004	9	1	4.18	2.10
A004	9	2	4.88	1.95
A004	9	3	3.82	1.54
A004	9	4	4.00	2.17
A004	9	5	3.91	1.74
A004	9	6	4.88	1.86

Table 7.2: Summary Data, Tensile Strain versus $N1$ (cont.)

Contract	Slab No.	Gauge No.	log life to *N1*	log με (initial)
A004	9	7	4.79	2.11
A004	10	1	3.82	2.41
A004	10	2	3.82	2.22
A004	10	3	3.88	2.13
A004	10	4	3.60	2.44
A004	10	5	3.65	1.92
A004	10	6	3.54	2.29
A004	10	7	4.00	2.35
A004	11	1	5.15	2.06
A004	11	2	4.18	1.89
A004	11	3	4.35	1.70
A004	11	4	4.62	2.13
A004	11	5	3.79	1.95
A004	11	6	3.79	1.88
A004	11	7	4.22	2.13
A004	12	1	3.46	2.46
A004	12	2	3.35	2.31
A004	12	3	3.41	2.14
A004	12	4	3.00	2.52
A004	12	5	3.00	2.06
A004	12	6	3.12	2.32
A004	12	7	3.24	2.13

Table 7.2: Summary Data, Tensile Strain versus *N1* (cont.)
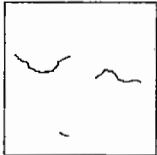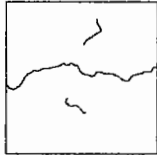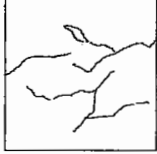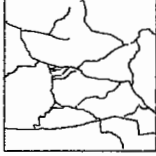
Index	Crack length/unit area	Illustration
1	Nil	
2	Not greater than 100mm/100mm^2	
3	Greater than 100mm/100mm^2 but not greater than 200mm/100mm^2	
4	Greater than 200mm/100mm^2 but not greater than 500mm/100mm^2	
5	Greater than 500mm/100mm^2	

Figure 7.3 : Classification System for Visual Cracking
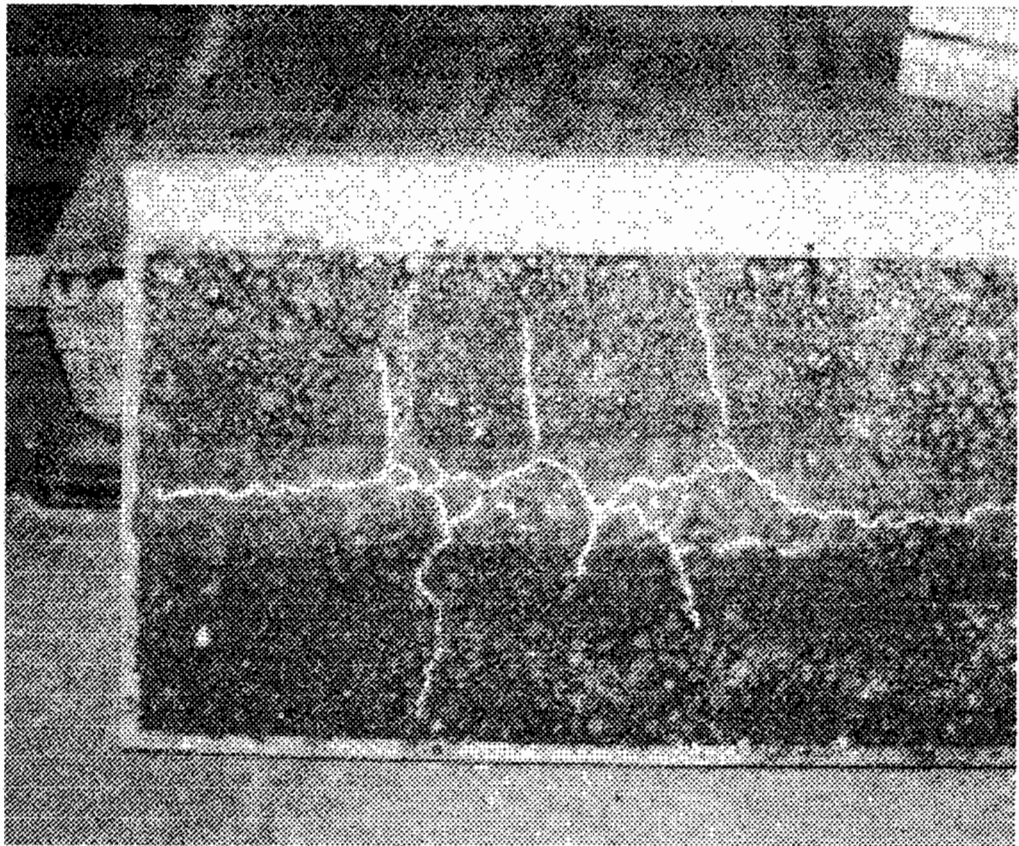
**Figure 7.4 : Typical Condition of Slab at End of Fatigue Wheel
Tracking Test, Top Surface**
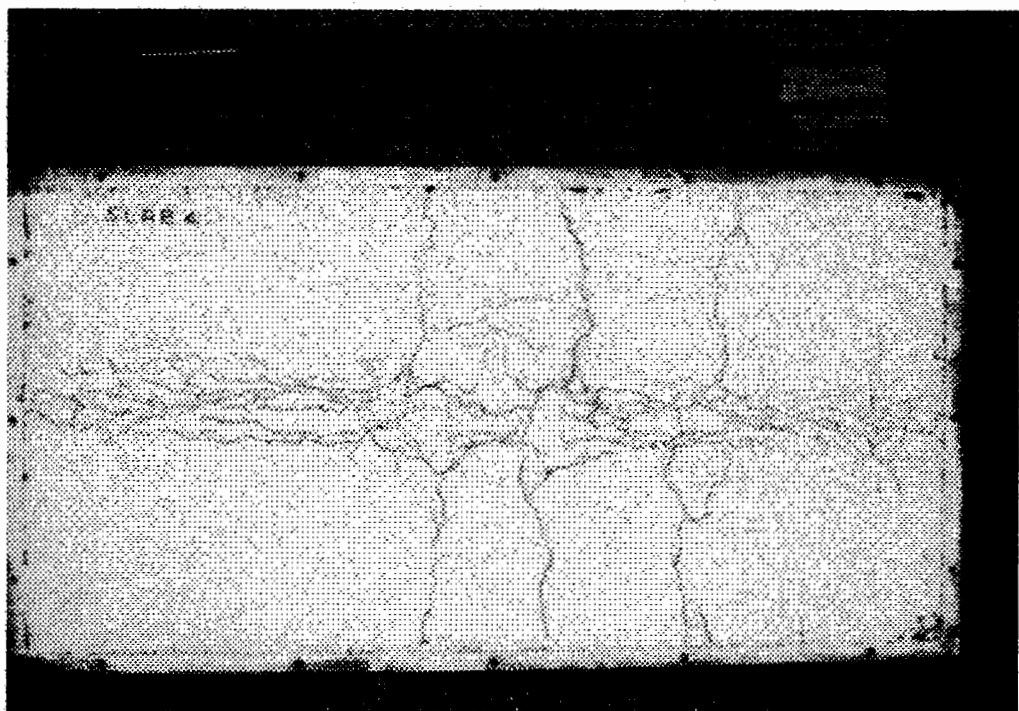
Figure 7.5 : Typical Condition of Slab at End of Fatigue Wheel Tracking Test, Bottom Surface

Index	CI_b		CI_t				CI_b-CI_t				Ranking with respect to crack propagation
Gauge	1/4/7	Ave.	1	4	7	Ave.	1	4	7	Ave.	
AAA-RD	4/5/5	4.7	3	2	3	2.7	1	3	2	2.0	=4
AAC-RD	4/4/4	4.0	1	2	2	1.7	3	2	2	2.3	=1
AAF-RD	4/5/4	4.3	3	2	3	2.7	1	3	1	1.7	=6
AAG-RD	4/4/5	4.3	2	2	3	2.3	2	2	2	2.0	=4
AAK-RD	5/5/5	5.0	3	4	3	3.3	2	1	2	1.7	=6
AAM-RD	4/4/4	4.0	2	3	3	2.7	2	1	1	1.3	8
AAG-RB	4/4/4	4.0	-	-	-	-	-	-	-	-	
	5/5/4	4.7	-	-	-	-	-	-	-	-	not ranked
	4/5/4	4.3	-	-	-	-	-	-	-	-	
	(4.3/4.7/4.0)	(4.3)	(-	-	-)	(-)	(-	-	-)	(-)	
M405-G-RB	5/5/5	5.0	3	3	3	3.0	1.7	1.7	1.7	2.0	
	5/4/5	4.7	2	2	2	2.0	1.7	2.0	2.5	2.7	
	5/5/5	5.0	-	-	-	-	-	-	-	-	=1
	(5.0/4.7/5.0)	(4.9)	(2.5	2.5	2.5)	(2.5)	(-	-	-)	(-)	
M415-G-RB	5/5/5	5.0	2	2	1	1.7	2.5	2.5	5.0	3.3	
	5/5/5	5.0	3	4	3	3.3	1.3	1.3	1.7	1.7	
	4/4/4	4.0	2	2	2	2.0	2.0	2.0	2.0	2.0	=1
	(4.7/4.7/4.7)	(4.7)	(2.5	2.5	2.5)	(2.3)	(2.3	2.0	2.7)	(2.3)	
M416-G-RB	3/5/3	3.7	3	3	3	3.0	1.0	1.7	1.0	1.2	
	4/4/4	4.0	3	3	3	3.0	1.3	1.3	1.3	1.3	
	4/4/4	4.0	3	4	3	3.3	1.3	1.0	1.3	1.2	9
	(3.7 4.3 3.7)	(3.9)	(2.3	2.7	2.0)	(3.1)	(0.7	1.0	0.7)	(0.8)	

(Left-side label spanning rows: Mix. Ref.)

Table 7.3 : Crack Indexes

The difference, CI_b-CI_t, is also presented in Table 7.3. The objective of this final parameter is that it should be related to the ability of a material to withstand the effects of crack propagation. Zero/low numbers would indicate rapid crack propagation whereas larger numbers indicate a material more able to resist crack growth and propagation.

7.4   TENSILE STRAIN VERSUS FATIGUE LIFE, *N1*

All the fatigue wheel tracking results have been compared at an equal strain level. In order to achieve this it has been assumed that the results lie on a log *N1* versus log ε_t relationship which has a negative slope of 0.25. This slope is suggested by analysis of fatigue results on similar mixtures by Tayebali et al. (1992). In addition when considering the combined data for the slabs, the observed slope tends to support this assumption, Figure 7.6.

Table 7.4 presents the mean fatigue life, log *N1*, and the standard deviation of each set of materials normalised to 200 micro strain (tension) assuming a slope of 0.25. The value of 200 microstrain is chosen because it is generally in the centre of the data collected and therefore there is minimum extrapolation of the results. Figure 7.7 illustrates the same results.

From individual tests it is impossible to obtain reliable strain-life relationships for the materials tested. When considering a larger number of tests, eg. 3 number tests, as for the A-004 (modified mixtures) testing, a relationship can be described in terms of tensile strain versus fatigue life, *N1*. The constants
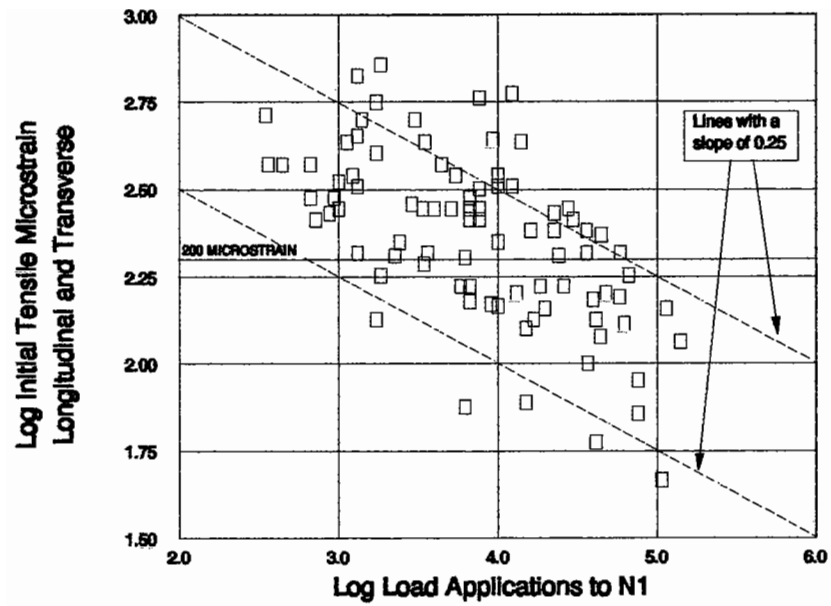
Figure 7.6 : Combined Test Results - Tensile Strain versus Fatigue Life *N1*

Mixture Reference	Average Life (Log)	Average Tensile Microstrain (Log)	Normalised to 200 Microstrain	
			Life (Log)	Standard Deviation
AAA-RD	4.000	2.636	5.341	0.505
AAC-RD	3.165	2.693	4.734	0.756
AAF-RD	4.479	2.183	4.006	0.381
AAG-RD	2.835	2.467	3.501	0.116
AAK-RD	4.235	2.429	4.746	0.223
AAM-RD	3.776	2.470	4.452	0.170
AAG-RB	3.099 4.488 3.574 (3.720)	2.546 2.015 2.313 (2.291)	4.079 3.345 3.620 (3.763)	0.294 0.742 0.368 (0.650)
M405-G-RB	3.756 4.392 3.233 (3.794)	2.343 2.017 2.347 (2.236)	3.924 3.254 3.416 (3.531)	0.355 0.810 0.545 (0.664)
M415-G-RB	3.749 3.976 4.602 (4.109)	2.508 2.432 2.189 (2.376)	4.577 4.499 4.155 (4.411)	0.320 0.491 0.566 (0.505)
M416-G-RB	3.104 4.235 4.547 (3.962)	2.702 2.296 2.038 (2.345)	4.708 4.215 3.495 (4.140)	0.329 0.566 0.307 (0.650)

Notes:1. Numbers in parenthesis are averages for data set.

Table 7.4 : Mean Fatigue Life and Standard Deviations for Each Slab Tested
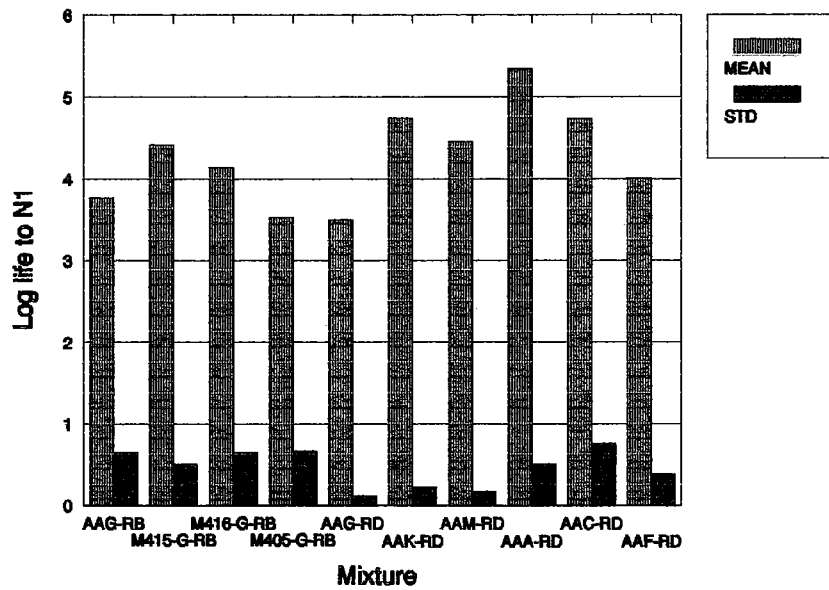
**Figure 7.7 : Normalised Fatigue Life (at 200 με),
Mean and Standard Deviation**

k1 and k2 for the relationship as defined in Equation 7.1 obtained are presented in Table 7.5.

$$N1 = k1 \left(\frac{1}{\epsilon_t}\right)^{k2} \tag{7.1}$$

It can be observed that when individual data points are used a poor correlation results. However, this is significantly improved if mean values are used for each data set.. Figure 7.8 illustrated the data points for the 4 mixtures evaluated as part of the A-004 test program.

7.5   STIFFNESS VERSUS FATIGUE LIFE, *N1*

Following the testing of the slabs, eight cores were taken from each slab and these were tested to obtain the Indirect Tensile Test Stiffness (for conditions see section 5.4.1), mixture density and volumetrics (see Table 7.6). The ITT Stiffness is correlated to the fatigue life as demonstrated in Figure 7.9. This correlation is of interest because the ITT Stiffness is correlated to the loss modulus (as indicated in Figure 7.10) which in turn is directly proportional to the materials ability to dissipate energy. Thus, in a cruder manner, the ITT Stiffness should rank the material in a similar order to that obtained from dissipated energy considerations. The use of this test device is discussed in more detail in Chapter 8.

Mix	Type	k1	k2	SE	R^2
AAG-RB	all data	4.710e+08	-2.1264	0.45	0.65
	mean data	5.822e+09	-2.6382	0.11	0.99
M415-G-RB	all data	4.033e+08	-1.8921	0.38	0.46
	mean data	2.591e+10	-2.6529	0.02	1.00
M416-G-RB	all data	9.595e+08	-2.1404	0.40	0.73
	mean data	1.544e+09	-2.2285	0.20	0.96
M405-G-RB	all data	1.928e+07	-1.56187	0.51	0.28
	mean data	8.569e+09	-2.74642	0.36	0.80

SE = Standard Error

Table 7.5 : Fatigue Life Relationship
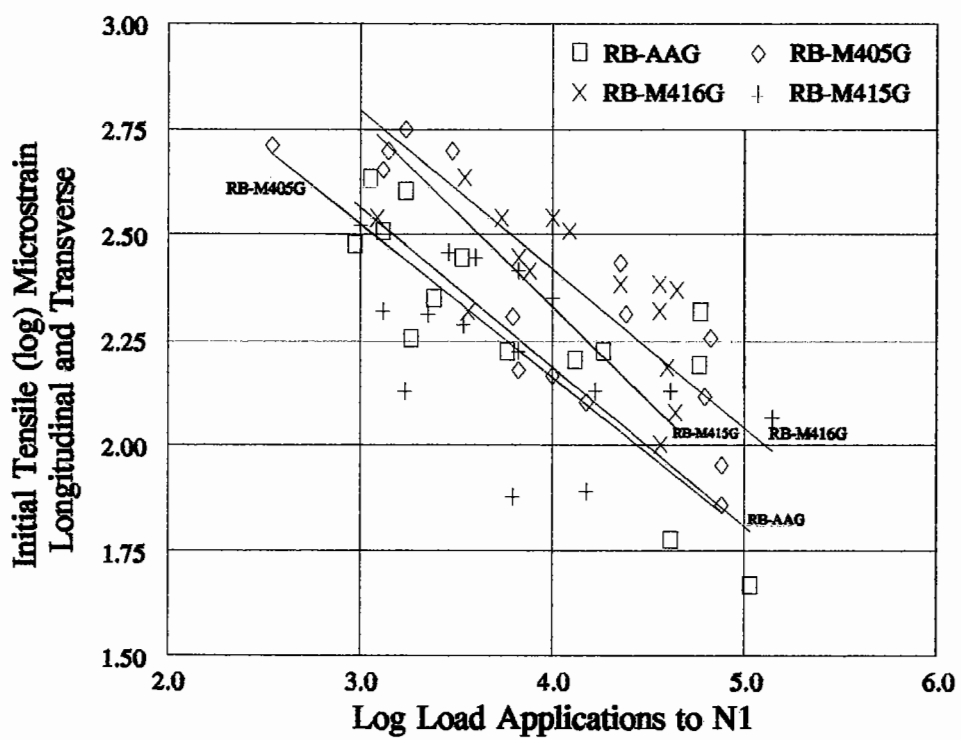
Figure 7.8 : A004 Test Results - Tensile Strain versus Fatigue Life *N1*

Contract	Slab No.	Material Ref	Date Slab Mixed	Date Slab Test Start	Date Cores Tested	No. of Cores	Density of Cores		ITT Stiffness (MPa)			
									Temp = 10°C		Temp = 20°C	
							Mean	SD	Mean	SD	Mean	SD
A003A	1	AAG/RD	19 Nov 91	13 Dec 91	17 - 20 Feb 92	8	2.294	0.019	11435	1035	7398	603
	2	AAK/RD	10 Dec 91	24 Jan 92	2 - 8 Oct 92	8	2.261	0.020	10219	1086	5561	149
	3	AAM/RD	29 Jan 92	11 Feb 92	2 - 8 Oct 92	8	2.309	0.042	8085	1572	4613	980
	4	AAA/RD	5 Feb 92	28 Feb 92	2 - 8 Oct 92	8	2.253	0.015	3412	262	1677	146
	5	AAC/RD	26 Feb 92	20 Mar 92	2 - 8 Oct 92	8	2.323	0.022	8993	691	4130	349
	6	AAF/RD	8 April 92	23 Apr 92	2 - 8 Oct 92	8	2.298	0.013	13595	631	8046	421
A004	1	AAG/RB	13 Nov 90	30 Jan 91	6 - 7 Mar 91	8	2.404	0.019	14513	1422	5782	300
	2	AAG/RB	04 Dec 90	19 Feb 91	21 - 25 Mar 91	8	2.375	0.022	11100	1119	5347	566
	3	AAG/RB	18 Feb 91	12 Apr 91	24 Jun 91	8	2.336	0.040	12578	934	5460	433
	4	415-G/RB	15 Apr 91	9 May 91	22 Jul 91	8	2.422	0.021	10780	1330	5080	440
	5	415-G/RB	25 Apr 91	24 Jun 91	23 - 24 Jul 91	8	2.351	0.031	9829	2000	3664	858
	6	415-G/RB	12 Jun 91	9 Jul 91	2 - 10 Feb 92	8	2.325	0.015	10209	1099	3711	426
	7	416-G/RB	26 Jun 91	13 Jul 91	10 - 12 Feb 92	8	2.296	0.016	11544	908	4151	366
	8	416-G/RB	12 Aug 91	Sep 91	11 - 12 Feb 92	8	2.446	0.015	15039	1461	6308	532
	9	416-G/RB	9 Sep 91	25 Oct 91	18 Feb 92	8	2.424	0.014	15084	751	6642	707
	10	405-G/RB	13 May 92	27 May 92	30 Sep - 9 Oct 92	8	2.388	0.012	21286	1459	12998	1121
	11	405-G/RB	19 May 92	10 Jun 92	1 - 8 Oct 92	8	2.336	0.011	14340	1206	10338	1511
	12	405-G/RB	2 June 92	7 Aug 92	5 - 8 Oct 92	8	2.346	0.023	16643	1789	10948	1435

Table 7.6 : Density and Stiffness Test Results
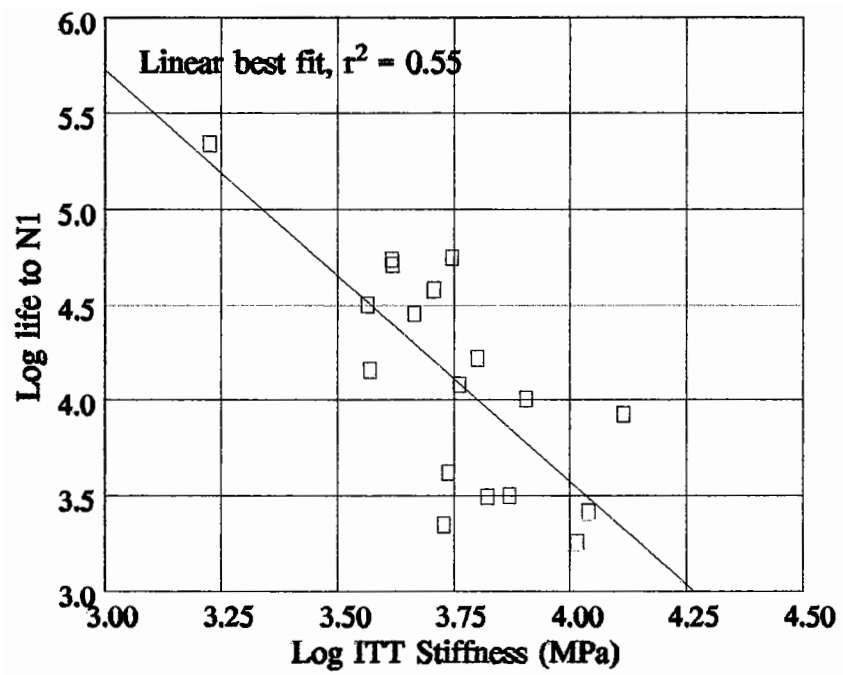
Figure 7.9 : Fatigue Life *N1* versus ITT Stiffness (at 20°C)
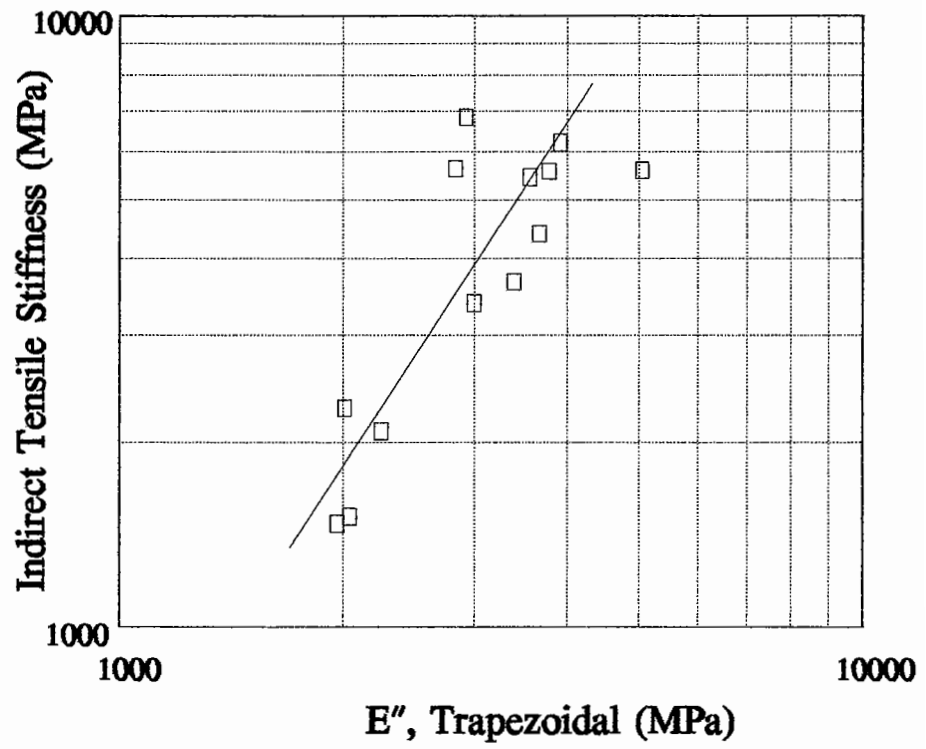
**Figure 7.10 : Relationship between E" (Trapezoidal Bending Beam)
and Indirect Tensile Stiffness at 20°C**

7.6   ANALYSIS OF BEAM FATIGUE TEST RESULTS

In addition to the wheel track testing work conducted at Nottingham the same mixtures (see Table 4.5) were tested at the University of California, Berkeley (UCB) in a bending beam fatigue test (Tayebali et al., 1992). The mixtures containing the RD aggregate where prepared at the University of California using a rolling wheel compaction method whereas those with the RB aggregate where prepared at Southwestern Laboratories (SWL) in Houston using a kneading compaction device. The results from this testing are summarized in Table 7.7.

The laboratory fatigue life obtained in the beam fatigue test was strongly correlated to the cumulative dissipated energy, Figure 7.11. However, the samples containing the RB aggregate all had shorter lives as illustrated in Figures 7.12 and 7.13. Considering, the fatigue wheel tracking data discussed earlier it was anticipated that the ranges in fatigue lives would overlap. In order to investigate this result, different aspects of the material behaviour were considered. A strong relationship had been observed between the complex stiffness modulus and the phase angle with data obtained from the trapezoidal fatigue testing and also for data reported by other workers (Francken, 1979). When considering the mixtures tested at UCB it is observed that three specimens obtained for the modified materials lie considerably off the trend line of data for the other materials produced, see Figure 7.14. This indicates that the rheology of these three samples is different when compared to the rest of the materials tested. The measure of mixture rheology "loss stiffness

Mixture Reference	k1	k2	r^2	Standard Error in Estimate (log)
AAA-RD	3.608×10^{-7}	-3.160	0.988	0.060
AAC-RD	2.184×10^{-7}	-3.383	0.996	0.037
AAF-RD	1.584×10^{-7}	-3.385	0.974	0.094
AAG-RD	3.064×10^{-9}	-3.776	0.910	0.205
AAK-RD	3.331×10^{-10}	-4.304	0.985	0.092
AAM-RD	3.360×10^{-9}	-4.044	0.977	0.107
AAG-RB	5.982×10^{-10}	-3.894	0.814	0.320
M405-G-RB	1.266×10^{-9}	-3.673	0.774	0.341
M415-G-RB	1.104×10^{-11}	-4.270	0.930	0.202
M416-G-RB	1.202×10^{-7}	-3.119	0.990	0.014

Table 7.7 : Beam Fatigue Test Results
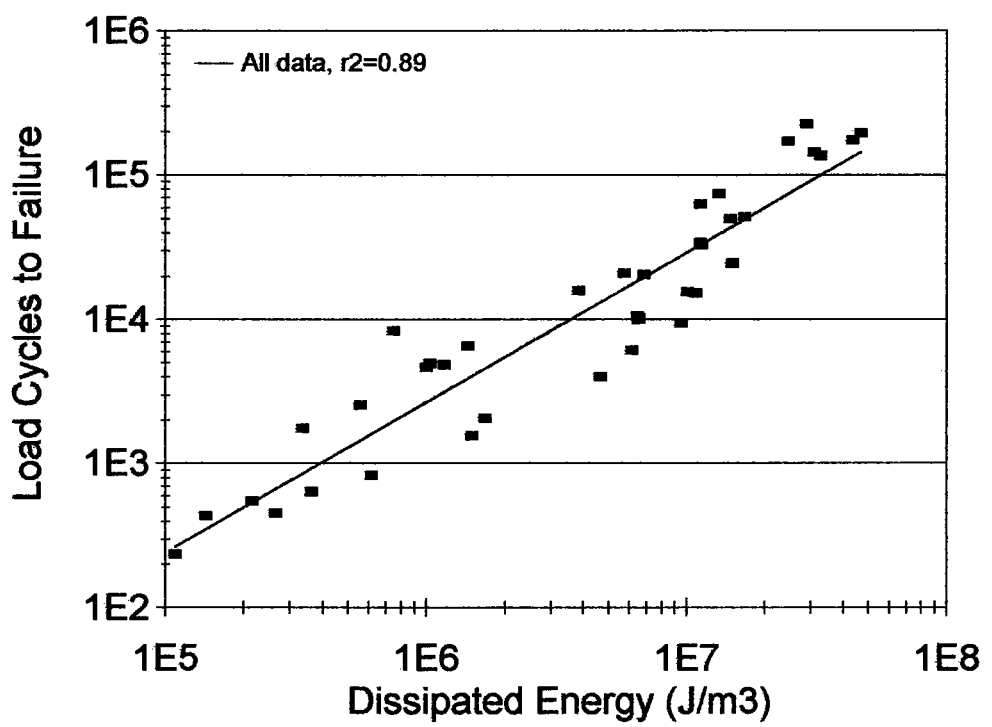
Figure 7.11 : Cumulative Dissipated Energy versus Fatigue Life, Flexural Beam Tests, All Data
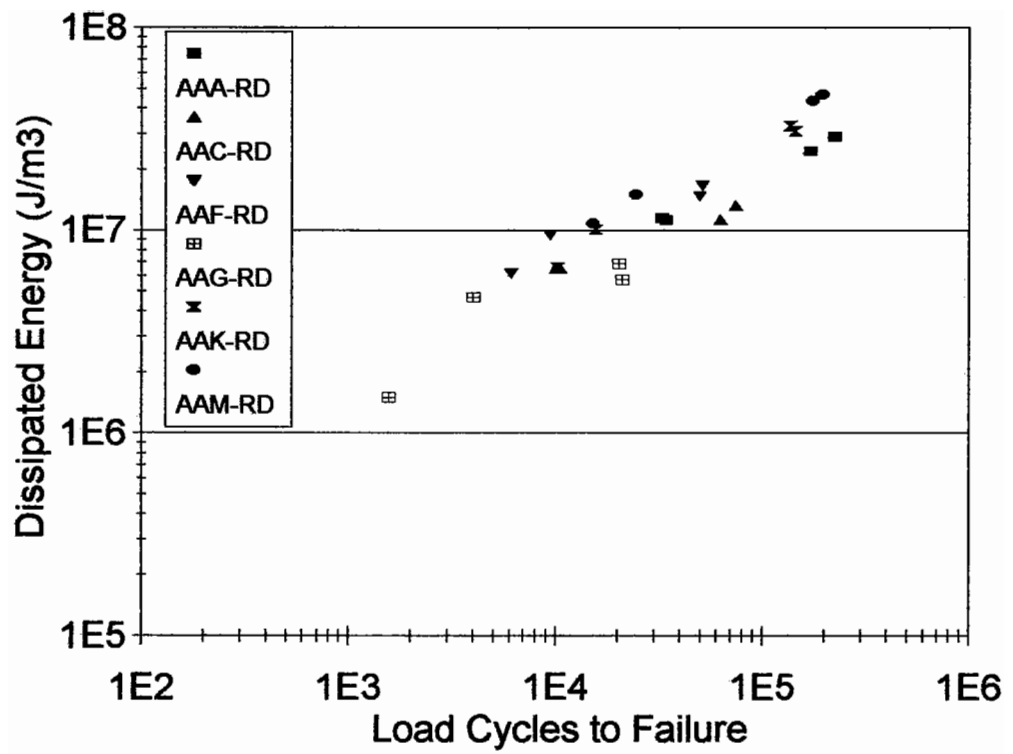
Figure 7.12 : Cumulative Dissipated Energy versus Fatigue Life, Flexural Beam Tests, RD Aggregate
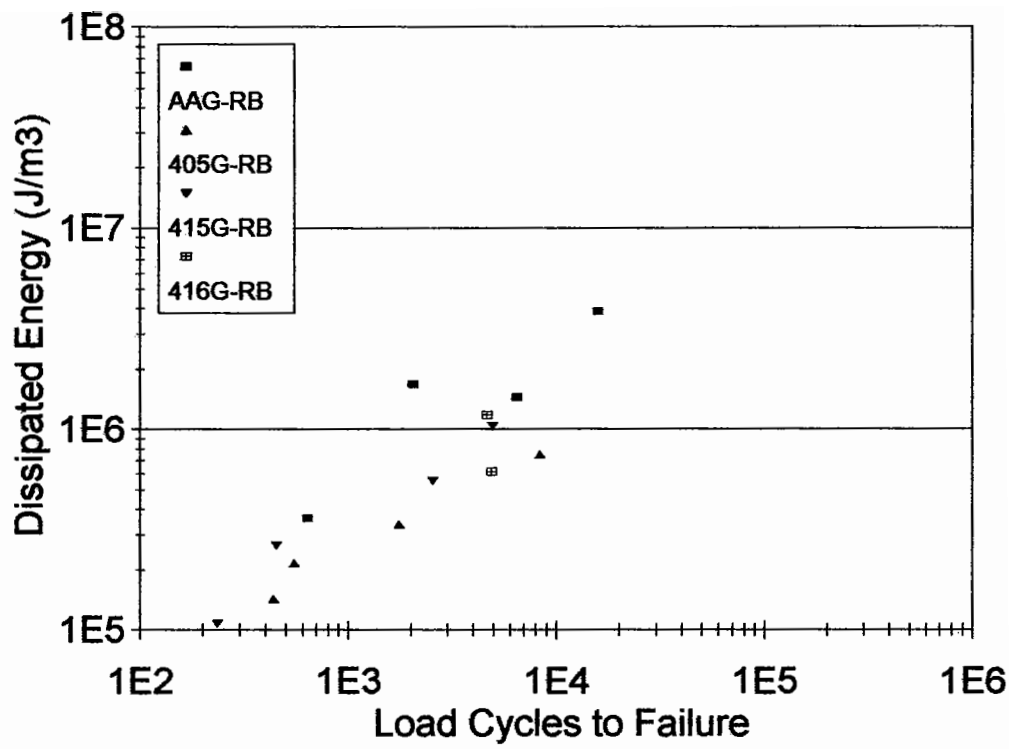
Figure 7.13 : Cumulative Dissipated Energy versus Fatigue Life, Flexural Beam Tests, RB Aggregate

-7.28-
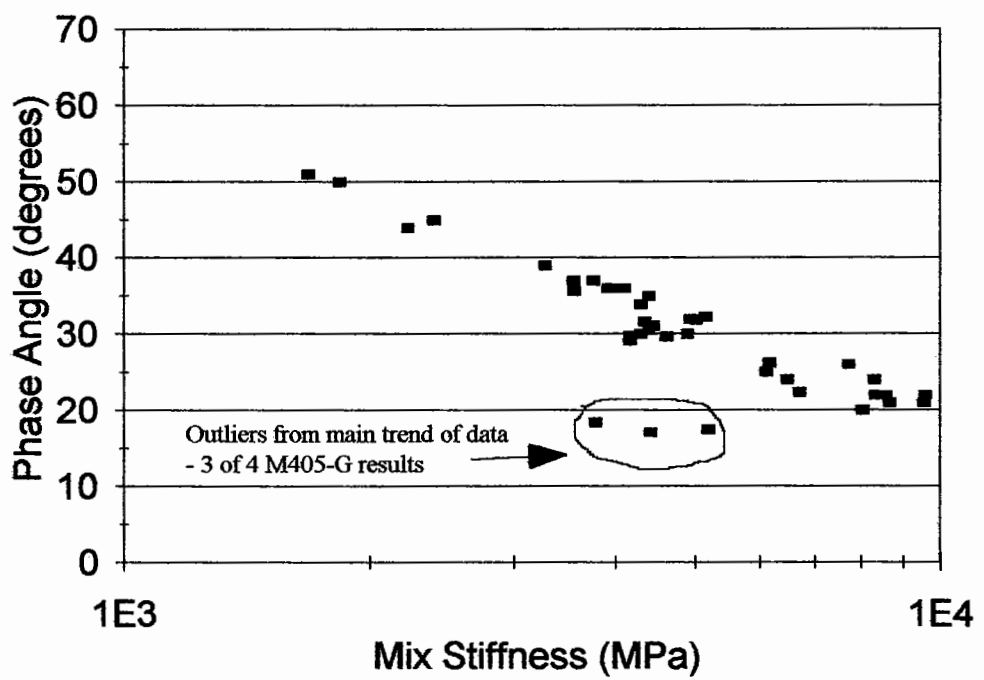
Figure 7.14 : Mixture Stiffness versus Phase Angle as measured in the Flexural Beam Tests, All Mixtures

modulus" should be directly correlated to fatigue performance since the product of this parameter with the square of strain and π is the dissipated energy in a cyclic fatigue test. Figure 7.15 illustrates the data obtained when plotting the mean values for each data set. It can be seen that two clear groups are obtained; 1) specimens produced at SWL (with kneading compaction), and 2) specimens produced at UCB (with rolling wheel compaction). It would appear that the compaction method is significantly effecting the performance of these materials in the fatigue test. The kneading compaction appears to be associated with a lower fatigue life compared to the rolling wheel method. This result is similar (but more severe) to that reported by Sousa et al., (1991). This gross difference is contrary to conventional understanding. However, it is possible that the fatigue specimens made by SWL in Houston were damaged in transit to UCB Berkeley for testing.

As discussed earlier, the fatigue wheel tracking results were compared at a level of 200 microstrain. This value was chosen to avoid large extrapolations of the data outside the range of data collected. Figure 7.16 illustrates the maximum, minimum and mean fatigue lives for all the mixtures tested in the beam fatigue test while Figure 7.17 illustrates the calculated lives using regression analysis for 200, 400 and 700 microstrain. It should be noted that the range in fatigue lives obtained from the laboratory testing is typically one order of magnitude. If the relationships are extrapolated to 200 microstrain, the total range of lives typically covers two orders of magnitude. In other words the extrapolation is approximately one order of magnitude which is the same range as that found in the original testing. By inspection of Figure 7.17
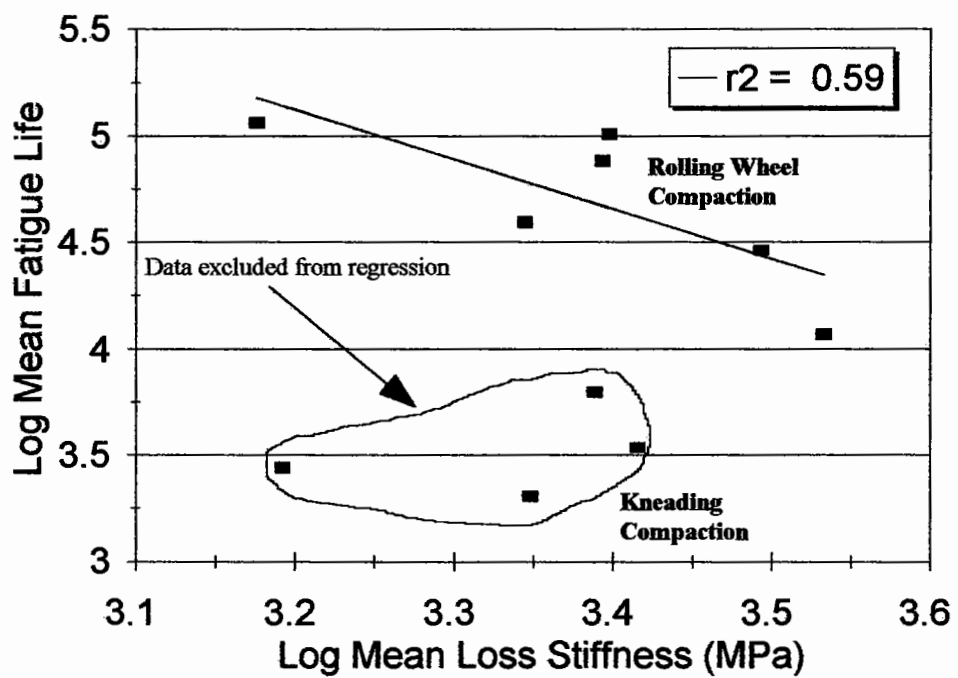
Figure 7.15 : Mean Mixture Loss Stiffness versus Mean Fatigue Life as measured in the Flexural Beam Tests, All Mixtures
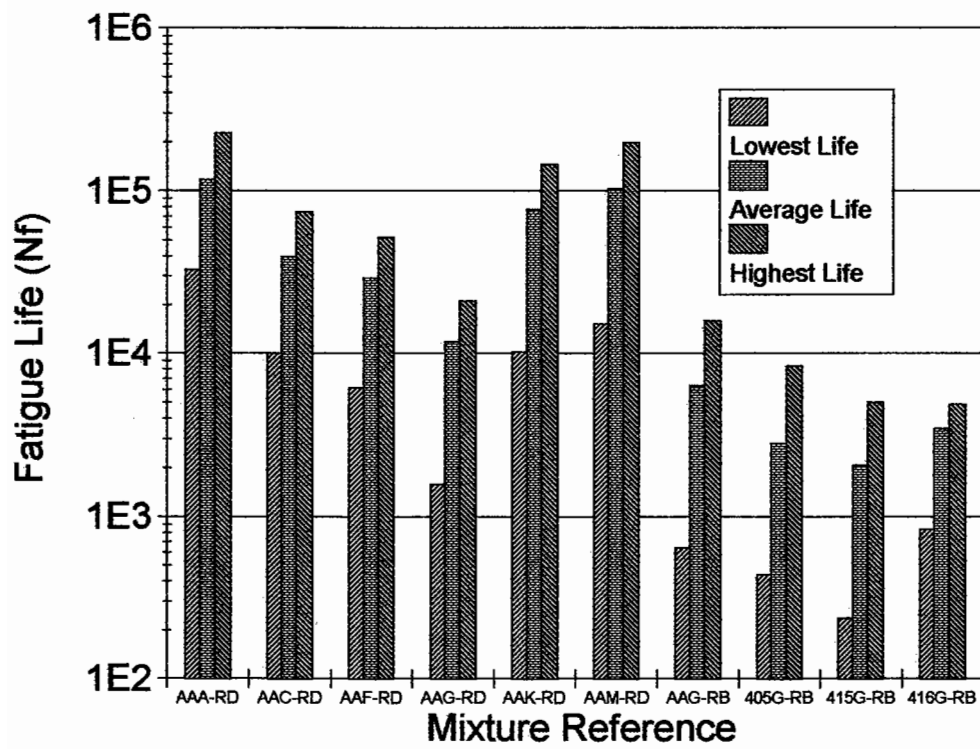
Figure 7.16 : Maximum, Minimum and Mean Fatigue Lives as measured in the Flexural Beam Tests, All Mixtures
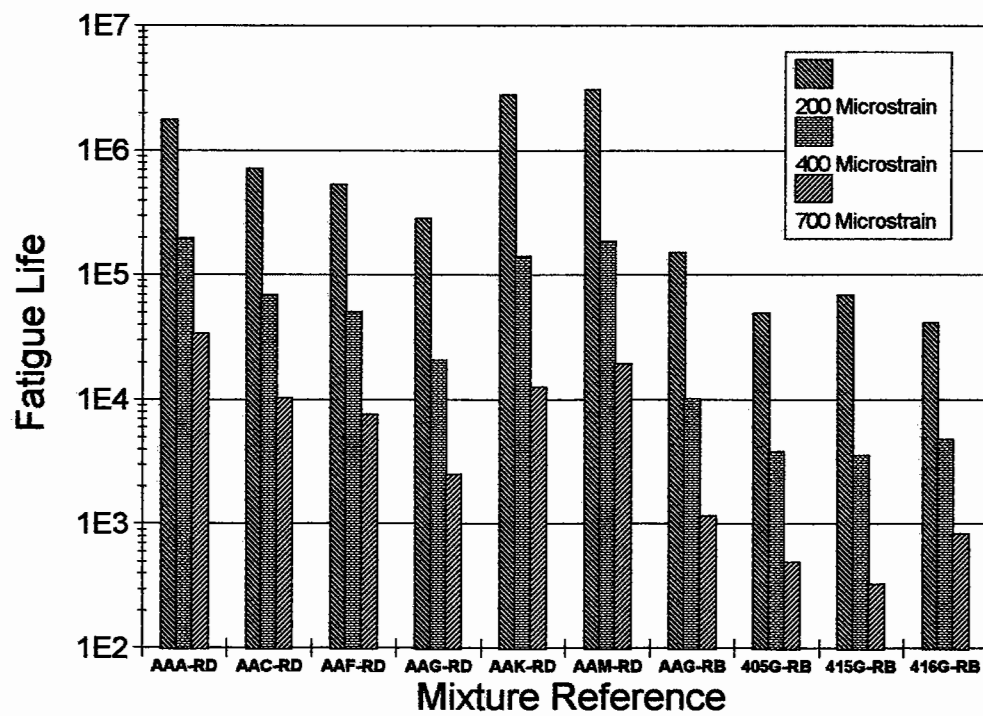
**Figure 7.17 : Fatigue Lives Calculated at 200, 400 and 700 Microstrain
from Regression Analysis of results from the Flexural Beam Tests**

it can be observed that the ranking of mixtures changes as the results are extrapolated with AAA-RD moving from rank 1 to 3. Two correlations between the laboratory fatigue data and the fatigue wheel tracking data were performed. The first compared element test data and wheel tracking results at the 200 $\mu\varepsilon$ level for all data excluding the RB aggregate (see Figure 7.18). The exclusion of the RB aggregate reduces the r^2 value from 0.49 to 0.39. However, when the same exercise was repeated with a level of 400 $\mu\varepsilon$ for the beam fatigue data (no extrapolation performed) and 200 $\mu\varepsilon$ for the fatigue wheel tracking data a r^2 of 0.43 is obtained with all the data which the increases to 0.73 if the doubtful RB data is excluded (see Figure 7.19). These results and the standard errors obtained are summarised in Table 7.8.

The exclusion of the RB aggregate from the data is further justified by inspection of additional results obtained from the fatigue testing, dissipated energy versus fatigue life, using the results from the University of California and the Trapezoidal tests reported herein. Figures 7.20 and 7.21 illustrate large amounts of data from both test programs. In Figure 7.20 the effect of different mixture types can be observed. The mixture with the Mesquite aggregate clearly gives a difference in level of performance. However, the UCB data with RB and RL aggregate generally appears to be similar to the trapezoidal data with the same aggregate type. The data obtained from the specimens fabricated by LCPC tends to have slightly higher values of dissipated energy for the failure condition (*Nf*).

In Figure 7.21 the results with binder AAG are plotted from both the UCB and
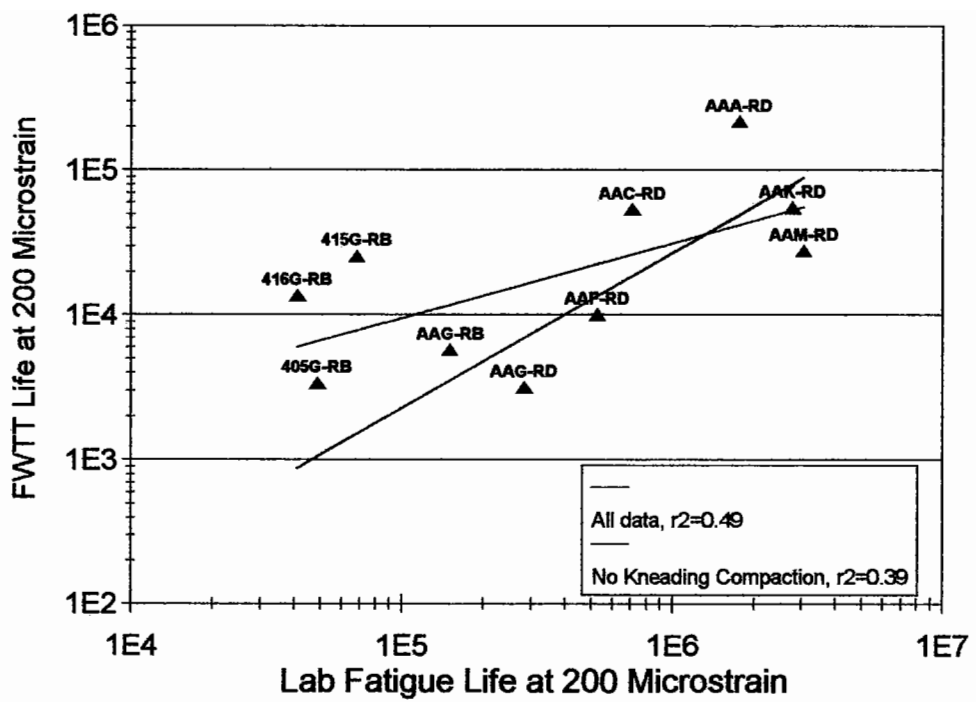
Figure 7.18 : Fatigue Wheel Track Test Results versus performance in the Flexural Beam Test at 200 Microstrain
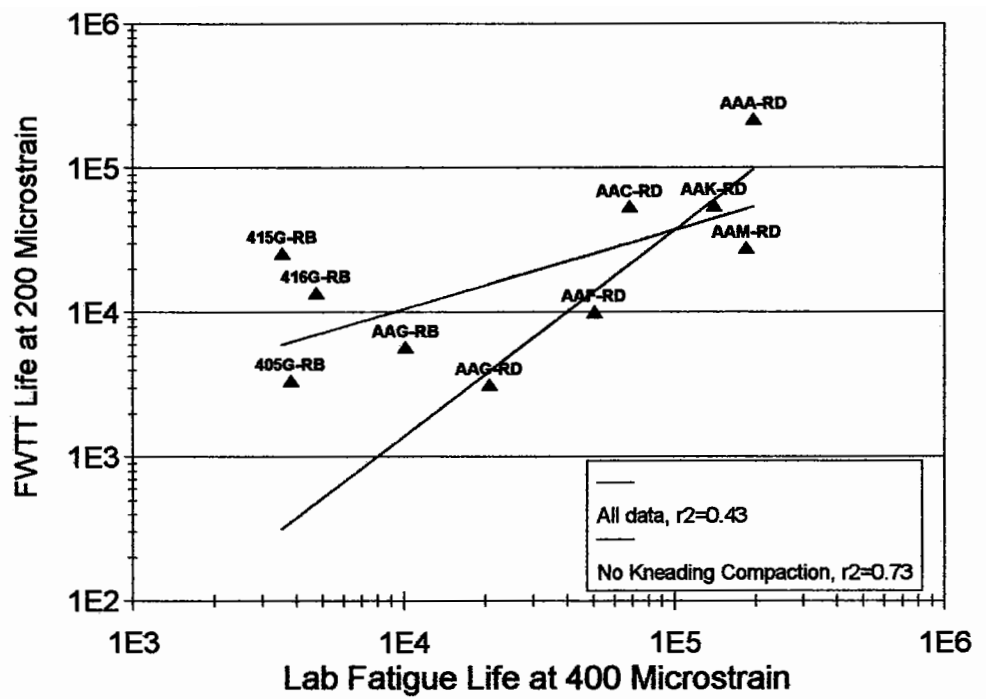
Figure 7.19 : Fatigue Wheel Track Test Results at 200 Microstrain versus performance in the Flexural Beam Test at 400 Microstrain

Strain Level in Beam Fatigue Test used for Regression	Modifier Data	a	b	r²	Standard Error in Estimate (log)
200	Included	1.387	0.518	0.391	0.488
	Excluded	-2.014	0.495	0.495	0.510
400	Included	1.831	0.548	0.428	0.473
	Excluded	-2.58	1.430	0.726	0.376

Equation is:

$$\log N_{stf} = a + b \log_{beam}$$

Table 7.8 : Fatigue Wheel Tracking Tests versus Beam Fatigue Results
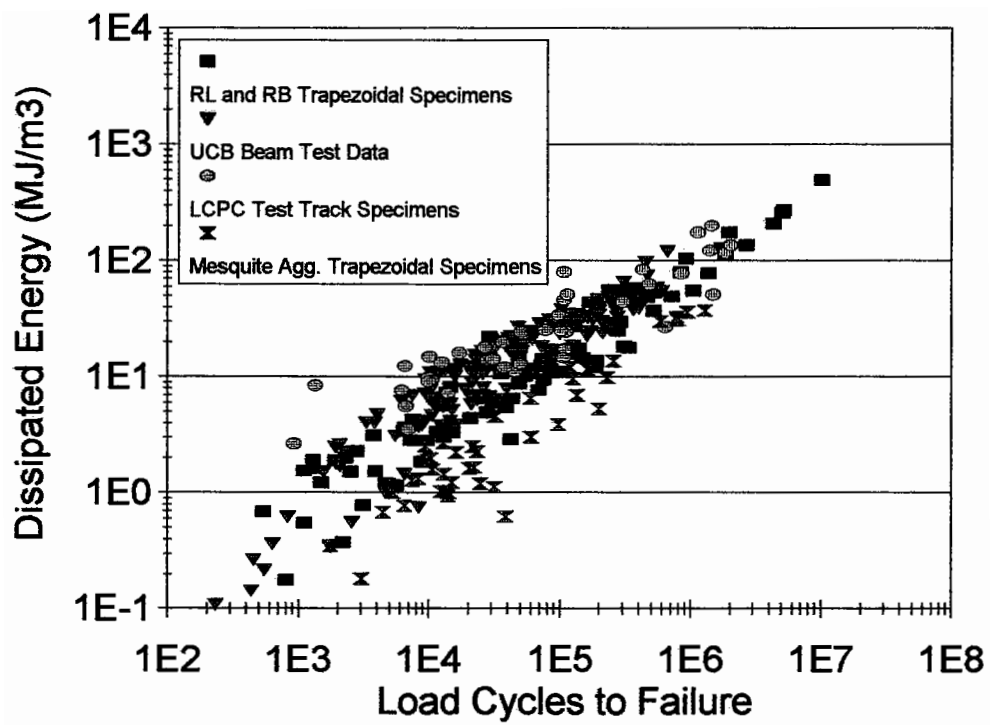
Figure 7.20 : Dissipated Energy Results - Nottingham Trapezoidal Tests versus University of California Data
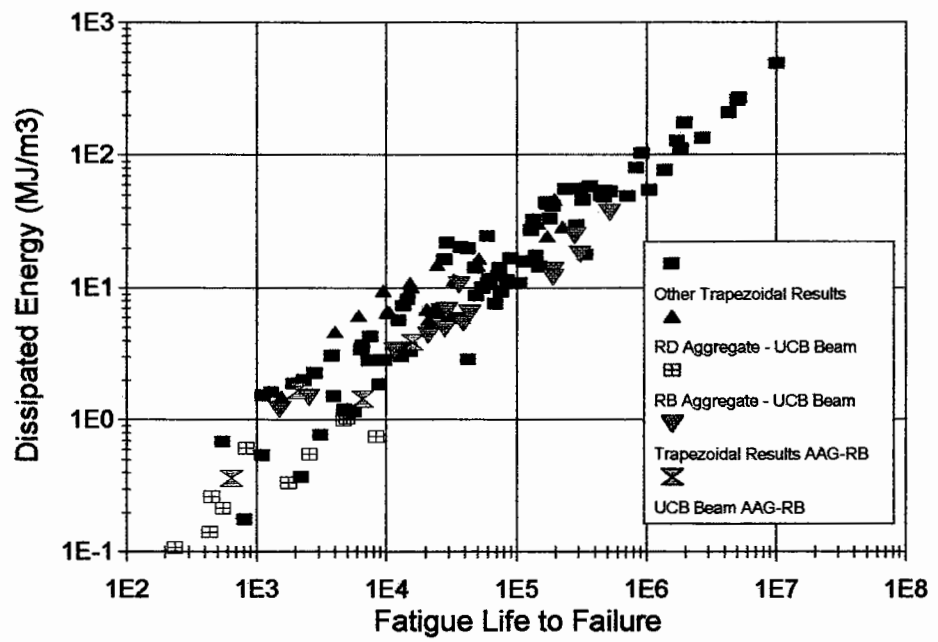
Figure 7.21 : Dissipated Energy Results - AAG-RB Results from Nottingham Trapezoidal Tests and University of California Flexural Beam Test

the Nottingham data. The UCB data obtained from specimens fabricated with the kneading device clearly gave lower fatigue lives compared to the levels obtained from the rolling wheel compaction method. It is hypothesized that this difference may be due to lack of uniformity of the specimens produced in the kneading device and/or some aggregate fracture or possible damage to the specimens in transit between Houston and Berkeley.

7.7   PERFORMANCE RANKINGS

The rankings from Fatigue Wheel Tracking, ITT Stiffness (at twenty degrees celsius), Dissipated Energy and Crack Index (CI_b - CI_t) are given in Table 7.9 for the mixtures tested in the A-003A test program. Rankings of dissipated energy results are not given for mixtures evaluated for the A-004 contract (modified mixture experiment). Consequently, these have not been included in Table 7.9. Ranking given for ITT Stiffness assumes that a higher stiffness will correspond to a shorter fatigue life consistent with controlled strain fatigue testing.

The rankings obtained from the fatigue wheel tracking for all the mixtures tested (both A-003A and A-004 tests) are given in Table 7.10 and are compared to the rankings indicated by the ITT Stiffness.

In most instances the fatigue wheel tracking and stiffness rankings give similar results with the exception of the Crack Index which appear not to be correlated with any of the parameters measured. It should be noted that considerable

Mixture Ref.	Ranking by			
	Fatigue Wheel Tracking	ITT Stiffness at 20°C	Dissipated Energy	Crack Index
AAA-RD	1	1	2	=2
AAK-RD	2	4	3	=4
AAC-RD	3	2	4	1
AAM-RD	4	3	1	6
AAF-RD	5	6	5	=4
AAG-RD	6	5	6	=2

Table 7.9 : Ranking of Fatigue Wheel Tracking Results
(A003A Results only)

Mixture Ref.	Ranking by		
	Fatigue Wheel Tracking	ITT Stiffness at 20°C	Crack Index
AAA-RD	1	1	=4
AAK-RD	2	6	=6
AAC-RD	3	2	=1
AAM-RD	4	4	8
M415-G-RB	5	3	=1
M416-G-RB	6	7	9
AAF-RD	7	9	=6
AAG-RB	8	5	not ranked
M405-G-RB	9	10	=1
AAG-RD	10	8	=4

Table 7.10 : Ranking of Fatigue Wheel Tracking Results
(A003A and A004 Results)

scatter exists in the fatigue wheel tracking data and in addition the ITT Stiffness is not a direct indicator of performance. In view of this the general agreement in the rankings obtained is considered encouraging.

7.8   SUMMARY

Eighteen slabs of asphalt/modified asphalt - aggregate mixtures were tested in the Slab Test Facility to determine their performance with respect to fatigue cracking. From the analysis of the test results, conclusions are made as follows:-

i.   The fatigue life to the *N1* condition was difficult to evaluate due to the crack pattern that occurred in the slabs being tested.

ii.   The results obtained indicate that the variability is relatively large. The standard deviations for the log of life when normalised to a constant value of strain ranged between 0.116 and 0.810.

iii.   The asphalt/modified asphalt - aggregate mixtures have been ranked according to their performance. The rankings obtained are similar to those obtained from stiffness measurement and measurement of fatigue performance using dissipated energy.

iv.   The beam fatigue results obtained at UCB correlated well to mixtures containing the RD aggregate.

v.   It appeared that the use of a kneading compaction device significantly effected the results of the modified asphalt mixtures tested at UCB or possibly specimens were damaged in transit between Houston and Berkeley.

The relationships obtained in this chapter are limited by the number of tests performed. Consequently, it is recommended that further studies with a larger set of materials be conducted to extend this work.

CHAPTER 8

Simplified Test Procedures

8.0   INTRODUCTION

During the test program, two simplified test procedures were used in order to study the results in comparison to the more fundamental trapezoidal bending beam fatigue tests. The two procedures were both Indirect Tensile Tests in which vertical load is applied which produces a horizontal tensile stress across the vertical diameter, Figure 8.1. In the first procedure the Stiffness Modulus was measured at three temperatures (0, 10 and 20°C). The second procedure involved complete fracture of a specimen during which measurements of horizontal and vertical deformation were taken. This data was subsequently reduced and analyzed to determine test parameters. This chapter presents an analysis of the results obtained and explores the use of simplified test procedures for the prediction of fatigue performance.

8.1   INDIRECT TENSILE STIFFNESS MODULUS

The Indirect Tensile Stiffness Modulus was measured in a device known as the Nottingham Asphalt Tester (NAT), (Cooper and Brown, 1989). This device is illustrated in Figure 8.2.
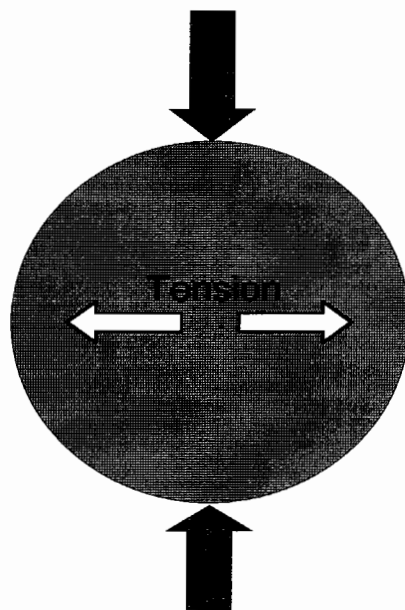
Figure 8.1 : Indirect Tension Test
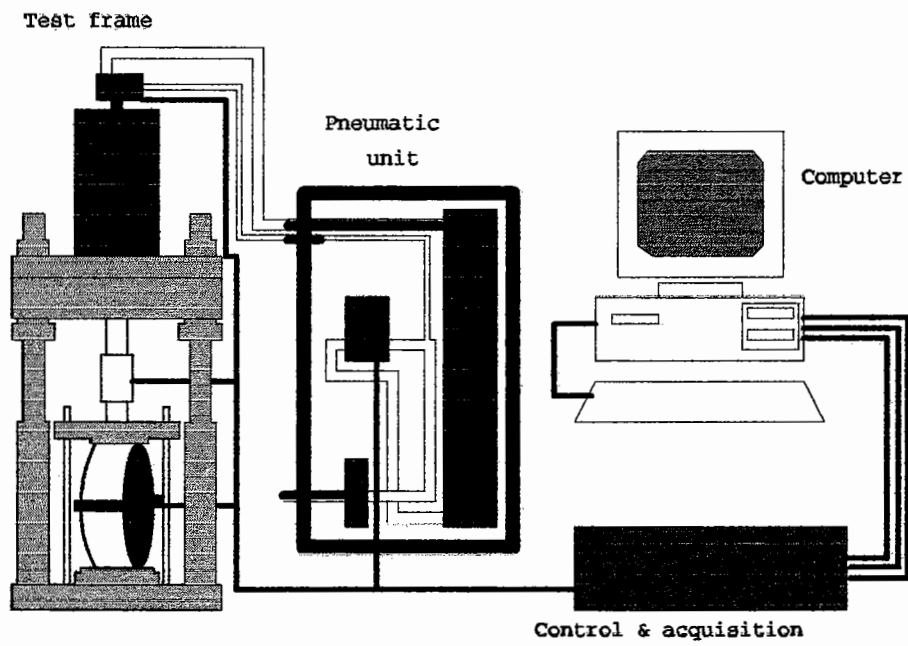
Figure 8.2 : The NAT Configured for the Indirect Tensile Test

In this method of stiffness measurement, repeated loading is applied across the vertical diameter of a cylindrical specimen. This loading produces a complex bi-axial stress distribution in the specimen as illustrated in Figure 8.3. The resultant extension of the horizontal diameter is measured and used to estimate the stiffness assuming that; 1) the specimen is subjected to plane stress, 2) the material is linear elastic, 3) the material is homogeneous and isotropic, 4) Poisson's ratio for the material is known and 5) the vertical load is applied as a line loading. When these conditions are satisfied, the stress conditions in the specimen are given by the closed form solution of the theory of elasticity (Hudson et al., 1968).

The maximum and average stresses acting on the x and y axis (using polar notation) are as follows:

$$\sigma_{\theta y}(\text{max}) = \frac{2\ P}{\pi\ d\ t} \qquad (8.1)$$

$$\sigma_{\theta x}(\text{max}) = \frac{-\ 6\ P}{\pi\ d\ t} \qquad (8.2)$$

$$\sigma_{\theta y}(av) = \frac{0.273\ P}{d\ t} \qquad (8.3)$$

$$\sigma_{\theta x}(av) = \frac{-\ P}{d\ t} \qquad (8.4)$$

where; P = vertical load

d = specimen diameter

t = specimen thickness
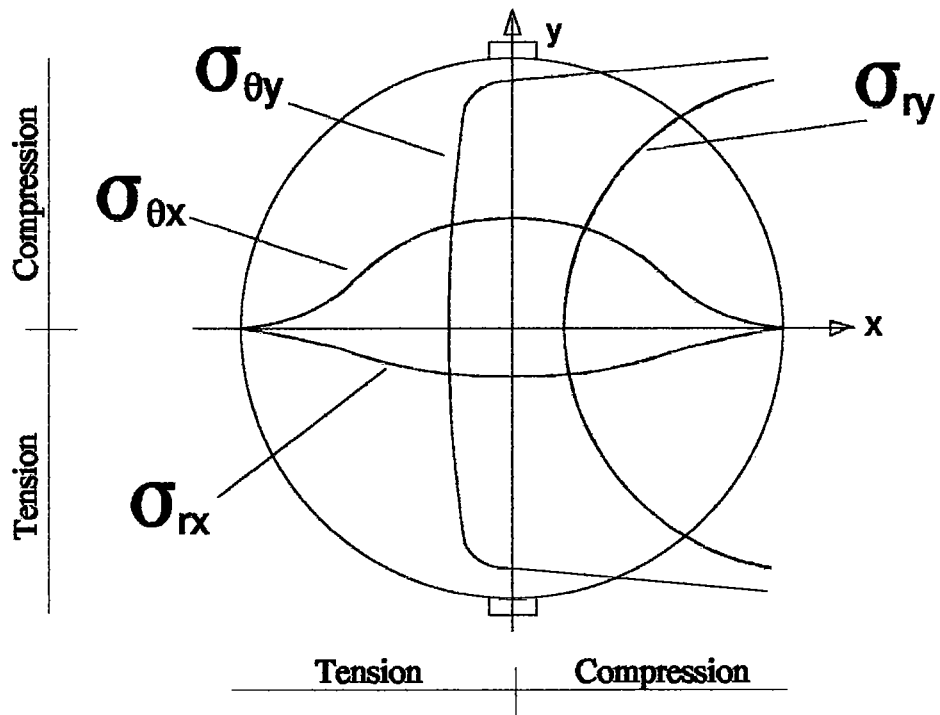
Notes :

r = radial distance of a point from the origin.

θ = angular displacement to a point from the y axis.

σ_θ = tangental stress.

σ_r = radial stress.

**Figure 8.3 : Stress across Horizontal and Vertical Diameters
(using polar notation)**

Determination of the stiffness modulus from the theoretical stress distribution is then calculated by considering the average principal stresses in a small element subject to bi-axial stress conditions. The horizontal strain of such an element is defined in Equation 8.5. By substitution the horizontal strain and displacement are calculated, Equations 8.6 to 8.8, which are then used to produce the expression which is used for the calculation of the indirect tensile stiffness modulus (Equation 8.9).

$$\epsilon_{\theta y}(av) = \frac{\sigma_{\theta y}(av)}{S_m} - v\frac{\sigma_{\theta x}(av)}{S_m} \qquad (8.5)$$

$$\epsilon_{\theta x}(av) = \frac{0.273\ P}{S_m\ d\ t} + \frac{v\ P}{S_m\ d\ t} \qquad (8.6)$$

$$\Delta h = \epsilon_{\theta y}(av)\ d \qquad (8.7)$$

$$\Delta\ h = \frac{0.273\ P}{S_m\ t} + \frac{v\ P}{S_m\ t} \qquad (8.8)$$

$$S_m = \frac{(0.273 + v)\ P}{\Delta\ h\ t} \qquad (8.9)$$

A Poisson's ratio of 0.35 was assumed at all temperatures. A load rise time of approximately 0.14 seconds was used with a load of approximately 3.1 kN. Figure 8.4 shows typical results obtained at the three temperatures tested for the mixtures containing the two types of binders and aggregates used in the test development programme. The results for these mixtures indicates a higher stiffness is obtained with the Valley binder compared to the Boscan binder. This was also the general trend observed in the test development program. However, when the stiffnesses obtained from the indirect tensile testing are
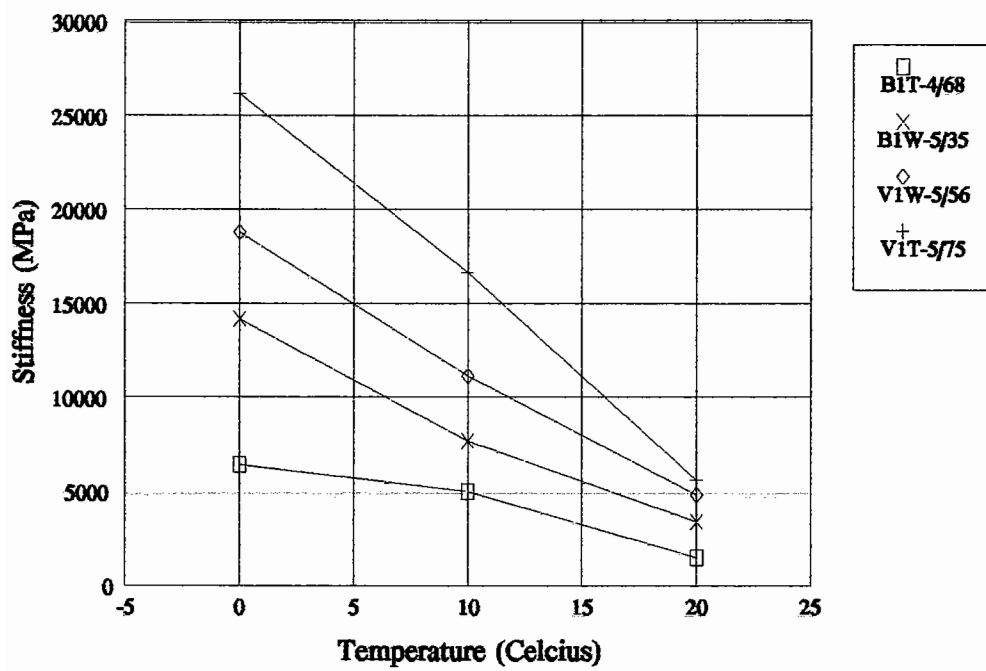
Figure 8.4 : **Typical Results for Mixtures with Boscan and Valley Binders, and Texas Chert and Watsonville Aggregate**

compared to those from the trapezoidal fatigue testing it is observed that the results at 20°C have a lower stiffness in the indirect tensile test but have higher values at a temperature of 0°C, see Figure 8.5. A bias in the results is expected due to the different loading speeds and in order to investigate this the results were initially adjusted to reflect the differences in loading speed. The adjustment factors are obtained from the use of Van der Poel's nomograph in conjunction with the Bonnaure et al., (1980) mixture stiffness prediction method. The stiffnesses were calculated for two loading times and three temperatures (0°C, 10°C and 20°C). From these stiffnesses, adjustment ratios were calculated which considered the difference in loading time and temperature of the test, see Table 8.1. The results adjusted for loading time only are presented in Figure 8.6 where it can now be seen that a linear relationship exists between the trapezoidal stiffness and that measured in indirect tension. This relationship has a r^2 value of 0.79 and is expressed as follows:-

$$S_m = 1.78 \ E^* - 957.8 \qquad (8.10)$$

The fact that such a good relationship exists between the Indirect Tensile Test and the stiffness measured in the Trapezoidal Fatigue Test suggests that the simpler Indirect Tensile Test can be used with a reasonable degree of confidence for stiffness measurement between fairly wide limits.

The above analysis is for the tests which were conducted at two temperatures 0°C and 10°C in the two test types (Indirect Tension and Trapezoidal Bending). However, Indirect Tensile Stiffness measurements were also obtained at the
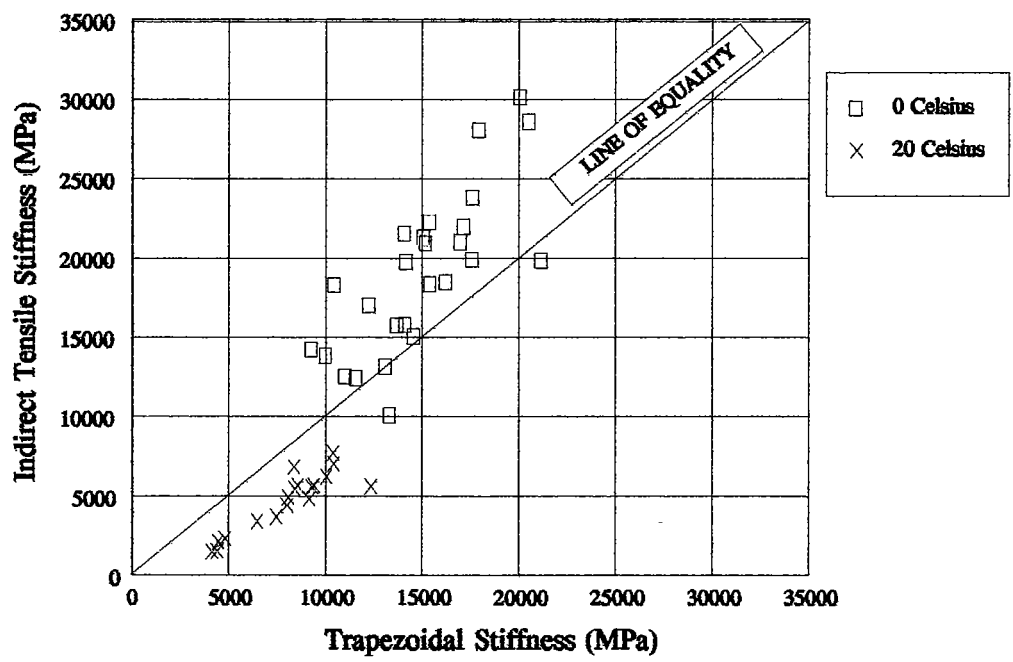
Figure 8.5 : Indirect Tensile Stiffness versus Trapezoidal Stiffness

-8.9-

Type of Test	Binder	Temperature (°C)	Stiffness (MPa)	
			Voids = 4%	Voids = 8%
Indirect Tensile Test	AAK-1 (Boscan)	20	3066	1909
		10	7298	4546
		0	13431	8706
	AAG-1 (Valley)	20	4496	2801
		10	13644	8872
		0	24122	17696
Trapezoidal Fatigue Test	AAK-1 (Boscan)	20	7292	4542
		0	19851	13975
	AAG-1 (Valley)	20	12641	8089
		0	30391	23411
Ratio's				
Trap./ITT	AAG-1	20	2.81	2.88
Trap./ITT	AAG-1	0	1.26	1.32
Trap./ITT	AAK-1	20	2.38	2.38
Trap./ITT	AAK-1	0	1.48	1.61
Trap./ITT	AAG-1	0/10	2.22	2.64
Trap./ITT	AAG-1	20/10	0.91	0.93
Trap./ITT	AAK-1	0/10	2.72	3.07
Trap./ITT	AAK-1	20/10	1.00	1.00

All Ratio's

Both @ 0°C AAG-1	Both @ 20°C AAG-1	Both @ 0°C AAK-1	Both @ 20°C AAK-1
1.29	2.845	1.545	2.38
Trap. @ 0°C ITT @ 10°C AAG-1	Trap. @ 20°C ITT @ 10°C AAG-1	Trap. @ 0°C ITT @ 10°C AAK-1	Trap. @ 20°C ITT @ 10°C AAK-1
1.29	2.845	1.545	2.38

Average Ratio's

Table 8.1 : Calculated Trapezoidal and Indirect Tensile Stiffnesses and Ratio's using the Bonnaure et al., (1980) method
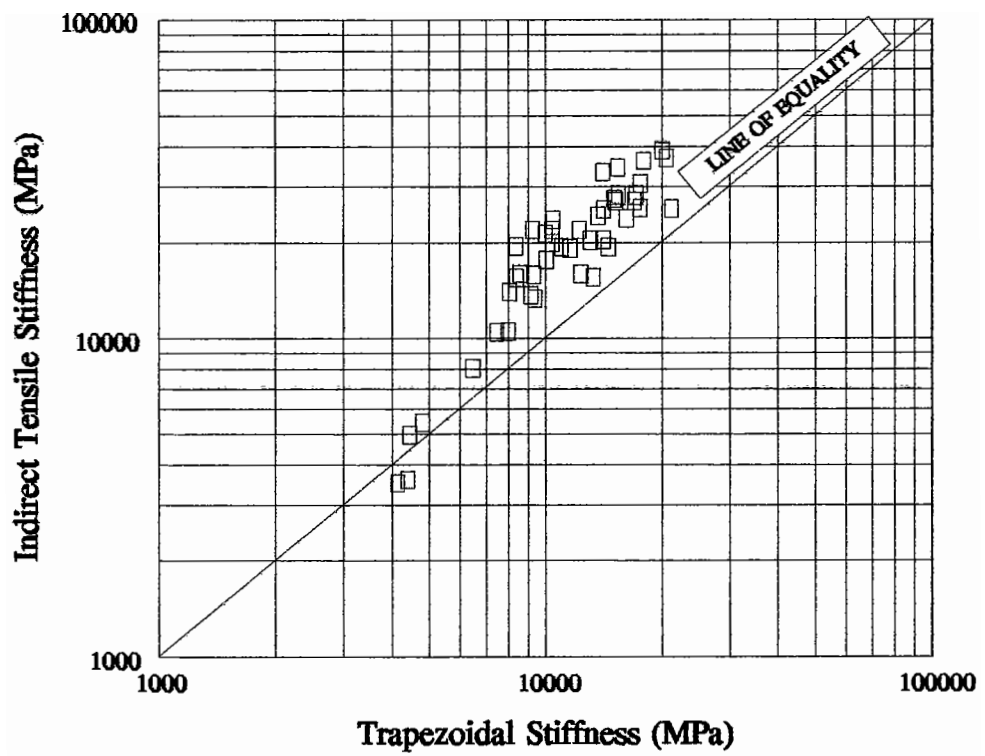
**Figure 8.6 : Indirect Tensile Stiffness versus Trapezoidal Stiffness -
Adjusted for Speed of Loading**

intermediate temperature of 10°C. It would be more desirable in a simple testing scheme to use this temperature in place of testing at the low temperature of 0°C since at temperatures around freezing, condensation can occur and generally temperature control is more difficult. Adjustment factors were also derived for this temperature and these are also presented in Table 8.1. The resulting adjusted stiffnesses are plotted in Figure 8.7. It can be seen from this figure that adjusted data lies in two distinct groups and a relationship cannot be established when results are adjusted for both loading time and temperature. It would appear that the stiffness adjustment is less reliable if both speed of loading and temperature adjustments are combined.

The analysis of fatigue test results in Chapter 6 illustrates that stiffness modulus plays a key role in the prediction of fatigue performance. To avoid the preparation of Trapezoidal beams which require extensive specimen preparation it would be desirable for the purpose of fatigue life prediction to replace the value of stiffness modulus used with that measured in the Indirect Tensile Test. However, one limitation of the Indirect Tensile Test is that no measure of phase angle can be made. Consequently, a method is required to estimate this.

Francken et al., (1974) published results for a series of mixtures covering a wide range of binders and volumetrics. If the logarithm of stiffness (E^*) is plotted against the phase angle (δ), see Figure 8.8, a relationship can be obtained as follows:-
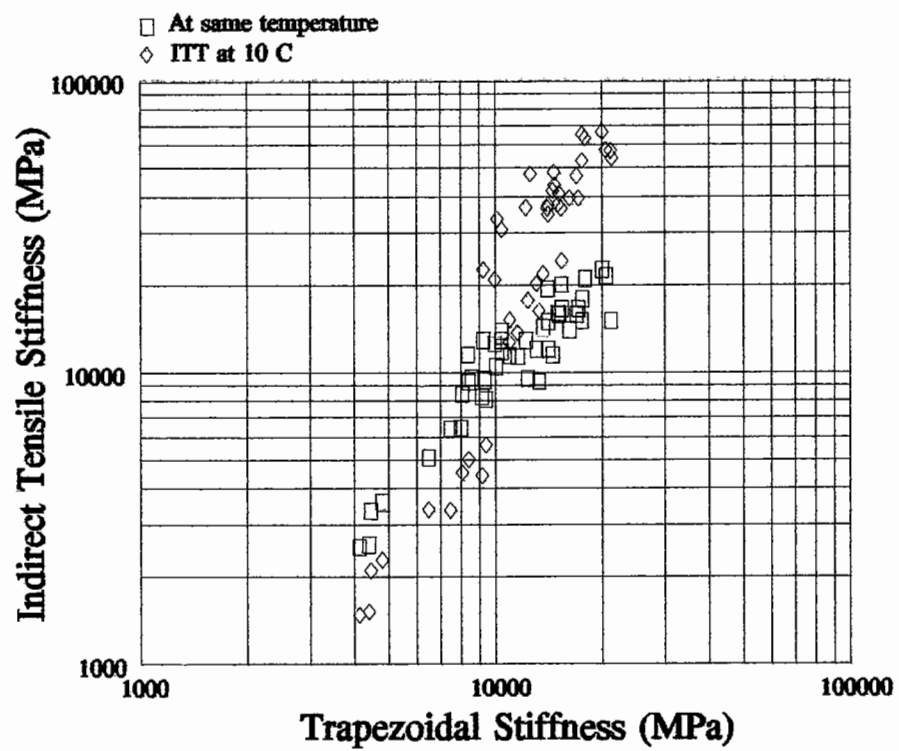
Figure 8.7 : Indirect Tensile Stiffness versus Trapezoidal Stiffness - Adjusted using $S_m = 1.78 E^* - 957.8$
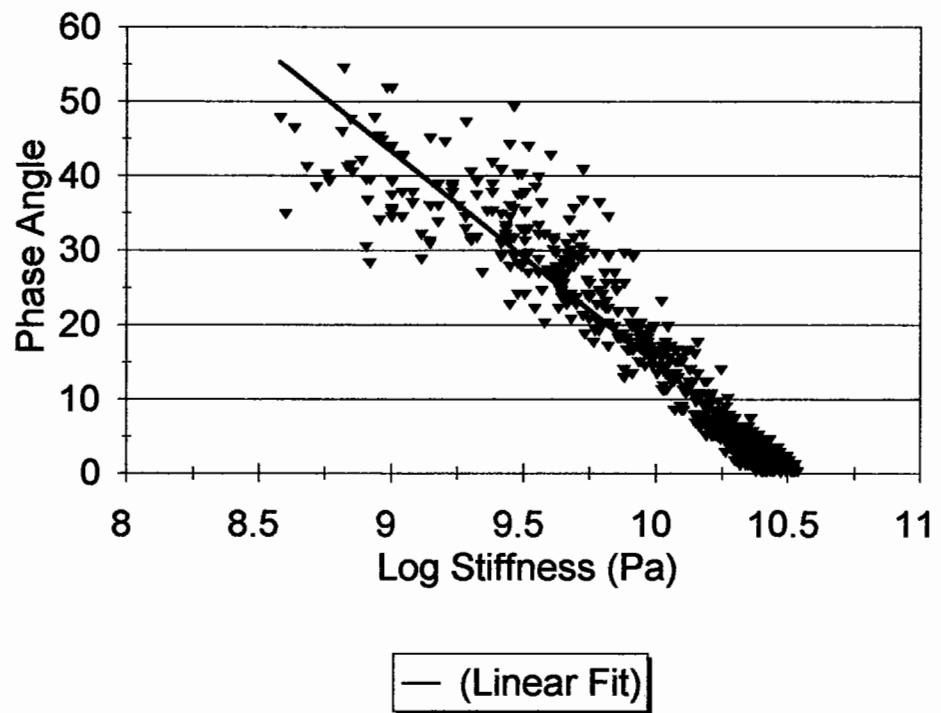
Figure 8.8 : Phase Angle versus Stiffness (after Francken et al., 1974)

$$\delta = 299.7 - 28.5 \log E^* \qquad \textbf{(8.11)}$$

Using this relationship the phase angle is calculated for the stiffness measured in the Indirect Tensile Test. This is compared to measured values from the Trapezoidal Fatigue Test in Figure 8.9. This data has been used with the method detailed in Chapter 6 for prediction of the fatigue life to the *Nl* condition for a number of mixtures. The results for this prediction are compared to the predicted results from the Trapezoidal Fatigue Test in Figure 8.10. It can be observed that while the stiffness from the Indirect Tensile Test does explain a significant amount of the variability, a bias does exist with longer lives being obtained. The relationship between the two methods of life prediction is as follows:-

$$\log Nl_{ITT} = 0.78 \log Nl_{Trap.} + 1.763 \qquad \textbf{(8.12)}$$

Thus, the use of stiffness values from the Indirect Tensile Test appears to be promising. From the limited data collected during this study, a large amount of variability in fatigue life can be explained by using a prediction method in which the Indirect Tensile Stiffness is used. However, problems were encountered in the area of time-temperature adjustments. The use of loading time adjustments appears more robust than trying to shift data for the effects of both loading time and temperature.

8.2   INDIRECT TENSILE FRACTURE TEST

The results from the Indirect Tensile Fracture Test were analyzed to determine the tensile strength and the work done to reach failure (see Equations 5.43 and
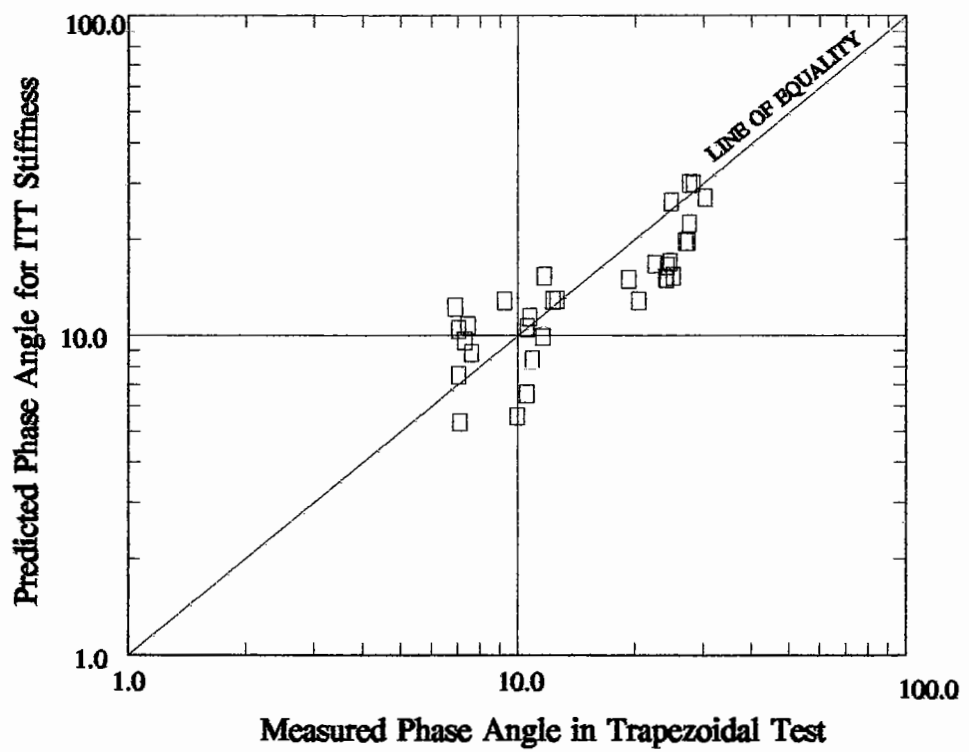
Figure 8.9 : Predicted Phase Angle versus Phase Angle Measured in the Trapezoidal Fatigue Test
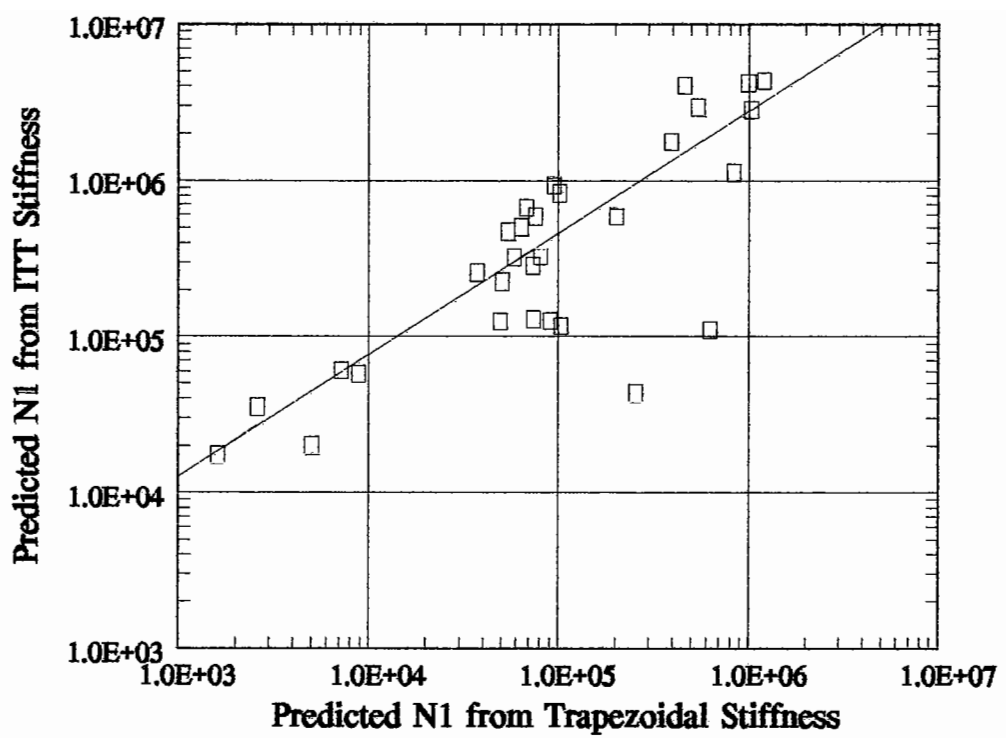
Figure 8.10 : Fatigue Life Predicted from NAT Results versus Predicted from Trapezoidal Fatigue Tests

5.45). A third parameter, the Poisson's ratio could not be calculated successfully due to the low resolution of the LVDT's measuring the horizontal deformation. The results, for the three temperatures , are presented in Table 8.2 and plotted in Figures 8.11 and 8.12.

The results indicate greater variability at 20°C compared to 0°C and 10°C. The tensile strength was found to be higher at lower temperatures for most of the mixtures. However, this was not the case for the energy to failure.

8.3 RANKINGS USING INDIRECT TENSION RESULTS

The ranking of Indirect Tensile Stiffness, Strength and Energy versus parameters measured in the Slab Test Facility experiments (rankings of mean life and crack index, see section 7.7) are given in Figure 8.13. It can be observed that the results from the Indirect Tensile Fracture test, in the form used here, do not discriminate between the materials in the same manner as did the Slab Test Facility (no trends in the data were apparent) or the Indirect Tensile Stiffness test.

8.4 STRESS STATE IN INDIRECT TENSILE TESTS

The state of stress in an indirect tensile test is significantly more complex than in a flexural beam test. Sousa et al. (1991) conducted a three dimensional Finite Element analysis of the specimen shape and concluded that the material properties would be dependent upon the stress level. This is due to the highly

Mixture	Tensile Stength (kN)			Energy to Peak Load (J/mm)		
Reference	0°C	10°C	20°C	0°C	10°C	20°C
AAG/RD	3.028	2.389	1.958	0.301	0.349	0.452
AAK/RD	3.134	2.726	1.483	0.301	0.404	0.269
AAM/RD	3.502	2.451	1.154	0.400	0.467	0.228
AAA/RD	-	-	-	-	-	-
AAC/RD	2.911	2.280	1.066	0.404	0.434	0.256
AAF/RC	2.838	2.682	1.693	0.215	0.348	0.363
AAG/RB	2.988 3.525 2.342 (2.951)	3.130 2.977 - (3.053)	2.642 2.289 - (2.764)	0.330 0.387 0.295 (0.337)	0.328 0.388 - (0.358)	0.583 0.598 - (0.591)
415-5/RB	4.554 3.888 2.943 (3.795)	- 2.499 2.427 (2.463)	2.760 2.086 1.637 (2.160)	0.462 0.409 0.275 (0.382)	- 0.293 0.362 (0.327)	0.530 0.471 0.375 (0.459)
416-G/RB	- 3.546 3.598 (3.572)	- 3.528 3.216 (2.872)	1.676 2.326 2.256 (2.086)	- 0.352 0.381 (0.366)	- 0.453 0.400 (.427)	0.537 0.462 0.541 (0.513)
405-G/RB	2.892 2.397 3.068 (2.786)	3.362 2.344 2.608 (2.772)	3.196 2.854 - (3.025)	0.251 0.173 0.272 (0.232)	0.322 0.198 0.276 (0.265)	0.379 0.333 - (0.356)

Table 8.2 : Tensile Strength and Energy to Peak Load in the Indirect Tensile Splitting Test
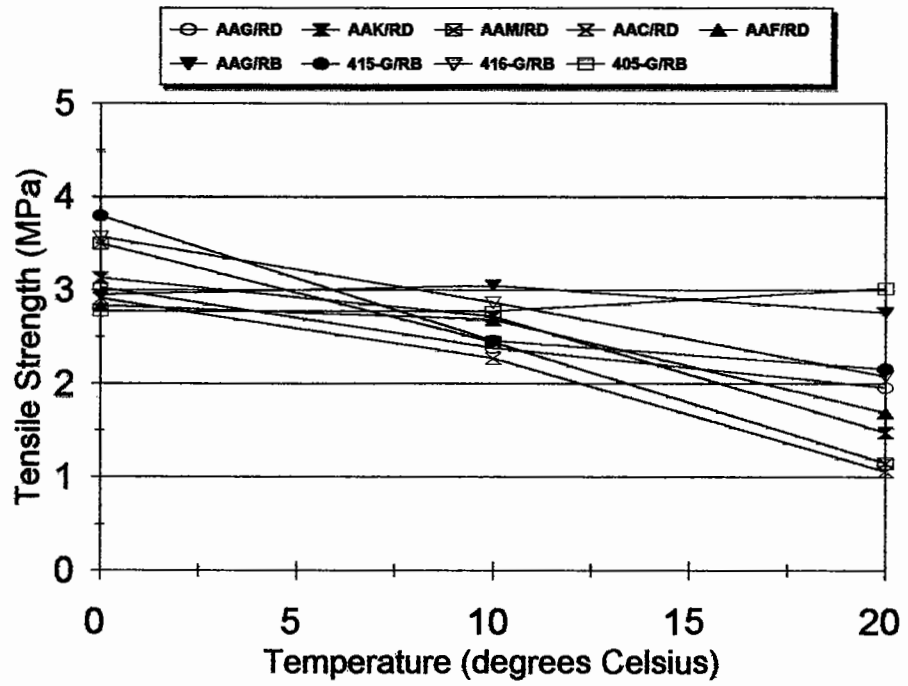
Figure 8.11 : Tensile Strength measured in the Indirect Tensile Splitting Test
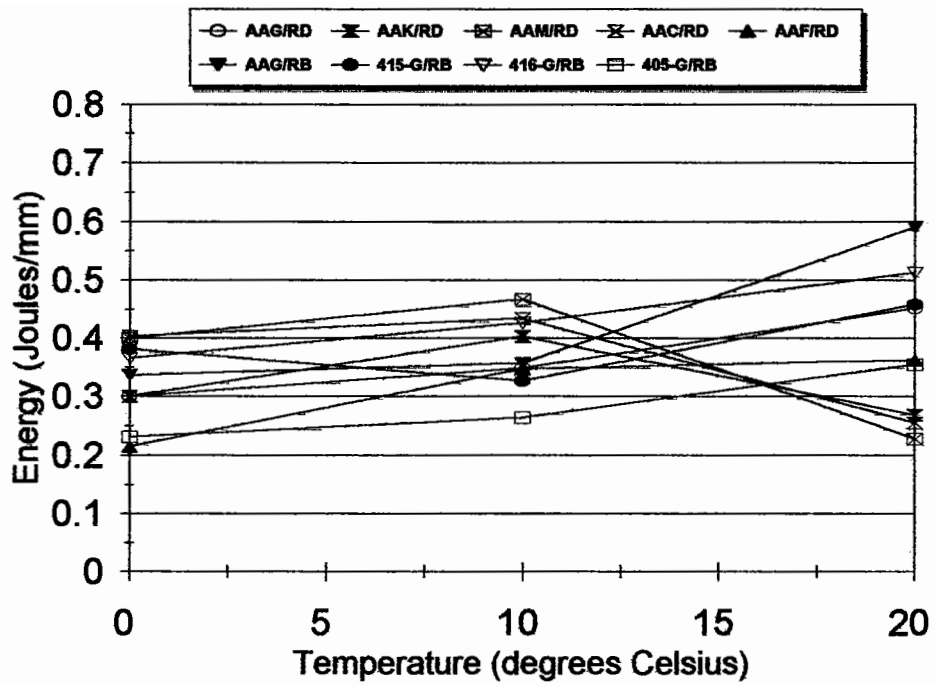
Figure 8.12 : Energy to Peak Load measured in the Indirect Tensile Splitting Test
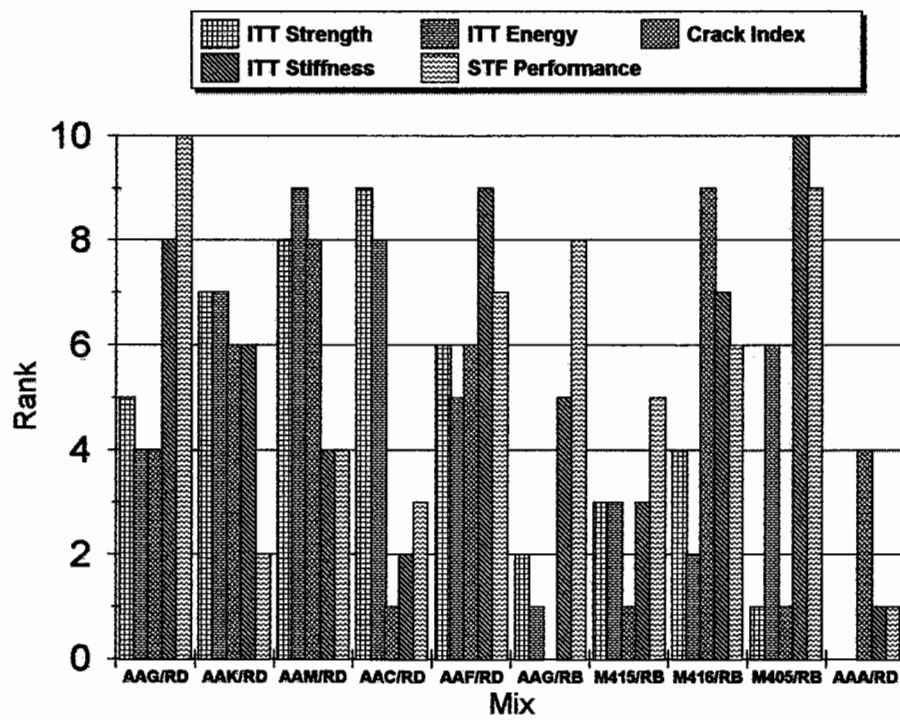
Figure 8.13 : Parameters Measured in the Indirect Tensile Test versus Performance Obtained in the Slab Test Facility

non-uniform stress distribution in the specimen. In addition, the value of Poisson's ratio is effected by this variable stress distribution.

The state of stress can be approximated to bi-axial as illustrated earlier. Using this form of approximation it can be observed that the stress increases to a very large value in the proximity of the loading strips. In addition, it has been observed that a relationship exists between the stiffness modulus and the Poisson's ratio (Sousa et al., 1991; Bouldin et al. 1993; Alavi and Monismith, 1994) and thus the true value for Poisson's ratio (or strain ratio) will be variable throughout the specimen. Consequently, the assignment of a single value could produce an incorrect result for the stiffness determination. Thus, it is considered that the test provides better results at lower temperatures when the strains are smaller. Recognizing, the problem with an assumed Poisson's ratio and variable stress/strain across the diameter of the specimen, Roque and Buttlar (1992) developed a method of measuring strains based upon measurements made towards the centre of the specimen faces. In this zone, the variation is significantly less than across the whole specimen. In addition Roque and Buttlar (1992) combined the analysis with an iterative procedure to minimize the errors associated with the Poisson's ratio determination. Hugo and Schreuder (1993) identified similar problems to Roque and Buttlar (1992) and made recommendations that specimen thicknesses also effect the test results.

8.5   THE RESILIENT MODULUS TEST (ASTM D 4123)

The test method specified in the ASTM standard is somewhat different from that developed by Cooper and Brown (1989) in that the resilient stain is used to determine the stiffness modulus rather than the total strain, see Figure 8.14. The resilient modulus test was extensively evaluated by Tayebali et al. (1994) who concluded that the use of the resilient stain can cause misleading values of stiffness modulus, particularly at high temperatures. In this condition, the resilient strain is small (ie. the specimen deforms only visco-plastically) and consequently the modulus is very high. This is the opposite trend to that obtained with bending tests in which the strain response includes elastic, viscous and plastic strain components.

8.6   EFFECTS OF STRESS PULSE IN INDIRECT TENSILE TEST

An additional factor which needs to be taken into consideration in the determination of stiffness modulus in the indirect tensile test is the shape of the stress pulse. Since asphaltic material is visco-elastic with time dependent properties, the stiffness is also a function of the area under the load time curve. A greater area under this curve will result in a higher stiffness. Consequently, care has to be taken when comparing results from tests which produce different load signals and when using different loading times. Nunn (1995) calculated the effects of different stress pulse shapes generated by commercially available equipment and concluded that, for tests conducted with identical times to peak load, the results could vary by about 20% dependent upon how quickly the
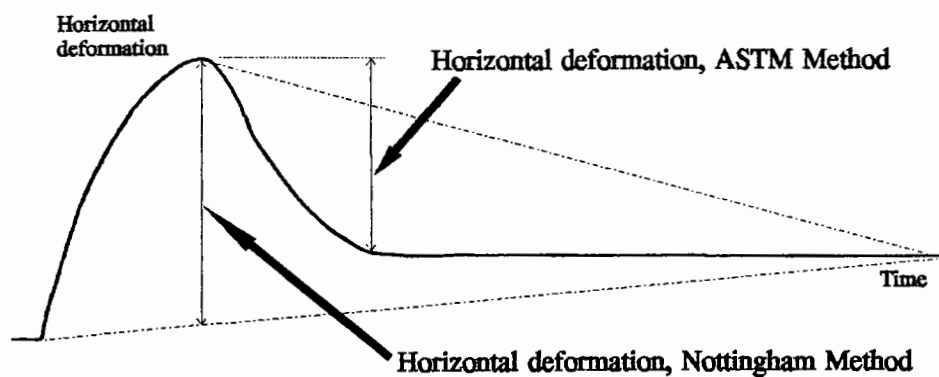
Notes:
Nottingham Method - 1) A line is constructed between the start (the initial reading) and the final reading. 2)   The horizontal deformation is taken as the distance between that line and the peak deformation reading.
ASTM Method - 1) A line is constructed between the maximum horizontal deformation and the horizontal deformation after a period of time. 2) A line is dropped from this line to determine the maximum ordinate between the constructed line and the strain. 3) This ordinate defines the end of the recovery of resilient strain. 4) The resilent srain is defined as the peak strain minus the strain and the time when recovery of the resilent strain is complete,

Figure 8.14 : Differences in the Definition of Horizontal Displacement, Nottingham versus ASTM Method

load was applied. This obviously is a cause of concern if the results are being used to substitute for other more fundamental test methods in which the shape and duration of the load pulse is more accurately defined.

8.7   SUMMARY

The results from this study demonstrated that a good relationship existed between the stiffness in indirect tension and the cantilever beam method when the results were compared at the same temperature. When shifting from one temperature to another, the relationship was found to be poorer. It is suggested that this could have occurred due to the different binder rheology in the mixtures which were tested. The results from the indirect tensile splitting tests proved to be inconclusive due to the lack of sensitivity of the instrumentation. In addition, several researchers have recently experienced problems interpreting results from this test. Some improvements to the instrumentation are recommended along with careful consideration of the problems discussed above. This test still appears to be promising but a significant amount of work is required to address the above concerns.

CHAPTER 9

Fatigue Analysis of Pavements

9.0   INTRODUCTION

This chapter considers methods to analyze pavement structures with respect to fatigue life prediction. Pavements have traditionally been analyzed with elastic analysis methods to compute the value of tensile strain at the underside of the bound pavement layer. This value is then used with a fatigue/life relationship to estimate the number of load repetitions which can be applied before fatigue cracking occurs. As part of the work reported herein, several pavements were tested with a wheel tracking device to determine the fatigue performance. Thus, if the relationships developed between energy and life are to be used, these need to validated against the results obtained from pavement analysis. However, it is not possible to calculate the amount of energy dissipated from a linear elastic analysis and, consequently, a method which makes use of visco-elastic pavement analysis has been developed. The use of the visco-elastic method (with a dissipated energy criteria) is compared to elastic analysis (using the strain criteria) for those pavements tested in Slab Test Facility (Chapter 7), and in addition for several other special cases. The computer program (which incorporates a visco-elastic model) developed by Rowe et al. (1995) uses a number of Maxwell elements in parallel (Figure 9.1). The program can contain any number of these elements acting in parallel using an overlay

n elements
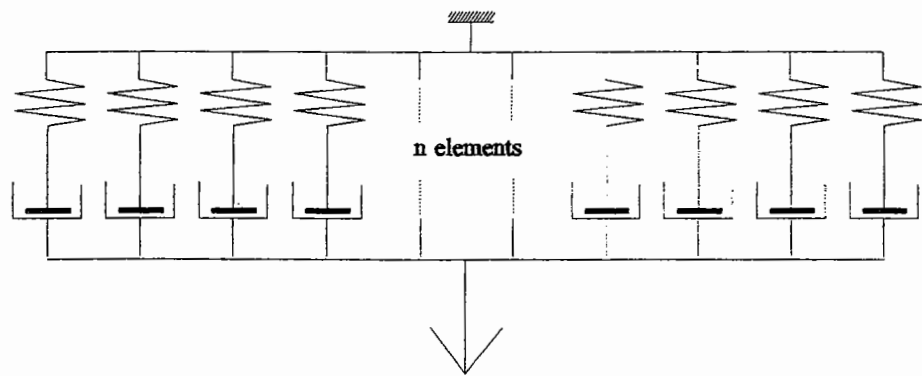
Figure 9.1 : Generalized Maxwell Model

technique (Pande, 1977). Methods currently in existence enable determination of the parameters for a model of this form from either frequency sweeps or other forms of repeated loading tests carried out on prepared specimens.

9.1   THE CASE FOR VISCO-ELASTIC ANALYSIS

Huhtala et al. (1990) reported strains measured in a test track. These showed that, in the longitudinal direction, compressive strains occur which are followed by a tensile peak and then compressive strains again, whereas, in the transverse direction, the strain is all tensile (see Figures 9.2 and 9.3). In the transverse direction, there is a residual strain following the passage of the wheel load, whereas in the longitudinal direction there are differences in the magnitude of the compressive strain that occurs before and after the tensile peak. If linear elastic analysis is used, the shape of the resulting strain curves are symmetrical. Therefore, Huhtala et al. (1990) presented strong evidence to suggest that linear elastic analysis is not correct in describing the strains (and indirectly, stresses) in an asphaltic pavement structure under the passage of a wheel load. However, if a visco-elastic model is employed, non-symmetrical stress/strain responses can be calculated as illustrated in Figures 9.4 and 9.5 (in this example, the material model for the asphaltic layers uses two Maxwell elements in parallel). The shapes of the curves in these figures have the same basic shape as observed by Huhtala et al. (1990). A further analysis by Huhtala et al. (1992) illustrated that using asphalt material properties associated with the Burgers' model (Figure 9.6) the effect of multiple wheel passes on the strain response could be explained with reasonable accuracy. The Burgers'
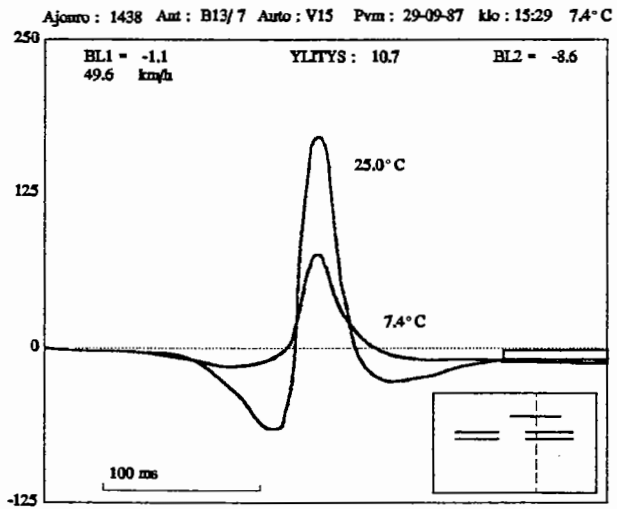
Figure 9.2 : Longitudinal Strains at underside of bound layer (after
Huhtala et al., 1990)
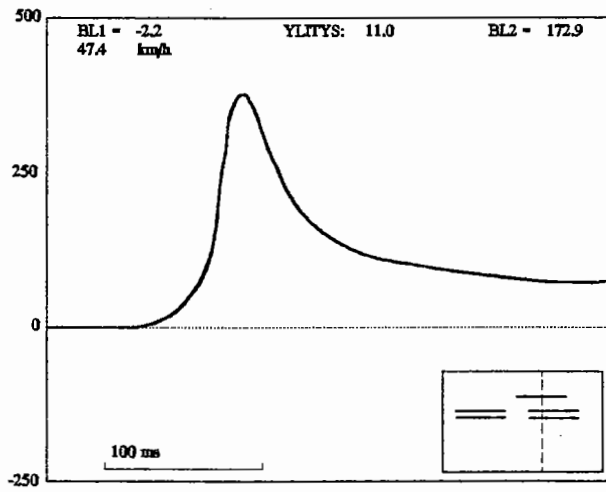
Figure 9.3 : Transverse Strains at underside of bound layer (after Huhtala et al., 1990)

-9.5-
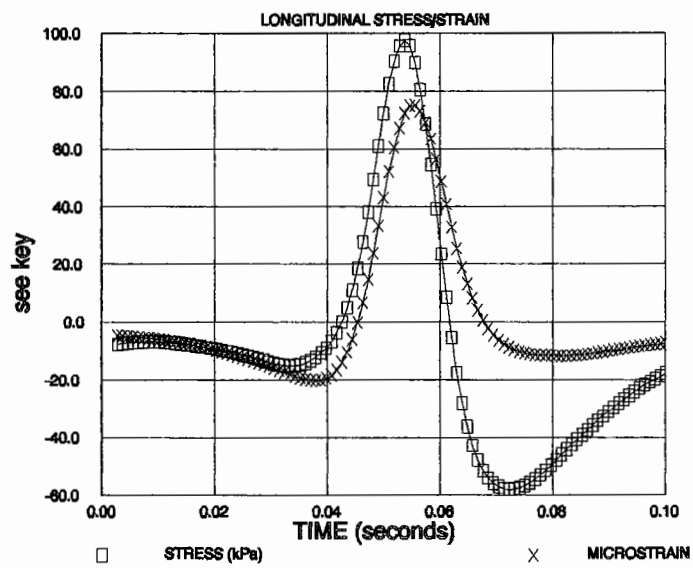
Figure 9.4 : Longitudinal Stresses and Strains Computed from the FE Model at underside of bound layer
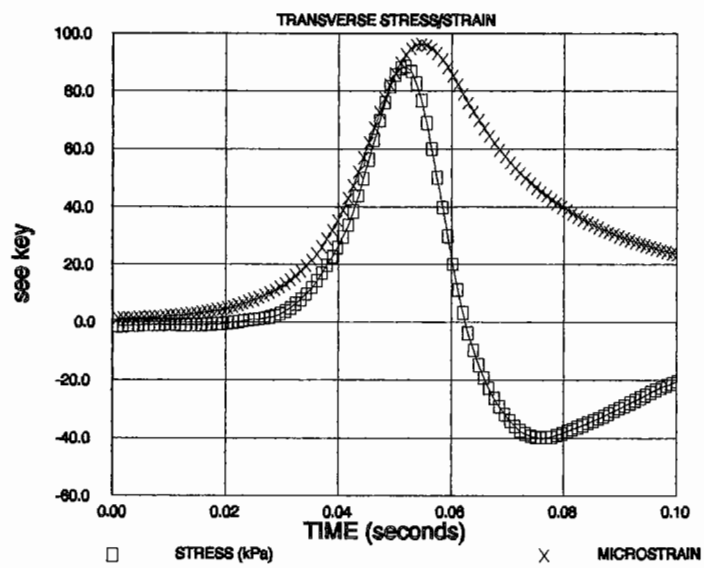
Figure 9.5 : Transverse Stresses and Strains Computed From the FE Model at underside of bound layer

Elastic

Viscous
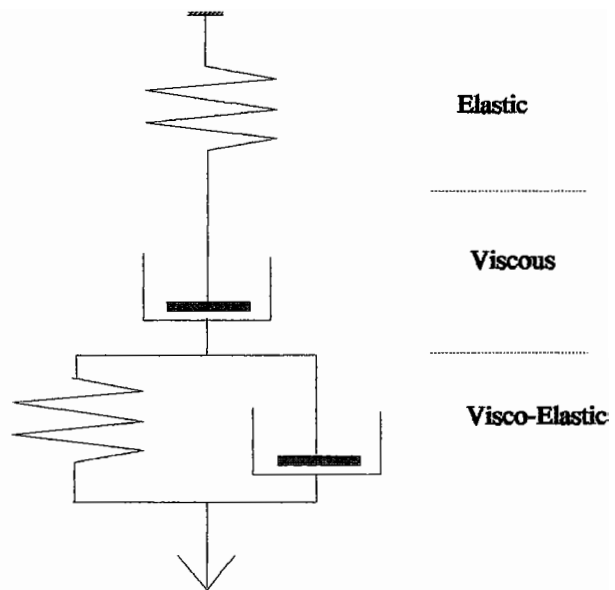
Visco-Elastic

Figure 9.6 : Burgers' Visco-Elastic Model

model parameters used by Huhtala et al. (1992) were estimated from a procedure developed by Gerritsen (1987) which makes use of the binder stiffness and other mixture properties as given in Equations 9.1 to 9.4.

$$\log E1 = 1.185 + (0.479 \times \log S_{bit}) - (0.072 \times VMA) \qquad (9.1)$$

$$\log E2 = 0.203 + (1.021 \times \log S_{bit}) - (0.083 \times VMA) \qquad (9.2)$$

$$\log V1 = 2.174 - (1.634 \times \log Pen) \qquad (9.3)$$

$$\log V2 = (0.796 \times \log E2_{pred}) - 1.083 \qquad (9.4)$$

where: E_1, E_2, V_1 and V_2 are the Burger parameters (E_1, V_1 a Maxwell element and E_2, V_2 a Kelvin element)

However, it should be noted that there is a direct equivalency between the Burgers' model and two Maxwell elements acting in parallel, as follows:

$$E_1 = E_i + E_{ii} \qquad (9.5)$$

$$V_1 = V_i \, V_{ii} \left(\frac{1}{V_i} + \frac{1}{V_{ii}} \right) \qquad (9.6)$$

$$E_2 = \cfrac{E_i E_{ii} \left(\cfrac{1}{V_i} + \cfrac{1}{V_{ii}}\right)(E_i + E_{ii})}{(E_i + E_{ii})\left[\left(\cfrac{E_i}{V_i} + \cfrac{E_{ii}}{V_{ii}}\right) - \cfrac{(E_i + E_{ii})\left(\cfrac{E_i E_{ii}}{V_i V_{ii}}\right)}{E_i E_{ii}\left(\cfrac{1}{V_i} + \cfrac{1}{V_{ii}}\right)}\right] - E_i E_{ii}\left(\cfrac{1}{V_i} + \cfrac{1}{V_{ii}}\right)} \tag{9.7}$$

$$V_2 = \cfrac{(E_i + E_{ii})^2}{(E_i + E_{ii})\left[\left(\cfrac{E_i}{V_i} + \cfrac{E_{ii}}{V_{ii}}\right) - \cfrac{(E_i + E_{ii})\left(\cfrac{E_i E_{ii}}{V_i V_{ii}}\right)}{E_i E_{ii}\left(\cfrac{1}{V_i} + \cfrac{1}{V_{ii}}\right)}\right] - E_i E_{ii}\left(\cfrac{1}{V_i} + \cfrac{1}{V_{ii}}\right)} \tag{9.8}$$

where: E_i, E_{ii}, V_i and V_{ii} are the parameters associated with two Maxwell elements in parallel

If stress and strain are both calculated then they can be plotted against each other to obtain hysteresis loops as shown in Figures 9.7 and 9.8. In addition, the FE code enables direct computation of deviatoric dissipated energy (see section 9.2) and a typical contour plot of deviatoric dissipated energy following the passage of a single wheel load is shown in Figure 9.9. The contour plot shows that peak dissipated energy occurs under the wheel load with high values also in areas near the edge of the load. With this particular pavement geometry (250 mm asphalt thickness on a granular base - see Table 9.1) fatigue cracking will be initiated at the underside of the pavement. The peak value of a dissipated energy at this location is 38.5 Joules/m^3 following the wheel passage.
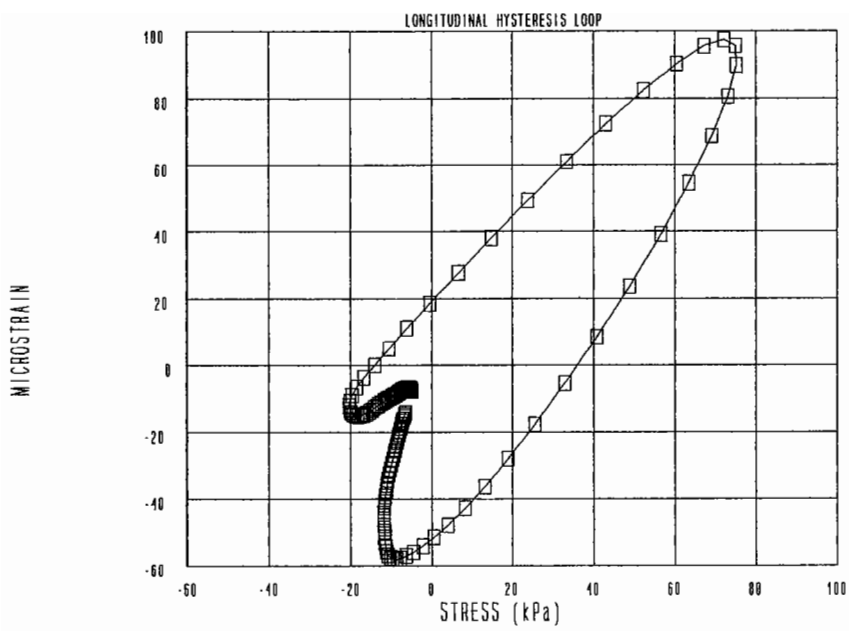
Figure 9.7 : Calculated Longitudinal Hysteresis Loop at underside of bound layer

-9.11-
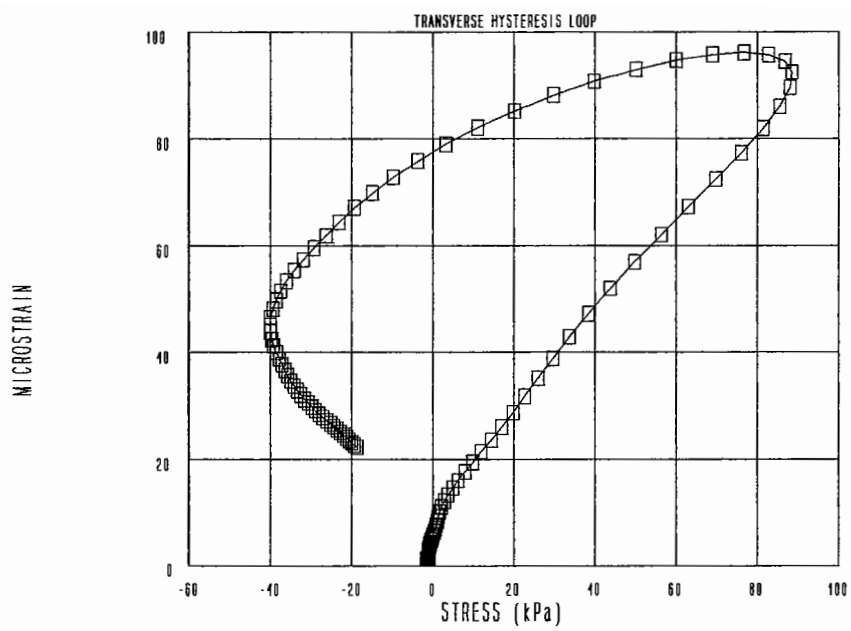
Figure 9.8 : **Calculated Transverse Hysteresis Loops at underside of bound layer**

SINGLE-WHEEL MODEL Refined 7x16 element mesh (PLANE STRAIN)   CONTOURS OF   ENERGY J/mcu
MINIMUM = 0.7   MAXIMUM = 38.5   14-FEB-1994 v 5   SPP.NSE

'92 RE-RUN
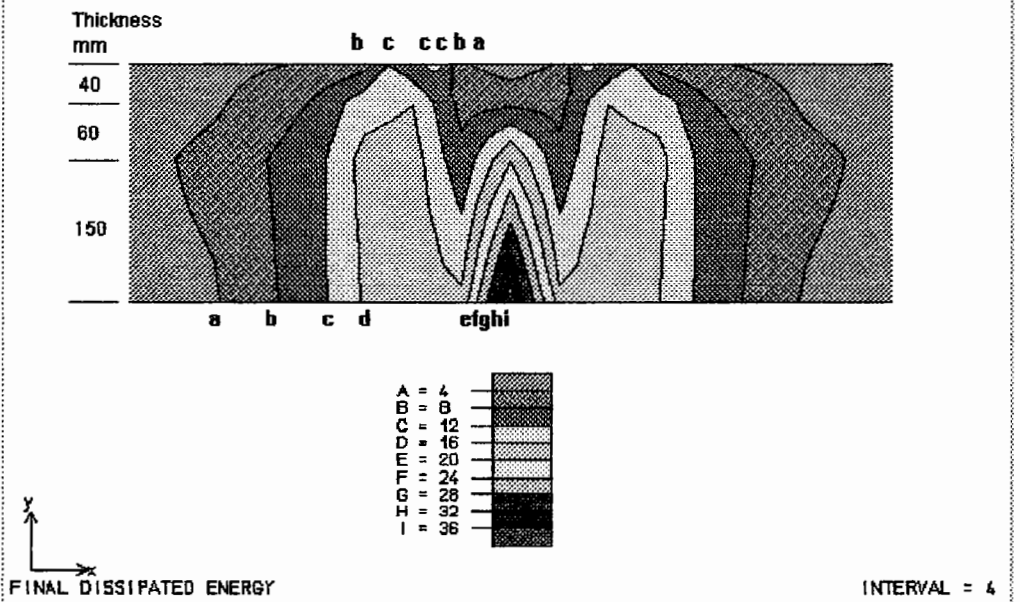
Figure 9.9 : Fatigue Damage Contour

Material Layers and Properties		
Layer	Thickness (mm)	Properties
Hot Rolled Asphalt Wearing Course	40	$E_i = 406.7$ MPa $V_i = 747.9$ MPa.sec $E_{ii} = 1273.3$ MPa $V_{ii} = 32.1$ MPa.sec
Hot Rolled Asphalt Basecourse	60	$E_i = 355.0$ MPa $V_i = 539.7$ MPa.sec $E_{ii} = 1,835.0$ MPa $V_{ii} = 33.0$ MPa.sec
Dense Bitumen Macadam	150	$E_i = 508.4$ MPa $V_i = 741.2$ MPa.sec $E_{ii} = 2,541.6$ MPa $V_{ii} = 33.0$ MPa.sec
Granular Foundation	3,570	$E = 200$ MPa
Loading		
Wheel load = 20 kN Contact Pressure = 600 kPa Load Pulse Duration = 9.27 milliseconds		

Notes: Visco-elastic properties for the asphaltic materials were calculated using the procedures developed by Gerritsen (1987).

Table 9.1 : Details of Typical 250 mm Thick Pavement

9.2   FINITE ELEMENT MODEL

The software developed for fatigue life prediction consists of a "core" FE program which interacts with other programs and subroutines that provide information on material properties, pavement temperatures and traffic conditions, Figure 9.10. The greater part of the existing finite element code, initially drawn upon for program development, is based on work described by Owen and Hinton (1980) and was coded by Sharrock (1990). The principle assumptions made in the FE code are described below.

Visco-elastic materials are treated as a special case of visco-elastic-plastic behaviour, in which the yield stress in the plastic slider element, for the onset of visco-plasticity, is reduced to zero (see Figure 9.11). Elastic material behaviour is also obtained as a special case, by specifying a very large yield stress for the plastic element so that visco-plastic flow cannot occur. Linear isotropic elasticity is assumed for modelling elastic behaviour with Young's modulus and Poisson's ratio being part of the input.

The total strain is assumed to be separable into elastic and visco-plastic components and, in terms of strain rates, as follows:

$$\dot{\epsilon} = \dot{\epsilon}_e + \dot{\epsilon}_{vp} \qquad\qquad (9.9)$$

where: $\dot{\epsilon}$ = total strain rate

             $\dot{\epsilon}_e$ = strain rate associated with elastic behaviour

             $\dot{\epsilon}_{vp}$ = strain rate associated with visco-plastic behaviour

-9.15-
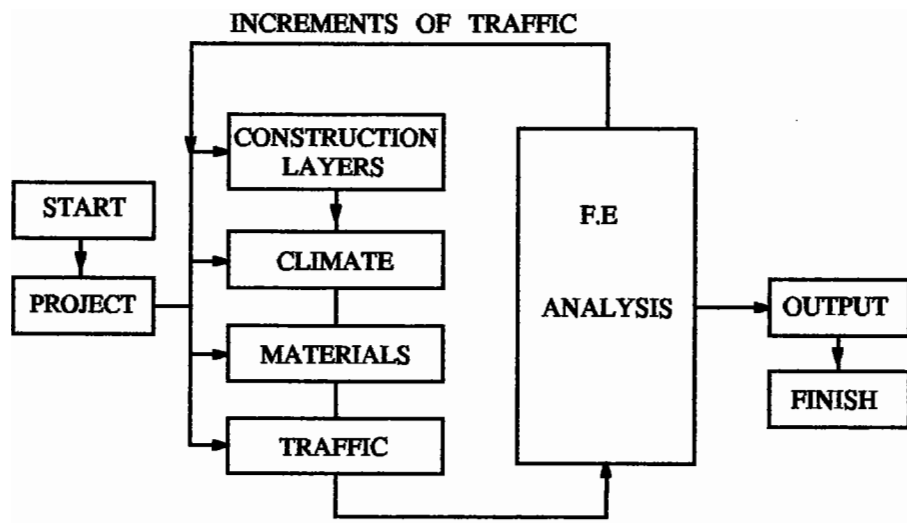
Figure 9.10 : Finite Element Program Elements

Linear elastic spring

Newtonian Viscous Dashpot

Plastic frictional slider yielding at F_o

Inactive if $F \le F_o$
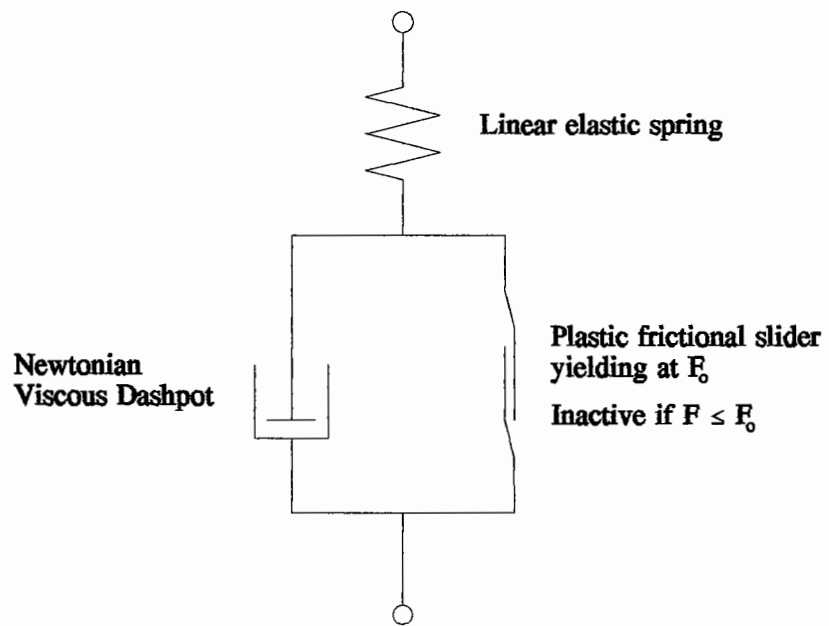
Figure 9.11 : Rheological Representation of Model Employed

The elastic component is assumed to experience the total stress acting and, therefore, the total stress rate depends on the elastic strain rate by way of the elasticity matrix D:

$$\dot{\sigma} = D \, \dot{\epsilon}_e \qquad (9.10)$$

The visco-plastic strain rate is determined from the current state of stress by the relationship:

$$\dot{\epsilon}_{vp} = \gamma \cdot [\mathscr{F}(F)] \cdot \frac{\partial F}{\partial \sigma} \qquad (9.11)$$

In Equation 9.11 $\partial F/\partial \sigma$ represents a plastic potential and γ is a fluidity (reciprocal of viscosity). The yield function F is that of Von Mises and the function $\mathscr{F}(F)$ is given by:

$$\mathscr{F}(F) = \frac{F - \sigma_y}{\sigma_y} \qquad (9.12)$$

For the case of purely viscous flow, with zero yield stress for plasticity:

$$\mathscr{F}(F) = F \qquad (9.13)$$

The resulting viscous strain increment is assumed to be entirely (shear) deviatoric (no volume change) and proportional to the current deviator stresses. The mixture "viscosity" is a shear viscosity in these circumstances. This is

considered to lead to a reasonable approximation of viscous flow with viscous or visco-elastic material behaviour.

Asphaltic materials cannot be characterized by the basic visco-elastic-plastic model used in the FE program as shown in Figure 9.11 but require more complex models to explain their behaviour. A method of obtaining more realistic material response, in the context of FE modelling, is to build up a composite action by using a number of different 'overlays' of simpler materials each with different characteristics. The material to be analyzed is assumed to be composed of several layers each of which undergoes the same deformation (strain compatibility). The total stress field in the material is then obtained by a summation to which each part of the 'overlay' contributes in proportion to the fractional weighting allocated in the total material. In a two dimensional situation, the total thickness is taken to be unity and the weighting for each material simply equals its thickness in the overlay (Zienkiewicz et al, 1972; Owen et al., 1974, and Pande et al., 1977). This concept is illustrated in Figure 9.12. The current version of the software (PACE Version 1.11, 7/3/95) uses a plain strain analysis. In order to produce deflections of the same magnitude as a full 3D analysis, the stiffness of the elastic base layers (sub-base and sub-grade) are increased by a factor of five[1]. This adjustment produces similar values of dissipated energy when using the plain strain

---

[1]This factor was determined by conducting both 2D and 3D Finite Element analysis. The factor of 5 applied to the subbase and sub-grade in the 2D calculations produced the same value of dissipated energy in the asphaltic materials that was obtained in the 3D case.
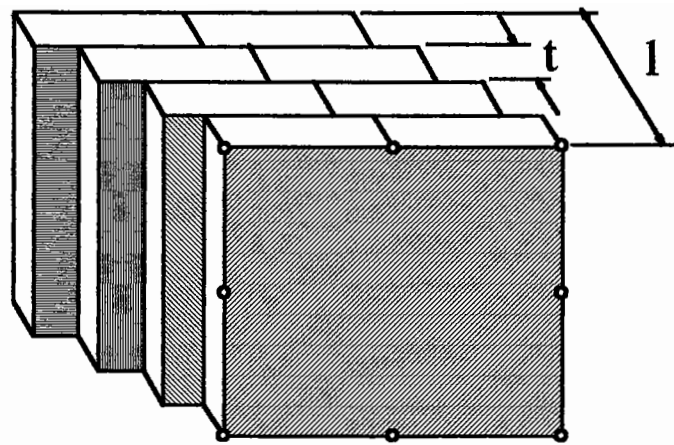
Unit thickness overlay composed of 4 materials, 2-D situation

Figure 9.12 : 'Overlay' Model

analysis compared to a 3D analysis.

9.3   VISCO-ELASTIC MATERIAL PROPERTIES

9.3.1   Relaxation properties

A method of analysis has been implemented to obtain a model which will allow input of parameters associated with a generalized Maxwell model, Figure 9.1. The current version uses properties associated with a four element Maxwell model for the fatigue life calculations. With 4-10 elements, excellent fits are obtained for the prediction of frequency sweep data over a wide range of loading times (Bouldin et al., 1994). The material properties are obtained from a computer program developed by Sharrock (1994) which determines a discrete relaxation spectrum for input consisting of frequency sweep data. The data is reduced to four sets of Maxwell parameters which can describe the complex properties of the material. A comparison between using two Maxwell units and four Maxwell units to describe a frequency sweep data set is illustrated in Figures 9.13 and 9.14. It can be seen that if two units are used then it is only possible to fit the data well at two specified frequencies while if four are used then a good fit is obtained over two decades of frequency.

9.3.2   Shear frequency sweep data

The SHRP A-003A contractor proposed a method of fatigue prediction based upon shear frequency sweep data and elastic analysis. Since shear apparatus
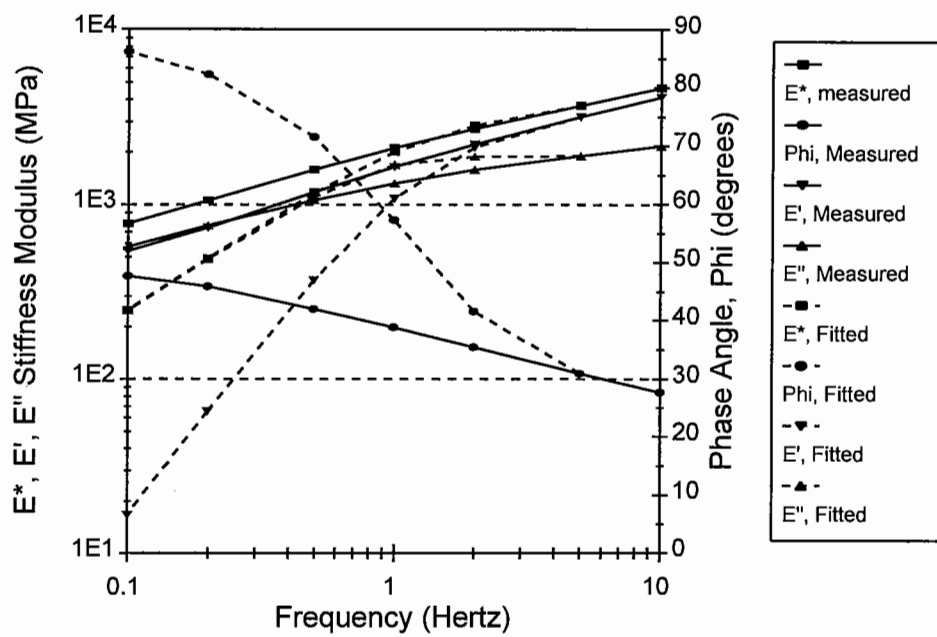
**Figure 9.13 : Complex Properties Measured and Fitted with Two
Maxwell Elements in Parallel**
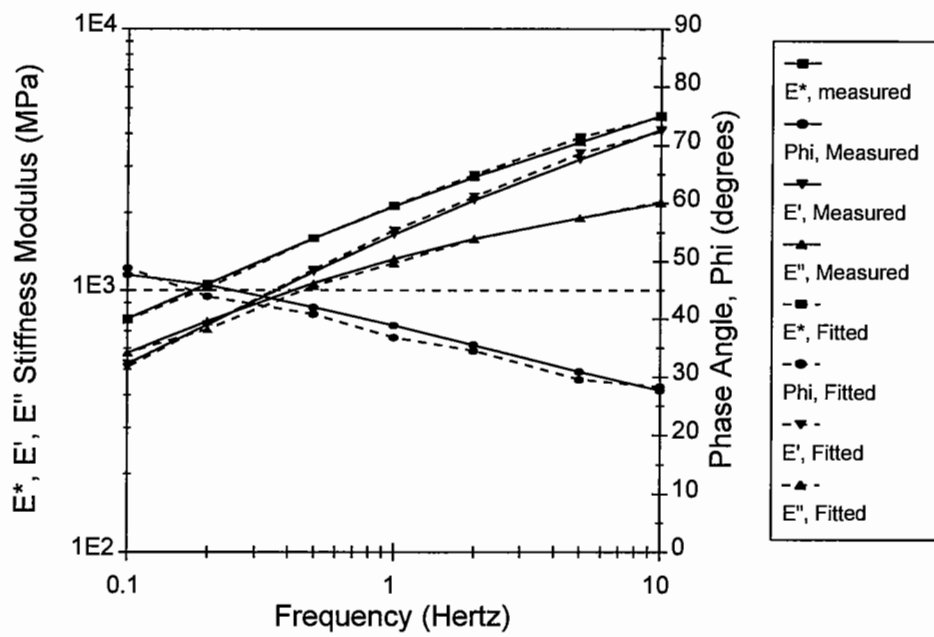
Figure 9.14 : Complex Properties Measured and Fitted with Four Maxwell Elements in Parallel

will be generally available it is considered desirable to investigate the use of this data in a prediction procedure. Relationships were proposed for conversion of the shear data to flexural data as follows:

$$S_o = 8.560 \, (G_o)^{0.913} \qquad (r^2 = 0.712) \quad (9.14)$$

$$S_o'' = 81.125 \, (G_o'')^{0.725} \qquad (r^2 = 0.512) \quad (9.15)$$

$$\sin \delta_{S_o} = 1.040 \, \left(\sin \delta_{G_o} \right)^{0.725} \qquad (r^2 = 0.810) \quad (9.16)$$

where S_o = Stiffness modulus, bending beam test.

S_o'' = Loss Stiffness modulus, bending beam test.

G_o = Stiffness modulus, shear test.

G_o'' = Loss Stiffness modulus, shear test.

δ = Phase lag (subscript indicates type of test).

The shear data were measured using the SHRP Test Method M-003 (Harrigan et al., 1994). This test method requires that the specimen height remains constant. This results in the application of an axial load in addition to the applied shear load. The test is conducted at a constant shear strain amplitude of 100 με.

In the comparison of shear and flexural data, it can be assumed that the relationship for the phase angle should pass through the ordinates (0,0) and (90,90) representing purely elastic and viscous behaviour respectively. However, the relationship proposed above (Tayebali et al., 1994) is a power

law which will result, for higher phase angles, in a mathematical error (sin δ > 1) if it is used for conversions. Since, a generalized relationship was needed for the visco-elastic model, a study was performed to fit a physical relationship which can be used over the entire range of possible phase angles thus permitting extrapolation from the original data set. It was considered that the best description of the data (forcing the relationship through the two ordinates discussed above) could be obtained using a sine function. An iterative analysis was performed (minimising the root mean square error) giving the result in Equation 9.17. This result which has a rms error value of 1.78 degrees compared to 1.88 degrees for the SHRP equation and 1.85 degrees for a linear best fit, is illustrated in Figure 9.15 along with the other relationships.

$$\delta_{S_o} = \delta_{G_o} + 9.65 \left(\sin 2\delta_{G_o} \right) \qquad (9.17)$$

The flexural and shear stiffnesses are related by a factor of three as illustrated in Figure 9.16. Shear frequency sweep data were published for each of the six A-003A Slab Test Facility experiments (see Table 9.2). These results have been analyzed to determine the Maxwell parameters and are presented in Table 9.3. In addition, to the estimation of parameters at 20°C from that data, it is also possible to construct master curves, shift these to any desired temperature and then predict a discrete relaxation spectrum (for four Maxwell elements) at that temperature. Figure 9.17 illustrates the master curve obtained for mixture AAG-RD. This has been shifted to temperatures between 4°C and 40°C and the discrete relaxation spectrum calculated at each temperature. The results for
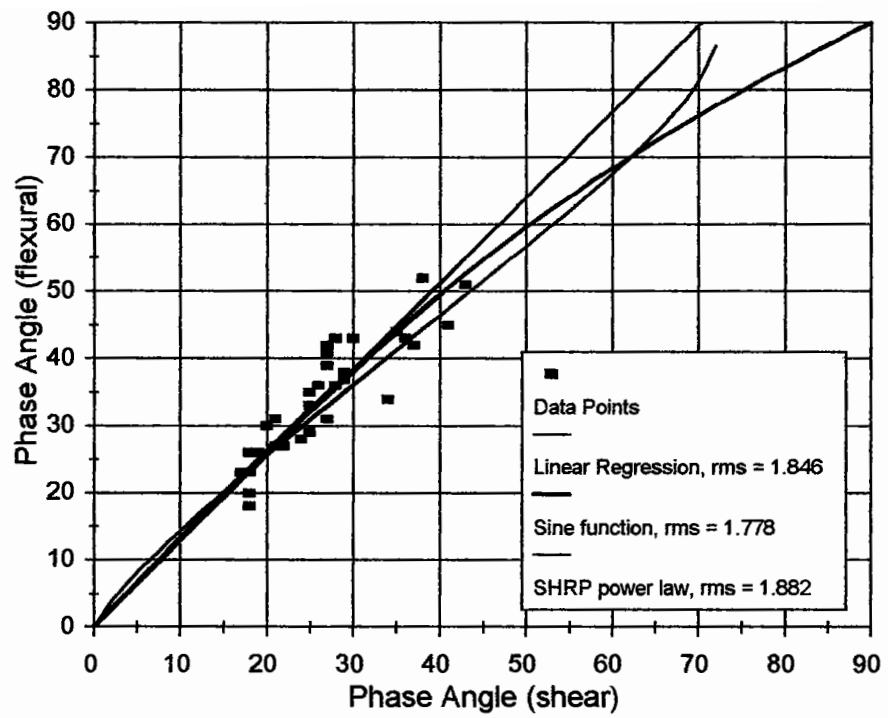
Figure 9.15 : Phase Angle Measurements, Flexural versus Shear
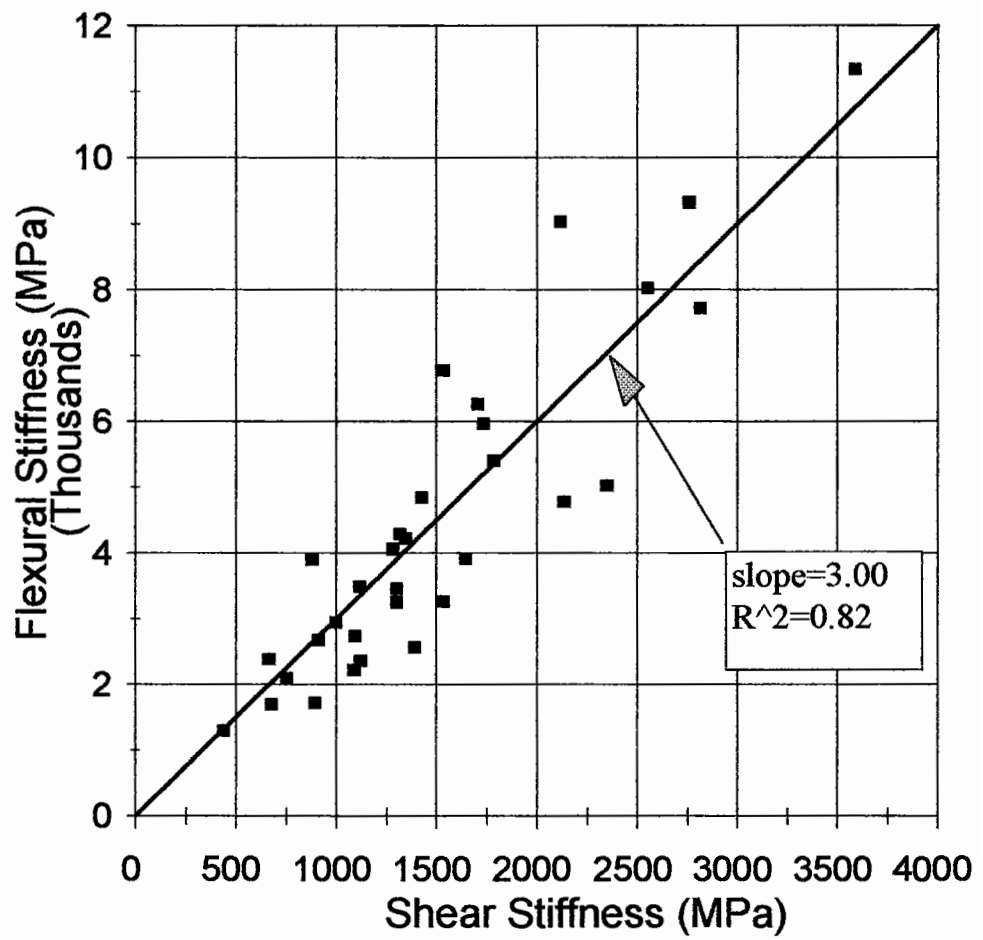
Figure 9.16 : Relationship Between Shear and Flexural Stiffness

Mixture Ref.	Freq.	Test temp 4°C		Test temp 20°C		Test temp 40°C	
		G* (MPa)	δ	G* (MPa)	δ	G* (MPa)	δ
AAA-RD	10	4118.5	22.0	1532.9	36.5	162.3	56.2
	5	3565.4	21.8	1152.3	40.1	120.5	52.8
	2	2913.7	24.9	782.3	44.5	83.0	47.2
	1	2418.1	27.5	570.5	47.5	65.3	42.4
	0.5	1973.1	30.9	409.7	50.0	53.6	39.1
	0.2	1457.3	35.0	257.6	52.3	43.4	34.3
	0.1	1124.0	38.4	182.6	52.7	38.2	31.2
AAC-RD	10	4256.9	14.0	1636.6	29.9	221.0	60.4
	5	3830.4	13.4	1329.1	31.7	158.3	61.0
	2	3349.6	14.4	1011.9	34.3	98.2	57.9
	1	3052.1	15.6	802.6	37.4	69.4	54.0
	0.5	2745.4	17.2	620.3	40.5	52.4	49.2
	0.2	2359.8	19.5	422.9	44.8	37.6	43.4
	0.1	2073.0	21.5	308.9	48.0	31.6	38.6
AAF-RD	10	4939.4	14.0	2787.2	19.7	563.1	48.6
	5	4605.4	12.0	2423.1	20.3	396.6	52.3
	2	4237.0	11.6	2026.5	22.3	254.7	56.1
	1	3972.4	12.1	1736.9	24.9	174.7	57.8
	0.5	3701.1	12.9	1457.2	28.2	121.0	58.1
	0.2	3317.1	14.7	1120.8	32.9	76.0	55.0
	0.1	3044.7	15.9	891.2	36.6	58.2	51.1
AAG-RD	10	3718.1	11.6	2360.7	27.6	330.8	65.5
	5	3755.2	7.1	2079.9	26.7	210.6	67.9
	2	3563.5	8.4	1663.8	31.2	113.8	65.6
	1	3364.1	9.6	1351.0	36.9	73.4	60.7
	0.5	3194.3	10.5	1036.0	43.5	51.2	54.4
	0.2	2899.9	12.3	673.5	53.2	37.6	45.2
	0.1	2722.2	13.8	448.0	60.0	31.6	41.4
AAK-RD	10	3226.7	14.2	1346.9	27.8	256.3	52.2
	5	2858.8	14.7	1064.3	31.3	183.9	52.8
	2	2497.5	17.6	776.1	36.4	117.5	51.7
	1	2231.2	19.4	597.2	40.0	86.1	49.9
	0.5	1947.6	21.4	446.7	43.0	63.7	46.9
	0.2	1613.0	24.8	297.3	46.3	44.5	42.7
	0.1	1363.9	26.9	217.5	48.0	37.3	38.7
AAM-RD	10	5748.5	12.3	2491.3	24.5	363.2	52.8
	5	5080.0	11.3	2010.9	25.6	253.2	54.4
	2	4567.2	12.3	1562.8	29.7	161.7	54.4
	1	4211.3	13.2	1256.4	33.1	115.1	53.8
	0.5	3825.7	14.6	993.2	36.0	84.4	52.1
	0.2	3384.9	16.4	705.3	40.0	59.2	48.6
	0.1	3035.1	17.9	534.8	43.2	46.4	44.8

Table 9.2 : Shear Frequency Sweep Test Results, RD Aggregate

	Maxwell Unit	Mixture					
		AAA-RD	AAC-RD	AAF-RD	AAG-RD	AAK-RD	AAM-RD
1	Elastic Modulus, MPa	1840.0	3560.0	11008.0	5789.0	2423.0	6476.0
	Viscosity, MPa.sec	2789.0	5469.0	20562.0	5980.0	3800.0	10637.0
	Time, sec	1.516	1.536	1.868	1.033	1.568	1.643
2	Elastic Modulus, MPa	3714.0	6945.0	9826.0	535.9	3686.0	7660.0
	Viscosity, MPa.sec	597.3	1113.0	2298.0	264.1	681.6	1526.0
	Time, sec	0.16079	0.16021	0.23391	0.49280	0.18490	0.19921
3	Elastic Modulus, MPa	7030.0	5541.0	11371.0	16744.0	7586.0	11763.0
	Viscosity, MPa.sec	301.9	215.5	645.9	1968.0	349.0	625.5
	Time, sec	0.04295	0.03889	0.05680	0.11753	0.04600	0.05318
4	Elastic Modulus, MPa	204771.0	80547.0	158267.0	107564.0	112800.0	148852.0
	Viscosity, MPa.sec	188.4	174.7	182.0	260.4	117.3	200.0
	Time, sec	0.00092	0.00217	0.00115	0.00242	0.00104	0.00134

Table 9.3 : Maxwell Parameters Fitted to Shear Frequency Sweep Data
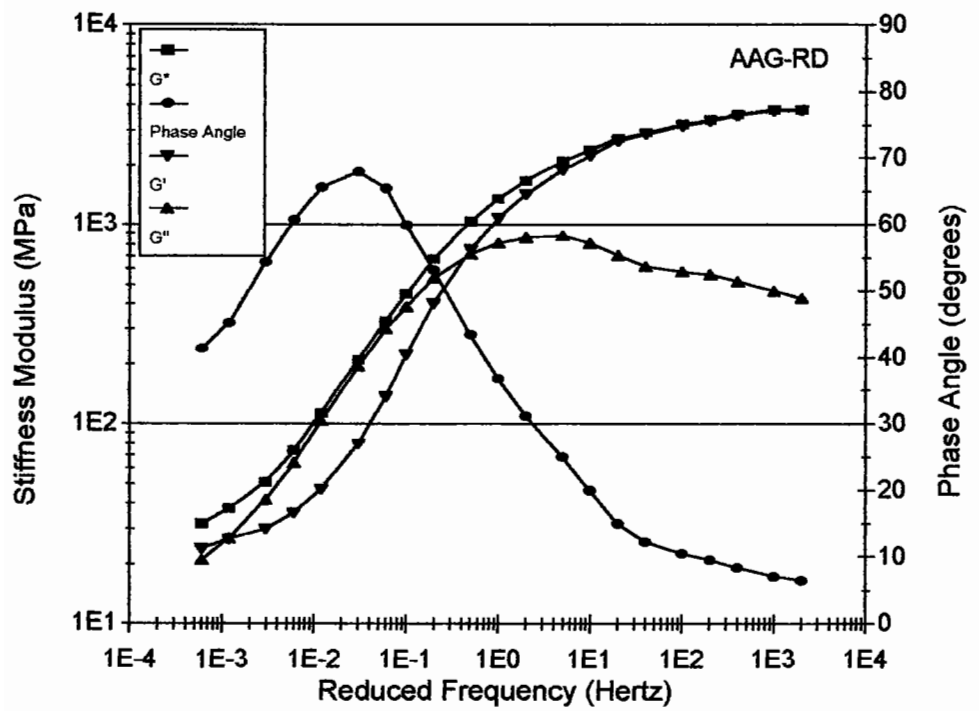
**Figure 9.17 : Master Curve Reduced to 20°C for Mixture AAG-RD
Measured in Simple Shear**

this analysis are illustrated in Figures 9.18 and 9.19.

9.4   ANALYSIS OF THE STF EXPERIMENT

9.4.1   *Visco-elastic analysis*

The STF experiment was analyzed by the PACE™ visco-elastic FE analysis
software at the load levels used in the experiment. For each slab, a dissipated
energy contour map was generated. The significant variables used for this
analysis were as follows:

Asphaltic Material:	Properties based upon Shear Frequency Sweep results as discussed earlier.
Base Support:	10 MPa stiffness rubber mat 92 mm thickness resting on a steel base with assigned stiffness of 500,000 MPa (ie. very stiff) 4.0 m thickness.
Temperature:	Constant with depth, 20°C.
Wheel speed:	2.3 km/hr.
Wheel load:	As given in Table 7.1.
Tyre pressure:	380 kPa.

An example of the dissipated energy contour plot (mixture AAF-RD) produced
by the software is presented in Figure 9.20. By inspection it can be seen that
the maximum value of dissipated energy occurs at the underside of the
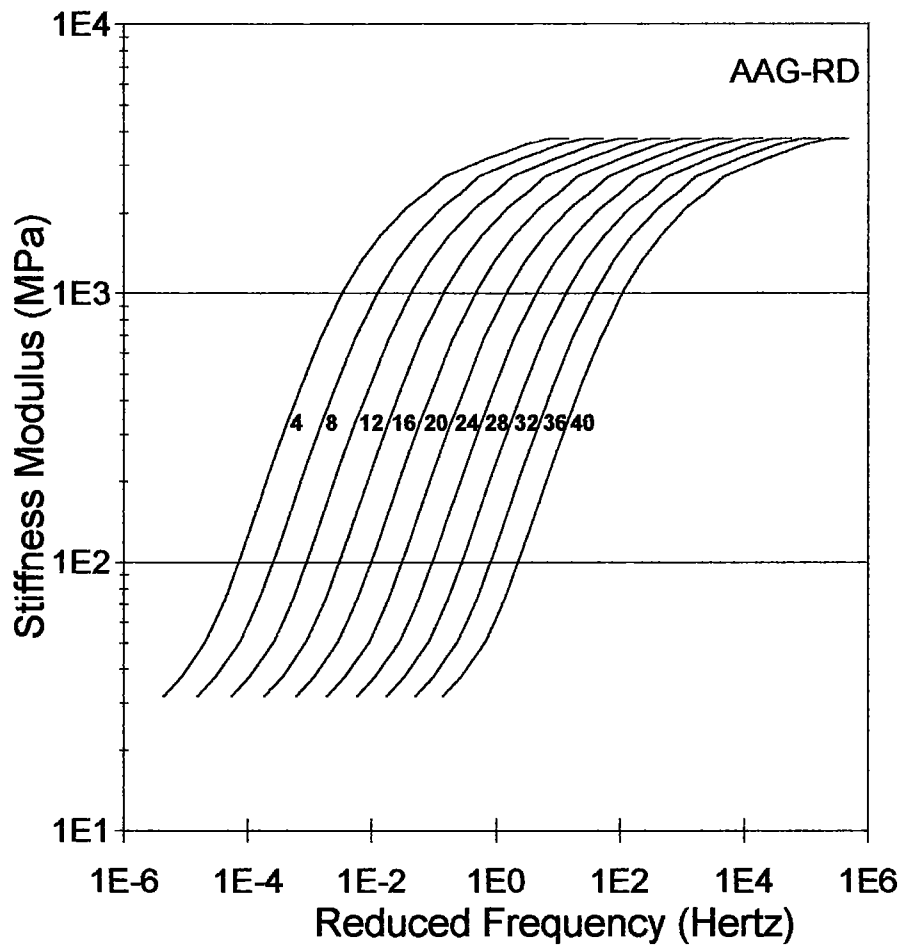
Figure 9.18 : **Complex Stiffness Modulus for Mix AGG-RD Shifted to 10 Temperatures Between 4°C and 40°C in 4°C Increments**
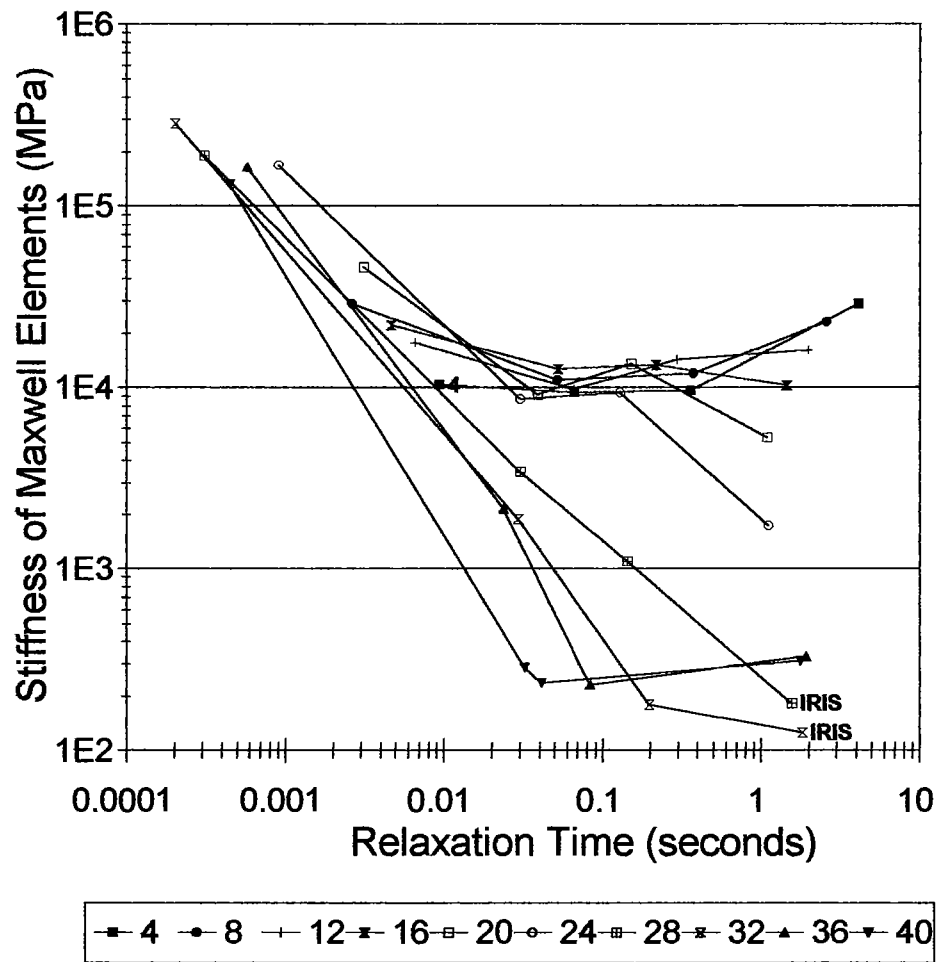
Figure 9.19 : Discrete Relaxation Spectrum for Various Temperatures for Mix AAG-RD

CROSS SECTION THROUGH ASPHALTIC MATERIAL

Wheel loading
380kPa

Key %
100
90
80
70
60
50
40
30
20
10
0

material
AAF-RD

Project Data c:\pace\prj\stfaafrd.vpp
CONTORS OF FATIGUE DAMAGE (%), IN PAVEMENT LAYERS

Estimated Life to Crack Initiation = 36000, Material Test Temperature = 20 (C)
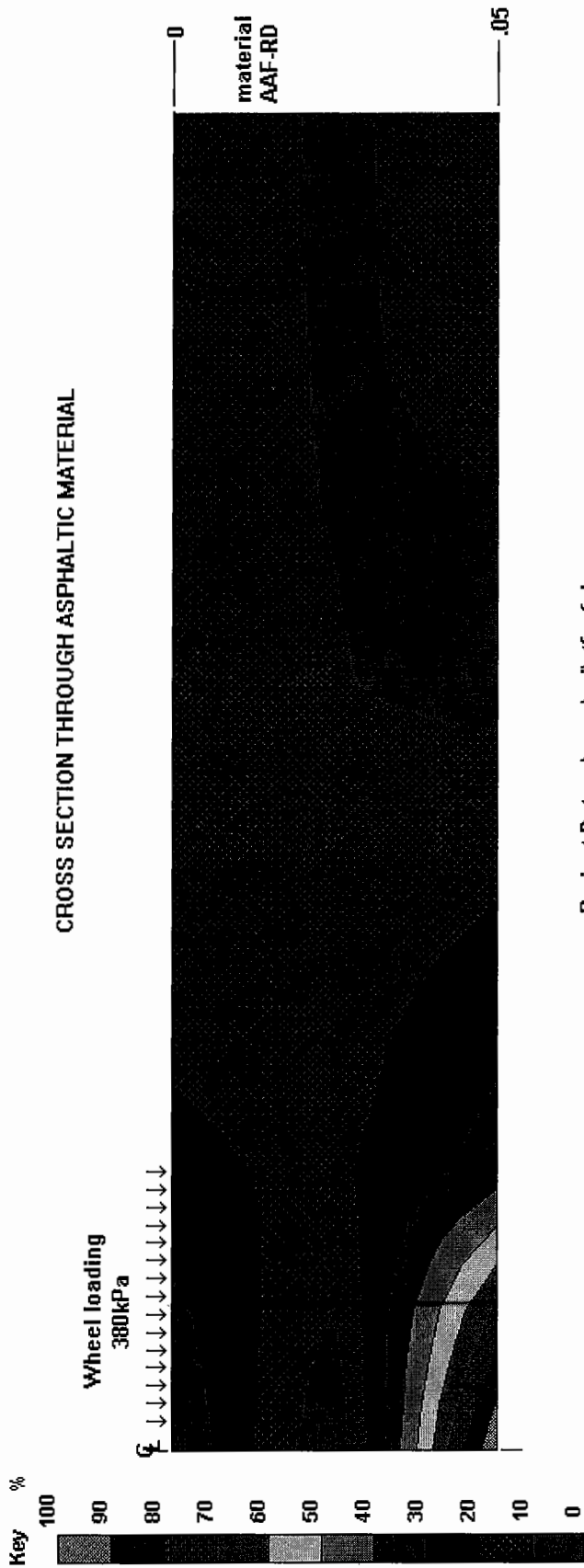
Figure 9.20 : Dissipated Energy Contour Map for STF Slab
with Mixture AAF-RD

asphaltic layer and this was true for all mixtures analyzed in the STF experiment. This value of dissipated energy was then used with Equation 6.31 to estimate the fatigue life to crack initiation, *N1*. The maximum value of dissipated energy and estimated life to the *N1* condition for each mixture is given in Table 9.4.

The FE analysis, generally, ranked the materials in the same order as the results obtained from the STF experiment with the exception of mixture AAK-RD (see Figure 9.21). The difference between the calculated lives versus that measured in the STF (both at the *N1* stage) are considered to be a result of rest periods which occur in the STF. The fatigue relationship used in the calculations (see Equation 6.30) was based on fatigue testing which contained no rest periods. Figure 9.22, which presents the data graphically, includes a line which represents a shift factor of ×25 as suggested by Raithby (1972) to account for rest periods. This line lies in the centre of the data collected. A regression line (excluding AAK-RD) is also shown and this indicates that the difference, in the measured and predicted results, is greater for slabs with longer lives. An alternate interpretation is that different shift factors apply for short and long fatigue lives. Shift factors based upon this data are illustrated in Figure 9.23. The mean shift factor for the long fatigue life results (AAA, AAF, AAK and AAM-RD) was 64 whereas that obtained for the shorter lives (AAC and AAF-RD) was 6. An alternative approach would be to consider that the shift factor is a function of the number of load cycles. Due to the lack of further data it is not possible to determine a more meaningful understanding. Consequently, it is proposed that in the design solution a shift factor of ×25

Mixture	Dissipated Energy (J/m^3)	*N1*
AAA-RD	263.68	50 066
AAC-RD	441.52	14 250
AAF-RD	294.11	35 990
AAG-RD	626.85	7 866
AAK-RD	588.46	8 001
AAM-RD	370.65	21 402

Table 9.4 : Dissipated Energy and Life to *N1* as Calculated using the PACE™ Software

RANK

STF   PACE

AAF   AAA

AAK   AAF

AAA   AAM

AAM   AAC

AAC   AAK

AAG   AAG
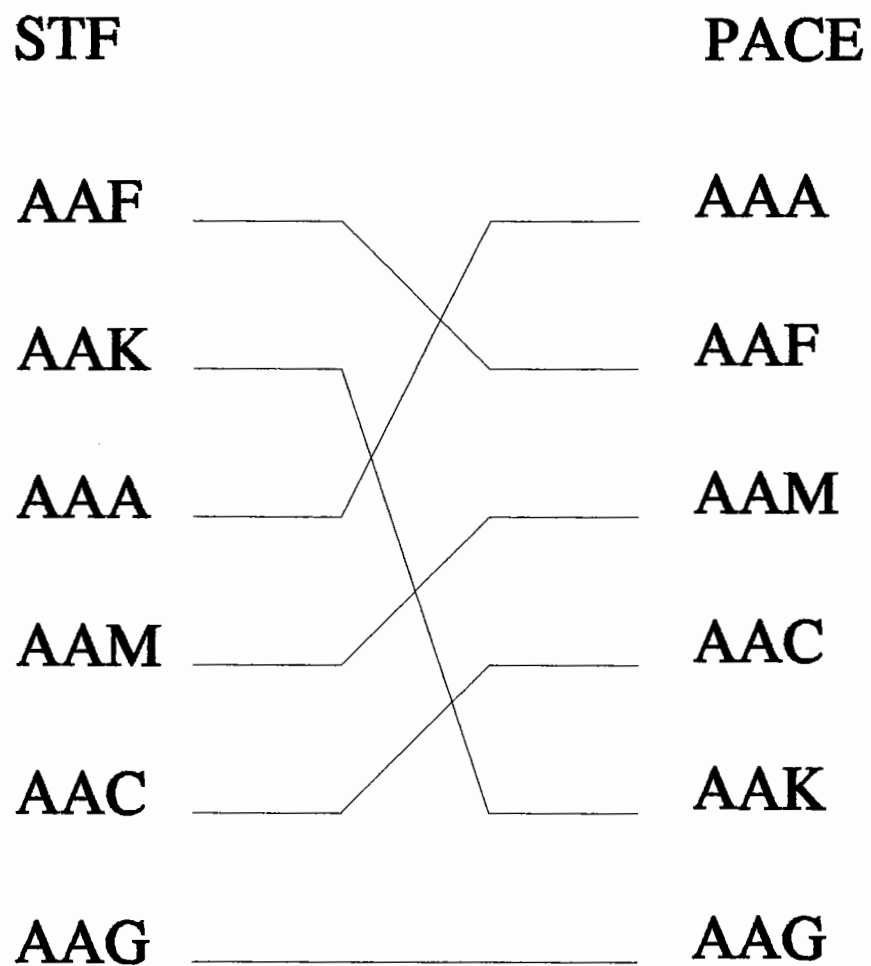
Figure 9.21 : Rankings in the STF Experiment and by using Visco-Elastic Analysis (PACE™) Software

-9.37-

Slab Test Facility Experiment

r2 = 0.814 (excluding AAK-RD data)

x 25

AAA-RD
AAF-RD
AAM-RD
AAC-RD
AAG-RD
AAK-RD

Predicted Fatigue Life

Measured Fatigue Life
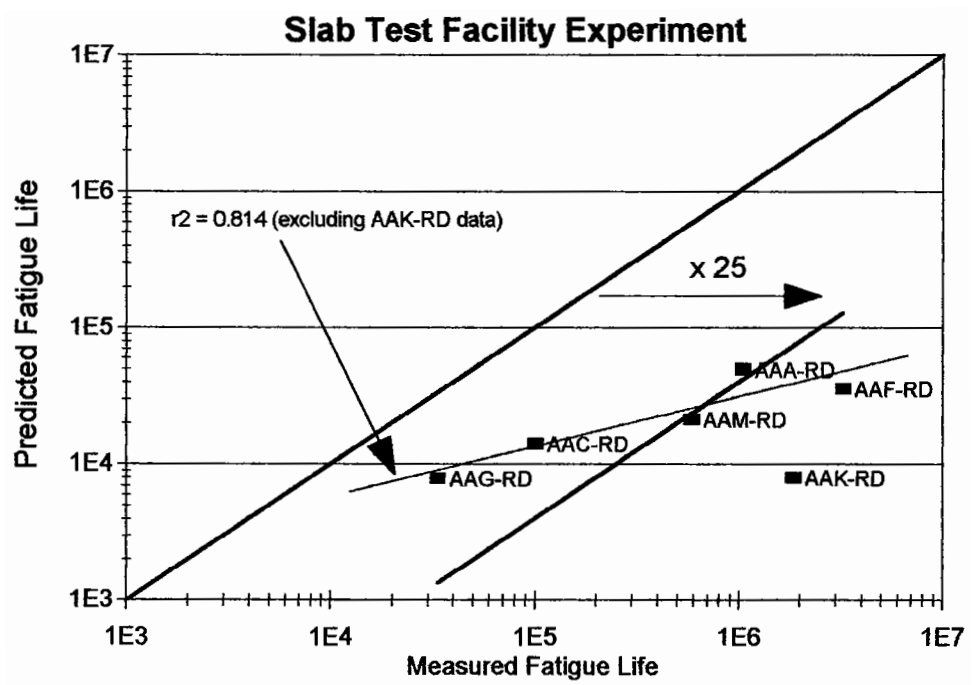
Figure 9.22 : Calculated versus Observed Results for the STF Experiment

-9.38-
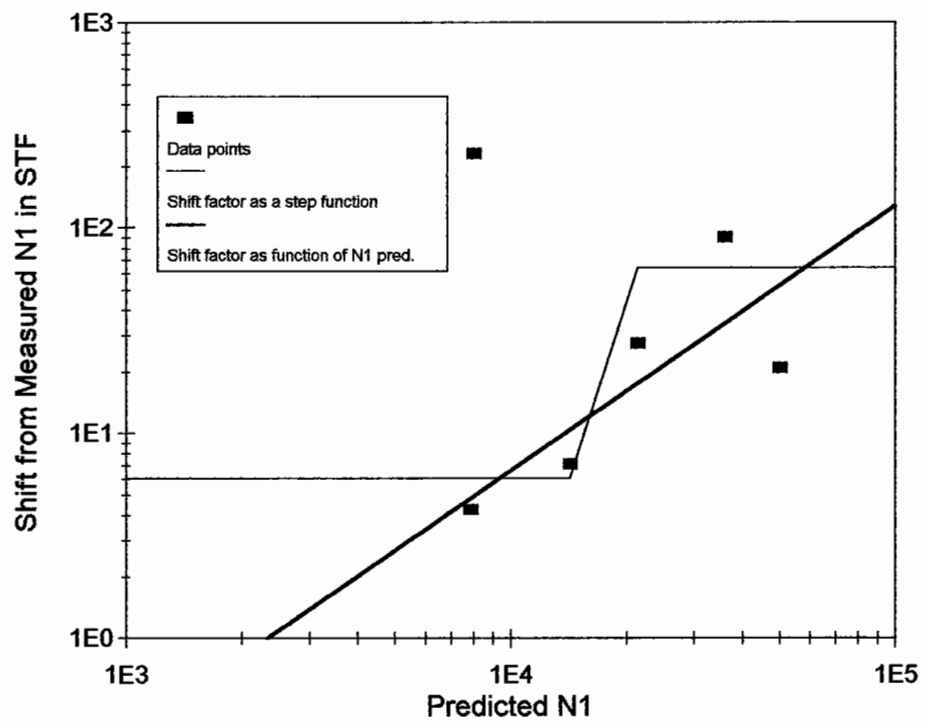
**Figure 9.23 : Shift factor as a Step Function
or as a Function of Predicted *N1***

should be adopted. This would be, generally, a conservative approach and considered wise for design.

9.4.2 Comparison with elastic analysis

Using the load data presented in Table 7.1 and mixture stiffness appropriate for the loading speed of the STF the fatigue life was calculated using strain life relationships and layered elastic analysis. The strain life relationships were obtained from analysis of controlled stain fatigue test data obtained by the University of California (Tayebali, 1992). The stiffness values used along with the constants for the fatigue equation are given in Table 9.5 along with the constants used in Equation 9.18.

$$N_{fat} = k1 \, (\epsilon_t)^{k2} \qquad (9.18)$$

The results from this analysis are presented in Figure 9.24 which also contains the results from the earlier analysis. It can be observed that whereas the visco-elastic procedure under-predicted the fatigue life by a factor of twenty five the elastic analysis over-predicts by a similar amount. Clearly, some of the differences could be attributed to the use of controlled strain fatigue data for the STF condition which is closer to the controlled stress mode of loading[2]. Both visco-elastic and elastic analysis appear to rank the data in a similar

---

[2] Tests conducted in the controlled strain mode of loading last longer than those conducted using controlled stress (see Chapter 3). Consequently, when controlled strain results are used for a pavement which is more representative of the controlled stress condition an over-prediction of fatigue life can occur.

Mixture Reference	Stiffness, E* (MPa)	k1	k2
AAA-RD	2978.1	3.61e-06	-3.1595
AAC-RD	3700.9	2.18e-07	-3.38268
AAF-RD	7363.2	1.58e-07	-3.3854
AAG-RD	5967.2	3.06e-09	-3.77549
AAK-RD	2977.8	3.33e-10	-4.30375
AAM-RD	5868.6	3.36e-09	-4.04387

Table 9.5 : Mixture Properties used for Elastic Analysis

Slab Test Facility Experiment

Predicted Fatigue Life

1E8

Life predicted based on
flexural beam and tensile
strain calculations

●AAM-RD

●AAA-RD

1E7

●AAF-RD

●AAK-RD

●AAC-RD

1E6

●AAG-RD

x 20   ←

x 25   →

1E5

■AAA-RD

■AAF-RD

■AAM-RD

■AAC-RD

1E4

■AAG-RD

■AAK-RD

Life predicted based on dissipated
energy calculations

1E3

1E3   1E4   1E5   1E6   1E7   1E8

Measured Fatigue Life
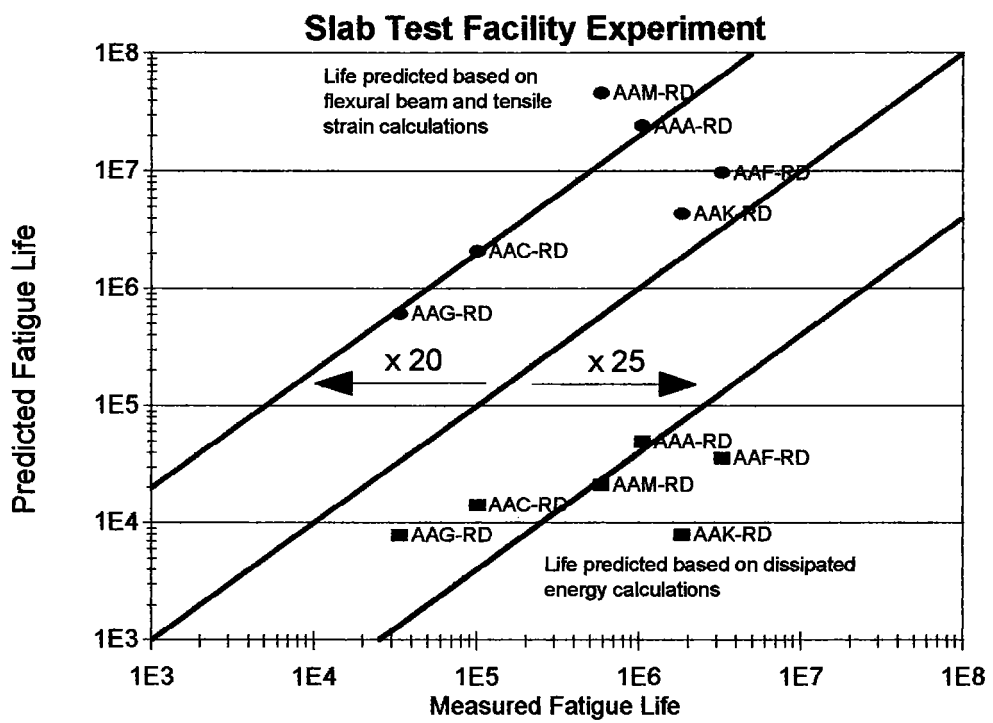
**Figure 9.24 :   Fatigue Life Predicted using UCB Controlled Strain
Fatigue Data in Comparison to PACE™**

manner but this result indicates that considerable care needs to be given to the choice of controlled stress versus controlled strain fatigue data. The energy method can, potentially, overcome this problem and use of the test type would not effect the position of the estimated life to crack initiation.

9.5   PAVEMENT THICKNESS AND TEMPERATURE

To investigate the effect of stiffness and temperature with the dissipated energy method a series of calculations where performed for; 1) the STF experiment, 2) a typical thick pavement structure, and 3) a typical thin pavement structure. All the calculations used mixture AAG-RD at different temperatures. The visco-elastic material properties are those that were presented earlier in Figure 9.19. In addition, computations were made using the University of Nottingham design method (Brown et al., 1985) but with the mixture stiffness values calculated using the Bonnaure nomograph (Bonnaure et al., 1977). The life calculations use the fatigue relationship developed by Cooper (1976) (no shift factors, ie. all lives are compared at the *N1* condition as defined earlier). The parameters used for the calculations are presented in Table 9.6.

9.5.1   Anticipated effect of temperature on the STF experiment results

The results obtained for the simulation of the STF at varying temperatures are presented in Figure 9.25. It can be clearly observed that, in this experiment, as the stiffness of the asphaltic material drops, the amount of dissipated energy increases and the calculated fatigue life decreases.

-9.43-

Mixture Properties (AAG-RD)	
Binder Properties (RTFOT used)	See Table 4.1
Volumetrics	
Voids, %	9.9
Volume of Binder, %	11.7
Voids in Mineral Aggregate, %	21.5
Stiffness at Temperature ($^{\circ}$C), MPa	
4	16799
8	14004
12	10407
16	7352
20	4935
24	3009
28	1825
32	1050
36-40	outside range of nomograph
Structure Features	
Asphalt Layer Thickness, mm	
Thin Pavement	50
Thick Pavement	300
Foundation Stiffness, MPa	50 and 300
Loading	
Axle	Dual
Speed of Loading, km/hr	50
Radius of Loaded Area, mm	113
Spacing of wheel centres, mm	376

Table 9.6 : Parameters used in Elastic and Visco-Elastic Comparison Study
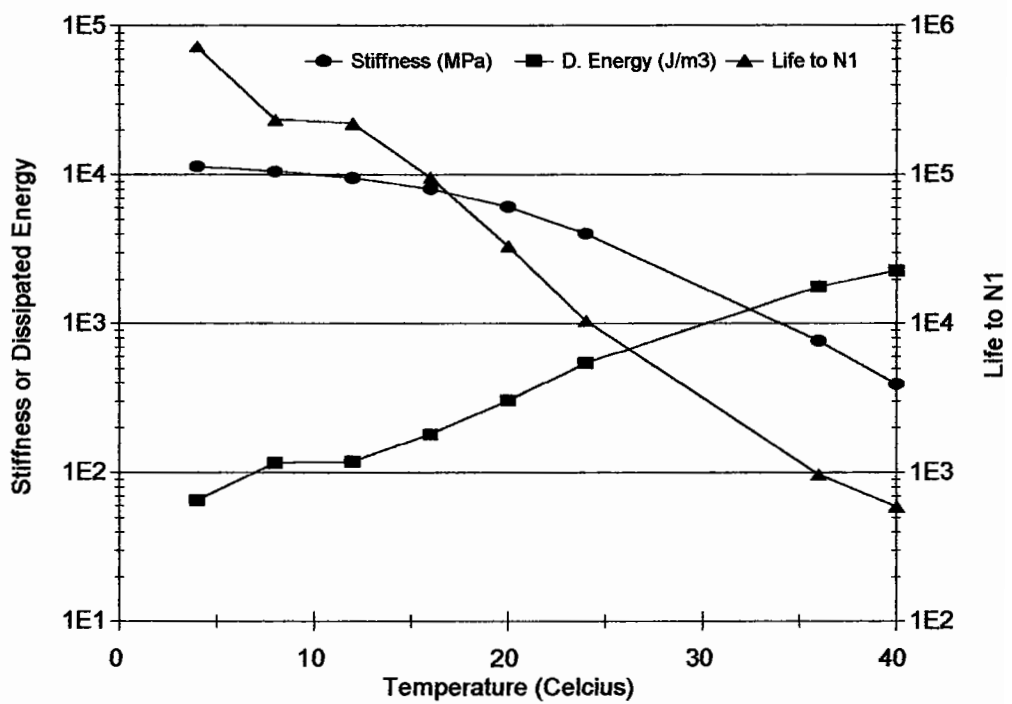
Figure 9.25 : Results from Visco-Elastic Analysis of the STF Configuration using various Temperatures for the Material Properties, Mix AAG-RD

9.5.2 Effect of temperature on typical thick and thin pavements

The results from the visco-elastic analysis (using the PACE™ software) and elastic analysis of the "thick" and "thin" pavements with "weak" and "strong" foundations" are presented in Figure 9.26. It can be observed that in all cases the fatigue life to crack initiation generally decreases[1] with increasing temperature. The result suggests that a stiffer material performs better in the prevention of crack initiation for both thin and thick pavement structures. Figure 9.27 illustrates a comparison between the life calculated by the two analysis methods including the STF experiment using both PACE™ and UCB data. It can be observed that the lives calculated for the thick pavement are relatively close (within ½ decade for lives 10000 to 10000000). However, the life calculated for the thin pavement structures by elastic analysis is considerably lower than the life calculated by visco-elastic analysis.

9.5.3 Thick and thin pavements versus the STF results

The results presented in Figure 9.27 show that the fatigue lives calculated for the thick pavement section have a similar trend line to that obtained for the STF analysis. This demonstrates that the visco-elastic analysis and elastic analysis using the Nottingham fatigue relationship (Cooper, 1976) give results which are similar (differing by about a ½ decade) for relatively thick

_____

[1]An increase in fatigue life is observed in the temperature range 10-15°C. This is considered to be due to variability in the accuracy of calculating the relaxation parameters from the frequency sweep data.
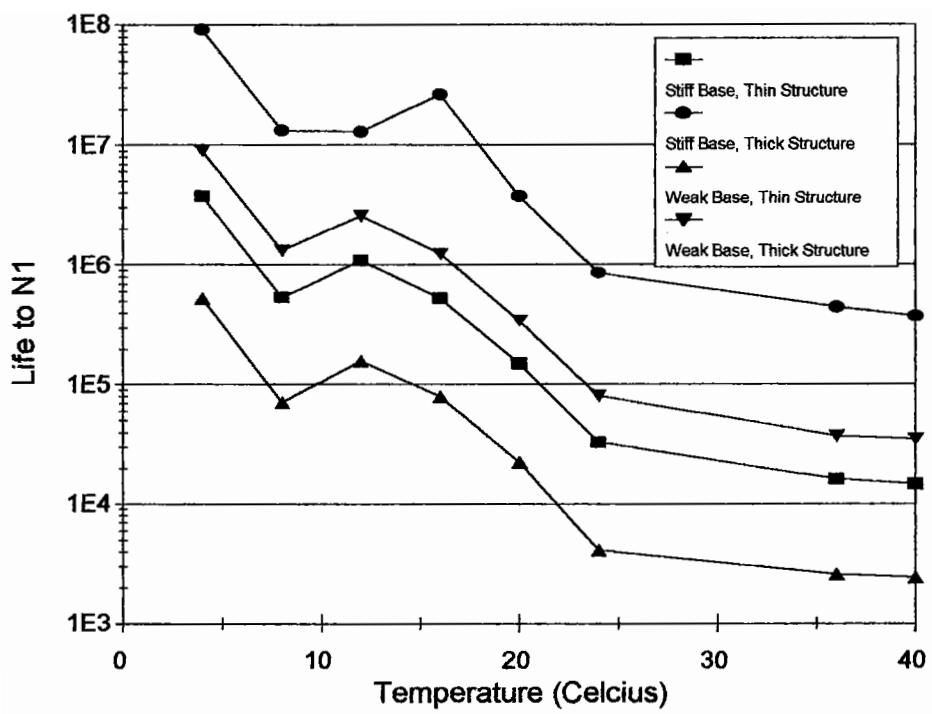
Figure 9.26 : Predicted Life using Visco-Elastic Analysis Software for Thick and Thin Pavement Stuctures on Weak and Strong Bases, Mix AAG-RD
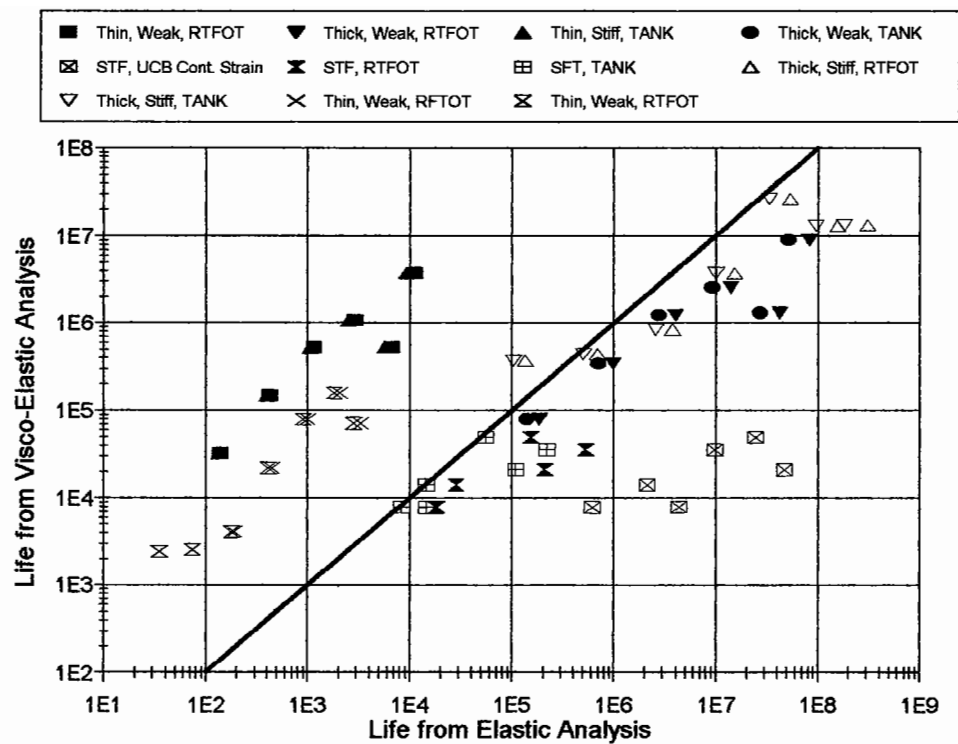
Notes: Thick = pavement structure 300 mm thick (see Table 9.6).
Thin = pavement structure 50 mm thick (see Table 9.6).
STF = 50 mm pavement tested in the Slab Test Facility
Weak = foundation stiffness of 50 MPa (see Table 9.6).
Stiff = foundation stiffness of 50 MPa (see Table 9.6).
UCB Cont. Strain = Calculations based on data collected at University of California in a controlled strain experiment.
TANK = Visco-elastic calculations performed using data from tests on materials with no ageing.
RTFOT = Visco-elastic calculations performed using data from tests on materials after Rolling Thin Film Oven ageing.

Figure 9.27 : Comparison of Various Structures, Elastic versus Visco-Elastic Analysis, Mix AAG-RD

pavement structures. For thinner pavement structures the tensile strain relationship results in low calculated lives compared to the visco-elastic analysis.

9.6   OTHER COMPARISONS TO ELASTIC ANALYSIS

The document, "An Introduction to the Analytical Design of Pavements - 3rd Edition," (Brown et al., 1985), which presents the University of Nottingham's simplified approach to pavement design, has been widely used for performing pavement design calculations. In order to compare the visco-elastic method more fully with this method, calculations have been performed using the pavement details given in the five cases contained in examples 1 and 2 of that document. The input data for the analysis is summarized in Table 9.7. All results are compared at the crack initiation stage (i.e. no factors for rest periods, crack propagation or lateral wander are used) for three pavement thicknesses (100, 200 and 300 mm).

9.6.1   Example 1 results

Example 1 compares four three layer structures consisting of an asphalt base material, sub-base and subgrade. No wearing course is used in this example. A typical example of a dissipated energy contour plot is given in Figure 9.28. From this figure, it can be observed that the highest value of dissipated energy is occurring at the surface and consequently, if this concept is valid, cracking would be expected to occur at this location first. In the majority of the

Mixture properties for asphaltic materials					
Mixture Type	Binder Content	Void Content	Voids in Mineral Aggregate	Volume Binder	Initial Penetration
Typical hot rolled asphalt wearing	7.9	4	21.8	17.8	50
Typical hot rolled asphalt base	5.7	5.0	18.1	13.1	50
Typical dense bitumen macadam base	3.5	10.0	17.9	7.9	100
Modified hot rolled asphalt base	5.0	4.0	15.7	11.7	50
Modified dense bitumen macadam base	4.5	6.0	16.4	10.4	50
Poisson's ratio assumed as 0.4 for above mixtures					

Binder properties assumed for typical mixes				
Initial Properties		Recovered Properties		
Penetration	Softening Point (°C)	Penetration	Softening Point (°C)	Penetration Index
50	53.6	32.5	58.6	-0.2
100	45.7	65.0	50.6	-0.4

Subbase/Subgrade Properties	
Subbase Thickness (mm)	200
Subbase Stiffness (MPa)	100
Subbase Poisson's Ratio	0.3
Subgrade Stiffness (MPa)	
Example 1	30
Example 2	50
Subgrade Poisson's Ratio	0.4

Design Criteria	
Number of Standard Axles (80 kN, Dual)	
Example 1	40,000,000
Example 2	10,000,000
Tyre Pressure (kPa)	500
Wheel centre spacing (mm)	376
Radius of loaded area	113
Speed of traffic (km/hr)	60
Design Temperature for Fatigue (°C)	
Example 1	17.3
Example 2	19.6
Wearing Course Present	
Example 1	No
Example 2	Yes

Note: Example 2 considers only the Modified HRA Base

Table 9.7 :   Design Parameters used in Comparison to University of Nottingham Method
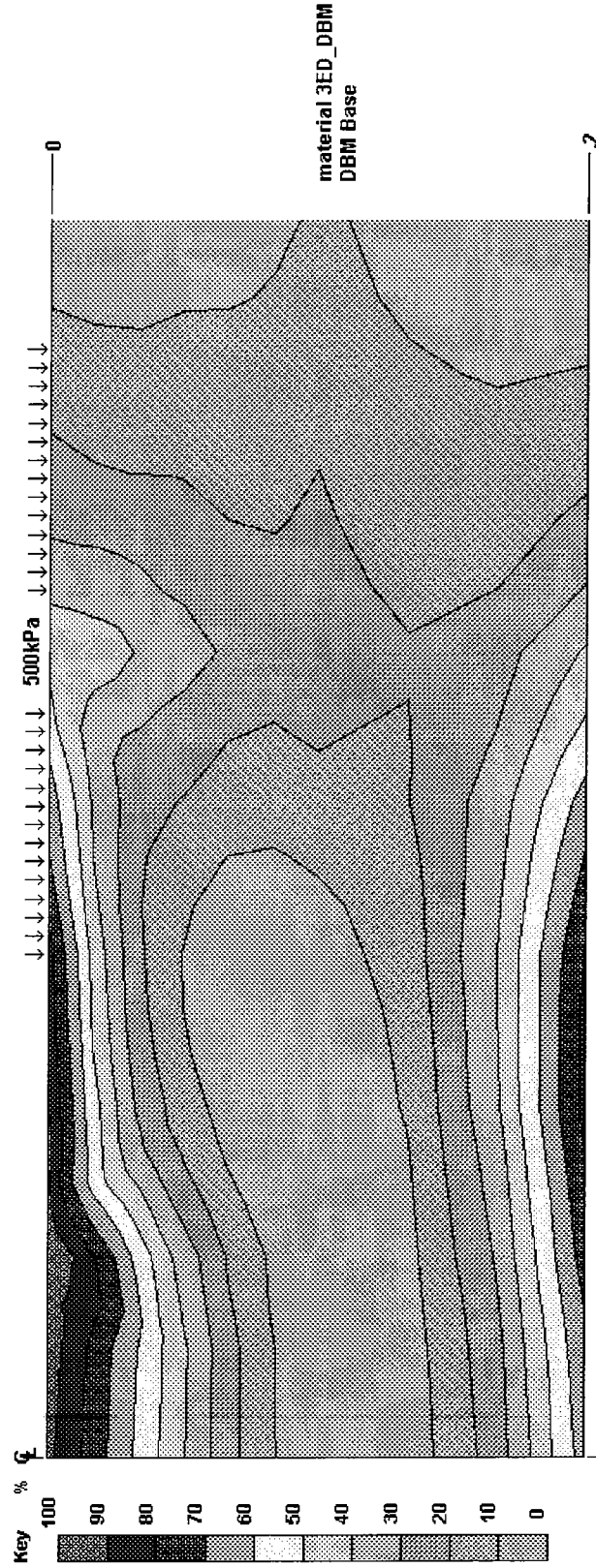
Figure 9.28 : Dissipated Energy Contour for Pavement with Single Layer of DBM, 200 mm Thick

calculations performed (with the exception of two 300 mm thick pavements) the highest value of dissipated energy occurs at the surface.

9.6.2 Example 2 results

Example 2 considers a structure which uses a modified HRA base along with a traditional 40 mm HRA wearing course. A typical example of a dissipated energy contour plot for this structure is given in Figure 9.29. It can be observed that the highest dissipated energy occurs in the less stiff wearing course material. However, unlike the example 1 result, the increased volume of binder in a wearing course results in the crack initiation being expected at the underside of the main structural layer.

9.6.3 Sensitivity to pavement thickness

The results of the visco-elastic analysis are illustrated in Figure 9.30. This figure illustrates that the HRA base material has the longest computed life. The results from both analysis techniques are plotted in Figure 9.31. This illustrates that the life computed from the visco-elastic analysis method is not as sensitive to pavement thickness compared to the elastic method. However, it also indicates that similar lives are obtained for the thicker pavement structure with the exception of that computed for the DBM base containing the softer 100 pen binder. The lower sensitivity with visco-elastic analysis to pavement thickness was also observed earlier (see Figure 9.28).
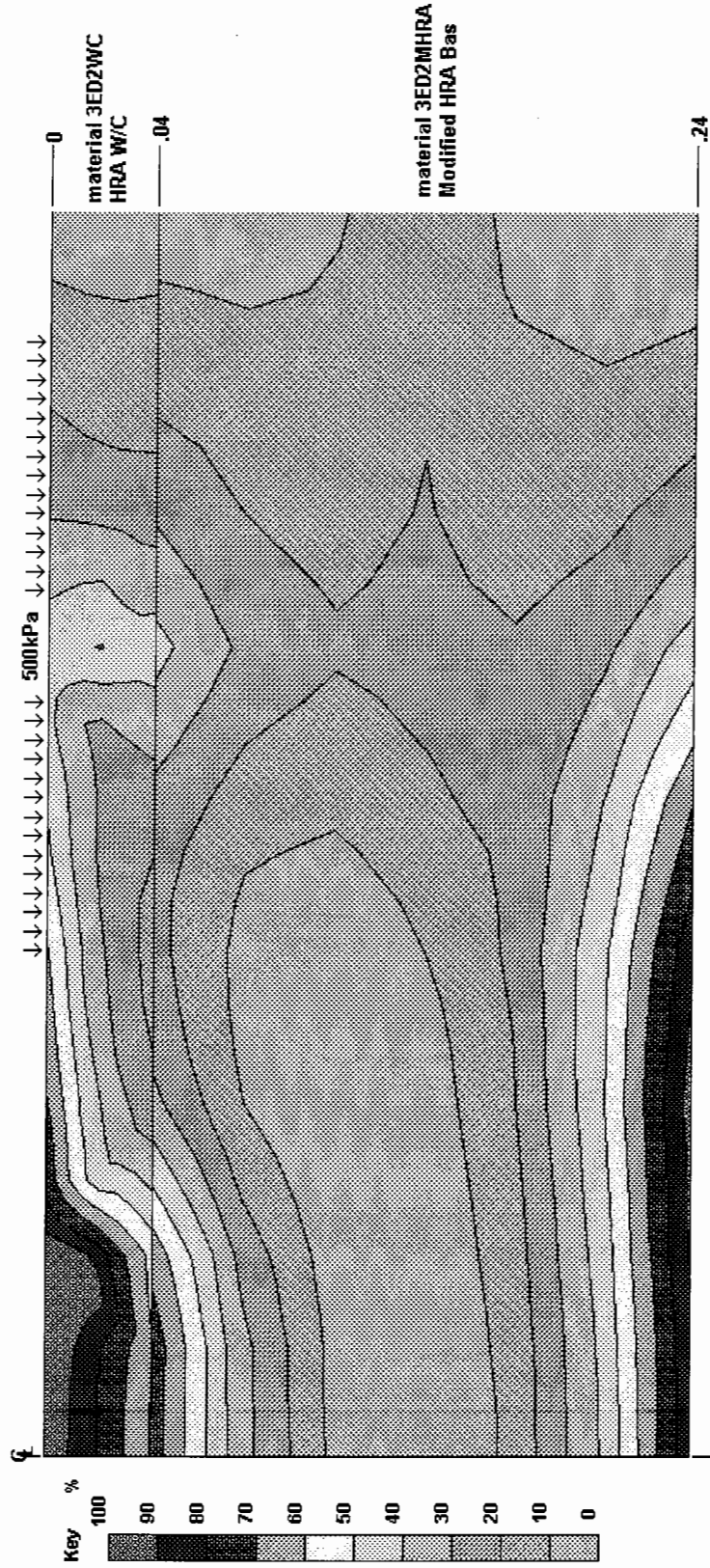
Figure 9.29 : Dissipated Energy Contour for Pavement with 200 mm Thick Modified DBM Base and 40 mm HRA Wearing Course
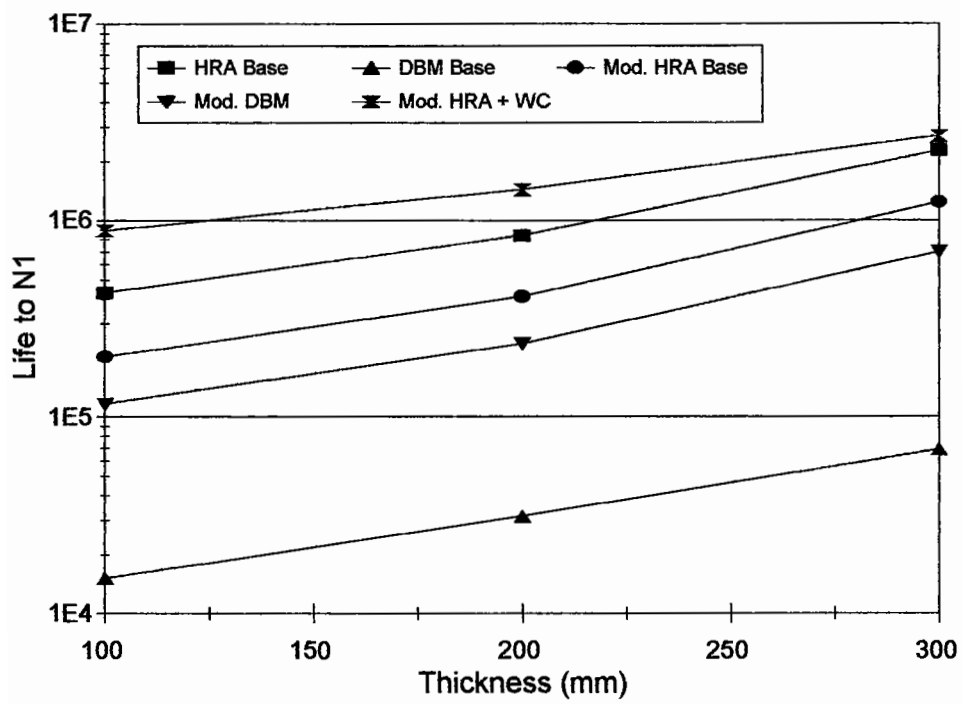
Figure 9.30 : Results Obtained From Visco-Elastic Analysis, Examples 1 and 2
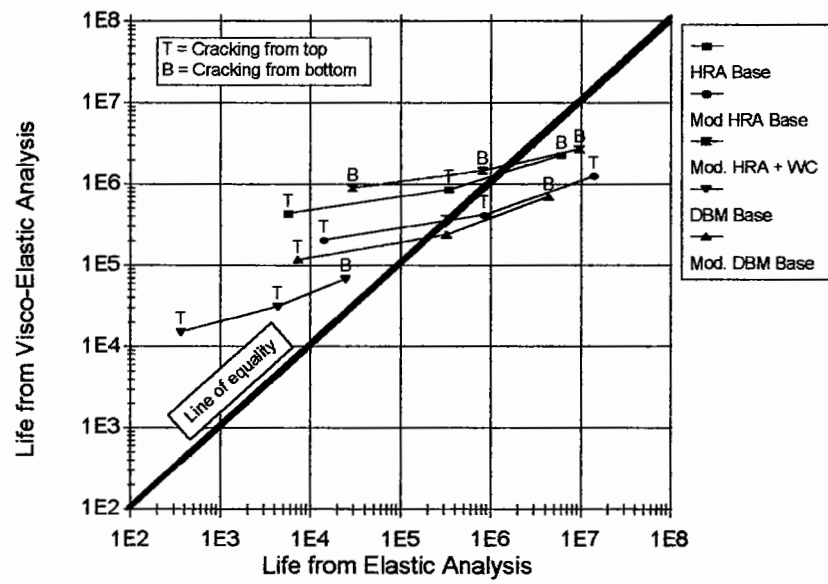
Figure 9.31 : Comparison of Results Between Elastic and Visco-Elastic Analysis, Examples 1 and 2

9.7   SUMMARY

Various structures have been analyzed using the visco-elastic analysis technique.   The analysis required   the derivation of visco-elastic material properties from frequency sweep data and from a prediction method.   These results were compared to conventional elastic analysis.

The relaxation properties of an asphaltic material can be fitted by a four Maxwell element model to achieve a good fit of properties over a two decade range of frequencies.   The fit of a two element model is, in comparison, very poor.   An improved method for converting shear frequency sweep data to flexural data was developed.   This method will enable the use of shear frequency data collected by devices which should be available during the implementation of the SHRP research program.   Data from shear testing was used to develop relaxation times for a mix in 4°C steps between 4°C and 40°C. In addition, relaxation times at 20°C were obtained for all RD aggregate mixtures.

Visco-elastic analysis of pavements containing aggregate RD produced a similar ranking to the performance obtained in the STF.   The results were shifted by a factor of approximately ×25 from the actual lives. This difference is considered to be a function of rest periods.   The results from controlled strain fatigue testing and elastic analysis over predicted the fatigue life.

Analysis performed for a pavement with mix AAG-RD at various temperatures

indicated that as temperature is increased, life decreases. This result is consistent with fatigue calculations by other techniques.

Analysis of pavements with different section thicknesses suggest that the visco-elastic plain strain analysis is not as sensitive to pavement thickness compared to elastic analysis.

CHAPTER 10

Prediction of Fatigue Life

10.0   INTRODUCTION

Fatigue performance predicted by using the energy dissipated (work done) in asphaltic materials under loading (with the damage being proportional to the cumulative dissipated energy) is similar to that used in the Shell Pavement Design Method (Shell International Petroleum Company, 1978).   Some additional features are made possible by the method described, including a direct calculation of dissipated energy from the FE analysis and incorporation of an improved model for determining pavement life from the consideration of dissipated energy.   This chapter presents a method of fatigue prediction that uses the concept of dissipated energy.

10.1   FATIGUE LIFE CALCULATION AND CUMULATIVE DAMAGE

For the analysis of real pavement structures (as opposed to laboratory pilot scale trails) consideration is needed of variable temperature gradients with depth, multiple applications of different axle loads and variation of traffic throughout the pavement life.

10.1.1 Traffic variations

The principle variation in traffic occurs on a daily basis. The traffic flow is generally low at night and then increases for day time hours. Peaks in vehicle traffic occur at the beginning and the end of the working day, although, commercial vehicle traffic (significant to fatigue damage) remains fairly constant throughout the working day. Brown et al. (1985) proposed the use of a trapezoidal variation of traffic over a twenty-four hour period, as illustrated in Figure 10.1, based on real data from the Transport and Road Research Laboratory (Croney, 1977). For simplicity a step function is proposed for use with the Finite Element Model as illustrated in Figure 10.2. The variation of traffic with time of year can be assumed to remain fairly constant and, consequently, this is not considered in the proposed method.

Variations of axle type and spacing between axles has been investigated by various workers. Raithby et al. (1972) suggested that the time between successive wheel loads was generally long enough to be regarded as a significant rest period. A shift factor of ×20 was used in the Nottingham design method (Brown et al., 1985) to account for rest periods (to adjust laboratory performance to observed life in pavements) using the results of Raithby et al. (1972). The basic assumption with this approach is that there is no complex interaction between successive wheel loads and the effect of an axle train versus discrete applications of the same number of wheel loads is equal. However, results published by Hutala et al. (1980) demonstrated that an interaction does exist when axle trains pass over a pavement structure,
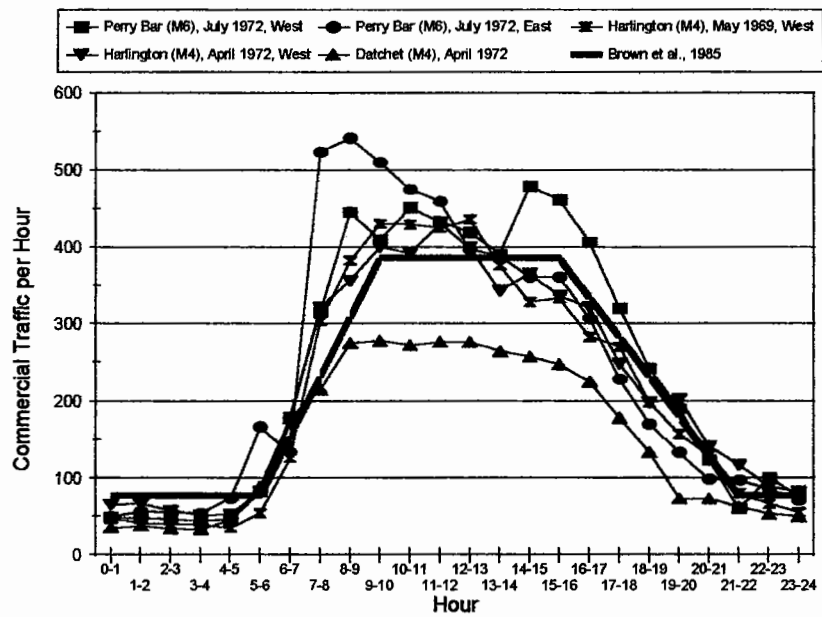
Figure 10.1 : Traffic Variation through a 24 hour period (after Croney, 1977 and Brown et al., 1985)
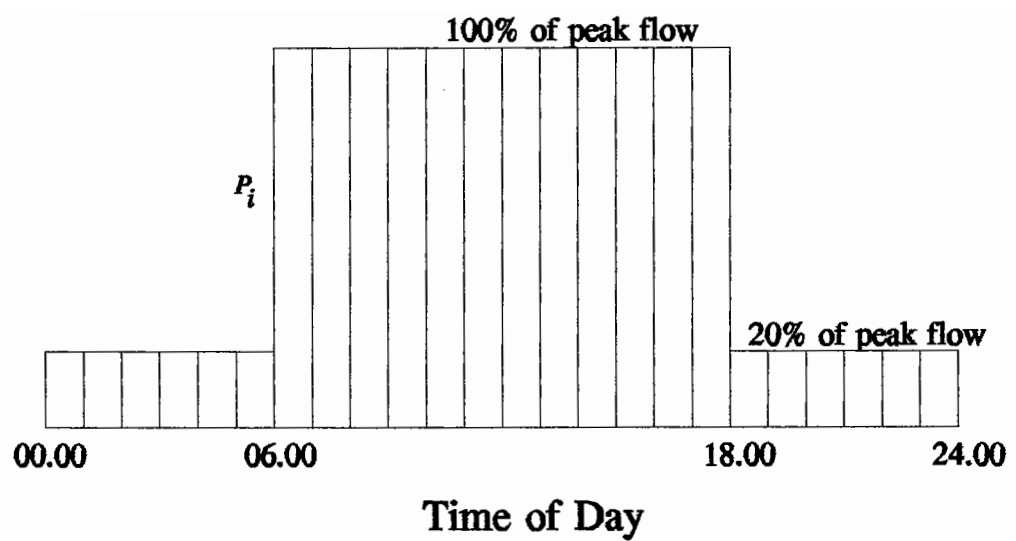
Notes: 1. P_i = Traffic in any hour (i)
       2.   Peak Traffic Flow = Total Commercial Vehicles divided by 14.4

Figure 10.2 : Simplified Traffic Variation through a 24 hour period

particulary with respect to the magnitude of the transverse strain. Dissipated energy can potentially provide a tool to investigate the combined effect of multiple axle loading but this would require relatively complex 3 dimensional analysis and significantly longer computation times compared to the 2 dimensional solutions resulting in long computation times for routine calculations.

The effect of axle loads with different weights has traditionally been considered by adoption of the theory that damage caused in any loading cycle is inversely proportional to the fatigue life of the material as discussed in Chapter 3 (see Equations 3.47 to 3.50). The current PACE™ software (as used earlier) allows axle loads to be analyzed individually and does not consider a spectrum of loading. However, equivalency values can be determined for a given axle by calculating the life for any axle load and comparing this to a standard axle.

10.1.2 Methods for determining pavement temperature

Since the properties of asphaltic materials are highly temperature dependent (as discussed in Chapters 2 and 3) detailed consideration is needed of temperature is needed to account for the effects.

The effect of temperature can be considered in a number of ways. Sophisticated climatic effect models can be used (Lytton et al., 1990) or, alternately, use can be made of simplified techniques to predict pavement

performance. Both these approaches are considered below.

The effect of varying temperatures both diurnally and annually can be obtained by calculating temperature depth gradients for discrete time periods. The effect of solar radiation and thermal properties of materials are fairly well established (Williamson, 1972; Lytton et al., 1990, and Solaimanian et al., 1993).

A method was developed using numerical procedures developed by Sharrock (1991) for calculating temperature-depth gradients. In Sharrock's method, rigorous analysis of climatic effects is performed which uses a FE heat flow model to generate 24 temperature-depth profiles, one for each hour of the day. The calculations are repeated for twelve periods corresponding to each of the twelve months of the year giving a total of 288 temperature depth gradients. The gradients are expressed in an exponential form as follows:

$$T_z = A_1 \; e^{\;b_1} + A_2 \; e^{\;b_2} + A_3 \; e^{\;b_3} + A_4 \; e^{\;b_4} + A_5 \; e^{\;b_5} + A_6 \; e^{\;b_6} \qquad (10.1)$$

where; A_1 to A_6 and b_1 to b_6 are curve fitting parameters.

Use of the above equation enables the calculation of pavement temperature at Gauss points in the Finite Element model.

Sharrock's procedure (Sharrock, 1991) uses an energy balance calculation with boundary conditions that consist of a heat transfer coefficient used in conjunction with air temperature, together with a radiation flux at the upper

surface and a fixed temperature at 1 m depth, equal to the average monthly air temperature. The computation is started at dawn, assuming a constant temperature with depth for simplicity. The heat flow equations are integrated by an explicit time stepping procedure, whilst, simultaneously, the heat transfer conditions at the surface are varied with time according to the predetermined patterns of air temperature together with direct and diffuse radiation. After 24 hours the temperature-depth variation found at this time is treated as a new estimate of the starting conditions and the time stepping process is repeated for another 24 hours. In this way, successive approximations to the initial boundary conditions are obtained. When the initial and final states of the 24 hour period match closely, the desired solution for the period has been determined. The radiation at the surface is obtained as follows:-

Day - A mean value of solar constant of 1362 W/m^2 is assumed, i.e. the radiation intensity normal to the Sun's direction above the earth's atmosphere. This is taken to vary seasonally by +/- 3.5% due to the varying radius of the Earth's orbit. Generally accepted published information on the proportion of the radiation reaching the ground is assumed, dependent on the elevation of the Sun, the height above sea level and cloud cover (Sharrock, 1991). An absorbtivity of 0.9 is taken for the asphaltic materials.

Night - A constant re-radiation of 120 W/m^2 to space is assumed. This is developed and terminated linearly during the first hour and last hour of darkness respectively, to give a pattern continuous with the daytime radiation input.

An approximate daily variation of air temperature for each month is constructed from average daily maximum and minimum temperatures, with an allowance of plus and minus a number of standard deviations to cover the required proportion of the extremes, varying linearly with maximum and minimum temperature over the year. Together with the computed surface temperature, this defines the remaining surface heat transfer, using a heat transfer coefficient of 23 $W/m^2/°C$.

Williamson (1972) conducted an extensive evaluation of the thermal properties for soils and asphaltic materials. In tests, he observed that the thermal conductivity for soils ranges between 0.518 to 2.742 W/m.°K with density being a major factor. For asphaltic mixtures, the thermal conductivity is a function of the thermal properties of the component materials. The binder component generally has fairly consistent properties typically ranging between 0.1360 to 0.1657 W/m.°K. However, the rock component has significant variability with typical values as follows:

Basalt	2.093 W/m.°K
Rhyolite	2.093 W/m.°K
Granite	2.637 W/m.°K
Limestone	3.140 W/m.°K
Quartzite	3.433 W/m.°K

The conductivity of the mixture can be approximated using the geometric mean equation, as follows:

$$K_{mix} = K_s^{V_s} \times K_b^{V_b} \times K_a^{V_a} \qquad (10.2)$$

where: V_s, V_b and V_a are volumes of stone, binder and air respectively.

K_s, K_b and K_a are conductivities of the stone, binder and air respectively.

Using a thermal conductivity for air voids of 0.024 W/m.°K and a mean value for the asphalt of 0.1509 W/m.°K, the conductivity can be considered as a function of the volumetrics and the aggregate type, as follows:

$$K_{mix} = K_s^{V_s} \times 0.1509^{V_b} \times 0.024^{V_a} \qquad (10.3)$$

For a typical dense asphalt mixture (air voids 7% and binder volume 11%) the range of conductivity expected for mixtures would lie between 1.146 and 1.720 W/m.°K. Since, this property is often unknown, a value of 1.5 W/m.°K has been adopted as a default value. Other typical thermal properties are assumed for the asphaltic mixture as follows:

Mass Density (ρ)   2400 kg/m^3

Specific Heat (c_p)   960 J/kg.°K

The above properties are used to obtain diffusivity, as follows:-

$$\kappa = \frac{K_{mix}}{(\rho \times c_p)} \qquad (10.4)$$

Thus, the default value used in the FE heat flow calculations for diffusivity is

$6.51 \times 10^{-7} \text{ m}^2/\text{s}$.

The heat flow calculation is done iteratively, employing the previously mentioned FE method. A typical example of calculated pavement temperature depth gradients is illustrated in Figure 10.3. It should be noted that the calculation of pavement temperature is not an exact science since the cloud cover, geographical location and thermal properties of materials all vary.

Various researchers have, using sophisticated models as described above, developed simplified methods for obtaining pavement temperatures. The Asphalt Institute method (Witczak, 1972) converts the mean monthly air temperature (*MMAT*) to mean monthly pavement temperature (*MMPT*) as follows:

$$MMPT = MMAT \left[1 + \frac{1}{(z + 4)} \right] - \frac{34}{(z + 4)} + 6 \qquad (10.5)$$

where;   *MMPT* and *MMAT* are measured in degrees Farenheight,

and   z is one third of the depth of asphalt in inches

The sensitivity of this equation to pavement thickness is relatively small (Brunton, et al., 1984) and thus a simplified relationship was proposed as follows:

$$MMPT = 1.15 \ MMAT + 3.17 \qquad (10.6)$$

A1 YORKSHIRE
Temp gradients, July 1991

KEY:

□ Sunrise + 0 hours
X Sunrise + 5 hours
◊ Sunrise + 10 hours
+ Sunrise + 15 hours
▽ Sunrise + 20 hours
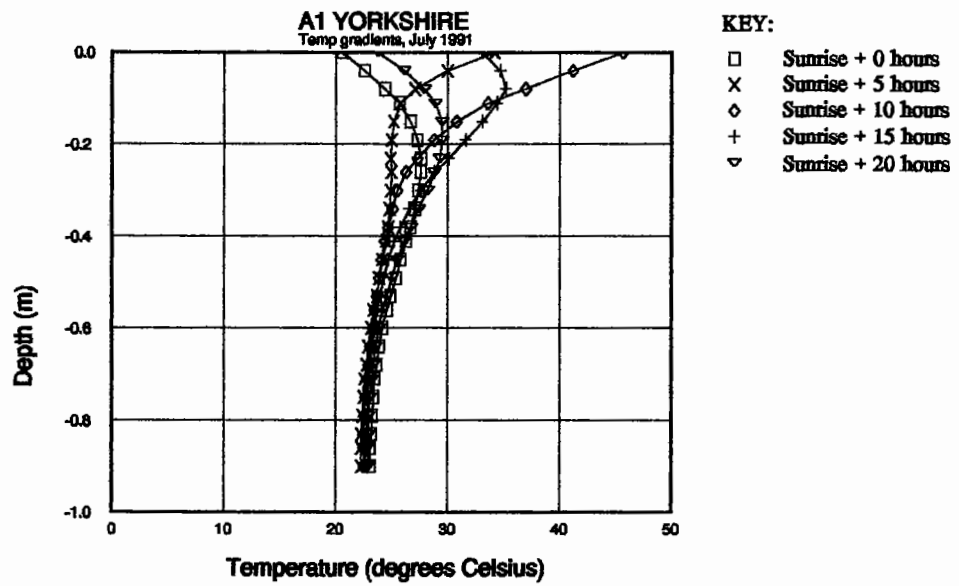
Figure 10.3 : A Typical Example of Calculated Pavement Temperature Depth Gradients

-10.11-

where;   *MMPT* and *MMAT* are measured in degrees Celsius,

If soil properties remain fairly constant over the year, this equation can be further simplified to reflect an equivalent annual pavement temperature for fatigue calculations (*EAPT_fat*), as follows:

$$EAPT_{fat} = AAPT + 11 \qquad\qquad (10.7)$$

where:

$$AAPT = \frac{1}{12} \sum_{m=1}^{m=12} MMPT \qquad\qquad (10.8)$$

(Note: *EAPT_fat* is in degrees Celsius)

Thus, depending upon the amount of temperature data available, two different approaches can be made to obtain the appropriate temperatures for performing the calculations. Either, a very detailed approach with calculated temperature depth gradients, or alternatively, a simplified approach with a single temperature assigned to the asphaltic layer based on mean monthly and annual pavement temperatures can be used. Often, the last of the two approaches has to be used because of the lack of good temperature data for a given location.

10.2   PROPOSED PAVEMENT DESIGN METHOD

Based upon consideration of pavement temperature data and material property relationships a tentative method is outlined for calculating fatigue life of road pavements. Due to ongoing development work with the PACE™ software the

calculation procedures have not currently been fully tested or validated. However, based on the work presented earlier in this thesis the following procedure is proposed:

i) Using the temperature depth gradients determine the pavement temperature at one third depth (Witczak, 1972) of the bound asphaltic layer. This temperature is used to describe the effective fatigue temperature for the asphaltic layers for a one hour period in a single month of the year. Using the temperature depth information from the model described earlier a total of 288 records are available (12 months $\times$ 24 one hour periods).

ii) The visco-elastic properties are obtained from frequency sweep data. This data is analyzed to obtain a master of properties and shift factors. The temperature range is split into five equal increments and relaxation properties (see section 9.3) are calculated for the upper and lower temperature of each increment. For example, if the total range is -10°C to +40°C then calculations are performed at -10, 0, 10, 20, 30 and 40°C.

iii) Calculate the dissipated energy contours in the pavement structure for each temperature obtained in step ii) which covers the highest to lowest expected.

iv) Calculate the fatigue life at each of the six temperatures, from the global relationship discussed earlier (see Equation 6.30) or using individual material relationships developed from fatigue testing, if these are available.

v)   Calculate the damage under a single axle load at each of the six temperatures, T, assuming Miners' linear damage rule to be valid:

$$D_T = \frac{1}{N} \qquad (10.9)$$

vi)   Determine a relationship between damage versus temperature.

vii)   For each month, using the relationship between damage and temperature, calculate the mean damage for the month. This is done by considering the traffic and temperature in 24, one hour increments, ie.:

$$D_m = \frac{\int_{t=1}^{t=24} P(t)\, D_T\, dt}{\int_{t=1}^{t=24} P(t)\, dt} \qquad (10.10)$$

where;   *P(t)* is the proportion of traffic in hour *t*

viii)   Assuming a uniform flow of traffic over the year, calculate the yearly traffic weighted mean damage from the following:

$$\bar{D} = \frac{1}{12} \int_{m=1}^{m=12} D_m\, dm \qquad (10.11)$$

ix)   Using the relationship established earlier between temperature and

damage under a standard axle load, it is possible to equate the yearly traffic weighted mean damage to temperature and material properties. However, this is not necessary since life can be computed from:

$$NI = \frac{1}{\bar{D}} \qquad (10.12)$$

If inadequate temperature data is available for a analysis in the manner outlined above, an alternate to the method outlined above is to consider the use of Equation 10.7 to define the pavement temperature and to perform a single calculation at this temperature, to define the fatigue life.

It is important to consider the cumulative damage and the interaction between vehicle loading/temperature must be considered. In addition, factors have to be introduced into the design to allow for crack propagation and the probability of survival. Thus the fatigue life is calculated as follows:

$$\log N_{fat} = \log NI + \log A_{rest} + \log A_{wander} + \log A_{prop} + \log A_{prob} \qquad (10.13)$$

where; NI =   life to crack initiation (as defined by Equation 6.30),

A_{rest} =   life adjustment associated with rest periods,

A_{wander} =   life adjustment due to lateral wander,

A_{prop} =   life adjustment associated with crack propagation,

and A_{prob} =   life adjustment associated with achieving the required probability of survival.

The work conducted herein has not been sufficient to evaluate most of the above parameters and, consequently, use has been made of parameters from other work. The values proposed for the parameters are as follows:

A_{rest} ×25 based on comparison of the STF crack initiation results (see Figure 9.21). This figure is also similar to the ×20 used in earlier work (Brown et al., 1985).

A_{wander} ×1.1 as used by Brown et al., 1985.

A_{prop} ×20 based upon van Dijk et al. (1977) and used in the Nottingham design method.

A_{prob} ×0.135 to obtain a 95% probability of survival based upon the standard error of fatigue results observed in the STF.

The above values give a total shift factor of 74.25 to give a 95% probability of survival. This value is very close to the factor of 77 adopted in the Nottingham method to obtain life to the critical condition (defined as the first appearance of cracking).

10.3   SUMMARY

Based upon consideration of dissipated energy, a pavement design method has been outlined which enables either a detailed evaluation of temperature effects

or, as an alternative, a relatively simplistic single design temperature can be adopted with one F.E. calculation performed. These methods require implementation in the F.E. code and further validation prior to adoption. In particular a comparison of 2 dimensional F.E. analysis versus 3 dimensional is needed. Also, no information is currently available on the possible loss of accuracy in using a single temperature versus the more detailed approach. This aspect should be investigated.

CHAPTER 11

Conclusions and Recommendations

11.0 INTRODUCTION

In order to investigate the behaviour of asphaltic materials with regard to their fatigue performance in relation to the concept of dissipated energy, a program of work was conducted which had three major components;

1)   Laboratory testing of materials to determine material relationships for fatigue performance with a particular emphasis on dissipated energy.

2)   Development of material relationships for obtaining visco-elastic properties of asphaltic materials.

3)   The investigation of analysis techniques to compute dissipated energy in pavement structures and comparison with elastic analysis techniques.

In addition, small scale pavement trials were evaluated in order to compare the data obtained from the analysis with validation tests and an assessment was made of the Indirect Tensile Test as a simplified method of testing.

11.1 FATIGUE TESTING

Based upon the results of trapezoidal flexural beam fatigue testing, several significant conclusions can be drawn:

i.   A parameter "a" has been defined (see Equation 6.8) which is dependant upon the initial rheology of the mixture and describes the damage to the mixture in terms of the relationship between the phase angle and the extensional complex modulus during an individual fatigue test. The relationships obtained from individual fatigue tests for extensional complex modulus versus phase angle can be considered to pass through a common point (a "focus"), which has enabled the development of a prediction procedure for "a" (see Figure 6.12).

ii.   A method has been developed which allows the definition of a failure criterion based on a crack initiation point, $N1$. The $N1$ criterion allows a comparison of materials at equal states of damage and avoids arbitrary definition of failure. It is concluded that this point is better defined in a controlled stress fatigue test than in controlled strain.

iii.   A method has been developed to predict fatigue life to crack initiation, $N1$. Parameters which significantly affect the performance of a given mixture are the initial dissipated energy, w_o, volume of binder, Vb and the work ratio parameter, ψ_{N1}, as described in Equation 6.30.

iv.   The volume of binder has been shown to significantly effect the parameter "A" in the relationship between cumulative dissipated energy (W) and the number of load cycles (N) ($W = AN^Z$) and if a simple volumetric correction is applied then the scatter in fatigue lines can be reduced considerably.

v.   A procedure has been developed to define a work ratio, ψ_{NI}, which is based upon the rheology of the mixture and a mode of loading factor, Γ, which can be used for the prediction of fatigue life. This allows the prediction of fatigue life for either controlled stress or strain conditions and also, more importantly, for intermediate modes of loading that exist in real pavement structures.

11.2   SLAB TEST FACILITY RESULTS

Eighteen slabs of asphalt/modified asphalt - aggregate mixtures were tested in the Slab Test Facility to determine their performance with respect to fatigue cracking. From the analysis of the test results, the following conclusions can be drawn:-

i.   The fatigue life to the NI condition was difficult to evaluate due to the crack pattern that occurred in the slabs being tested.

ii.   The results indicated that variability is relatively large with the standard deviations for the log of life when normalised to a constant value of strain

between 0.116 and 0.810.

iii.   The asphalt/modified asphalt - aggregate mixtures have been ranked according to their performance. The rankings obtained were similar to those based on the measurement of stiffness and of fatigue performance using dissipated energy.

iv.   The 4 point beam fatigue results obtained at the University of California at Berkeley for mixtures manufactured using rolling wheel compaction correlated well with those obtained using the trapezoidal beam test.

v.   It appeared that the use of a kneading compaction device (at South Western Laboratories) or other unknown factors significantly effected the results of the modified asphalt mixtures shipped to, and tested at the University of California at Berkeley.

11.3   EVALUATION OF SIMPLIFIED TEST PROCEDURES

Testing of specimens in indirect tension for stiffness and tensile strength was conducted and from this work the following conclusions can be drawn:-

i)   A good relationship existed between the stiffness in indirect tension and the cantilever beam method when the results were compared at the same temperature. When shifting from one temperature to another, using the Bonnaure et al. (1980) method, the relationship was found to be poorer. It is

suggested that this could have occurred due to the different binder rheology in the mixtures tested.

ii)   Using a relationship between phase angle and stiffness modulus, developed from data collected by Francken et al. (1974), an estimation of dissipated energy was made of the fatigue life to the *N1* condition. This demonstrated that the stiffness in indirect tension could account for a large amount of the variability in life.

iii)   The results from the indirect tensile splitting tests proved to be inconclusive due to the lack of sensitivity of the instrumentation used.

11.4   VISCO-ELASTIC ANALYSIS OF PAVEMENT STRUCTURES

Various structures have been analyzed using a visco-elastic analysis technique. The analysis required the deviation of visco-elastic material properties from frequency sweep data. These results were compared to analysis from conventional elastic analysis and from these the following conclusions can be drawn:-

i)   The relaxation properties of an asphaltic material can be fitted by a four Maxwell element model with good accuracy over a two decade range of frequencies. The fit of a two element model is, in comparison, very poor.

ii)   An improved method for converting shear frequency sweep data to

flexural data was developed. This method will enable the use of shear frequency data collected by devices which should be available during the implementation of the SHRP research program.

iii)   Visco-elastic analysis of pavements containing aggregate RD produced a similar ranking to that observed in the STF. The results were shifted by a factor of approximately ×25 from the actual lives. This difference is considered to be a function of rest periods.

iv)   The results from controlled strain fatigue testing and elastic analysis over predicted the fatigue life.

v)   Analysis performed for a pavement with mix AAG-RD at various temperatures indicated that as temperature increased life reduced. This result is consistent with fatigue predictions by other techniques.

vi)   Analysis of pavements with different section thicknesses suggest that the visco-elastic plain strain analysis is not as sensitive to pavement thickness as compared to elastic analysis.

11.5   RECOMMENDATIONS FOR FURTHER WORK

While this work has contributed to the understanding of the fatigue process using the concept of dissipated energy the results of the work presented in this thesis is limited to a relatively small data set and limited implementation of

the calculation procedures. For example, the trapezoidal fatigue testing was conducted at only three temperatures. Consequently, to verify material relationships and to implement the calculation procedures further work is proposed as detailed below.

11.5.1 Laboratory Fatigue Testing

Further work is required to verify that the parameter "*a*" (which describes the stiffness loss in a fatigue test - see Section 6.2.2) can be adequately predicted from the initial mixture stiffness and phase angle. This work should extend the data set to encompass larger variations in mixture volumetrics and test temperatures. Further work should also consider improvements to the definition of mixture stiffness. This parameter was observed to change very rapidly at the beginning of laboratory fatigue tests. Since it is used in the prediction equations, any errors in its estimation will effect the calculated fatigue life.

The estimation of crack growth parameters needs to be considered by conducting tests which measure fracture properties. The effect of rest periods and healing should be evaluated with both forms of fatigue testing. This would enable more accurate consideration of the crack propagation phase.

11.5.2 Pilot Scale Testing

A series of tests should be conducted using identical materials to those used

in the laboratory fatigue testing. These mixtures should be evaluated to obtain master curves of stiffness using axial, flexural and shear modes of loading to enable evaluation of the interrelationships in an efficient manner. This work would probably be best conducted in the Nottingham Pavement Test Facility (PTF) since more realistic structures can be built than in the Nottingham Slab Test Facility (STF). The PTF also allows the effects of lateral wheel distribution and rest periods to be evaluated.

11.5.3 Visco-Elastic Analysis

This works needs to be extended to explore the potential of visco-elastic analysis over other analysis techniques. In particular, the work should include the following:

i.   The implementation of a 3 dimensional method to produce a more realistic loading arrangement.

ii.   The use of an automated calculation procedure to sum damage associated with each season as discussed in Chapter 10.

iii.   Further validation of the dissipated energy technique against pavements of known performance is needed to extend the results presented in Chapter 9.

REFERENCES

Alavi, S.H. and Monismith, C.L., "Time and Temperature Dependent Properties of Asphalt Concrete Mixes Tested as Hollow Cylinders and Subjected to Dynamic Axial and Shear Loads," Journal of the Association of Asphalt Paving Technologists, Volume 63, 1994, pp. 152-181.

AASHTO M-003 "Determining the Shear and Stiffness Behavior of Modified and Unmodified Hot Mix Asphalt with the Superpave® Shear Test Device - The SUPERPAVE Mix Design System Manual of Specifications, Test Methods, and Practices," Strategic Highway Research Program, National Research Council, 1994, pp. 103-120.

AASHTO TP1 "Test Method for Determining the Flexural Creep Stiffness of Asphalt Binder Using the Bending Beam Rheometer (BBR)".

AASHTO TP5 "Test Method for Determining Rheological of Asphalt Binder Using a Dynamic Shear Rheometer (DSR)".

American Gillsonite Company, "Gillsonite," Salt Lake City, Utah.

Attwooll, A.W. and Broome, D.C., "Trinidad Lake Asphalt," Baynard Press, 1962.

Bonnaure, F., Gest, G., Gravois, A and Uge, P., "A New Method of Predicting

the Stiffness of Asphalt Paving Mixtures," Proceedings, Association of Asphalt Paving Technologists, 1977.

Bonnaure, F., Gravois, A., and Udron, J., "A New Method for Predicting the Fatigue Life of Bituminous Mixes," Proceedings, Association of Asphalt Paving Technologists, 1980, pp. 499-529.

Bonnaure, F.P., Huibers, A.H. and Boonders, A., "A Laboratory Investigation of Rest Periods on the Fatigue Characteristics of Bituminous Mixes," Proceedings, Association of Asphalt Paving Technologists, Vol. 51, 1982, pp. 104-128.

Bouldin, M.G., Rowe, G.M., Sousa, J.B. and Sharrock, M.J., "Repetitive Creep as a Tool to Determine the Mix Rheology of Hot Mix Asphalt," Journal of the Association of Asphalt Paving Technologists, Volume 63, 1994, pp. 182 - 223.

British Standards Institution, BS 598: Part 3: 1985, "Sampling and Examination of Bituminous Mixtures for Roads and other Paved Areas - Part 3. Methods for design and physical testing," 1985.

Brown, S.F., "Stiffness and Fatigue Requirements for Structural Performance of Asphaltic Mixes," Proceeding, Eurobitume Symposium,, 1978, pp. 141-145.

Brown, S.F. and Brunton, J.M., "An Introduction into the Analytical Design of Bituminous Pavements," 3rd Edition, University of Nottingham, Nottingham,

England, 1985.

Brown, S.F., Brunton, J.M. and Stock, A.F., "The Analytical Design of Bituminous Pavements," Proceedings, (Paper 8834 Transportation Engineering Group), Institution of Civil Engineers, Part 2, 1985, 79, Mar. 1-31.

Brown, S.F., Rowlett, R.D. and Boucher, J.L., "Asphalt Modification," Highway Research, Sharing the Benefits, Proceedings of the conference - The United States Strategic Highway Research Program, 1990, pp 181-204.

Brunton, J.M. and Brown, S.F., "Design of Asphalt Pavements with Polymer Grid Reinforcement for North American Conditions," Report submitted to The Tensar Corporation, University of Nottingham, Department of Civil Engineering, 1984.

Burgers, J.M., "Mechanical considerations - model systems - phenomenological theories of relaxation and of viscosity," Academy of Sciences, Amsterdam, first report on viscosity and plasticity, 1935.

Burmister, D. M., "The theory of stresses and displacement in layered systems and applications to the design of airport runways," Proceedings, Highway Research Board, Washington, 1943, 23, pp. 126-144.

Christensen, D.W. and Anderson, D.A., "Interpretation of Dynamic mechanical Test Data for Paving Grade Asphalt Cements," Journal, Association of Asphalt

Paving Technologists, Volume 61, 1992, pp. 67-116.

Chomton, G. and Valayer, P.J., "Applied Rheology of Asphalt Mixes - Practical Applications," Proceedings, Third International Conference on the Structural Design of Asphalt Pavements, London, England, 19972, pp. 214-225.

Collins, J.H., Bouldin, M.G., Gelles, R. and Berker, A., "Improved Performance of Paving Asphalts by Polymer Modification," Journal, of the Association of Asphalt Paving Technologists, Volume 60, 1991, pp. 43-79.

Cooper, K.E., "The Effect of Mix and Testing Variables on the Fatigue Strength of Bituminous Mixes," M.Phill Thesis, University of Nottingham, 1976.

Cooper, K.E. and Brown, S.F., "Development of Simple Apparatus for the Measurement of the Mechanical Properties of Asphalt Mixes," Proceedings, Eurobitume Symposium, Madrid, 1989, pp. 494-498.

Corbett, L.W. and Swarbrick, R.E., "Clues to Asphalt Composition," Proceedings, Association of Asphalt Paving Technologists, Vol. 27, 1955, p. 107.

Croney, D., "The Design and Performance of Road Pavement," HMSO, London, 1977.

Deacon. J.A., Tayebali. A.A., Coplantz. J.S., Finn F.N. and Monismith C.L., "Fatigue Response of Asphalt - Aggregate Mixes: Part III Mix Design and Analysis," Strategic Highway Research Program, National Research Council, Washington, D.C. 1994.

Dobson, G.R., "The Dynamic Mechanical Properties of Bitumen," Proceedings, Association of Asphalt Paving Technologists, Volume 38, 1969, pp. 123-139.

Ferry, J.D., "Viscoelastic Properties of Polymers," John Wiley & Sons, Third Edition, 1980.

Finn, F.N., Saraf, C., Kulkarni, R., Nair, K., Smith, W. and Abdullah, A., "The Use of Distress Prediction Subsystems for the Design of Pavement Structures," Proceedings, Fourth International Conference on the Structural Design of Asphalt Pavements, University of Michigan, Ann Arbor, Vol. 1, August 1977, pp. 3-38.

Francken, L., "Fatigue Performance of a Bituminous Road Mix under Realistic Conditions," Transportation Research Record 712, Washington 1979, pp 30-37.

Francken, L. and Clauwaert, C., "Characterization and Structural Assessment of Bound Materials for Flexible Road Structures," Proceeding, Sixth International Conference, Structural Design of Asphalt Pavements, 1987, pp. 130-144.

Francken, L. and Verstraeten, J., "Methods for Predicting Moduli and Fatigue Laws of Bituminous Road Mixes under Repeated Bending," Paper presented at the 53rd Annual Meeting of the Highway Research Board, 1974.

Gerritsen, A.H., "Prediction of The Dynamic Visco-Elastic Behaviour of Asphalt Wearing Course Mixes using Burgers' Model," Koninklijke/Shell-Laboratorium, Amsterdam, Report MF 88-0809, 1987.

Gerritsen, A.H., van Gurp, C.A.P.M., van der Heide, J.P.J., Molenaar, A.A.A., and Pronk, A.C., "Prediction and Prevention of Surface Cracking in Asphaltic Pavements". Proceedings, Sixth International Conference, Structural Design of Asphalt Pavements, Michigan, July 13-17 1987, pp 378-391.

Griffith, A.A., "The Phenomena of Rupture and Flow in Solids," Philosophical Transactions of the Royal Society, London, Series A, Vol. 221, 1921.

Hadley, W.O., and Vahida, H., "Fundamental Comparison of the Flexural and Indirect Tensile Tests," Transport Research Record 911, 1970, pp. 42-51.

Harrigan, E.T., Leahy, R.B. and Youtcheff, J.S., "The SUPERPAVE Mix Design System Manual of Specifications, Test Methods, and Practices," SHRP Report SHRP-A-379, Strategic Highway Research Program, National Research Council, Washington, DC, 1994.

Heukelom, W., "A Bitumen Test Data Chart for Showing the Effect of

Temperature on the Mechanical Behaviour of Asphaltic Bitumens," Journal, Institute of Petroleum Technologists, Volume 55, 1969, pp 404-417.

Hopman, P., "Energy Dissipation," Proceedings, European Flexible Pavement Study Group, 1990.

Hopman, P.C., Kunst P.A.J.C and Pronk A.C., "A Renewed Interpretation Method for Fatigue Measurement, Verification of Miner's Rule," 4th Eurobitume Symposium, Volume 1, Madrid, 4-6 October 1989, pp 557-561.

Hudson, W.R. and Kennedy, T.W., "An Indirect Tensile Test for Stabilized Materials," Research Report 98-1, Project 3-8-66-98, Center for Highway Research, The University of Texas at Austin, January, 1968.

Hugo, F. and Schreuder, W.J., "Effect of Sample Length on Indirect Tensile Test Parameters," Journal of the Association of Asphalt Paving Technologists, Volume 62, 1993, pp.422-449.

Huhtala, M., Alkio, R., Pihljamaki, J., Pienmaki, M. and Halonan, P., "Behavior of Bituminous Materials Under Moving Wheel Loads," Journal of the Association of Asphalt Paving Technologists, Vol. 59, 1990, pp 422-442.

Huhtala, M. and Pihajamäki, J., "New Concepts on Load Equivalency Measurements," Proceedings, 7th International Conference on Asphalt Pavements, Volume 3, 1992, pp. 194-208.

Hveem, F. N., "Pavement deflections and Fatigue Failure," Highway research Board, Bulletin 144, Washington, 1955, pp. 43-73.

Irwin, G.R., "Analysis of Stresses and Strains Near the End of the Crack Traversing a Plate," Journal of Applied Mechanics, Volume 24, Sept. 1957, pp. 361- 364.

Jenq, Y. and Perng, J., "Analysis of Crack Propagation in Asphaltic Concrete Using Cohesive Crack Model," Transportation Research Record 1317, 1990, pp. 90-99.

Kallas, B.F. and Shook, J.F., " Factors Influencing Dynamic Modulus of Asphalt Concrete," Proceedings, Association of Asphalt Paving Technologists, Volume 38, 1969, pp. 140-178.

Little, D.N., "Investigation of Microdamage Healing in Asphalt and Asphalt Concrete," Task K, Semi-Annual Technical Report Western Research Institute, FHWA Project DTFH61-92-C-00170 - Fundamental Properties of Asphalts and Modified Asphalts, October, 1995.

Lytton, R.L., Pufahl, D.E., Michalak, C.H., Liang, H.S. and Dempsey, Bl J., "An Integrated Model of the Climatic Effects on Pavements", Texas Transportation Institute, Texas A & M University, Final Report, February, 1990.

Lytton, R.L., Shanmugham, U. and Garrett, B.D., "Design of Asphalt Pavements for Thermal Fatigue Cracking," Report FHWA/TX-83-284-4, Texas Transportation Institute, Texas A&M University, 1983.

Lytton, R.L., Uzan, J., Fernando, E.G., Roque, R., Hiltunen, D. and Stoffels, S.M., "Development and Validation of Performance Prediction Models and Specifications for Asphalt Binders and Paving Mixes," SHRP-A-357, Strategic Highway Research Program, National Research Council, Washington, DC, 1993.

Majidzadeh, K., Kaufmann, E.M. and Ramsammoj, E.M., "Application of Fracture Mechanics in the Analysis of Pavement Fatigue," Proceedings, Association of Asphalt Paving Technologists, Volume 41, 1971.

Majidzadeh, K., Buranarom, C. and Karakouzian, M., "Application of Fracture Mechanics for Improved Design of Bituminous Concrete. Vol. I, Plan of Research, State of the Art and Mathematical Investigations," Report FHWA-RD-76-91, Federal Highway Administration, Washington, DC, 1976.

Majidzadeh, K., Dat, M. and Madisi-Ilyas, F., "Application of Fracture Mechanics for Improved Design of Bituminous Concrete. Vol. II, Evaluation of Improved Mixture Formulations and the Effect of Temperature Conditions on Fatigue Models," Report FHWA-RD-76-92, Federal Highway Administration, Washington, DC, 1976.

Majidzadeh, K., Talbert, L.O. and Karakouzian, M., "Development and Field Verification of a Mechanistic Structural Design System in Ohio," Proceedings 4th International Conference on the Structural Design of Asphalt Pavements, Ann Arbor, 1977.

Matsuno, S. and Nishizawa, T., "Mechanism of Longitudinal Surface Cracking in Asphalt Pavement," Proceedings, 7th International Conference on Asphalt Pavements, Volume 2, 1992, pp. 277-291.

McCarthy. P.F., "Factors Affecting the Fatigue Characteristics of Bitumen Sand Mixtures", PhD Thesis, University of Nottingham, 1960.

McElvaney, J., "Fatigue of a Bituminous Mixture under Compound Loading," Ph.D. Thesis, University of Nottingham, 1972.

McElvaney, J. and Pell, P.S., "Fatigue Damage of Asphalt, Effect of Rest Periods," Highways and Roads Constructions, October, 1973.

Miller, J.S, Uzan, J. and Witczak, M.W., "Modification of the Asphalt Institute Bituminous Mix Modulus Predictive Equation," Transportation Research Record 911, 1981, pp. 27-36.

Miner, M.A., "Cumulative Fatigue Damage," International Conference on the Fatigue Damage of Metals, London, 1954.

Molenaar, A.A.A., "Structural Performance and Design of Flexible Pavements and Asphalt Concrete Overlays," PhD Dissertation, Delft University of Technology, 1983.

Molenaar, J., "Dynamic Properties of Asphalt Concrete," Proceedings, European Flexible Pavement Study Group, 1990.

Monismith, C.L. and Deacon, J.A., "Fatigue of Asphalt Paving Mixtures," ASCE Transportation Engineering Journal, Volume 95:2, 1969, pp. 317-346.

Monismith, C.L., Epps, J.A., and Finn, F.A., "Improved Asphalt Mix Design," Proceedings, Association of Asphalt Paving Technologists, San Antonio, Texas, February 11,12 and 13, 1985, pp. 347-406.

Murdock, J.W. and Kesler, C.E., "The Effect of Range of Stress on the Fatigue Strength of Plain Concrete Beams," Journal of the American Concrete Institute, August, 1958.

Nunn, M.E., "The Measurement of Stiffness Modulus Using the Indirect Tensile Test," Draft Unpublished Report, PR/CE/14/95 E082A/HM, Transport Research Laboratory, 1995.

Owen, D.R.J. and Hinton, E., "Finite Elements in Plasticity. Theory and Practice," Pineridge Press, Swansea, 1980.

Owen, D.R.J., Prakash, A. and Zienkiewicz, O.C., "Finite Element Analysis of Non-linear Composite Materials by use of Overlay Systems," Computers and Structures, Vol. 4, 1974, pp. 1251 -1267.

Pande, G.N., Owen, D.R.J., and Zienkiewicz, O.C., "Overlay Models in Time Dependent Nonlinear Material Analysis," Computers and Structures, Vol. 7, 1977, pp 435-443.

Paris, P.C. and Erdogan, F., "A Critical Analysis of Crack Propagation Law," Transactions of the ASME, Journal of Basic Engineering, Series D, 85, No. 3, 1963.

Pell, P.S., "Fatigue Characteristics of Bitumen and Bituminous Mixes," Proceedings, International Conference on the Structural Design of Asphalt Pavements, 1962.

Pell, P.S. and Cooper, K.E., "The Effect of Testing and Mix Variables on the Fatigue Performance of Bituminous Materials," Proceedings of the Association of Asphalt Paving Technologists, 1975, Vol. 44, pp 1-37.

Pell, P.S., McCarthy, P.F. and Gardner, R.R., "Fatigue of Bitumen and Bituminous Mixes," International Journal of Mechanical Science, Pergamon Press Ltd, 1961, pp. 247-267.

Perl, M., Uzan, J. and Sides, A., "Visco-elastic-plastic Constitutive Law for a

Bituminous Mixture Under Repeated Loading," Transportation Research Board, No. 911, 1981, pp. 20-27.

Pfeiffer, J. Ph. and Van Doormall, P.M., "The Rheological Properties of Asphaltic Bitumens," Journal, Institute of Petroleum, Volume 22, 1936, pp 414-440.

Pronk, A.C., "Fatigue Research on Asphalt Beams," Proceedings, European Flexible Pavement Study Group 1990.

Raithby, K.D., "Laboratory Fatigue Tests on Rolled Asphalt and their Relation to Traffic Loading," Roads and Road Construction, August/September 1972, pp 219-223.

Raithby, K.D. and Sterling, A.B., "Some Effects of Loading History on the Performance of Rolled Asphalt," Transport and Road Research Laboratory, Report TRRL-LR 496, Crowthorne, England, 1972.

Rowe, G.M. "Fatigue Life Prediction Based on Energy Considerations," Attachment No. 4, April 1991 Quarterly Report, SHRP A003A Project.

Rowe, G.M., Brown, S.F., Sharrock, M.J. and Bouldin, M.G., "Visco-Elastic Analysis of Hot Mix Asphalt Pavement Structures," Paper presented at the Annual Meeting of the Transportation Board, Washington, DC, January, 1995.

Roque, R. and Buttler, W.G., "The Development of a Measurement and Analysis System to Accurately Determine Asphalt Concrete Properties using the Indirect Tensile Mode," Journal of the Association of Asphalt Paving Technologists, 1992, pp. 304-332.

Ruth, B.E. and Potts, C.F., "Changes in Asphalt Concrete Mixture properties as affected by Absorption, Hardening and Temperature," Transportation Research Record 515, pp. 55-66, 1974.

Sadanada, K. and Shahinian, P., "Elastic-Plastic Fracture Mechanics for High Temperature Fatigue Crack Growth," Fracture Mechanics: Twelfth Conference, ASTM STP 700, American Society for Testing and Materials, 1980, pp.152-163.

Schapery, R.A., "A Theory of Crack Growth in Viscoelastic Media," Report 2, MM 2764-73-1, Journal of the Franklin Institute, Volume 279, No. 4, pp. 268-289.

Schmidt, R.J., "A Practical method for Measuring the Resilient Modulus of Asphalt Treated Mixes," Highway Research Record No. 404, Highway Research Board, 1972.

Sharrock, M.J., "FEPS - Finite Element Plain Strain," Scott Wilson Kirkpatrick and Partners, 1983.

Sharrock, M.J., "Computer Program to Predict Pavement Performance," Progress Report Submitted to Shell Development Company, SWK Pavement Engineering, 1990.

Sharrock, M.J., "Computer Program - HiRoad," PACE™ Software, SWK Pavement Engineering, 1991.

Sharrock, M.J., "Computer Program - Frequency Domain," PACE™ Software, SWK Pavement Engineering, 1994.

Shell International Petroleum Company, "Shell Pavement Design Manual," London, 1978.

Solaimanian, M. and Bolzan, P., "Analysis of the Integrated Model of Climatic Effects on Pavements," SHRP Unpublished Report SHRP-A-637, Strategic Highway Research Program, National Research Council, Washington, DC, 1993.

Sousa, J.B., Taylor, R. and Tanco, J.A., "Analysis of some Laboratory Testing Systems for Asphalt-Aggregate Mixtures," Transport Research Board, Paper No. 91-0743, 1991.

SPSS/PC+ 4.0, SPSS UK Ltd, London Street, Chertsey, Surrey, 1991.

Strategic Highway Research Program, "Strategic Highway Research Program -

Research Plans - Final Report". Strategic Highway Research Plans - Final Report," Transportation Research Board, Washington, D.C., 1986.

Tayebali, A., "Fatigue test results, R^2 for exponential regression fit for dissipated energy versus number of cycles," A-003A Project Communication between Akhtar Tayebali and Geoff Rowe, November 7, 1991.

Tayebali, A.A., Deacon, J.A., Coplantz, J.S., Harvey, J.T. and Monismith, C.L., "Fatigue Response of Asphalt-Aggregate Mixes, Part 1 - Test Method Selection," SHRP Project A-003A, Strategic Highway Research Program, National Research Council, Washington, D.C., November 1992.

Tayebali, A.A., Rowe, G.M. and Sousa, J.B., "Fatigue Response of Asphalt-Aggregate Mixtures," Paper Presented at the Annual Meeting of the Association of Asphalt Paving Technologists, Charleston, 24-26 February 1992, pp 333-360.

Tayebali, A.A., Tsai, B. and Monismith, C.L., "Stiffness of Asphalt-Aggregate Mixes," Report SHRP-A-388, Strategic Highway Research Program, National Research Council, Washington, DC, 1994.

The Asphalt Institute, "Research and Development of the Asphalt Institute Thickness Design Manual (MS-1) Ninth Edition," The Asphalt Institute, RR-82-2, 1982.

The Asphalt Institute, "Thickness Design - Asphalt Pavements for Highways and Streets," Manual Series No. 1 (MS-1), October, 1984.

The Asphalt Institute, "Mix Design Methods for Asphalt Concrete and Other Hot-Mix Types," Manual Series No. 2 (MS-2), May, 1984.

van Dijk, W., Moreaud, H., Quedeville, A. and Ugé, P., "The Fatigue of Bitumen and Bituminous Mixes," Proceedings, Third International Conference on the Structural Design of Asphalt Pavements, London, 1972, pp. 355-366.

van Dijk, W., "Practical Fatigue Characterisation of Bituminous Mixes," Proceedings, Association of Asphalt Paving Technologists, Technical Sessions, Phoenix, Arizona, February 1975, Volume 44, pp 38-74.

van Dijk, W. and Visses, W., "The Energy Approach to Fatigue for Pavement Design," Proceedings, Association of Asphalt Paving Technologists, Technical Sessions, San Antonio, Texas, February 1977, Volume 46, pp 1-40.

Van der Poel, C.J., "A General System Describing the Visco-Elastic Properties of Bitumens and its relation to routine test data," Journal of Applied Chemistry, Volume 4, 1954, pp. 221-236.

Verstraeten, J., Veverka, V. and Francken, L., "Rational and Practical Design of Asphalt Pavements to Avoid Cracking and Rutting," Proceedings, Fifth International Conference on Structural Design of Asphalt Pavements, Vol. 1,

1982, pp. 45-58.

Whiteoak, D., "The Shell Bitumen Handbook," Shell Bitumen U.K., 1990.

Williamson, R.H., "Environmental Effects in Road Engineering and Their Engineering Significance," PhD Report Volumes 1 and 2, University of Natal, Durban, December, 1972.

Witczak, M.W., "Development of Regression Model for Asphalt Concrete Modulus for Use in MS-1 Study," University of Maryland, College Park, 1978.

Witczak, M.W., "Design of Full-Depth Asphalt Airfield Pavements," Proceedings, Third International Conference on the Structural Design of Asphalt Pavements, London, 1972, pp. 550-567.

Zienkiewicz, O.C., Nayak, G.C. and Owen, D.R.J., "Composite and Overlay Models in Numerical Analysis of Elasto-plastic Continua," International Symposium on Foundations of Plasticity, Warsaw, 1972.

APPENDIX A

STRAIN GAUGE RESULTS FROM
FATIGUE WHEEL TRACKING

SHRP A003A
SLAB 1 CH1

SHRP A003A
SLAB 1 CH2

SHRP A003A
SLAB 1 CH3

SHRP A003A
SLAB 1 CH4

SHRP A003A
SLAB 1 CH5

SHRP A003A
SLAB 1 CH6

SHRP A003A
SLAB 1 CH7

SHRP A003A
SLAB 1 CH8

SHRP A003A
SLAB 2 CH1
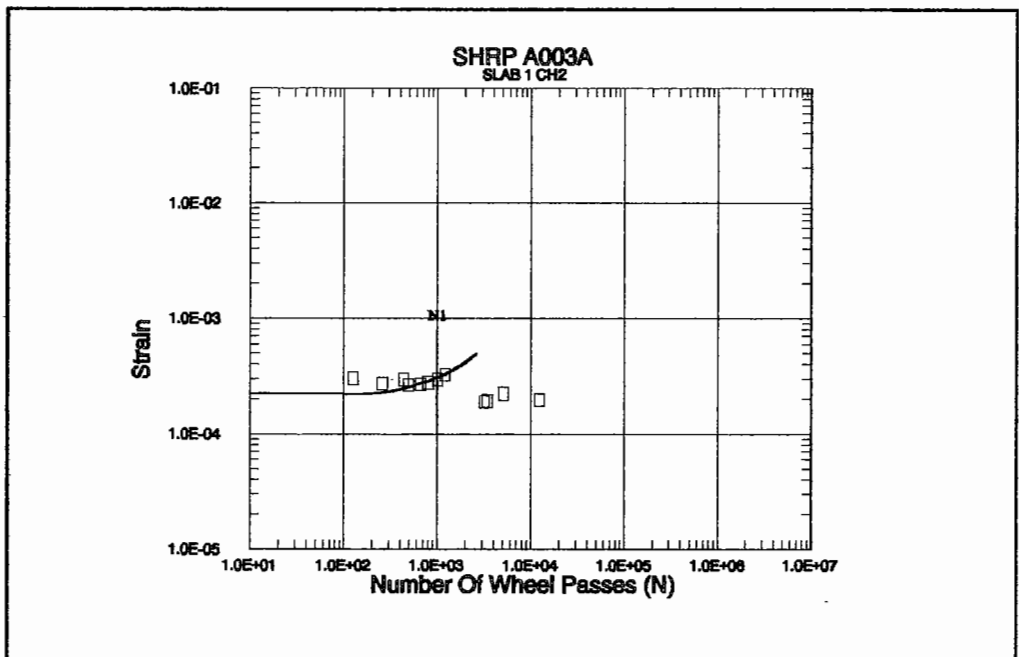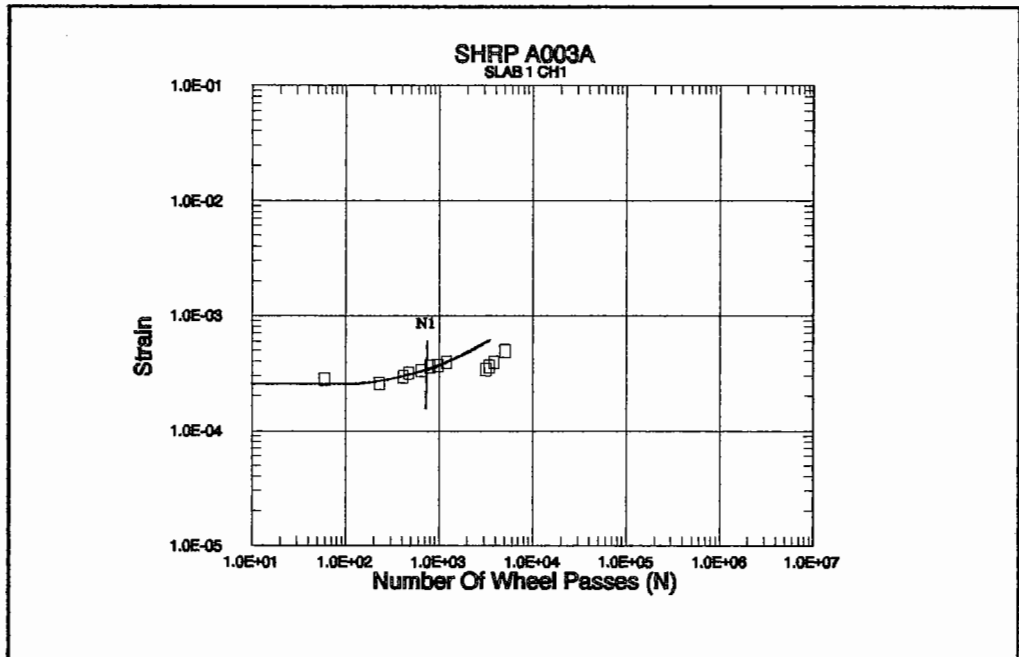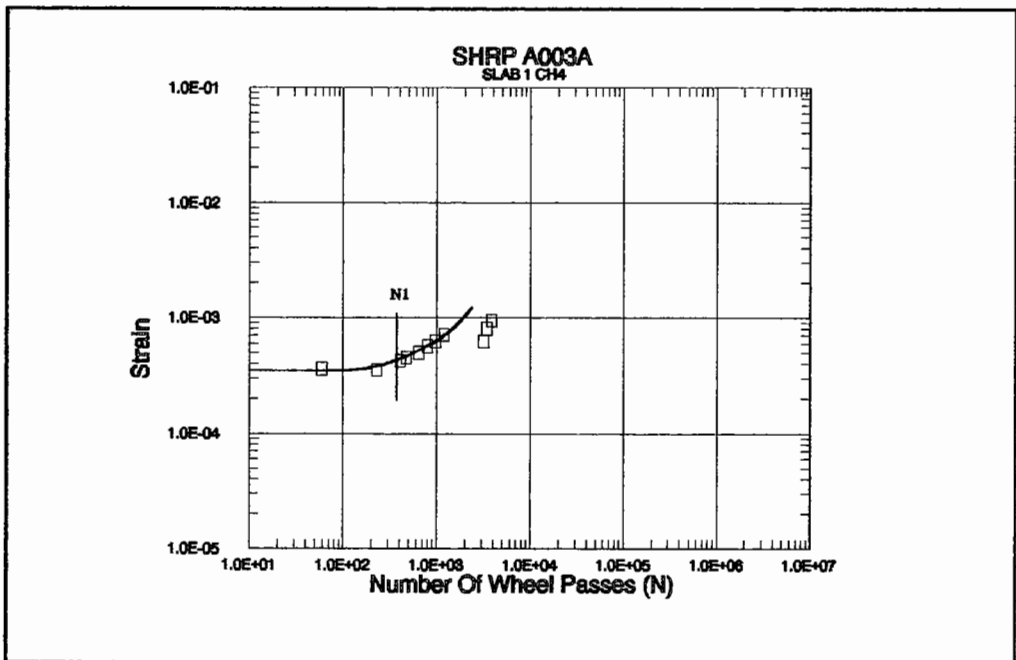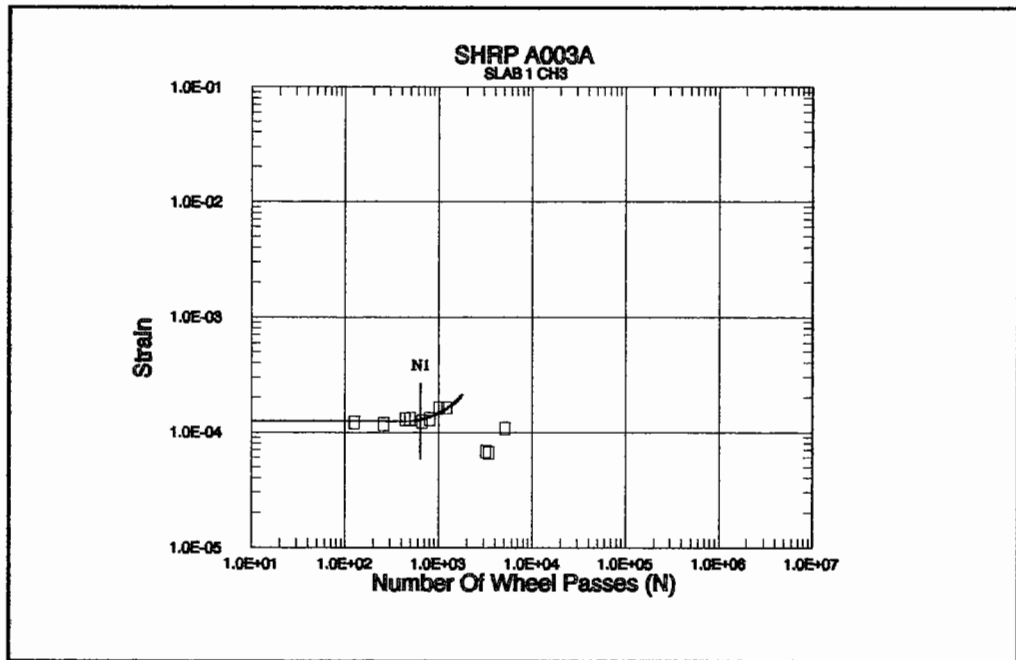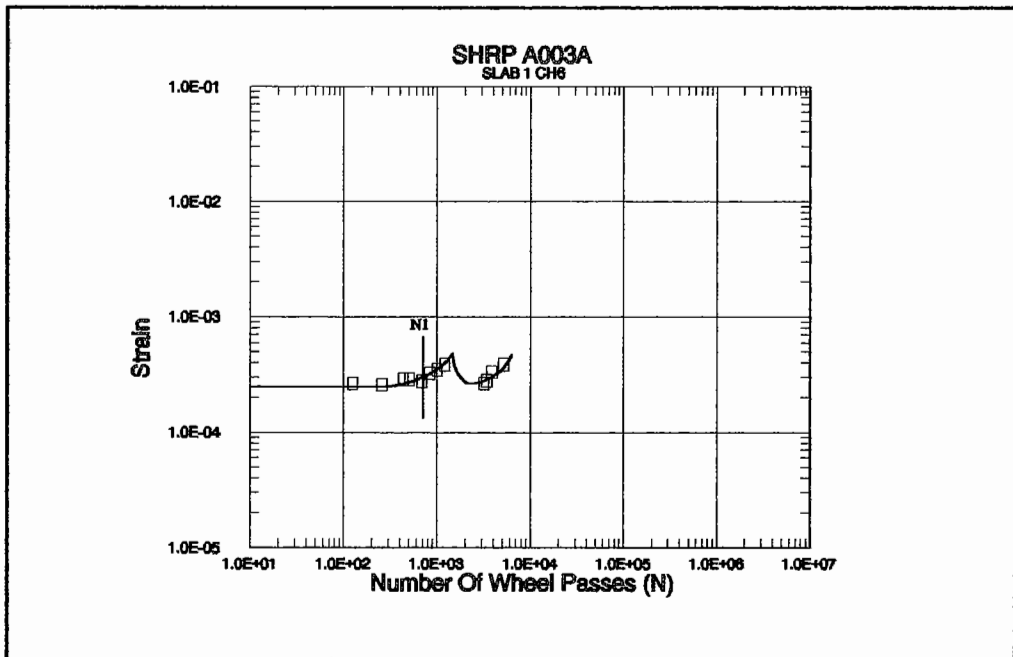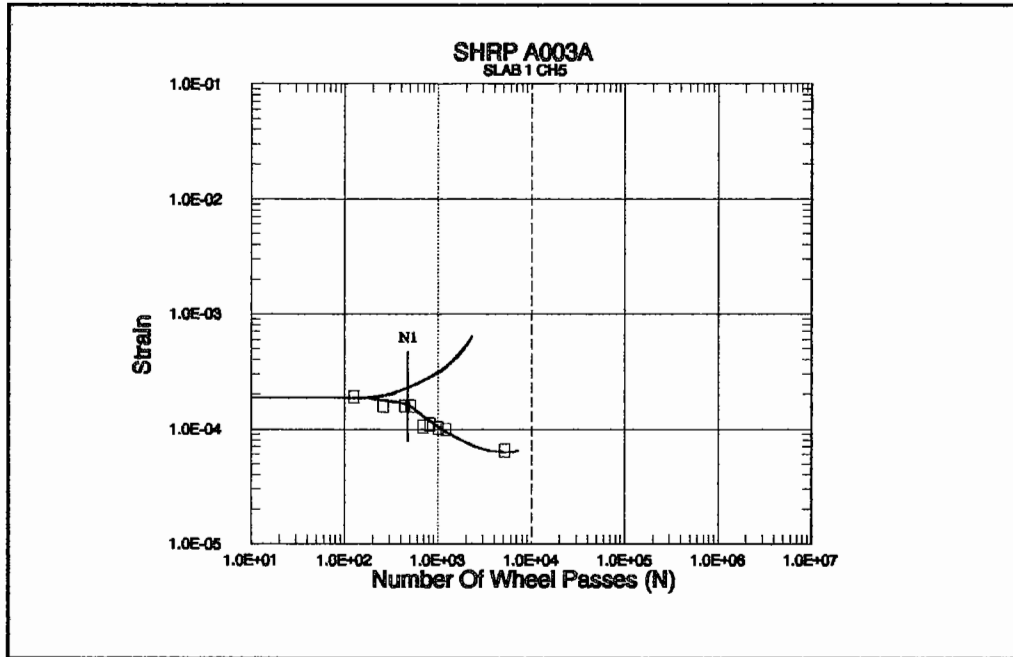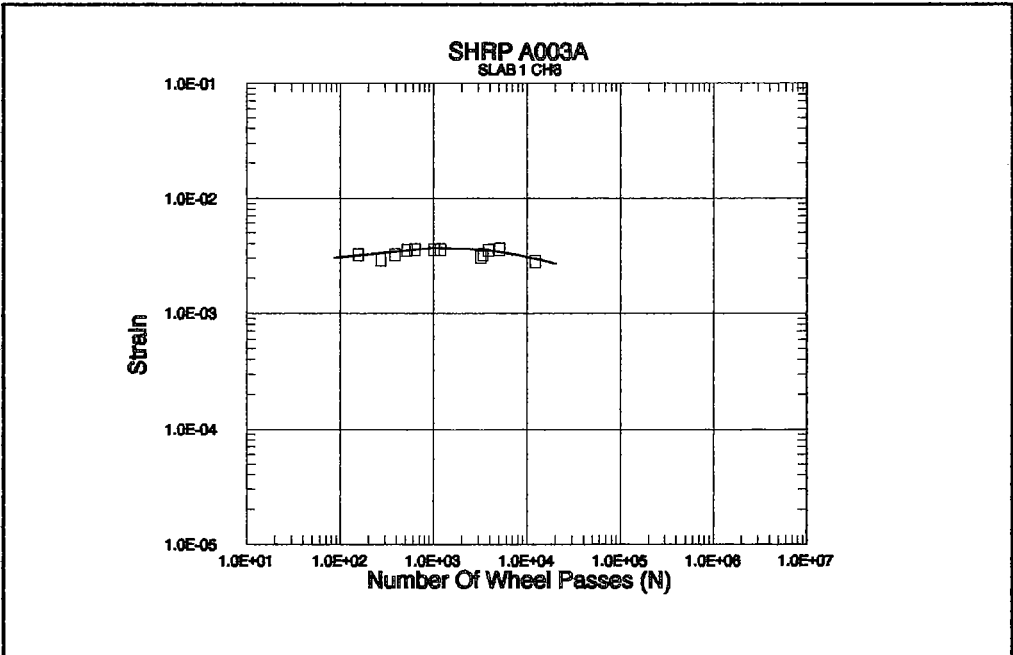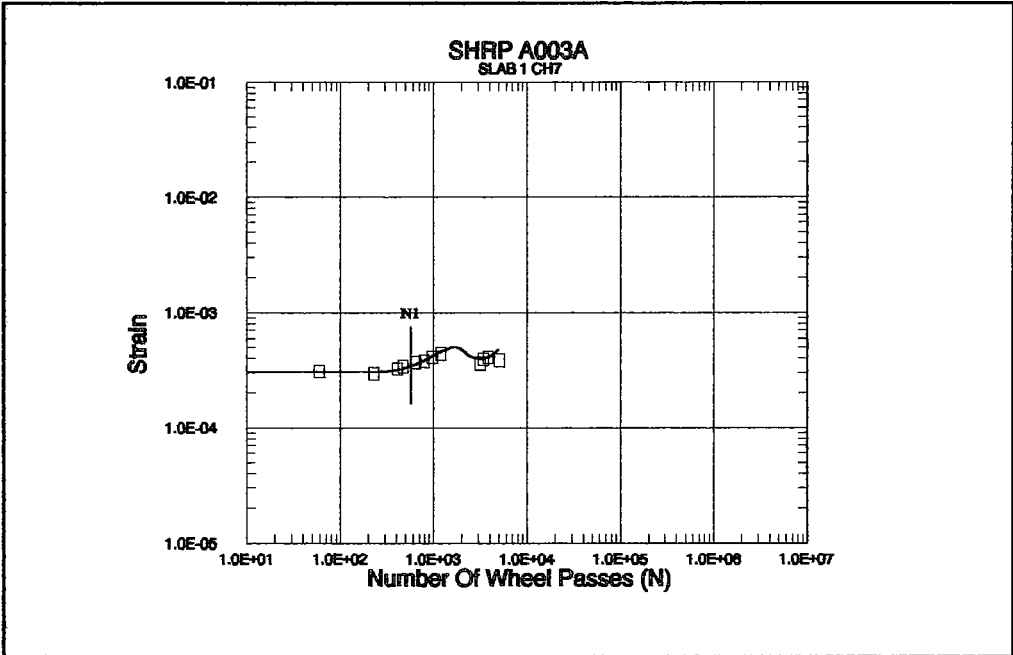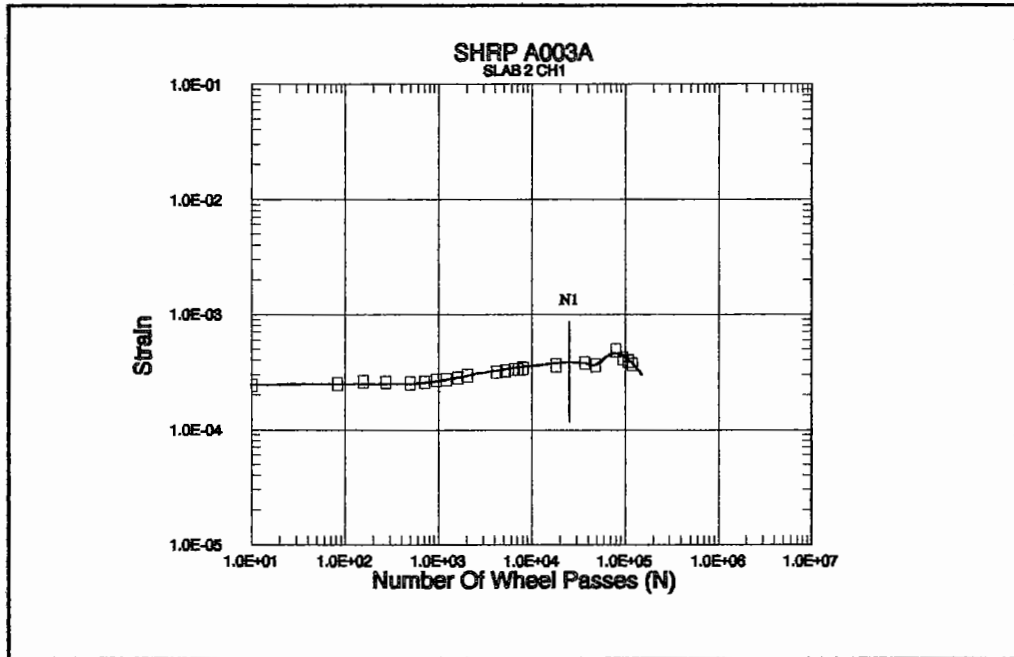
**STRAIN GAUGE BROKE
A003A SLAB 2 CH2**

SHRP A003A
SLAB 2 CH3

SHRP A003A
SLAB 2 CH4

SHRP A003A
SLAB 2 CH5

SHRP A003A
SLAB 2 CH6

SHRP A003A
SLAB 2 CH7

SHRP A003A
SLAB 2 CH8

SHRP A003A
SLAB 3 CH1

SHRP A003A
SLAB 3 CH2

SHRP A003A
SLAB 3 CH3

SHRP A003A
SLAB 3 CH4

SHRP A003A
SLAB 3 CH5

SHRP A003A
SLAB 3 CH6

SHRP A003A
SLAB 3 CH7

SHRP A003A
SLAB 3 CH8

SHRP A003A
SLAB 4 CH1

SHRP A003A
SLAB 4 CH2

-A.14-

SHRP A003A
SLAB 4 CH3

SHRP A003A
SLAB 4 CH4

-A.15-

SHRP A003A
SLAB 4 CH5

SHRP A003A
SLAB 4 CH6

SHRP A003A
SLAB 4 CH7

SHRP A003A
SLAB 4 CH8

SHRP A003A
SLAB 5 CH1

SHRP A003A
SLAB 5 CH2

SHRP A003A
SLAB 5 CH3

SHRP A003A
SLAB 5 CH4

SHRP A003A
SLAB 5 CH5

SHRP A003A
SLAB 5 CH6

-A.20-

SHRP A003A
SLAB 5 CH7

SHRP A003A
SLAB 5 CH8

SHRP A003A
SLAB 6 CH1

SHRP A003A
SLAB 6 CH2

SHRP A003A
SLAB 6 CH3

SHRP A003A
SLAB 6 CH4

SHRP A003A
SLAB 6 CH7

SHRP A003A
SLAB 6 CH8

SHRP A004
SLAB 1 CH1

SHRP A004
SLAB 1 CH2

SHRP A004
SLAB 1 CH3

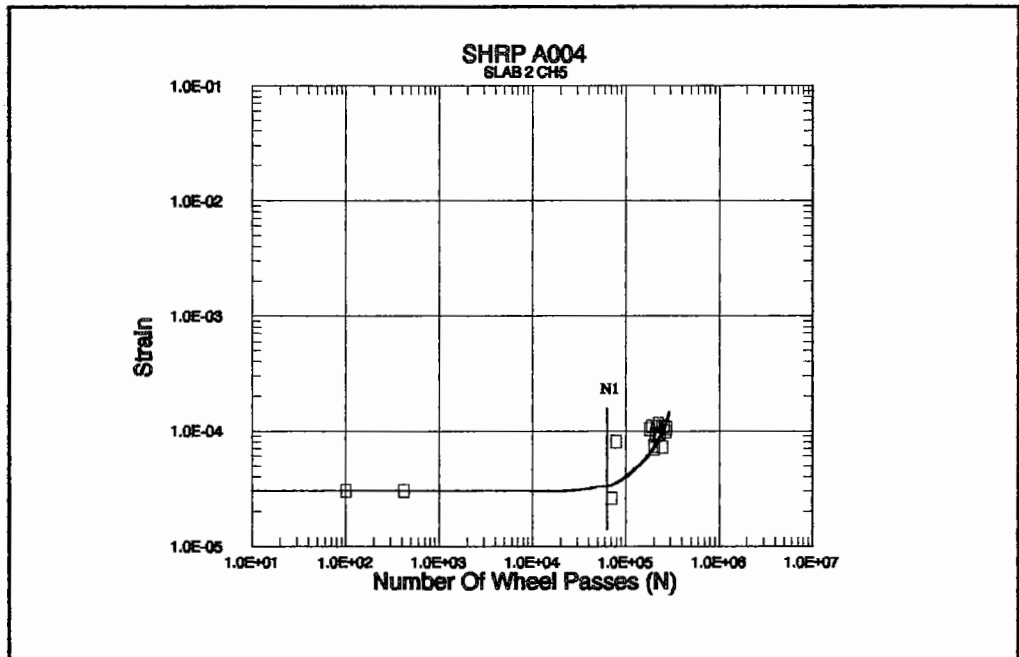SHRP A004
SLAB 1 CH4

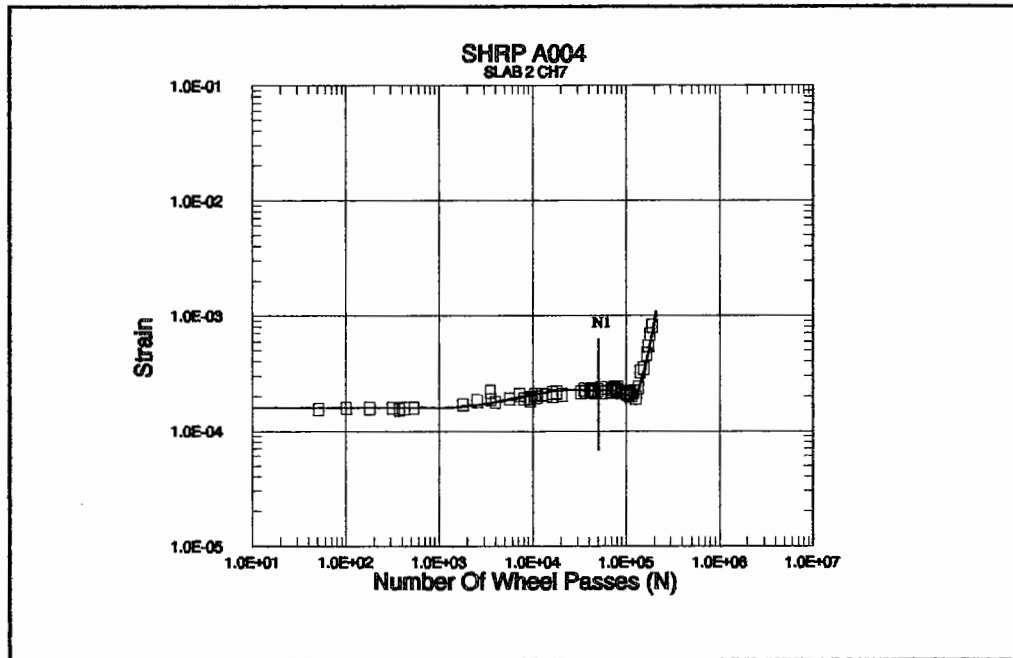SHRP A004
SLAB 1 CH5

SHRP A004
SLAB 1 CH6

SHRP A004
SLAB 1 CH7

NO GAUGE 8 (CH8) WAS USED FOR A004 SLAB NO 1

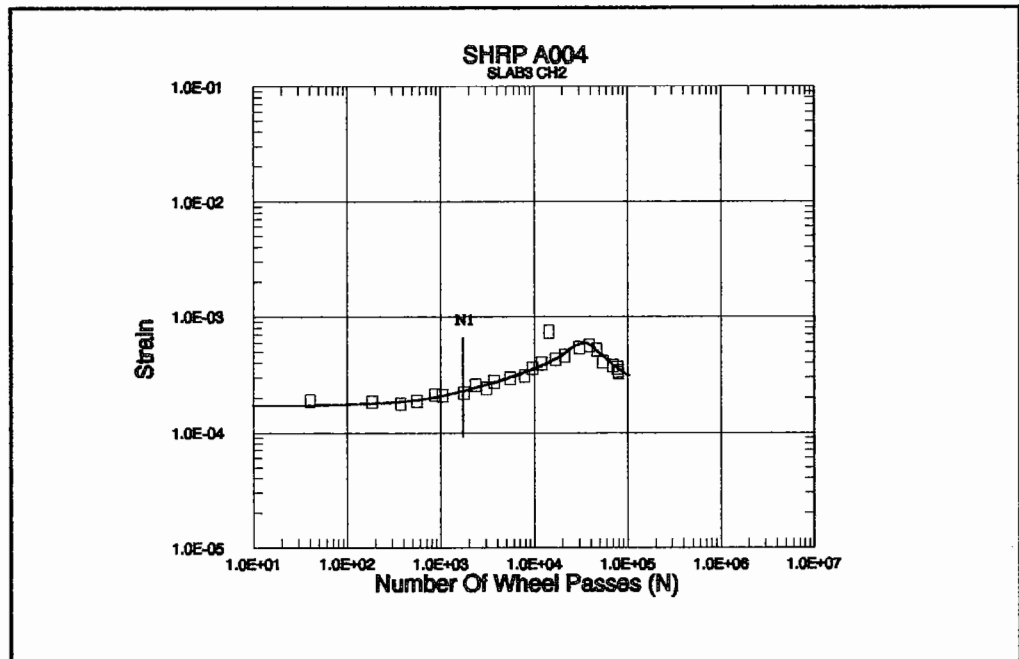SHRP A004
SLAB 2 CH1

SHRP A004
SLAB 2 CH2

SHRP A004
SLAB 2 CH3

SHRP A004
SLAB 2 CH4

SHRP A004
SLAB 2 CH5

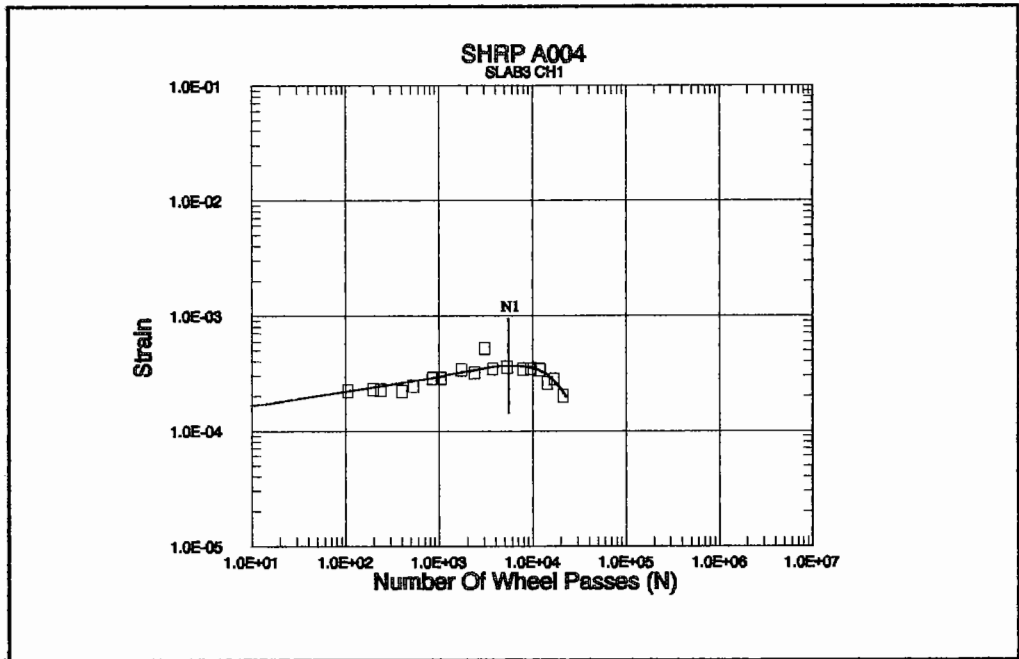SHRP A004
SLAB 2 CH6

SHRP A004
SLAB 2 CH7

NO GAUGE 8 (CH8) WAS USED FOR A004 SLAB NO 2

SHRP A004
SLAB3 CH1

SHRP A004
SLAB3 CH2

SHRP A004
SLAB3 CH3

SHRP A004
SLAB3 CH4

-A.35-
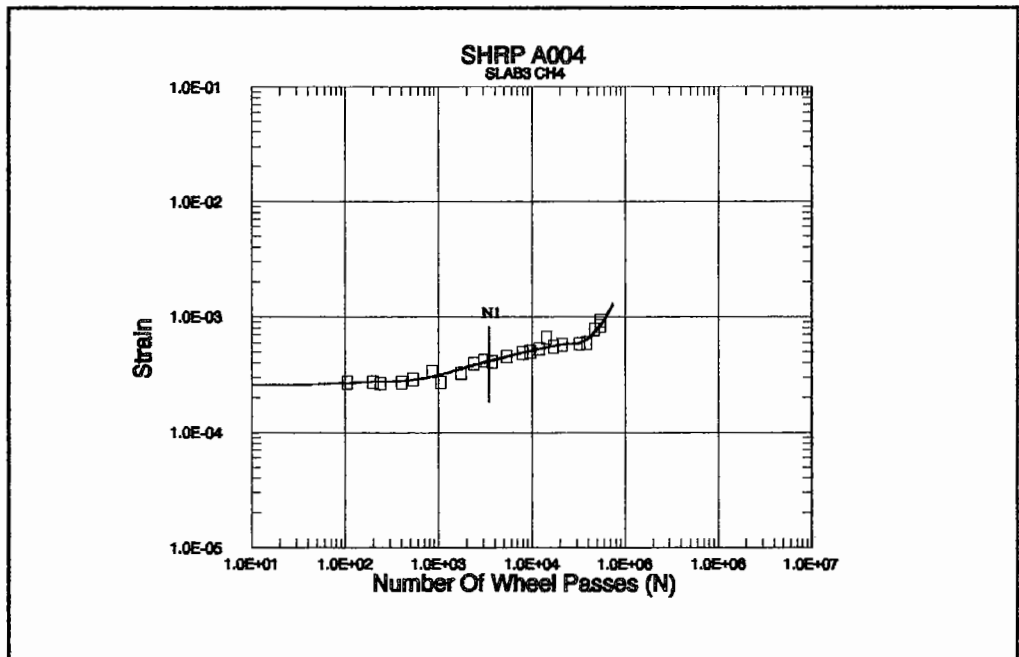
STRAIN GAUGE BROKE
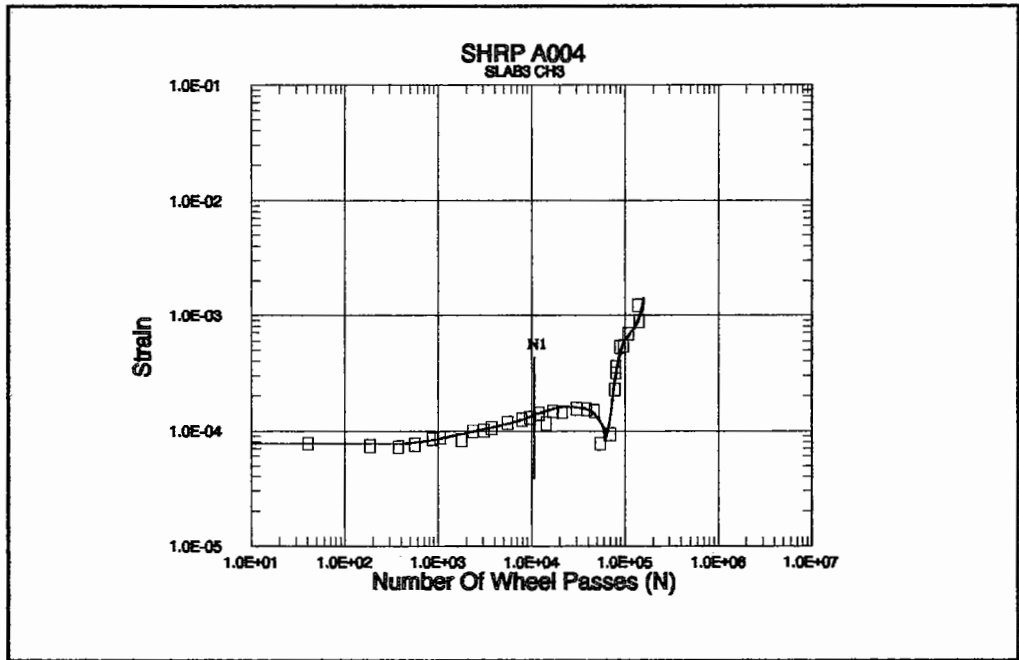## A004 SLAB 3 CH6

SHRP A004
SLAB3 CH6

-A.36-

SHRP A004
SLAB3 CH7

NO GAUGE 8 (CH8) WAS USED FOR A004 SLAB NO 3

SHRP A004
SLAB4 CH1

1.0E-01

1.0E-02

N1

1.0E-03

Strain

1.0E-04

1.0E-05
1.0E+01 1.0E+02 1.0E+03 1.0E+04 1.0E+05 1.0E+06 1.0E+07
Number Of Wheel Passes (N)

SHRP A004
SLAB4 CH2

1.0E-01

1.0E-02

N1

1.0E-03

Strain

1.0E-04

1.0E-05
1.0E+01 1.0E+02 1.0E+03 1.0E+04 1.0E+05 1.0E+06 1.0E+07
Number Of Wheel Passes (N)

-A.38-

SHRP A004
SLAB4 CH3

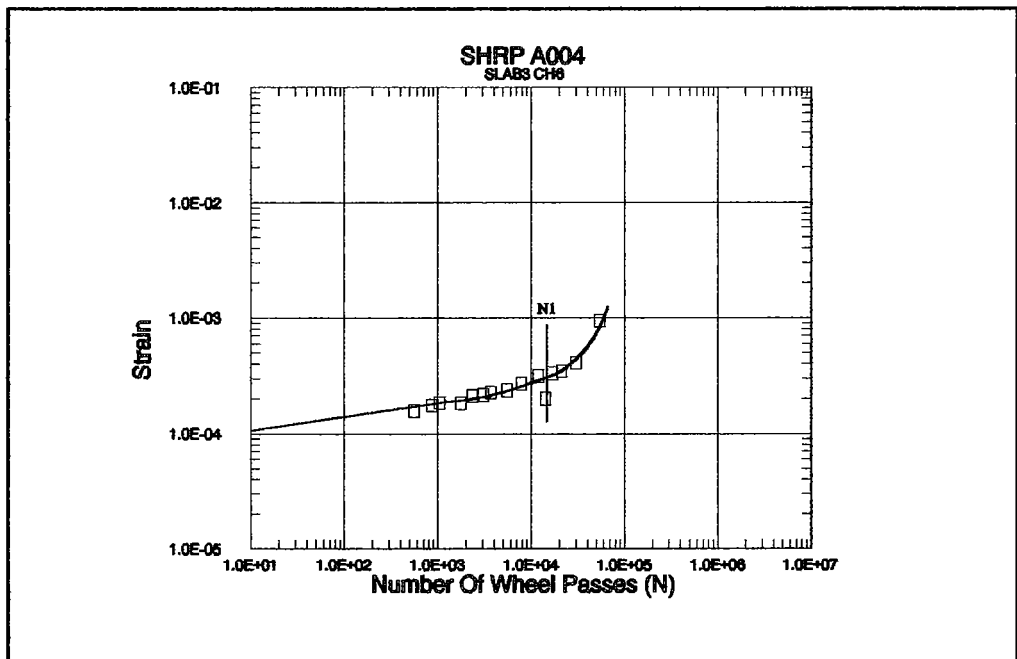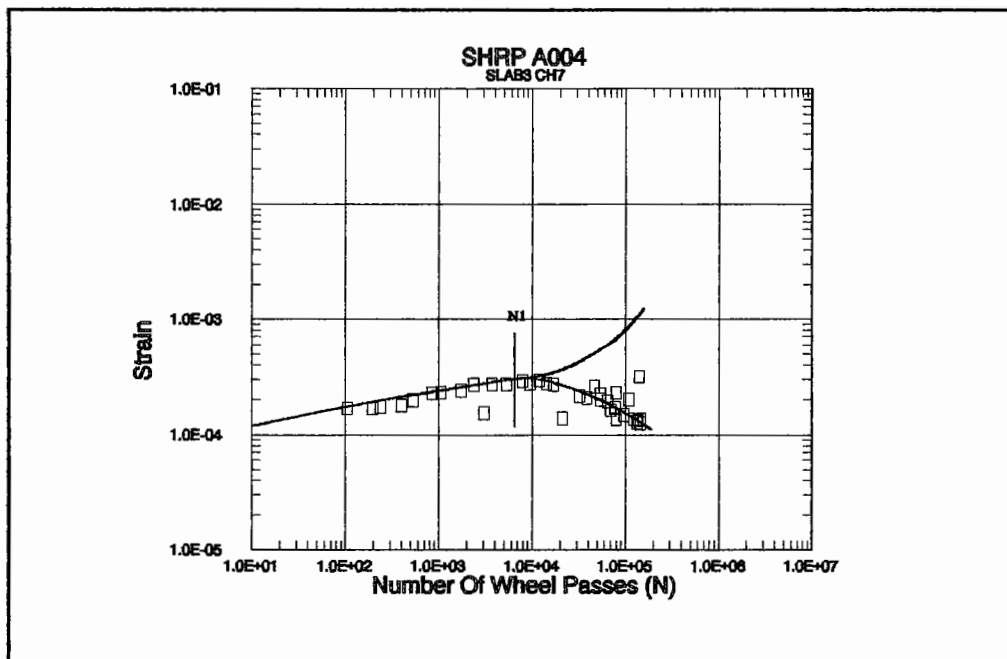SHRP A004
SLAB4 CH4

SHRP A004
SLAB4 CH5
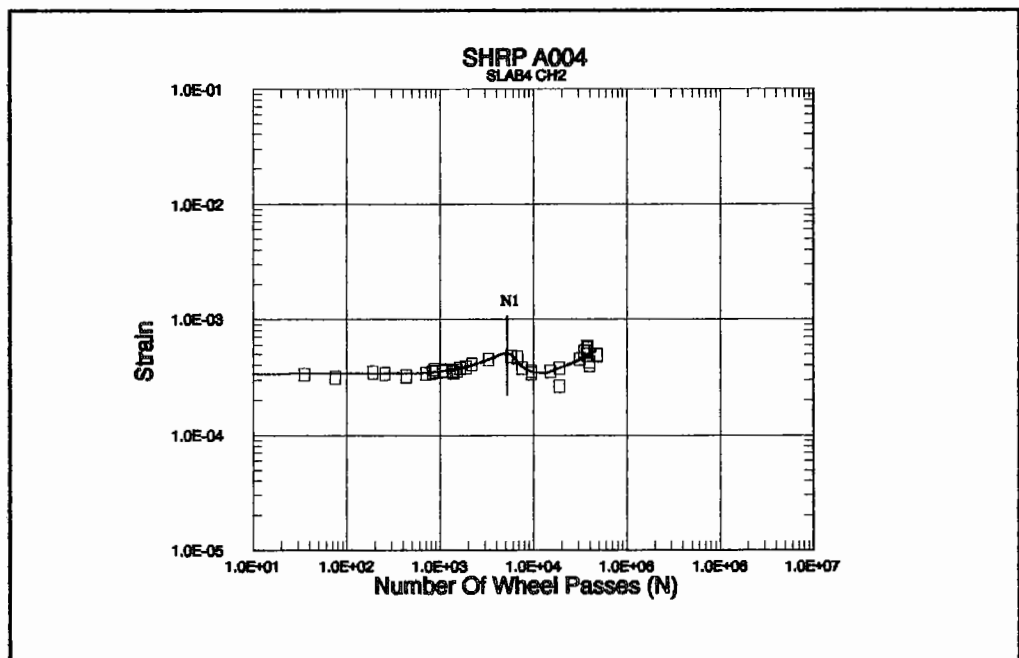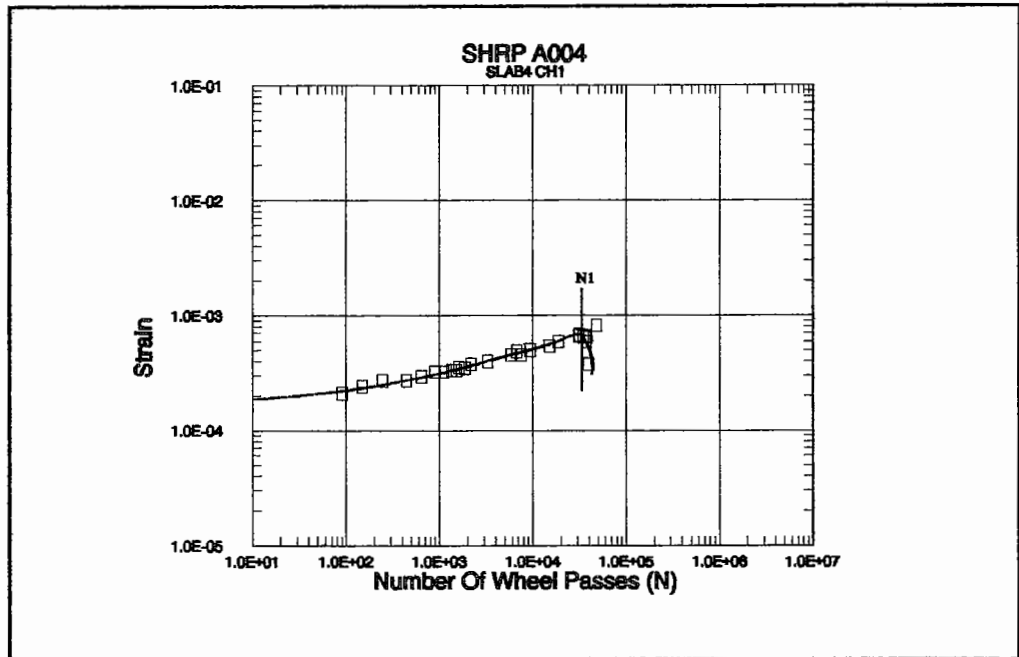

SHRP A004
SLAB4 CH6

SHRP A004
SLAB4 CH7

NO GAUGE 8 (CH8) WAS USED FOR A004 SLAB NO 4

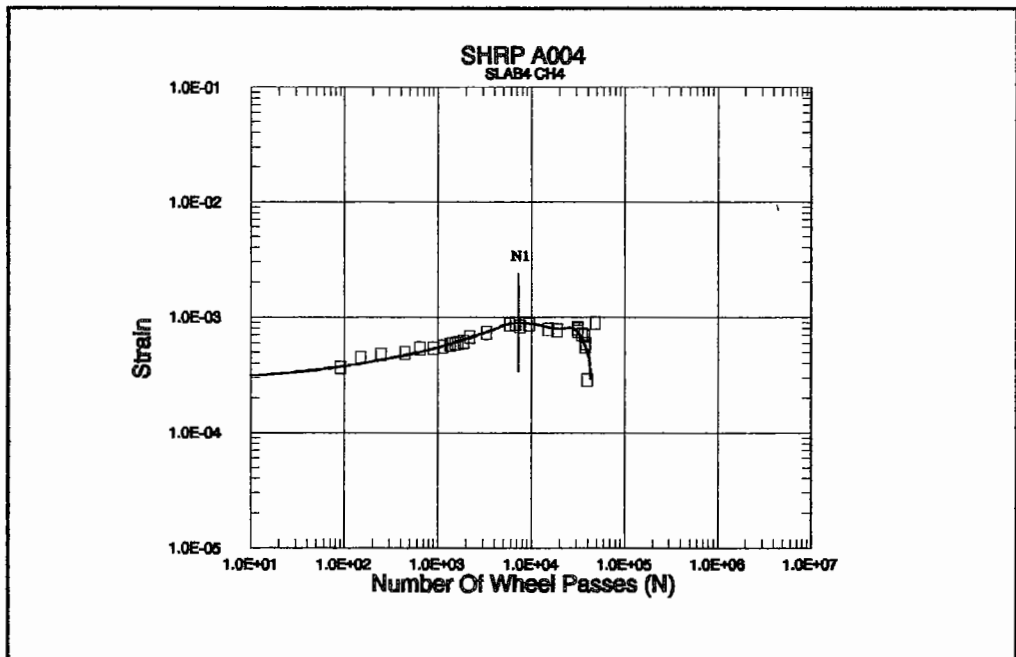SHRP A004
SLAB5 CH1

SHRP A004
SLAB5 CH2

SHRP A004
SLAB5 CH5

SHRP A004
SLAB5 CH6

SHRP A004
SLAB5 CH7

SHRP A004
SLAB5 CH8

SHRP A004
SLAB6 CH1

SHRP A004
SLAB6 CH2

SHRP A004
SLAB6 CH3

SHRP A004
SLAB6 CH4

SHRP A004
SLAB6 CH5

SHRP A004
SLAB6 CH6

SHRP A004
SLAB6 CH7

SHRP A004
SLAB6 CH8

SHRP A004
SLAB7 CH1

SHRP A004
SLAB7 CH2

SHRP A004
SLAB7 CH3

SHRP A004
SLAB7 CH4

SHRP A004
SLAB7 CH5

SHRP A004
SLAB7 CH6

SHRP A004
SLAB7 CH7

SHRP A004
SLAB7 CH8

SHRP A004
SLAB8 CH1

SHRP A004
SLAB8 CH2

SHRP A004
SLAB6 CH3

SHRP A004
SLAB6 CH4

SHRP A004
SLAB8 CH5

SHRP A004
SLAB8 CH6

SHRP A004
SLAB8 CH7

SHRP A004
SLAB8 CH8

SHRP A004
SLAB9 CH1

SHRP A004
SLAB9 CH2

SHRP A004
SLAB9 CH3

SHRP A004
SLAB9 CH4

SHRP A004
SLAB9 CH5

SHRP A004
SLAB9 CH6

-A.60-

SHRP A004
SLAB9 CH7

SHRP A004
SLAB9 CH8

SHRP A004
SLAB10 CH1

SHRP A004
SLAB10 CH2

SHRP A004
SLAB10 CH3

SHRP A004
SLAB10 CH4

SHRP A004
SLAB10 CH5

SHRP A004
SLAB10 CH6

SHRP A004
SLAB10 CH7

SHRP A004
SLAB10 CH8

SHRP A004
SLAB11 CH1

SHRP A004
SLAB11 CH2

SHRP A004
SLAB11 CH3

SHRP A004
SLAB11 CH4

SHRP A004
SLAB11 CH5

SHRP A004
SLAB11 CH6

SHRP A004
SLAB11 CH7

SHRP A004
SLAB11 CH8

SHRP A004
SLAB12 CH3

SHRP A004
SLAB12 CH4

SHRP A004
SLAB12 CH5

SHRP A004
SLAB12 CH6

SHRP A004
SLAB12 CH7

SHRP A004
SLAB12 CH6